SIMULATION OF FLUID FLOW IN FRACTURED ROCK;
A PROBABILISTIC APPROACH

by

JOSE ANTONIO SAMANIEGO, BSc., MSc. DIC.

A thesis submitted to the University of London

(Imperial College of Science and Technology)

for the degree of

Doctor of Philosophy in the Faculty of Engineering

March, 1985.

THIS WORK IS DEDICATED TO THE MEMORY

OF MY BROTHER ALBERTO

ABSTRACT

A statistical computer model was developed, capable of generating in two dimensions a random discontinuity network and calculating fluid flow through the interconnected discontinuities. The aims of this work were firstly to identify and study those discontinuity characteristics that are crucial in dictating the hydraulic behaviour of the discontinuity network, and secondly to assess when a network of discontinuities can be validly represented as a continuous anisotropic porous medium.

The input data for the model were obtained from field measurements; both scanline sampling and surface sampling by photographs were used. Additional data for the model included the mean discontinuity aperture of each set, usually estimated from borehole pressure tests, and the hydraulic boundary potentials which, for a specific problem, can be estimated from piezometric measurements. A field trip to Pembrokeshire provided the necessary input data. The model, based upon a bi-factorisation routine, calculates the flow quantities and the equivalent permeability tensor for any random, two-dimensional network comprising up to 5000 discontinuities. A numerical validation of the model, carried out against an idealized extensive discontinuity network, indicated that calculations of flow quantities and permeability tensor are free of numerical error. Geometrical validation of the model, carried out against discontinuity field data, was only successful for highly fractured rock exposures. Parametric studies of the characteristics of discontinuity networks showed that trace length is immportant in determining permeability and that discontinuity frequency, if used solely as an index of permeability, can often be misleading. As expected, it was found that the permeability tensor is proportional to the cube of the discontinuity aperture. Two indices of network interconnectivity were defined: the node index and the discontinuity index. These indices tended to unity as the density of discontinuities and/or trace length increased. The validity of the continuum approximation was studied utilising these connectivity indices. It was found that even when the permeability tensor was symmetric, some errors in predicting flow could be expected. A study of the representative elementary volume indicated that, as size of the test area increased the permeability tensor became constant. A Monte Carlo simulation was carried out in order to provide substantiation for the results obtained in the parametric studies since these were performed on the basis of a single realisation. Two practical applications were presented, the first involved the analysis of water flow into circular tunnels of different diameters. The second provided a case study which involved the prediction of water inflow at the tunnel face at a site in Derbyshire.

TABLE OF CONTENTS

TABLE OF CONTENTS

TABLE OF CONTENTS

TABLE OF CONTENTS

TABLE OF CONTENTS

LIST OF FIGURES

LIST OF FIGURES

LIST OF FIGURES

LIST OF FIGURES

LIST OF FIGURES

LIST OF FIGURES

LIST OF TABLES

LIST OF TABLES

LIST OF TABLES

LIST OF SYMBOLS

$\vec{a}$	Unit vector of a discontinuity normal	
A	Area (A_i)	(L^2)
2b	Parallel plate aperture	(L)
B	Number of nodes at the boundaries	
c	Fracture conductance	(L^2/T)
	or censoring level	(L)
	or coefficient of variation	
C	Correlation coefficient	
D_h	Hydraulic diameter	(L)
e	Discontinuity aperture	(L)
e_m	Aperture of the mth channel	(L)
EPT	Equivalent permeability tensor	(L/S)
f	Roughness factor	
$f(x)$	Probability density function of x	
F	Over-relaxation factor	
$F(x)$	Cummulative distribution function of x	
g	Gravitational acceleration	(LT^{-2})
h	Hydraulic head	(L)
h_i	Hydraulic head at input line	(L)
h_o	Hydraulic head at output line	(L)
I_1, I_2, I_3	Invariants of permeability tensor	
I_D	Discontinuity index	
I_N	Node Index	
J_i	Potential gradient = $\partial h/\partial x_i$	
	or = $\partial\phi/\partial x_i$ (in Chapter 2)	

k	Intrinsic permeability (k_{ij})	(L^2)
K	Hydraulic conductivity (K_{ij})	(L/T)
	or Fisher's constant (in Chapter 2 and 3)	
K_F	Fracture hydraulic conductivity	(L/T)
k_F	Fracture intrinsic permeability	(L^2)
K_g	Permeability measured in the direction of the gradient	(L/T)
K_f	Permeability measured in the direction of the flow	(L/T)
K_1, K_2, K_3	Principal permeabilities	(L/T)
ℓ	Random trace length	(L)
L	Fracture length	(L)
	or scanline length (Chapter 2 and 3)	(L)
	or side length of test area (Chapter 4)	(L)
$\overline{\ell}_i$	Mean censored semi-trace length	(L)
$\overline{\ell}$	Mean generated trace length	(L)
ℓ_m	Length of the mth channel	(L)
n	Number of elements in a sample population	
	or number of nodes (Chapter 3 and 4)	
N	Discontinuity density	(L^{-2})
	or total number of nodes in a discontinuity mesh	
p	Pressure, $\partial p/\partial x$ pressure gradient	(MLT^{-2})
q	Flow quantity	(L^3/T)
	or specific discharge (Chapter 2)	(L/T)
Q	Flow quantity across a boundary	(L^3/T)
q_m	Flow quantity along the mth channel	(L^3/T)
r	Number of discontinuities with semi-trace length less than censoring level, c	(L)
RE	Flow relative error	

r_e	Radius of the zone of influence	(L)
r_w	Radius of borehole	(L)
R_e	Reynold's number	
s	Flow direction vector	
SD	Standard deviation	
v	Flow velocity	(L/T)
$\overline{V}_i$	Specific discharge	(L/T)
v_m	Flow velocity along the mth channel	(L/T)
w	Width of the fracture	(L)
	or weighting factor (Chapter 2)	
x_i	Coordinate system	
z	Geometrical head	(L)
α	Angle between normal to the discontinuity and the scanline	
β	Discontinuity trend	
γ	Discontinuity plunge	
λ	Discontinuity frequency	(L^{-1})
λ_s	Discontinuity frequency along the scanline	(L^{-1})
δ_{ij}	Kronecker delta $\delta_{ij} = \begin{cases} 1 & i = j \\ 0 & i \neq j \end{cases}$	
Δh	Drop in potential head	(L)
ε	Absolute roughness	(L)
ψ	Friction factor	
ρ	Fluid density	(ML^{-3})
μ	Coefficient of viscosity	$(ML^{-1}T^{-1})$
	or $1/\mu$ = mean trace length	(L)
Θ	Angle of orientation of a discontinuity	
Θ_i	Angles between normal to the discontinuity and the coordinate axis	
ν	Kinematic viscosity	$(L^{-2}T)$

Fundamental Terminology

The following are definitions and descriptions of terms used in this thesis.

Aperture

Perpendicular distance between adjacent walls of a discontinuity.

Areal Frequency

Number of discontinuity centres per unit area.

Censored Semi-trace Length

The length of the trace from the scanline to one end of the trace or a fixed distance (known as the censoring level) whichever is the least.

Coefficient of Permeability

See permeability.

Discontinuity

Break or interruption in the mechanical properties of a rock mass. It is also the collective term used for joints, bedding planes and fractures, so that, for the purposes of this thesis, these are used interchangeably.

Discontinuity Network

Also discontinuity mesh, is the system formed by discontinuity traces (or planes) in two (or three) dimensions.

Discontinuity Set

Is a group or family of discontinuities that are grouped according to their orientation.

Frequency

The number of discontinuities intersected per unit length of sampling line.

Intrinsic Permeability

See permeability.

Hydraulic Aperture

The equivalent parallel plate aperture as computed from borehole pressure tests assuming the validity of the cubic law.

Hydraulic Conductivity

See permeability.

Linear Flow

Or Darcian flow, the flow in which the pressure gradient is proportional to the specific discharge.

Orientation

Is the attitude of the discontinuity plane in space, and, in the two dimensional model is the angle measured anti-clockwise from the right hand end of the horizontal axis.

Permeability

For the purposes of this work the term is used in a generic sense. The meaning can be; hydraulic conductivity, coefficient of permeability or sometimes intrinsic permeability. See Section 2.3.2 for precise definition of each of these terms.

Rock Mass

A physical system formed of intact rock and geological discontinuities.

Rock Material

Also rock matrix, is the intact rock portion of a rock mass.

Scanline Sampling

Is a line sampling method which basically consists on recording, the orientation, position, semi-trace length, type of termination and aperture of each of the discontinuities that intersect a tape held along a rock exposure.

Semi-trace Length

Is the portion of the trace length measured between the scanline intersection point and one end of the trace.

Spacing

Is the perpendicular distance between two adjacent discontinuities that belong to the same discontinuity set.

Trace Length

Is the length of the intersection of a discontinuity plane with a rock exposure or a selected plane of analysis.

ACKNOWLEDGEMENTS

This work has been commmissioned by the Department of the Environment as part of its radioactive waste management research programme and coordinated by the Building Research Establishment.

I would like to express my sincere gratitude to the following for their advice and assistance while this work was being done.

To Dr. S.D. Priest, Supervisor of this project, for his support and guidance throughout this research and also for his critical comments on the manuscript; To Professor E.T. Brown for his stimulating discussions; To Dr. J.W. Bray for his help and encouragement in the initial stages of this work; To Dr. J.O. Watson for his immense help and advice during the development of the computer program; To Dr. J.A. Hudson for his helpful criticism of the research; To Dr. D.L. Hodkin of G.H. Hill and Sons Consulting Engineers, for his kind help and guidance during the field trip to Derbyshire; To Mr. J. Harrison for his co-operation and hard work during the field trip to Pembrokeshire; To Messrs. L.D. Wilson, P. Huckle, W. Harman and T. Allen for their help in various aspects of this work; To Maritza Arispe and Karin De Rycker for their excellent drafting; To Elizabeth Dowden for her efficient typing of the manuscript; To Angela Smith and her colleagues at the Rock Mechanics Information Service, for their collaboration in finding useful information; To Adrian Clark and Ruth Cooper for their patience and humour during the continuous overdues on my library loans; To

Margaret Burr and Noel Treacy for proof reading the text; To all my research colleagues of the Imperial College Rock Mechanics Section for their fruitful discussions and warm friendship; To many other persons within Imperial College and outside who were connected with various aspects of the study and the production of this thesis; Finally to my parents for their continuous encouragement and support throughout my studies.

CHAPTER 1 INTRODUCTION

The work described in this thesis was carried out under a research contract supported by the Radioactive Waste Professional Division of the Department of the Environment, as part of its programme of radioactive waste management research coordinated by the Building Research Establishment. The aim of this research is firstly to identify and study those properties of discontinuous rock masses that are crucial in controlling its hydrological characteristics. Secondly, to analyse whether it is possible to define an Equivalent Permeability Tensor (EPT) for a discontinuity network, and determine when this tensor can be used in conjunction with the theory of anisotropic porous media in order to predict permeability and flow in all directions.

Rock masses are generally physical systems formed of intact rock and geological discontinuities. The discontinuities are present in families or sets and are the results of tectonic stresses. The description or characterisation of these systems of discontinuities can only be studied from a statistical and probabilistical point of view since the exact information describing the discontinuity geometry cannot be determined without destroying the very features that are being measured. Permeability to fluid flow in these types of rock masses is critically dependent upon the frequency and geometry of discontinuities within the mass. This is especially true in hard non-porous rocks that are brittle enough to develop fracture systems, and that are strong enough to sustain significant discontinuity apertures in a given stress field. Consequently, any analysis of flow through the discontinuity network must be based upon a representative sample of the relevant discontinuity characteristics, coupled with some form of idealised model of discontinuity geometry and fluid flow. In this work a statistical computer model was developed which performs a numerical analysis of fluid flow through a random two-dimensional discontinuity network and then calculates the equivalent permeability tensor for the network.

The interest in this type of study has been prompted by the possibilities of underground disposal of radioactive waste, however, these studies can also be applied to ground water flow through fractured masses and to fractured reservoirs in the petroleum industry. Nevertheless at this early stage of modelling one should be aware of the difficulties encountered in trying to represent a three-dimensional problem by a two-dimensional model.

In Chapter 2 of this work a survey of the literature is presented, which includes a brief description of the two main approaches in studying discontinuous rock masses, this is followed by a review of the previous work that has been carried out in statistically representing discontinuity geometry characteristics as observed in the field. In the third part of the chapter, the ways of simulating flow in fractured rock are examined and related topics including: theory of anisotropic porous media, Darcy's Law, directional permeability and parallel plate analogue are discussed. Finally in this chapter there is a review of the deterministic and statistical models used in studying flow in fractured rock.

In Chapter 3, the theory used in developing the model along with the description of the model itself is presented. The first section describes the methods of collecting data in the field plus their interpretation and processing by the SCANL and PHOCOM programs. This is followed by the description of: DICHA, the mesh generator program; DICONN, the connectivity analysis program and, DIFLOW, the program which calculates fluid flow and the equivalent permeability tensor. Finally in this chapter a series of validation runs is presented.

The applications of the model are presented in Chapter 4. The first section includes some applications of the discontinuity mesh generator program such as the study of the relationship between discontinuity density, trace length and frequency as well as an analysis of the anisotropy of discontinuity frequency. This is followed in the second section by a Monte Carlo type of study and then by an analysis of factors affecting permeability. This analysis includes the effects of changing discontinuity trace length and density, aperture, relative orientation of discontinuity sets and the size of the test area. The analysis of the test area size is an attempt to define the representative elementary volume. In the third section a study of the anisotropy of permeability in discontinuity networks is presented by means of rotating the test area. Finally in section four a practical application of the model is introduced, which includes the effects on water flow into underground excavations when the size of the excavation is changed and also a case study performed in a tunnelling site in Derbyshire, England which involves the prediction of water flow into the tunnel.

CHAPTER 2 LITERATURE SURVEY

The prediction of rock mass behaviour is of vital importance in the design of various types of engineering structures. It is well known that discontinuities such as joints, fractures, fissures, faults and bedding planes can have a major influence on the engineering properties of a rock mass, in particular its deformability, strength and permeability. The following discontinuity characteristics are recognised as controlling the nature and extent of this influence on the engineering properties: (1) orientation, (2) frequency, (3) size, (4) surface geometry and aperture, (5) nature of fill materials. Piteau (1970).

The study of discontinuities has been carried out in several ways, ranging from laboratory and insitu testing to physical and numerical modelling. In the course of this review more emphasis will be given to the latter since this is more relevant to this work. The literature survey is divided into the following sections. The first describes briefly the two main approaches to the general study of discontinuities, the second section covers previous work that has been done in representing discontinuity geometry, the third section concentrates on a review of studies of the permeability of discontinuous rock and the attempts to establish an equivalent porous medium.

2.1 The Deterministic and Probabilistic approaches

The deterministic approach in rock mechanics relies upon the knowledge of the different parameters that characterise the rock mass, because this is almost impossible these parameters are usually described by their mean values. These mean values are then used in design and the results are expressed in deterministic terms. Einstein and Baecher (1982, 1983) pointed out that uncertainty in geotechnical engineering has three major sources: (1) the innate spatial variability of geological formations, (2) errors introduced in measuring and estimating engineering properties and (3) inaccuracies caused by modelling physical behaviour. In an engineering study, one can never know what has been left out of an analysis, thus in addition to the above uncertainities, there is an uncertainty due to omissions.

These uncertainities have led to many authors taking a probabilistic approach. The main difference between this and the deterministic approach is that input parameters are described by statistical techniques so that a degree of uncertainty is attached and therefore the results of the analysis are described in probabilistic rather than deterministic terms.

The statistical approach to geotechnical problems has become common only in the last few decades and several attempts have been made to implement these methods in the different branches of rock mechanics. Statistic and probabilistic approaches to the field of slope stability analysis were investigated by authors such as McMahon (1974), Young (1977), Lamb (1970) and Priest and Brown (1983), they all considered that the geometric and stength characteristics of the discontinuities are not unique but distributed and, therefore, carry a degree of uncertainity, hence the result i.e. factor of safety, has to be expressed in probabilistic terms.

Statistics have also been used in the field of ground water flow in continuum models, notably by Freeze (1975) and Newman et al (1979).

They performed simulations in which the properties of individual elements (or nodes) within the computational mesh were treated as random variables; the assembly of elements into a numerical model then produces a representation of a heterogeneous material. Newman (1982) did a comprehensive literature survey on this topic and he presents, in that paper, the state of the art on stochastic modelling for porous materials.

Previous studies on the use of statistics to describe fracture networks for computational models are limited to the work of Long (1983), Robinson (1982) and Cundall (1983). These models calculate the flow of water through realistic fracture patterns, based on statistical data collected in field surveys, in order to predict the hydraulic behaviour of rock masses.

Although a fair amount of work has already been done on the statistical and probabilistical approach to geotechnical engineering, some of the density distributions describing the discontinuity parameters still need to be better understood, in order to avoid introducing inaccuracies that can have greater effect than the uncertainty of individual parameters.

2.2 Discontinuity Geometry

The most commonly measured geometrical properties of discontinuous rock masses are spacing, trace length, orientation and aperture. Authors such as Piteau (1970) and Baecher (1977) have pointed out that the above parameters are crucial for the design and stability of any structure built in or above a discontinuous rock mass.

2.2.1 Discontinuity Spacing

Priest and Hudson (1976) presented a theoretical approach to the study of discontinuity spacings and RQD based on the statistical distributions that occur when a rock mass is sampled by the scanline method. They have shown the influence of spacing distributions on the RQD and the sensitivity of this to mean discontinuity spacing. By assuming that discontinuity spacing values follow a negative exponential distribution they developed the following RQD expression for an arbitrary threshold value, t;

$$RQD_t^* = 100\, e^{-\lambda t}\, (\lambda t + 1) \qquad (2.1)$$

they compared the predictions of this formula against the actual RQD as calculated from spacings values measured in three different tunnels in the U.K. and found a maximum discrepancy of 5%.

Priest and Hudson (1976) recommended that in order to estimate the number of discontinuities per metre to acceptable precision it is necessary to have a scanline of at least fifty times the mean discontinuity spacing and at least two hundred values had to be measured before the negative exponential distribution became clear on a histogram plot.

In a later paper Priest and Hudson (1981) introduced some concepts of the central limit theorem in order to assess the precision of the mean discontinuity spacing and discontinuity frequency estimates. In that way they managed to calculate the number of spacing values required to obtain a given error bandwidth for various confidence levels.

Baecher et al (1977) measured values of discontinuity spacing for two types of rocks in the USA. Using scanlines of different orientations, they then fitted theoretical distributions to the observed spacings and found that spacings followed an exponential distribution. They also pointed out that the distribution holds regardless of the orientation of the scanline relative to discontinuity orientation, though the parameters vary. Priest and Hudson (1976) reached the same conclusion.

Call et al (1978) presented a detailed account of the scanline sampling method and they referred to the need for special mapping methods when the line sampling fails to intersect sufficient number of discontinuities for less obvious discontinuity sets. They analysed the rock mass geometry of several open pit mines and found that the negative exponential distribution best fitted the measured values for discontinuity spacing.

Hudson and Priest (1983) pointed out that discontinuity frequency (the reciprocal of mean spacing) measured along a scanline or borehole is usually quoted as a single figure yet this value can be highly dependant on the scanline orientation. They presented the theory for the variation of discontinuity frequency for several sets, the work they presented is similar to that of Terzaghi (1965) and the more recent methods suggested for the quantitative description of discontinuities in rock masses by the International Society for Rock Mechanics. The equation proposed as formulated by Hudson and Priest is:

$$\lambda_s = \lambda|\cos\alpha|$$

where λ_s is the frequency along the scanline and λ is frequency along the normal to the discontinuity set and α is the angle between the normal to the discontinuities and the scanline, as can be seen in Fig. 2.1.

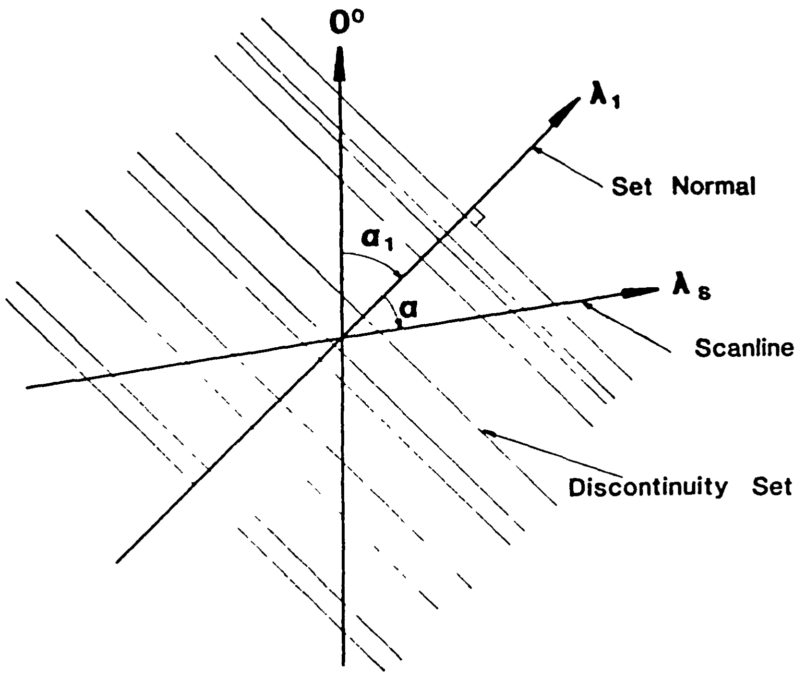

Fig. 2.1 A set of parallel persistent discontinuities sampled by a scanline of orientation α

They expanded this theory to three-dimensional space by using a left-handed cartesian coordinate system, and derived expressions that give the magnitudes and directions of the maximum and minimum frequency in rock mass, and also that allow prediction of discontinuity frequency in arbitrary directions. They also found that their results were applicable to any distribution of discontinuity spacings and also to non-persistent discontuities. Although their results apply mainly when the rock mass is statistically homogeneous, the concept of frequency variability may be useful in the study of heterogeneous rock masses by incorporating geostatistical techniques.

2.2.2 Discontinuity Trace Length

Robertson (1970) has pointed out that discontinuity size, i.e. trace length is closely related to the formation of potential failure surfaces in a slope. Presenting data from the De Beers Mine he found that the distribution of trace lengths was best represented by the negative exponential distribution. An important contribution was the estimation of discontinuity shape, this was done by measuring strike trace lengths and dip trace lengths which were then plotted on a Bivariate plot. He found that for the igneous rocks of the De Beers Mine these values were approximately equal suggesting either that the discontinuities are equidimensional or that their major axes are randomly orientated. Other authors, including Barton (1977) and Bridges (1975), have indicated that discontinuities may be equidimensional, but without explicitly presenting data.

Baecher et al (1977) fitted exponential, lognormal and gamma distributions to data on trace length. They used maximum likihood estimators to define these theoretical distributions and also performed goodness of fit tests and discovered that the lognormal distribution most accurately fitted the measured data.

Reported distributions of discontinuity trace length are less consistent than those for spacing. This is perhaps partly caused by strong biases inherent in the sampling techniques and by the way data are grouped into histograms prior to analysis. Baecher and Lanney (1978) and Baecher (1980) pointed out that in sampling for discontinuity trace length there are three well defined biases, these are: size bias, through which probability of being sampled is proportional to discontinuity size; truncation bias, through which small discontinuities are systematically excluded from samples, and censoring bias, through which the full trace length of some discontinuities is not observable. They presented formulations for the correction of truncation and size biases and for the censoring bias pointed out that there is no easy correction unless a negative exponential distribution is assumed, but this assumption may not be realistic as it has been found that on many occasions the best fit provided a log-normal or gamma distribution.

Priest and Hudson (1981) have stated that when using scanline survey methods, estimation of discontinuity frequency is a problem of precision while estimation of mean trace length is a problem of both accuracy and precision. The inaccuracy, or bias, in trace length measurements is caused by the scanline preferentially intersecting longer trace lengths on a rock mass of limited extent. This concept is similar to the one expressed for size bias by Baecher and Lanney (1978).

They proposed four probability density distributions in order to study the bias introduced into trace length measurements by the use of scanline surveys.

These were:

f(l) - the distribution of actual trace lengths exposed at a rock face

g(l) - the distribution of complete trace lengths intersected by a scanline

h(l) - the distribution of semi-trace lengths intersected by a scanline

i(l) - the distribution of censored semi-trace lengths

They centered their discussion on the problem of preferential intersection of the longer trace lengths, measuring trace lengths on one side of the scanline only and the problems of trace length censoring at limited exposure areas, and defined the population means and estimated means as shown in table II.1

Table II.1

Probability density Distribution	Population Mean	Estimated Mean
f(1)	$1/_\mu$	$\bar{1}$
g(1)	$1/\mu_g$	$\bar{1}_g$
h(1)	$1/\mu_h$	$\bar{1}_h$
i(1)	$1/\mu_i$	$\bar{1}_i$

They showed that when the trace length of a discontinuity is measured by using a scanline, a bias is introduced. Thus g(1) represents the biased distribution of sampled trace lengths for any actual distribution of trace lengths, f(1). Also, when f(1) is negative exponentially distributed, g(1) is of general log-normal form. This result agrees with the one proposed by Baecher and Lanney (1978). Table 2.II shows a summary of the four distribution parameters as well as particular formulae for uniform, normal and negative exponential distribution as presented by Priest and Hudson (1981).

They drew attention to the fact that the value of the mean trace length, $1/\mu_g$, can, for certain distributions, exceed $1/_\mu$, i.e. $1/\mu_g = 1/_\mu + \sigma^2\mu$, where σ^2 is the variance or second moment of

	Distribution of actual trace lengths, l 0			Distribution of intersected trace lengths		Distribution of semi-trace lengths	
	Probability density f(l)	Cumulative probability	Mean	Probability density g(l)	Mean $\frac{1}{\mu_g}$	Probability density h(l)	Mean $\frac{1}{\mu_h}$
Negative	$\mu e^{-\mu l}$	$1 - e^{-\mu l}$	$\frac{1}{\mu}$	$\mu^2 l e^{-\mu l}$	$2/\mu$	$\mu e^{-\mu l}$	$\frac{1}{\mu}$
Uniform	$\mu/2, l \leq \frac{2}{\mu}$	$\mu l/2$	$\frac{1}{\mu}$	$\mu^2 l/2$	$4/3\mu$	$\mu(1-(\mu l/2)$	$2/3\mu$
Normal	$\frac{1}{\sigma\sqrt{2\pi}} \exp A$	F(l) from tables	$\frac{1}{\mu}$	$\frac{\mu l}{\sigma\sqrt{2\pi}} \exp A$	$\frac{1}{\mu} + (\sigma^2\mu)$	$\mu(1-F(l))$	$\left(\frac{1}{\mu} + (\sigma^2\mu)\right)\Big/2$

where $A = \left[-\left(l - \frac{1}{\mu}\right)^2 \Big/ 2\sigma^2\right]$

Table 2.II The Theoretical densities and associated means for various trace length distribution

(After Priest and Hudson, 1981)

f(l) about the mean. In the case of the negative exponential distribution, this excess leads to an overestimate of $1/_{\mu}$ by 100%.

In many situations, it is not possible to measure the full length of the trace so that the semi-trace length is usually measured. The distribution that represents the population of semi-trace lengths is h(l). Priest and Hudson pointed out that when the actual distribution of trace lengths, f(l), is of negative exponential form, the distribution of actual trace lengths is exactly the same as the distribution of sampled semi-trace lengths. This is because the bias towards longer lengths caused by scanline sampling has cancelled the bias caused by only measuring the semi-trace length.

Another interesting finding by Priest and Hudson (1981), was that $\mu_h = 2\mu_g$, which confirms the intuitive idea that the mean semi-trace length should be half of the mean of the complete trace length intersected by the scanline. They also defined the distribution i(l) of censored semi-trace lengths at an exposure where the maximum observable semi-trace length equals c, as:

$$i(l) = h(l)/H(\ell) \qquad (2.3)$$

where H(l) is the probability that a randomly intersected semi-trace length is less than c.

Finally, they proposed two methods of estimating the form of the four distributions mentioned before. One is a graphical method: provided that a large number of measurements of censored semi-trace lengths are taken, a histogram of observed semi-trace lengths can be plotted and compared to the theoretical distributions, this will provide a basis for selecting the appropriate form of f(l). The mean semi-trace length $\bar{l}_i$ can be used as an estimate of the mean of i(l) and hence h(l), g(l) and f(l) by the following relation

$$\bar{l}i = 1/\mu_i \qquad (2.4)$$

Sets of curves were produced for different types of distribution and values of censoring level. The second method of estimating is more formal and, although developed for the negative and uniform distributions of trace lengths, could be applied to any other form of distribution.

Barton (1978) showed that a distribution of cord lengths, generated from random normal intersections of a series of parallel, circular shaped lognormal discs, shows a good correlation with field joint trace populations. Barton found that cords from circles with lognormally distributed diameters had a similar distribution to the trace lengths of the discontinuities mapped on the rock walls at the CSA mine, Cobar. He also showed that the standard deviation of the trace length populations were higher than the parent population. This became clear when he considered that the parent discs are all the same size but the traces are not. The model also showed that as the variability in size of the population increased, the relative value of the derived mean trace length also increased. The trend finally results in the mean trace exceeding the mean parent diameter, in other words, size bias becomes more important as the variability in size increases.

Cruden (1977) analysed discontinuity trace length data from Nchanga Open Pit Mine and found a negative exponential distribution. His main interest, however, was to estimate the probability of a discontinuity in the rock mass exceeding a certain size. He suggested that this information is vital in the design of rock slopes. He also explained in detail, the techniques and problems associated with trace length measurements.

Phal (1981) presented a technique for estimating the mean trace length of discontinuities observed in mine drive walls and applied his theory to data from the King Island Scheelite Mine. His method is distribution independent and no knowledge of the actual lengths of the observed traces are required. Although the flexibility of the estimation procedure of this method resides in its independent distribution nature, in many cases, it is necessary to know the type of distribution in order to carry out a stochastic simulation. However his technique is specially appropriate to underground exposures where there are no facilities or time to measure trace lengths. A disadvantage which exists is that only a few distributions, such as the exponential, are fully specified when their mean is known.

Broadbent (1970) suggested that all discontinuities of less than 60 cm are random and do not help in defining discontinuity sets, and therefore need not be measured, however, the majority of other authors stress the importance of measuring all discontinuities.

2.2.3 Discontinuity Orientation

Although a great deal of statistical work has been done on the description of discontinuity plane orientations, perhaps more than on the other rock mass properties, little success has been achieved in fitting analytical distributions. Einstein and Baecher (1983) analysed several types of distributions, the Fisher, the Bingham, the Elliptical and the Uniform, that are defined on the limit sphere; and the bivariate Normal and bivariate lognormal that are defined on the plane. Using maximum likelihood estimates to fit the distributions, they found that only when an ideal pole distribution occurred, i.e. when the density contour lines are nearly symmetrical, can an analytical distribution be fitted. They suggested that, in the case of a complicated pole distribution, a visual clustering may lead to better results.

Knoring (1970) presented a study of the correlation of discontinuity orientation with elements of tectonic structures. He analysed data from six different tectonic regions. The Fisher distribution was used to fit the data and was then tested for goodness of fit. When the observed frequencies did not correspond to the Fisher distribution they were assumed to reflect a heterogeneous rock mass or complex deformations that had affected the rock mass after the formation of the main discontinuity sets. He determined that a combination of discontinuities whose poles distribution belonged to a particular Fisher distribution, with a parameter K greater than 4, formed a discontinuity set.

Robertson (1970) suggested that orientation data should be plotted in rectangular plots instead of hemispherical projections because they can easily be represented by a computer with limited plotting facilites. He also presented a formulation to correct the sample bias. This bias results in a greater number of discontinuites which are normal to the sample line being sampled, while discontinuities exactly parallel to the sampling line are missed entirely. The correction he proposed gives the number of discontinuities which a line, equal in length to the sample line, would be expected to encounter had it had an orientation normal to the plane of the discontinuity set considered. No attempt was made, however, to fit any theoretical distribution to the measured orientations.

Robertson (1970) decided that the bias should be corrected for any class interval and he presented the following expression

$$N_i^* = \frac{N_i}{\mathrm{Cos}|\Theta_s - \Theta_i|\mathrm{Cos}|(\delta s + \delta_i) - 90|} \qquad (2.5)$$

where δ_s and Θ_s are the plunge and trend of the sampling line and δ_i and Θ_i are the mid-points of the class interval for dip and dip direction of all discontinuities present in the ith interval of the rectangular plot. N_i is the number of discontinuites in such an interval and N_i^* the corrected number of discontinuities.

Furthermore to facilitate comparisons between surveys of different lengths (L) he suggested that a correction to a standard survey length (L_s) is needed.

$$N_i^{**} = N_i^* \, Ls/L \qquad (2.6)$$

Priest (1983) pointed out the occurrence of the same bias in orientation data when sampled by a linear method. He suggested the introduction of a "weighting factor" which is defined as

$$w = 1/\cos\delta \qquad (2.7)$$

where δ is the acute angle between the normal to a given discontinuity and the sampling line. The factor w was also expressed as:

$$w = \frac{1}{\cos(\alpha_p - \alpha_s).\cos\beta_p \cos\beta_s + \sin\beta_s \sin\beta_s} \qquad (2.8)$$

where α_s and β_s are the trend and plunge of the sampling line and α_p and β_p are the trend and plunge of the normal to the discontinuity plane. The above equation is similar to that used by Terzaghi (1965) but differs in that Terzaghi's correction factor considers the angle between the discontinuity plane and the scanline rather than the angle between the normal to the discontinuity plane and the scanline as considered by Priest. There are a number of complications with this approach, one is the possibility of a high "weight" being assigned to those discontinuities whose normal makes a high angle with the line of sampling. This can be overcome by using at least three mutually orthogonal sampling lines. In practical experience, however, this case can seldom be achieved and hence the bias remains. Priest also recommends a method of analysing the clustering of discontinuity poles; he introduces the normalised "weighing factors" in order to standarise the sample size. He then, similarly to Knoring (1970), uses Fisher's theory to define discontinuity sets.

Fisher (1953) proposed a method of estimating the mean orientation of a population of unit vector poles. This mean vector is the sum of all the unit vector poles and is called the resultant vector, R. He assumed the probability density distribution was proportional to $e^{K \cos\theta}$, where

Θ is the angular displacement from the mean and K is a measure of the dispension and estimated as:

$$K = \frac{N - 1}{N - R} \tag{2.9}$$

where N is the sample size. Fisher found that K is a good estimate when $N-R < 2$.

Mahtab et al (1972) presented a computerized approach to analysing orientation data, this involved dividing the surface of the upper hemisphere into 100 equal area patches and then counting the number of poles that fell within each patch. The resulting density is then used to define clusters. He introduced the Poisson distribution model in order to provide a threshold density which is used to define the clusters. The next step was to compare a cluster of the poles with the hemispherical normal distribution by applying the chi-square test. Levels of confidence were then selected to define a confidence interval around the mean value. Mahtab et al applied this method to data taken from the San Miguel Copper mine. He found that there are three prominent sets of discontinuities, two nearly vertical with stikes north-south and east-west respectively and a third set nearly horizontal. Data of only one of these sets, however, managed to pass the chi-square test when compared with the Arnold's hemispherical normal distribution. This was probably due to the problems associated with complicated pole distributions as shown by Baecher et al (1983).

2.2.4 Discontinuity Aperture

Measurements of discontinuity aperture have essentially followed two approaches. One involves direct measurement in the field such as that described by Bianchi and Snow (1968), Sharp (1970) and Rocha and Franciss (1977). The second involves indirect measurement such as that performed by Snow (1968, 1970), Rissler (1978).

Bianchi and Snow (1968) pointed out the need for a method for measuring apertures because of their importance in determining the equivalent permeability of a fractured rock mass, and proposed a method using macrophotography and fluorescent liquid penetrants. The technique consisted of applying a fluorescent dye to the rock surface, which penetrates the discontinuites. After allowing sufficient time for penetration, a solvent is sprayed on to clean the surface, followed by a developer to form a thin coating; this developer soaks the penetrant remaining in the fractures and when exposed to ultraviolet light the dyed developer fluoresces and reveals the presence of fractures. This method has to be modified for fractures exceeding 1 mm in aperture because capillary action cannot bring the penetrant to the surface. In this case it is preferable to dye the surface instead of the fracture and to omit cleaning before and after developing. Photographs were taken of the surface with a camera fitted with a telephoto lens and a flash covered with an ultra-violet filter. The negatives were projected and enlarged approximately 76 times and then the fracture apertures measured on the screen. Five measurements were made of each fracture by using a metric caliper with an accuracy of $\pm$ 0.025 mm. The values were then corrected for the enlargement, obtaining in this way the real aperture. The accuracy of the method was tested with artificial fractures of known aperture, and results showed a ± 4% discrepancy in the values. The distribution of apertures was found to be lognormal, agreeing with Snow's (1965) predictions. The range of apertures measured by this method was of the order of 0.12 mm to 5.4 mm. At present this type of measurement is restricted to surface exposures, Bianchi and Snow claimed that this method can be adapted for use in boreholes, where disturbance would be less.

Sharp (1970) attempted to measure aperture on rock samples in the laboratory, he used the "Quantimet" image analysis computer. The instrument consists of a microscope, television camera and a small computer. The microscope image is scanned by the television camera, and the signal is monitored by a series of brilliance controls. This can be improved if the analysis is carried out on a photo of the surface rather than the surface itself. In this case the photos had to be reduced to a suitable size for the 'Quantimet'. The fracture zone was divided into sections 3mm long and the aperture of these sections was then measured. The overall range of apertures ranged from 0.01 - 0.8 mm. Sharp did not fit any theoretical distribution to his measurements, however, he recorded the variation in aperture of a single fracture and measured the maximum and minimum aperture every time.

Rocha and Franciss (1977) attempted to measure apertures by using the method known as integral sampling. This method basically consists of obtaining an oriented core sample from the rock mass previously reinforced with a bar, (which ensures the integrity of the whole sampled material), the final aim being to determine the permeability tensor. Direct aperture measurements were performed on the integral samples by using micrometric oculars or by comparison with standard marks with thicknesses ranging from 0.05 mm. Although this method is an improvement since the samples come from boreholes with little disturbance, it has the disadvantage of being an expensive method making it difficult to carry out a large number of measurements. Rocha and Franciss did not fit a distribution in their aperture data.

Snow (1970) argued that apertures can be measured at surface exposures or possibly in boreholes, but the determination of in situ apertures, not affected by stress release, requires indirect methods of measurement. In a previous paper, Snow (1968), attempted to measure discontinuity aperture by means of interpreting water-injection tests. One of the disadvantages of this method was the assumption that all the discontinuities were alike. In later work, Snow (1970) showed that the aperture computed on the assumption that the fracture apertures are the same, gave the same value as the mean of the distribution of fracture apertures actually measured. He also developed a method to find the second moment of the aperture distribution and the type of the distribution. In order to evaluate his theory Snow first standarized all the water-injection tests by adjusting them to produce equal net head, equal diameter and equal length conditions. To do this he assumed that the medium behaved like a continuum. He then produced the cumulative distribution of the standardized discharges and noted the presence of zero discharges, from test lengths intersecting non-conducting fractures. Snow interpreted these continuous distributions as compounded of two variables which have their own distributions: the fracture frequency in the test length and the aperture of those fractures. Further he showed that the distribution of the number of fractures intersected by the test length can be represented by the Poisson distribution. He arrived at this conclusion by means of surveys carried out in boreholes using a TV camera. He then analysed the composite distribution of total discharge and, concluding that fracture aperture follows the lognormal distribution, found expressions for the mean and standard deviation of aperture. This method does not differentiate between the aperture distributions of individual sets and all the fractures are assumed to be perpendicular to the boreholes. The data Snow used in his theory came from Grand Coulee Dam, in Washington and Morrow point, Colorado.

Rissler (1978) developed a method to calculate aperture from water-pressure tests, in his solution he argued that the critical energy head should be used - this is the energy head at which the laminar flow in the fracture changes to a turbulent flow at the borehole wall. His equation also introduced the effect of relative roughness and because the equations developed are too large he constructed a set of curves to calculate aperture for a range of values of kinematic viscosities and borehole diameters. The radius of influence was assumed to be 100 m. The success of the method relies on a clear determination of the critical energy head taken from the curves produced by plotting heads against discharge as obtained from the pressure tests. He recommended plotting the results on graphs Ho/q against Ho, where Ho is the head and q the associated discharge. This produces a horizontal line for the laminar range with the critical energy head shown by the clear break from this horizontal line, as can be seen in Fig. 2.2. Rissler expanded his equations to cope with inclined discontinuity sets intersecting a vertical borehole and also inclined discontinuity sets orientated normal to the borehole axis. In the investigation he used a finite element method and concluded that the correlation between aperture and critical energy head is almost negligibly influenced by the change in the type of intersection between the discontinuities and the borehole. Therefore for practical purposes the inclination of the discontinuities can, usually, be neglected in the determination of aperture. This method was further extended to include several joints belonging to the same discontinuity set. The results were not, however, satisfactory. The author argued that the instruments used on the site, particularly those for flow rate measurements, were not precise enough.

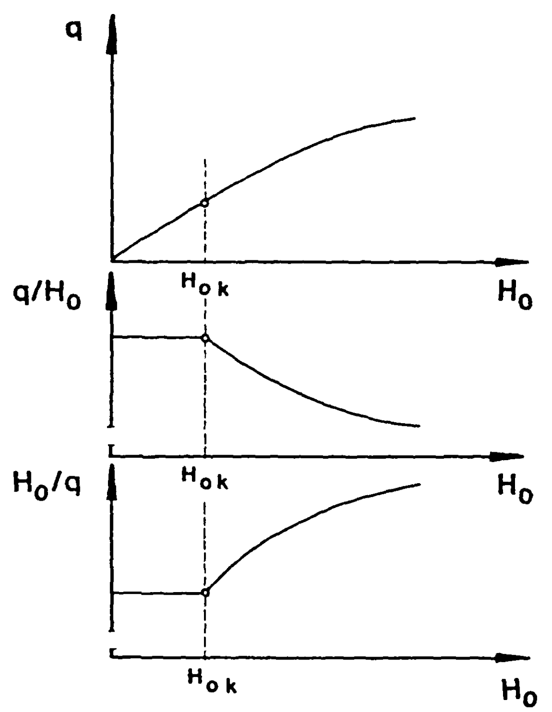

Fig. 2.2 Representation of the results of tests for the determination of the critical energy head H_{OK} (after Rissler, 1978)

Witherspoon and Gale (1983) showed a probability plot of the distribution of fracture apertues determined from injection test carried out at the Stripa mine, Sweden. Two type of tests were performed: one of fixed test length assuming that a single fracture occurred within the 2m test length regardless of the actual number, and the second, where single fractures were isolated and tested. In both cases they found a good correlation and concluded that aperture follows a lognormal distribution. Based on that interpretation they then calculated mean values and standard deviations. Gale (1982) later pointed out that the standard assumption of smooth parallel plates may introduce an error caused by ignoring the effects of roughness. In order to correct for roughness he then carried out some laboratory tests on natural fractures in a core, again without differentiating the distributions of apertures for each discontinuity set.

2.2.5 Concluding Remarks

The review of the literature on discontinuity geometry had shown that, before the statistical interpretation is undertaken, the sampling bias should be removed. Although, authors such as Terzaghi (1965), Robertson (1970) and Priest (1983) have presented methods for correcting bias of the discontinuity orientation, there are no easy ways to corect the bias introduced in measuring trace length. Priest and Hudson (1981) and Baecher and Lanney (1978) have presented approximate methods of removing the bias of the mean discontinuity trace length. Both methods make some inferences about the distribution of trace length and are valid when used in two dimensional sampling.

The review has also shown that the distribution of spacings between discontinuities along a sampling line is usually well modelled by an exponential density distribution. Reported distributions of trace length are less consistent than those for spacing, log-normal and negative exponential forms being most frequently reported. Discontinuity orientation distributions are even less consistent than those for the above two parameters. Arnold's and Bingham distributions were reported, however Fisher's distribution seems to be most frequently used because of its simplicity. Discontinuity aperture is mainly measured by indirect methods; the log normal distribution was reported to model the distribution of apertures.

2.3 Simulation of fluid flow in fractured rock

Flow through fractured rock has generally been modelled as one of the following cases: the equivalent continuum; where the number of discontinuities per unit area (volume) is large, and the discrete method where the individual behaviour of every fracture in the formation is considered. The first method of analysis is most suitable when the scale of the particular problem is large compared with mean discontinuity spacing The discrete discontinuity model is best suited for local, small scale analysis, where only a few discontinuities need to be considered.

As the equivalent continuum approach makes use of the theory of fluid flow in homogeneous anisotropic porous media the first part of this section includes a review of the relevant aspects of this theory, including, Darcy's Law, its derivations and generalizations and also, directional permeability. In the second part a review of the parallel plate analogue for flow through a single fracture is presented. Finally a review of the existing models which analyse flow in fractured rock is also presented.

2.3.1 Homogeneous Anisotropic Porous Media, Darcy's Law

A basic relationship describing the motion of a fluid through homogeneous porous media was first presented by Darcy. This relationship was later expressed in different ways by several authors. Hubbert (1940) presented a comprehensive discussion of the merits of the various generalizations of Darcy's Law. The most commonly accepted form is:

$$v = -k \frac{\rho g}{\mu} \frac{\partial \phi}{\partial s} \qquad (2.10)$$

where v is the volumetric flow, k is the intrinsic permeability, ρ is the mass density of the fluid, μ is the coefficient of viscosity of the fluid, g is the acceleration due to gravity and $\partial\phi/\partial s$ is the applied gradient in the s direction.

A more general expression is obtained when the differentiations are carried out with respect to a system of orthogonal cartesian coordinates,

$$v_i = - k \frac{\rho g}{\mu} \frac{\partial \phi}{\partial x_i} \qquad i= 1,\ 2,\ 3 \qquad (2.11)$$

The above equation applies for a medium where the permeabilities are the same in all directions. Porous media like this are said to be isotropic with regard to permeability, however not every porous medium posseses isotropic permeability. In order to account for such anisotropic properties Darcy's Law can be generalised to:

$$v_i = -\frac{\rho g}{\mu} k_{ij} \frac{\partial \phi}{\partial x_j} \qquad i, j = 1, 2, 3 \qquad (2.12)$$

the double index convention or Einstein's solution convention is used here. (Refer to Jeffreys (1931) for detailed information about this convention

The nine components of k_{ij} in three dimensional space (or four components in two dimensions) define the permeability tensor; they can be written in matrix form as:

$$\begin{bmatrix} v_1 \\ v_2 \\ v_3 \end{bmatrix} = -\frac{\rho g}{\mu} \begin{bmatrix} k_{11} & k_{12} & k_{13} \\ k_{21} & k_{22} & k_{23} \\ k_{31} & k_{32} & k_{33} \end{bmatrix} \begin{bmatrix} \frac{\partial \phi}{\partial x_1} \\ \frac{\partial \phi}{\partial x_2} \\ \frac{\partial \phi}{\partial x_3} \end{bmatrix} \qquad (2.13)$$

Because k_{ij} is generally assumed to be a symmetrical tensor, there will be only six different components (or three in the two dimensional case) i.e. $k_{ij} = k_{ji}$.

The direction in space specified by the unit vector μ_i is called the principal direction of the tensor k_{ij} if the associated vector $k_{ij}\mu_i$ is parallel to μ_i, in other words if this vector can be written in the form $k\mu_j$, where k is a scalar (Bear 1972). For a principal direction μ_i and a symmetrical tensor k_{ij} this relation can be written:

$$(k_{ij} - k\delta_{ij})\, \mu_i = 0 \qquad \delta_{ij} \begin{cases} = 1 \text{ for } i = j \\ = 0 \text{ for } i \neq j \end{cases} \qquad (2.14)$$

δ_{ij} is known as the Kronecker δ. The above relation represents a set of linear equations for the components of μ_i. To solve this the determinant of coefficients must vanish, i.e.

$$|k_{ij} - k\delta_{ij}| = 0 \tag{2.15}$$

expanding this determinant leads to a cubic equation for k, known as the characteristic equation:

$$k^3 - I_1 k^2 - I_2 k - I_3 = 0 \tag{2.16}$$

Where I_1, I_2, I_3 are scalars that being independent of the co-ordinate system are known as the invariants of the symmetrical tensor k.

$$\begin{aligned} I_1 &= k_{ii} \\ I_2 &= \tfrac{1}{2}(k_{ii}\, k_{jj} - k_{ij}\, k_{ji}) \\ I_3 &= \text{determinant of matrix } k_{ij} \end{aligned} \tag{2.17}$$

the roots k_1, k_2, k_3 of the characteristic equations are called principal values or eigen values of the symmetrical tensor k_{ij}. Each of them is associated with a unit vector μ_1, μ_2 and μ_3 respectively. These unit vectors indicate the principal directions in space. In matrix form this can be expressed as:

$$k_{ij} = \begin{vmatrix} k_1 & 0 & 0 \\ 0 & k_2 & 0 \\ 0 & 0 & k_3 \end{vmatrix} \tag{2.18}$$

so that Darcy's Law applied in principal directions becomes

$$v_i = - k_i \frac{\rho g}{\mu} \frac{\partial \phi}{\partial x_i} \qquad i = 1, 2, 3 \qquad (2.19)$$

Thus, each component of v_i is proportional to the corresponding component of the potential gradient but the constants of proportionality are not equal since k_i are not all equal.

Most of the derivations presented above, as well as the generalization of Darcy's Law to three dimensions, were first suggested as heuristic generalizations, and were only later justified by experimentation using conceptual models. Bear (1972) presents a good review of these models. One of these conceptional models is the capillary tube model. The starting point in all these type of models is the application of Hagen-Poiseuille's law to the capillary tubes. This leads to a linear relationship between the velocity and the piezometric head gradient. The difference among the various models is only the relationships they yield among k and properties of the porous medium. Scheidegger (1954, 1974) suggested a capillary model which relates the average diameter of the capillary tubes to the pore size distribution of the medium. He also considered the case where the capillary tubes are tortuous and of variable diameter by introducing a term named tortuosity factor, defined as the ratio of the length of the actual flow channel to the length of the porous medium.

A second class of models as discussed by Bear (1972), are the fissure models. This type of model was developed notably by Irmay (1955). He employed narrow capillary fissures to represent the porous medium.

He then applied the solution of the Navier-Stokes' equation and found an expression for the average velocity as a function of the geometrical properties of the model, the properties of the fluid and the hydraulic gradient. This gave a link between permeability and the geometry of the model. Similar models were produced by Snow (1965) and Parsons (1966) but since they were directed towards a representation of flow in fractured rock they will be discussed later on.

A third class of conceptual models are the Hydraulic Radius models which are a refinement of the capillary models. The hydraulic radious is defined as the ratio between area of cross-section and wetted perimeter. Another way to define the hydraulic radius is the ratio of volume of a conduit filled with fluid to its wetted surface. The last definition combined with a visualization of the porous medium as a network of interconnected channels leads to the definition of an equivalent hydraulic radious for the complicated flow channels within the porous medium.

Kozeny (1927) proposed a relation between permeability and the geometrical properties of a porous medium. He represented the porous medium as an assemblage of channels of various cross sections, but of a definite length. He then solved the Navier-Stokes equations simultaneously for all channels passing through a plane normal to the flow in the porous medium, and thereby obtained an expression for permeability k, of the form $k = cP^3/S^2$. Where P is porosity factor, S is the surface area per unit volume (the latter being a similar concept to the "hydraulic radius") and c, a number, known as the Kozeny constant, that varies with the shape of the cross section. Kozeny's theory was later modified by several workers, notably by Carman (1938). In all these modifications, the result was that the permeability remained essentially proportional to $1/S^2$ but an uncertainty was attached to the porosity factor, P.

Statistical models have also been used in an attempt to validate Darcy's law. Scheidegger (1974) pointed out that the previous conceptual models and theories assumed models of the porous medium that are ordered and regular to such an extent that the Navier-Stokes equations can be used. Natural porous media, however, are generally extremely disordered so it is not strictly valid to represent them by an intrinsically ordered model. Scheidegger (1974) therefore, suggested that the problem be treated as an intrinsically disordered porous medium with a random pore geometry. It is clear that the Navier-Stokes equations would not be applicable in this case; instead statistical methods have to be applied.

2.3.2 Permeability and hydraulic conductivity

The term, permeability k, as used in the preceding section is also called the intrinsic permeability of a porous matrix and depends solely on the properties of the solid material. Originally, in the derivation of Darcy's Law the coefficient of proportionality K was termed the hydraulic conductivity; this is sometimes called the coefficient of permeability. In an isotropic medium hydraulic conductivity, which can be defined as the specific discharge per unit hydraulic gradient, is a scalar value which expresses the ease with which a given fluid is transported through the porous matrix. It is, therefore, a coefficient that depends on both matrix and fluid properties. The fluid properties are the density, ρ, and viscosity, μ, or kinematic viscosity, υ, and the relevant solid matrix properties are pore size distribution, shape of grains, tortuosity, specific surface and porosity. From dimensional analysis, it follows that:

$$K = \frac{\rho g}{\mu} k = \frac{g}{\upsilon} k \tag{2.20}$$

Commonly adopted units for permeability, k, (dimension L^2) are cm^2 or m^2; those for hydraulic conductivity, K, (dimensions L/T) are usually cm/sec.

2.3.3 *Directional Permeability*

Anisotropy is a common property of many porous media. As the direction of flow and the hydraulic gradient in an anisotropic porous medium are generally not parallel there are two different methods for defining directional permeability.

Scheidegger (1954), Marcus (1962) and Bear (1972) have shown two ways of defining directional permeability. In the first, here termed directional permeability in the direction of the flow, permeability is expressed as the ratio of the flow velocity to the component of the hydraulic gradient in the direction of the flow. In the second, here termed directional permeability in the direction of the gradient, permeability is expressed as the ratio of the component of the velocity in the direction of the hydraulic gradient to the magnitude of the hydraulic gradient (see Fig. 2.3).

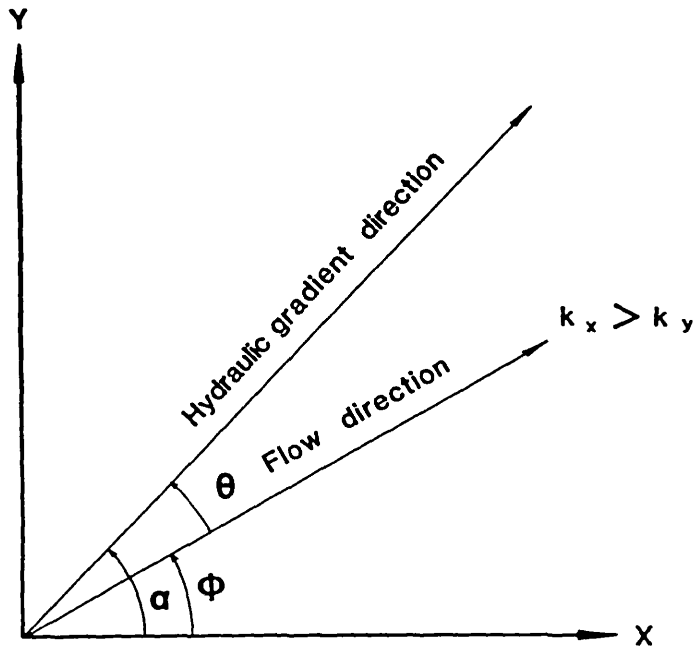

Fig. 2.3 Hydraulic gradient and flow direction in anisotropic porous medium.

Scheidegger (1954), by considering two-dimensional flow, showed that in most cases the difference between the two types of directional permeability was negligible. However, Marcus (1962) stated that the two definitions do not yield the same result, and that the difference between them is a function of the anisotropy of the material and of the directions of flow or gradient with respect to the principal permeabilities. Marcus also used a two-dimensional case to demonstrate this point. It seems that the proof of Marcus is a more realistic one since it takes into account the degree of anisotropy.

Following the ideas and definitions of Bear, Scheidegger and Marcus, a summary of the formulation of the two types of directional permeability is presented here.

In the following discussion the equations will be written in vectorial notation for the sake of simplicity. Generally Darcy's Law for an anisotropic, porous medium can be expressed in vectorial terms as:

$$\vec{q} = K.\vec{J} \tag{2.21}$$

It follows from the above equation that the specific discharge, $\vec{q}$, and hydraulic gradient, $\vec{J}$, are non-colinear vectors, except when they are in the direction of one of the principal axes. The angle Θ between the vectors $\vec{q}$ and $\vec{J}$ is given by

$$\text{Cos } \Theta = \vec{q}.\vec{J}/_{qJ} \tag{2.22}$$

where $\qquad q = |\vec{q}| \text{ and } J = |\vec{J}|$

Firstly, considering the directional permeability in the direction of flow, here denoted by K_f:

$$K_f = q/J \text{ Cos } \Theta \tag{2.23}$$

assuming that x, y, z are the three principal axes, from (2.21) and (2.22)

$$\text{Cos } \Theta = K_xJ_x{}^2 + K_yJ_y{}^2 + K_zJ_z{}^2/_{qJ} \tag{2.24}$$

Substituting (2.24) in (2.23)

$$K_f = \frac{q}{J\text{Cos}\Theta} = \frac{q^2}{K_xJ_x{}^2 + K_yJ_y{}^2 + K_zJ_z{}^2} \tag{2.25}$$

from (2.21) and (2.25)

$$K_f = \frac{K_x{}^2J_x{}^2 + K_y{}^2J_y{}^2 + K_z{}^2J_z{}^2}{K_xJ_x{}^2 + K_yJ_y{}^2 + K_zJ_z{}^2} \tag{2.26}$$

If the angles α_1, α_2, α_3 denote the angles between the direction of $\vec{q}$ and the three principal axes, x, y, z respectively then

$$K_x J_x = q \text{ Cos } \alpha_1; \quad K_y J_y = q \text{ Cos } \alpha_2; \quad K_z J_z = q \text{ Cos } \alpha_3 \tag{2.27}$$

From (2.26) and (2.27) it is possible to obtain

$$\frac{1}{K_f} = \frac{\text{Cos}^2\alpha_1}{K_x} + \frac{\text{Cos}^2\alpha_2}{K_y} + \frac{\text{Cos}^2\alpha_3}{K_z} \tag{2.28}$$

assuming $\vec{r}$ is a unit vector in the direction of $\vec{q}$ and has the following components

$$x = r\cos\alpha_1 \; ; \quad y = r\cos\alpha_2; \quad z = r\cos\alpha_3$$

Then equation (2.28) becomes

$$\frac{r^2}{K_f} = \frac{x^2}{K_x} + \frac{y^2}{K_y} + \frac{z^2}{K_z} \tag{2.29}$$

by selecting a radius $r = \sqrt{K_f}$ in the direction of $\vec{q}$, and subtituting in (2.29), this becomes

$$\frac{x^2}{K_x} + \frac{y^2}{K_y} + \frac{z^2}{K_z} = 1 \tag{2.30}$$

This is the equation of an ellipsoid in the x, y, z coordinate system, its semiaxes are $\sqrt{K_x}$, $\sqrt{K_y}$ and $\sqrt{K_z}$ in the x, y, z directions respectively.

In the second case, the directional permeability in the direction of the gradient, K_g, is expressed as:

$$K_g = q \text{ Cos}\Theta/J \tag{2.31}$$

the components of $\vec{J}$ in the principal directions are:

$$J_x = J \cos\alpha_1; \quad J_y = J \cos\alpha_2; \quad J_z = J \cos\alpha_3 \tag{2.32}$$

in this case α_1, α_2, α_3 are the angles between the direction of $\vec{J}$ and x, y, z respectively. From (2.21), (2.31) and (2.32)

$$K_g = \frac{1}{J^2}\left(K_x J_x{}^2 + K_y J_y{}^2 + K_z J_z{}^2\right) \tag{2.33}$$

assuming a unit vector $\vec{r}$ such that $x = r\cos\alpha_1$, $y = r\cos\alpha_2$, $z = r\cos\alpha_3$ and substituting in (2.33) this becomes

$$\frac{r^2}{1/K_g} = \frac{x^2}{1/K_x} + \frac{y^2}{1/K_y} + \frac{z^2}{1/K_z}$$

by selecting a radius $r = 1/\sqrt{K_g}$ in the direction of $\vec{J}$ it can be shown that

$$\frac{x^2}{1/K_x} + \frac{y^2}{1/K_y} + \frac{z^2}{1/K_z} = 1 \tag{2.35}$$

The above equation also describes an ellipsoid, but in this case its semi-axes are $1/\sqrt{K_x}$, $1/\sqrt{K_y}$, $1/\sqrt{K_z}$. From equations (2.30) and (2.35) it can be seen that for permeability measured in the direction of flow the major axis of the ellipsoid is in the direction of maximum permeability, while for permeability measured in the direction of gradient the major axis of the ellipsoid is in the direction of minimum permeability.

2.3.4 The parallel plate analogue

The parallel plate analogue for flow through a single fracture has been studied by many researchers; experimental work by Lomize (1951) and Huitt (1956) provided the basis for the development of more formal expressions. They assumed that Darcy's law can be applied to flow in a fractured rock mass where the permeability term, or the hydraulic conductivity, is derived by idealizing each fracture as a parallel plate opening - as shown in Fig. 2.4. Equations describing the flow between a pair of parallel plates have been developed by authors such as Polubarinova-Kochina (1962), Romm and Pozinenko (1963), Lamb (1932), De Wiest (1965) and Snow (1965). Each of these started from the Navier-Stokes equation for single phase, non-turbulent flow and assumed an incompressible, viscous fluid. The equation obtained is a relation between flow rate, q, and pressure gradient dp/dx

$$q = ((2b)^3/12\mu)dp/dx \qquad (2.36)$$

where 2b is the fracture aperture, and μ is the fluid viscosity.

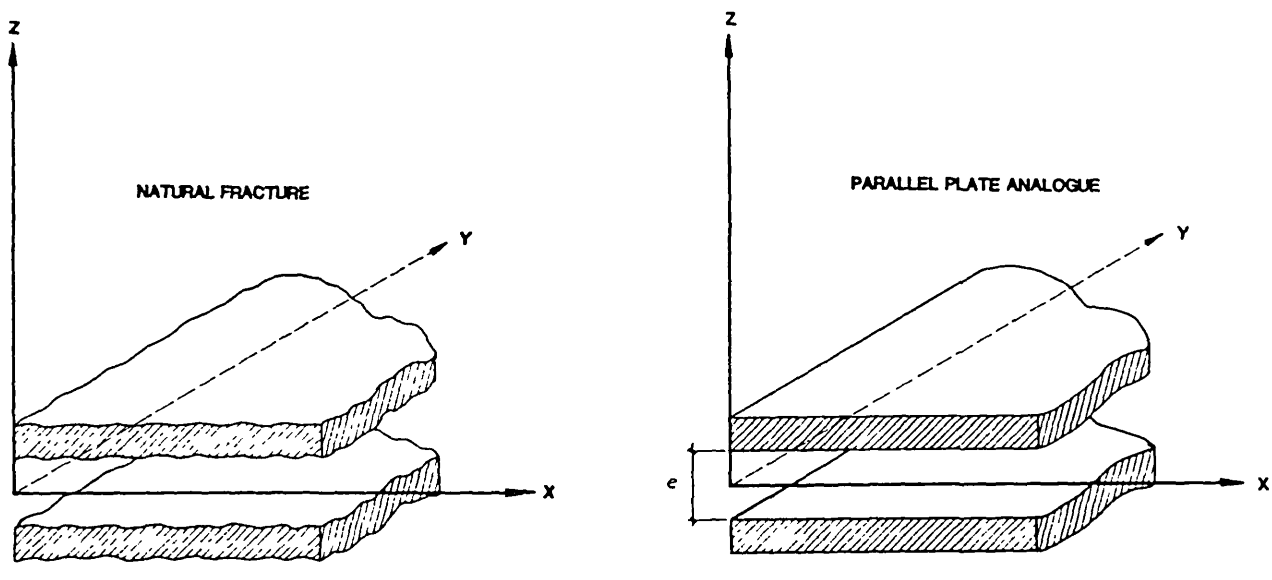

Fig. 2.4 Natural fracture and the parallel plate analogue

Since the cross sectional area for flow is (2b).1, the average velocity is simply:

$$v = \left[{(2b)^2}/{12\mu} \right] \frac{dp}{dx} \qquad (2.37)$$

It can be seen from equation (2.36) and (2.37) that flow in a fracture is a sensitive function of aperture size. These equations are valid only in a laminar flow regime, but Louis (1969) has pointed out that this type of flow is indeed dominant in most field situations.

The intrinsic permeability of a fracture with an aperture of 2b is given by

$$k_F = (2b)^2/12 \qquad (2.38)$$

When converted to a hydraulic conductivity of a fracture this gives:

$$K_F = k_F \frac{\rho g}{u} = (2b)^2 \rho g/12\mu \qquad (2.39)$$

If the flow is steady and isothermal, the flow per unit drop in head, Δh, can be developed from Darcy's law and may be written as:

$$Q/\Delta h = c(2b)^3 \qquad (2.40)$$

where c is a constant called the conductance of the fracture, which in the case of radial flow is given by

$$c = \frac{\rho g}{12\mu} \frac{2\pi}{Ln(r_e/r_w)} \qquad (2.41)$$

where r_w is the well bore radius and r_e the outer radius of the zone of influence. In the case of straight flow this constant is given by

$$c = \frac{\rho g w}{12\,\mu L} \tag{2.42}$$

where w is the width of the fracture and L is its length.

Equation (2.40), which is often called the "cubic law" (Witherspoon et al 1980), can be generalized in terms of the Reynolds number, Re, and friction factor, ψ. Lomize (1951), Romm (1966) and Louis (1969) introduced a factor D equal to 4 times the hydraulic radius, i.e. 8b. In this case:

$$Re = \frac{Dv}{\upsilon} \tag{2.43}$$

$$\psi = \frac{D}{(\upsilon^2/2g)}\frac{dh}{dx} \tag{2.44}$$

From (2.36), (2.43) and (2.44) the cubic law for laminar flow in an open facture can be expressed as:

$$\psi = 96/Re \tag{2.45}$$

Lomize (1951) used parallel glass plates and demonstrated the validity of the cubic law, as long as the flow was laminar. He also investigated the effect of surface roughness and the influence of fracture shape. Lomize introduced a method for defining the roughness, ε, in terms of absolute height of the asperities and developed the following empirical equation:

$$\psi = \frac{96}{Re}\left[1 + 6.0\left(\frac{\varepsilon}{2b}\right)^{1.5}\right] \tag{2.46}$$

which is valid when $\varepsilon/2b > 0.065$. He also studied the effect of flow through fractures with planar but non-parallel sides.

Witherspoon et al (1980) have simplified equation (2.46) by re-writing it in the form:

$$\psi = \frac{96}{Re} f \tag{2.47}$$

where f is a factor that accounts for deviations from the ideal conditions that were assumed when deriving (2.45). For instance if roughness is taken into account, f > 1 and equation (2.40) becomes

$$Q \quad \Delta h = \frac{c}{f} (2b)^3 \tag{2.48}$$

Lomize (1951) developed a flow regime chart with several semi-empirical flow laws to take into account the effects of roughness and turbulent flow in open fractures. Louis (1969) has independently performed experiments similar to Lomize's and reached basically the same conclusions. Romm (1966) performed two series of experiments; the first in fractures with apertures ranging from 10 to 100 μm, the second in fractures with apertures ranging 0.25 to 4.3 μm. He proved that the cubic law is valid for laminar flow in these models. The critical Reynolds number at the transition from laminar to turbulent flow was found to be 2400. This same critical value was reported by Lomize (1951); Louis (1969) reported the value to be 2300.

Sharp (1970) reported results of laboratory flow tests carried out on a natural fracture in a rock specimen of hard granite porphry whose matrix permeability was very small. In questioning the applicability of the cubic law in describing laminar flow under his laboratory conditions he concluded that the fracture discharge was related to the aperture by some exponential factor less than 3. Sharp (1970) and Sharp and Maini (1972) proposed an empirical flow law for natural fractures that was based on the "effective" aperture. The effective aperture was assumed to be zero when the two halves of the specimen were in contact. Sharp (1970) did, however, report a measurable flow under these conditions.

Iwai (1976) has confirmed the validity of the cubic law by testing induced tension fractures under radial and linear flows. The tests were carried out in 3 types of rocks: basalt, granite and marble. Normal loads were applied in an attempt to close the fracture. Although he concluded that the cubic law is generally valid, he found that in some cases the radial flow data tended to deviate from the ideal cubic law. He explained that this may be due to roughness effects being more complex in radial than linear flow.

Iwai (1976) and Gale (1975) performed laboratory tests with deformable fractures and studied the effect on flow when axial stresses were applied. This topic is not directly relevant to the present work, and therefore has not been pursued further.

2.3.5 Models for fractured rock

This part of the review will concentrate only on those models that analyse fluid flow in fractured rock for which the permeability of the matrix is assumed to be very small, so that all the fluid flow occurs through the discontinuities of the rock mass. It was noted earlier that two approaches have been used for analysing fluid flow in fractured rock: the equivalent continuum approach and the discrete approach.

The basic assumption in the equivalent continuum approach is continuity and statistical homogeneity of the rock and fluid properties. The discrete approach assumes that the specific geometrial chacteristics of the fracture system can be determined. The choice between these approaches depends essentially upon the relative scale of the problem being studied, and on the availability of the necessary input data. Deterministic models which attempt to duplicate the actual geometry of the fractured system by specifying individual fracture locations, size, orientation and aperture variations are usually limited to relatively small geotechnical problems. The equivalent continuum approach is more realistic in ground-water and petroleum engineering problems.

In many of the deterministic models, each fracture is modelled separately using an approach based on network analysis. Wilson (1970) presented a review of some of these models, including work by Crawford and Collins (1954), Crawford and Landrum (1955), who used electric analogue models, and Ollos (1963), who utilized a model made of a network of pipes.

Serafim and del Campo (1965) developed a mathematical model involving steady state flow in a network of three orthogonal sets of fractures. They used the parallel plate model and considered all fractures in a given set to be parallel and of equal aperture and spacing, a further assumption was that flow in each fracture was independent of the flows in any other fracture. Although this assumption may be correct for infinitely long discontinuities it cannot be true when the discontinuities are of finite length.

Louis (1969) presented two methods, one graphical and the other analytical for solving the potential distribution in his model of fractured rock. In the graphical method he considered two-dimensional problems by assuming that the flow processes in rock are the same in all vertical planes that are perpendicular to the strike of the fracture system. His graphical method was applicable to models containing two sets of discontinuities, each with parallel fractures. The first of these sets had extensive water bearing fractures; the second set comprised a group of minor fractures. The potential flow grid was determined for arbitrarily hydraulic and geometric boundary conditions. In the analytical method, when two main water-bearing fracture sets were to be considered the assumptions concerning geometry of the fractures were extended to include orientation and the degree of continuity. Again in this case the geometric and hydraulic boundary conditions were set arbitrarily. He then considered conservation of energy and continuity of flow firstly at every intersection, and then at each closed circuit of fracture segments. This generated a system of linear equations which were solved to determine the potential distribution within the system. Flow was initially assumed to be laminar to give a first approximation for flow velocities. The flow velocities were then examined at each fracture segment to determine whether turbulence would develop. If turbulent flow was discovered the equation for the conservation of energy was amended for those segments, and the system of equations was again solved, this time using an iterative technique to cope with the resulting non-linear equations. He considered losses of energy at intersections to be negligible.

Wittke (1972) and Wittke et al (1972) presented a three-dimensional model which represented a rock mass containing a discrete network of discontinuity planes. By assuming a given set of boundary conditions the distribution of potential, velocity and discharge were established with the aid of a finite element program. The regions of turbulence were not known initially, but were found and solved iteratively. The water table surface was also found iteratively. Wittke's assumptions that the flow is laminar along the intersections and that the piezometric head did not change, were verified by means of a physical tunnel model built of plexiglass blocks with axisymmetric fractures intersecting the tunnel. Wittke measured piezometric heads at 140 points adjacent to the tunnel and reported a reasonable agreement between the numerical and physical models.

Wilson (1970) developed a model utilizing the finite element method to solve two-dimensional problems in the laminar flow regime for arbitrary, but known, fracture geometries and boundary conditions. He presented some simple examples to demonstrate his model. This model has the advantage of being able to analyse the flow through the rock matrix as long as the overall flow remains laminar. This model is also capable of representing fractures with different wall configurations and shapes and can be extended to couple the stress/flow behaviour to analyse how permeability changes with the application of loads. The main disadvantage of this and all of the deterministic models, apart of the difficulty in obtaining realistic input parameters, is that as the number of fractures involved in a given problem increases (and often before reaching the point where the equivalent continuum representation becomes valid) the solution becomes very expensive and computationaly impractical.

An alternative approach, using the continuum method, is the application of statistical models. These can be applied when the fracture density is large and when comprehensive measurements of discontinuity characteristics are available in the form of mean values, standard deviations and distribution types. The general approach, described earlier, is to define an equivalent porous medium model that describes the hydraulic behaviour of the fractured system, and that can be analysed using the theory applicable to anisotropic porous media. Gringarten (1982) pointed out that an "equivalent" system is one whose calculated behaviour is equivalent to the observed behaviour of a real system. He added that the word "equivalent" only applies to the basic theoretical model and that the boundary conditions should be the actual ones, when they are known.

Important contributions to the statistical approach have been made by Snow (1965). He developed an expression for the permeability tensor of a single extensive fracture of arbitrary orientation and aperture relative to a fixed relative coordinate system. He then expanded his theory to a medium with several parallel extensive discontinuities and more than one set. The permeability tensor for a network of fractures can then be calculated by adding the respective components of the permeability tensor for each individual fracture. The basic approach used is summarized below, and follows that of Snow (1965, 1969) and Bianchi and Snow (1969). Flow in a single fracture of aperture (2b) under a field gradient, I_i, can be expressed as

$$q_j = \frac{(2b)^3}{12\mu} \rho g \left(\delta_{ij} - m_{ij}\right) I_i \qquad (2.49)$$

where q_j is the flow per unit width of fracture (L^3/T), δ_{ij} is the Kronecker delta, $m_{ij} = n_i n_j$ is a matrix formed by direction cosines of the normal to each fracture plane, ρ, μ are density and viscosity of the fluid and g is the acceleration due to gravity. Snow asserted that each fracture intersecting a sample line has its image at a distance L equal to the length of the sample line measured in the direction of the sample line. Thus the spacing between each fracture and its repetition is given as:

$$w = L|n_\ell \; D_\ell| \tag{2.50}$$

where w is spacing between fractures, n_ℓ are the direction cosines of the normal to the fracture set and D_ℓ are the direction cosines of the sampling line. The intrinsic permeability of a medium containing a single fracture is then given by:

$$k_{ij} = \frac{2}{3L} \frac{b^3}{n_\ell D_\ell} (\delta_{ij} - m_{ij}) \tag{2.51}$$

Where more than one fracture set is present at each location and when more than one location considered, Bianchi and Snow (1969) recommend using the average for all locations given by:

$$k_{ij} = \frac{1}{N} \sum_1^N \frac{2}{3L} \sum_1^S \frac{b^3}{|n_\ell D_\ell|} (\delta_{ij} - m_{ij}) \tag{2.52}$$

where N is the number of locations and S is the number of sets at each location.

Snow (1969) by applying equation (2.52) found the permeability tensor for a model generated from a random set of fracture apertures taken from a normal distribution paired with random orientations taken from the Fisher distribution. He repeated the experiment with different input parameters, and studied the effect of changing the size of the sample and changing the dispersion of orientation for a constant fracture spacing.

Snow examined the influence of sample size on the permeability tensor and concluded that dispersions of principal axes and permeabilities decreased for samples of increasing size. He also found that median permeability values increased slightly with sample size. He suggested that model permeability becomes independent of sample size when there are 100 or more joints. Snow also showed that as the dispersion of orientation decreases there is a progressive reduction of the dispersion of axes and permeabilities. He found also that for three orthogonal sets, if each set has fractures of similar aperture distribution, spacing is more important than orientation dispersion in determining anisotropy.

Irmay (1958) pointed out that flow across three inclined or different sets of straight seams leads to a second rank tensor permeability. Romm and Pozinenko (1963) have derived equation 2.51 without the weighting factor $|n_i D_i|$. Their solution proved to be adequate for any system containing sets of parallel fractures but could not be applied to sets with variable orientation.

Castillo (1972) presented an independent development of Darcy's Law for idealized two dimensional systems of continuous uniform laminar fractures. It may be argued, however, that the utility of such a model does not extend to real applications because fractures in rocks are not characterized by uniform, smooth, individually isotropic, continuous planes arranged in parallel sets with the same aperture. Similar formations such as Lomize (1951), Romm and Pozinenko (1963), Snow (1965), Louis (1970), Wittke (1972) and Wilson (1970) also have this limitation. However, these theories prepare the way for better methods of field measurement and better interpretation of the measurements.

Rocha and Franciss (1977) developed a method for determining the permeability tensor in fractured rock from a characterization of its fracturing by means of integral sampling. Although their theoretical analysis was similar to Snow's model, and made similar assumptions, it did include an additional factor to correct for simplifying assumptions such as continuity of each fracture plane, roughness and head losses at fracture intersections. The correction factor was derived by comparing the results of permeability tests in boreholes with those obtained from the theoretical analysis. They performed a pressure test and measured the discharge for a given diameter and section length of borehole and found the correction factor, ρ, for the theoretical permeability tensor, by equating the flow that corresponds to the principal permeabilities, ρK_1, ρK_2 and ρK_3, to the measured discharges. Rocha and Franciss then extended this correction to include the case of two discontinuity sets. They proposed an iterative method for applying a different correction factor for each of the two discontinuity sets separately.

This analysis does not permit rotation of the principal axes and was developed for the case of radial flow only.

Parsons (1966) studied regular fracture networks containing one or more fracture sets within which all fractures were parallel, had the same spacing and aperture. He found that the behaviour of this model was equivalent to that of an anisotropic porous medium. Fatt (1956) arrived at the same conclusion. Parsons also developed a heterogeneous fracture network in which the fracture conductivities were randomly selected within the two-dimensional network. The boundary conditions were then applied and the pressure distribution found by means of a computer program, to give the permeability of the network. Parsons concluded that the permeability calculated depends upon the distribution of the fracture conductivities and the geometry of the fracture network into which they are placed. Although he did not find any clear correlation between the overall permeability and the distribution of fracture conductivities, he did conclude that the larger the standard deviation of the conductance distribution, the larger is the spread (standard deviation) of permeabilities calculated from different random realizations. He found that the distribution of permeabilities was approximately normal. He also found that if the conductance distributions have a relatively low standard deviation, the geometric mean value of permeabilities is a fair approximation to permeability for square networks. Parsons also experimented with some properties of discontinuous systems. By doubling the conductance of all the fractures in the x direction, he found that the permeability in the y direction also increased. This effect would not be seen in persistent fractures, however, by considering impersistent fractures, the flow in the y direction will be affected by fluid flowing in individual fractures in the x direction . Increasing the conductances of fractures in the x direction would, therefore, tend to increase the total flow, thereby increasing permeability in the y direction. For a similar reason the permeability in the x direction was less than doubled.

Cadwell (1972) constructed two-dimensional resistivity analogues of network flow and measured the potential distribution within the model. The value of the permeability tensor for each test was then calculated. This tensor was input to a finite difference computer program and the resulting potential distribution was determined. The measured and the calculated potential distributions were then visually and statistically compared. By using statistical fitting techniques, he then determined the permeability tensor value. It was clear, however, that other permeability tensors would give fits equally as good as those obtained. This casts some doubt on the accuracy of the method. Cadwell also studied a model that contained two orthogonal, but different sets of persistent fractures. Statistical comparisons of the measured and calculated model potentials showed that a small difference in mean and standard deviation existed. Also, he studied models with three sets of random, impersistent fractures. In this case the statistical agreement between measured and calculated potentials was not as good as with two sets. Another model with two orthogonal sets was also studied, one set consisted of persistent, regularly spaced fractures, the second set had fracture lengths that were randomly selected from a negative exponential distribution and spacings equal to one-quarter of those for the persistent set. Cadwell found that when the set with variable fracture lengths had a mean length 2 or more times the spacing of the persistent set, the overall permeability was the same as that where both sets were persistent. This was because all fractures were hydraulically active. When the mean trace length of the inpersistent fracture set was equal to the spacing of the persistent set less than half of the fractures were hydraulically active. Cadwell's analysis was one of the first in addressing the influence of fracture continuity on the permeability tensor in two dimensions. One of the main disadvantages of the electrical analogue method is that it is difficult to extend to three dimensions and also a realistic modelling of discontinuity aperture is limited.

Sagar and Runchal (1982) also addressed the problem of fracture continuity. By assuming that a single fracture can be represented by a parallelopiped they derived an equivalent permeability tensor using an approach similar to Snow's (1965). In trying to extend their formulation to a multiple set of fractures they assumed that, for an elemental block, the flow in any fracture is "virtually" independent of that in the other fractures as long as the flow is laminar and disturbances at the fracture intersections are negligible. Obviously this assumption is incorrect no matter how small the elemental block is. In presenting an application of their model they considered the elemental block to be a cube of 5m size; the assumption of independent fracture flow severely limits the accuracy of the results at this scale.

Robinson (1982), Cundall (1983), Long (1983) and Priest and Samaniego (1983), have independently developed statistical models based on fracture field data in order to analyse flow and determine the equivalent permeability tensor in two dimensions. This work follows the general approach of representing fracture networks as random realisations, developed by Baecher (1979), La Pointe and Hudson (1980) and Samaniego (1981). Robinson (1982), Long (1983) and Samaniego (1981) have developed similar computer models that generate random networks of fracture systems. Each of these models is based on four discontinuity characteristics: orientation, length, density and aperture. The location of each discontinuity is assumed to follow a two-dimensional Poisson process and therefore is statistically homogeneous. A more comprehensive explanation is presented in Chapter 3. Cundall (1983) presented a discontinuity mesh generator that is basically the same as those listed above except but his model takes the spacing between joints to be a random variable that may be specified independently of the other parameters. He also introduced a parameter, called gap length, to simulate the breaks in fracture persistence that certain rock types present. Non-homogeneous characterisations can be generated by assigning spatial gradients to some or all of the parameters describing the discontinuity network.

Flow through the fracture network can be calculated using a variety of approaches. After the boundary conditions have been fixed, the solution involves setting up a linear equation, for each node or intersection, based upon the principle of conservation of fluid rock mass. For a network of n nodes, there are n simultaneous linear equations in which the unknowns are the potentials at the inner nodes; the potentials at the boundary nodes are fixed. Cundall (1983) used an iteration procedure which does not require the coefficient matrix to be stored in core at all times. This is achieved by making adjustments node by node until the change in potentials falls below some given threshold value, at which point the iteration stops. Although this method is attractive in its simplicity, in the author's experience the convergence is extremely slow when a large number of discontinuities are analysed. Cundall found this method satisfactory because the type of problems that he solved had relatively homogeneous potential distributions.

Robinson (1982) used a banded gaussian elimination method to solve the potentials in a fracture network. This required a renumbering routine to reduce the bandwidth of the coefficient matrix. The renumbering of the network implies that the solution vector would have to be reordered into its original numbering in order to calculate the flow rates at each discontinuity segment.

Long (1983), in order to calculate flow through the network, used a finite element program developed by Wilson (1970). For this purpose fractures are represented as line elements and the rock matrix is assumed to be impermeable. The system of linear simultaneous equations was generated in the manner described earlier, the solution vector is evaluated by triangular decomposition of the coefficient matrix.

There can only be flow along those fractures that are connected to at least two other fractures or to a boundary and another fractures. Robinson (1982) and Priest and Samaniego (1983) presented a method for removing the dead ends, i.e. non-active fractures, from the network of fractures. This was done in order to simplify the subsequent flow calculations. Even after this process isolated fracture groups could still remain inside the interconnected network. In a later paper Samaniego and Priest (1984) presented a method for removing these isolated networks. They then applied an efficient bi-factorisation method in order to solve the system of linear equations.

After solving the flow across the boundaries and within the network, Long (1983) and Robinson (1982) determined permeability in the direction of the gradient by applying Darcy's law to a sample of fractures, using:

$$K_{ij} = \frac{Q_i}{A_i \nabla \phi_i} \qquad i = 1,\ 2 \qquad (2.55)$$

where A_i is the gross area perpendicular to the i direction and Q_i is the flow rate in the direction of the gradient $\nabla\phi_i$. A problem they found with this approach was that inflow does not equal outflow on opposite sides of the sample area. Obviously this creates a problem when using equation (2.53). To overcome this difficulty Long (1983) arbitrarily defined that permeability is proportional to the inflow, ignoring the outflow on the opposite side. Robinson (1982) used the average of the inflow and outflow in order to define permeability. Results obtained using this approach are highly sensitive to the location of the boundary. In fact Long (1983) showed examples where the flow in opposite sides of the sample differed by up to 10^6 (cm^3/s) orders of magnitude. This is due to the authors having ignored the vectorial characteristics of the specific discharge. Cundall (1983) and Samaniego and Priest (1984) developed an alternative approach to overcome this difficulty. The method involves calculating the average velocity in the region of interest and then, by putting the result into

Darcy's equation (equation 2.12) the permeability tensor can be obtained. It is necessary to carry out flow tests in at least two orthogonal directions to obtain the full permeability tensor. It was found that for dense networks with a high degree of connectivity, the permeability tensor becomes symmetric. This method of demonstrating symmetry of the permeability tensor differs from that of Long (1983). She argued that the only way to show that a given network has a symmetric permeability tensor was actually to measure the directional permeability. To do this Long rotated the sampled network around an axis that passed through the centre of the sample area. At each step of the rotation the permeability in the direction of gradient was calculated and the inverse of its square root plotted in polar coordinates. As the sample area selected was square, a slightly different sample of fractures was being considered at every step of the rotation. Ideally a circular shaped sample area would be required to overcome this difficulty. After completing the rotation of the sample, Long (1983) performed a regression analysis in order to determine the permeability tensor. The method for solving the regression equations was similar to that given by Scheidegger (1954). This method consists of finding the parameters K_{11}, K_{12} and K_{22} - where 1 and 2 are the axis of a local system of coordinates which best fit the data obtained from the rotation (Fig. 2.5). From these parameters Long calculated the principal permeabilities and directions. She then defined the mean square error as the ratio of the square of the deviations of the data points from the theoretical elliptical variation to the total number of data points measured. In order to compare different results she normalized the mean square error by dividing it by the product of the principal permeabilities. Unfortunately this approach becomes very expensive if a Monte Carlo type analysis is performed. This is because the normalised mean square error found for a single mesh realization only describes the behaviour of that particular mesh; it is not possible to make any confident extrapolations.

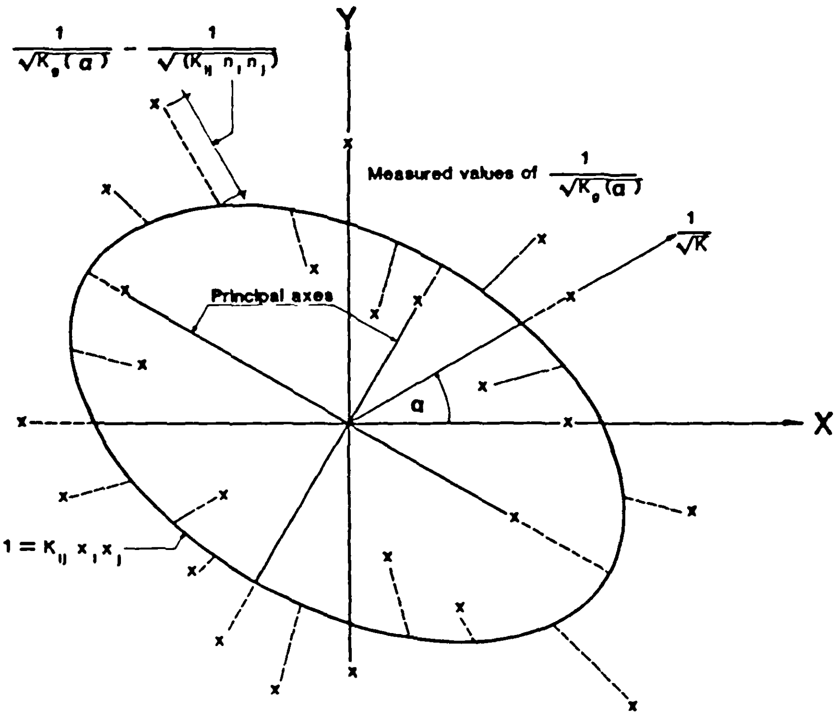

Figure 2.5 A set of directional permeability measurements plotted as $1/\sqrt{kg}$ in polar coordinates (after Long, 1983)

Long (1983), using the procedure outlined above, studied the effects of fracture density, aperture, orientation distributions and scale on the equivalent permeability tensor. She pointed out that although all her results conformed to intuition, it was the first time that they had been numerically sustained, and thus formed a basis for a better understanding of fracture system behaviour.

Robinson (1982) analysed a mesh composed of 2 orthogonal sets, each with a fixed discontinuity length and aperture but with an orientation that was allowed to vary randomly according to a uniform distribution within $\pm 5°$ of the mean value. He performed an experiment by increasing the sample size in 30 steps of 0.2 m each, carrying out six realizations at each step. As expected he showed that there are large fluctuations in permeabilities for small regions but that this fluctuation decreases as the size of the flow region is increased.

Cundall (1983) used circular sample areas to measure the permeability tensor. He performed sixty runs and did parametric studies in meshes with two or three sets. He also studied in-homogeneity. Finally he performed a study of dispersion of marker particles. Cundall's general conclusions are that the average permeability tensor is unreliable when it is used to characterise discontinuity systems that contains less than one hundred joints. He also found that the most sensitive parameter in establishing the average permeability tensor was the trace length; he found that the size of the gaps in a discontinuity did not have much influence on permeability. A limitation of the studies made by Cundall is that he assumed the aperture to be constant throughout his experiments. This is a serious limitation since, as has been discussed in previous sections, the distribution of discontinuity apertures is of paramount importance in the determination of flow in fractured rock. Another limitation is that he used only a uniform probability distribution for all of the discontinuity parameters. These limitations do not, however, invalidate the general conclusions that he arrived at.

2.3.6 Concluding Remarks

When flow through fractured rock is simulated by a statistical model one of the aims is to determine an equivalent continuum permeability tensor that represents the anisotropic flow properties of the complex, discontinuous, in-homogeneous rock mass. In order to make use of the equivalent continuum permeability tensor, it is necessary to understand the nature of porous medium permeability. Darcy's law which is a basic relationship describing the motion of fluid through homogeneous porous media has been discussed and its different generalizations presented. Of particular relevence to this work was the generalization of Darcy's law based upon simplified fissure models. The review of the theory of directional permeability showed that, for a symmetric permeability tensor, if the permeability kg is measured in the direction of the gradient, then a plot of $1/\sqrt{kg}$ in polar coordinates against α (the direction of measurement) is elliptical in shape.

The experimental work and theory developed for the parallel plate analogue indicated that this is an appropriate way to simulate fluid flow in a discontinuity under laminar flow conditions. The effects of discontinuity roughness and also turbulent flow were studied and several semi-empirical flow lows were presented (Lomize, 1951 and Louis, 1969).

A review of the deterministic models used for analysing fluid flow in fractured rock showed that they can be satisfactorily applied to relatively small geotechnical problems and where the continuum approach cannot be defined. Some of the reviewed discrete models incorporated finite element techniques (Wilson, 1970 and Wittke, 1972), this allows them to study the stress/flow behaviour and hence to analyse how permeability changes with the application of loads. The review of the fracture rock models using the continuum approach indicated that the permeability of fractured rock with persistent discontinuities is well defined. Provided that some assumptions are made with regard to the discontinuity geometry, it is possible to find an expression for the permeability tensor as a function of the geometrical properties of discontinuities (Snow, 1969). The permeability of fractured rock where the fractures are inpersistent has only recently been studied. Initially these studies were carried out using electric analogues (Cadwell, 1972). Statistical and probabilistic modelling of fracture rock was introduced by Robinson, (1982), Cundall (1983), Long (1983) and Priest and Samaniego, (1983). All these authors presented models that statistically generated discontinuity networks. Then by applying hydraulic boundary conditions the potentials in the interval nodes of the network were solved. They all used different techniques, these ranged from iterative methods to more rigorous methods. Such as; banded gaussian elimination, triangular decomposition and bi-factorization methods. Although it is difficult to generalize about the relative merits of each method, some advantages of the bi-factorization approach to solving large systems of space matrices were observed.

Parametric studies of the discontinuity networks characteristics were discussed by Long (1983). These included the effects of fracture density, aperture, orientation distribution and scale on the equivalent permeability tensor. These studies, however, were of limited extent because Long's discontinuity density meshes were limited by the capacity of the computer she used. In order to solve this difficulty some streamlining of the network has to be performed and also more efficient techniques for solving large space matrices have to be introduced.

CHAPTER 3 THEORY AND DESCRIPTION OF MODEL

The theory used in developing the probabilistic model presented in this work is explained along with the description of the model itself. In the first section of this Chapter the methods of gathering data in the field, their interpretation and processing to determine the discontinuity geometry parameters are fully described. Two computer programs were developed for this purpose, the program SCANL which analyses data from scanlines and the program PHOCOM which analyses data from photographic prints.

In Section 2, DICHA, the mesh generator program is decribed and in Section 3, DICONN, the program that performs the connectivity analysis is explained. In the following section the program DIFLOW, which calculates the flow and the equivalent permeability tensor, EPT, is presented, followed by the deduction of the expression for EPT. Finally a validation of the model is presented under three categories; geometrical, numerical and flow validation.

3.1 Preparation of input data

The input data for the models presented in this work are normally obtained from field surveys of rock mass structure. The methods used for this purpose include scanline sampling, surface sampling, borehole loggings and water pressure tests. Only the first two methods were performed in the course of this work; the remaining results are taken from other published works. This section is divided in three parts: the first includes the basic assumptions concerning the geometry of the discontinuity characteristics which are needed to define the discontinuity network. The second part gives a brief description of the methods used in the field surveys and finally in the third part the data processing, using the computer programs SCANL and PHOCOM, are discussed. An explanation of the theory used in developing these programs is also included.

3.1.1. Basic assumptions

The following basic assumptions set the conceptual frame-work for the development of the statistical model presented here:

(i) Discontinuities are assumed to occur in sets that can be represented by a continuous distribution of orientations and characterised by a mean orientation and a measure of orientation variability.

(ii) Discontinuities are assumed to be planar and of finite extent so that their intersection, by an additional arbitrary plane, produces a group of linear traces. It is assumed that these traces can be represented by a continuous distribution of lengths and characterised by a mean length and a measure of length variability. It is also assumed that the discontinuity planes have an equidimensional geometry, so that their trace length distribution on an intersecting plane is effectively independent of the orientation of that plane.

(iii) The aperture of a given discontinuity is assumed to be *constant*. It is also assumed that the apertures for a set of discontinuities can be represented by a continuous distribution of values and characterised by a mean aperture and a measure of aperture variability.

(iv) Finally it is assumed that all discontinuities occur randomly throughout the rock mass; this means that the mid-points of discontinuity traces on a given intersecting plane obey a statistically homogeneous, two dimensional Poisson process.

The distributions listed above, and their associated parameters have been studied already by several authors. This work will make use of the currently available knowledge for the characterization of fractured rock masses. An extended review on this aspect has already been presented in Chapter 2.

3.1.2 Description of field sampling methods

The selection of a particular sampling method is firstly dependent on the type of geotechnical problem that is being tackled, and secondly on the type of exposures available at a specific site. The sampling methods described here are only those that are appropriate in collecting discontinuity parameters to serve as input data to the statistical models referred to at the beginning of this Chapter. The type of information required for this purpose was summarized in the previous section. Much of the necessary information can be obtained from rock mass exposures, which usually constitute road cuttings, quarry benches or coastal cliffs. Apertures must, however, usually be measured indirectly by performing water pressure tests. When data from unexcavated zones are required the best apprach is borehole sampling. The disadvantage with boreholes is that they only provide limited information on discontinuity size, therefore reliable measurements of this property can only be obtained by examining larger rock exposures.

Measurements at a rock face can be based upon either linear or surface sampling. In linear sampling the properties of only those discontinuities that intersect an arbitrary sampling line, or scanline, are recorded. This approach has the advantage of being compatible with a borehole sample and of providing information on discontinuity frequency and spacing along a line. The disadvantage of this approach is that it tends to sample preferentially the larger discontinuities and also those whose normals make small angles with the scanline. Analyses of the scanline sample bias are discussed by several authors including Terzaghi (1965), Baecher (1978), Priest and Hudson (1981) and Hudson and Priest (1983). Priest and Hudson (1981) also proposed methods for removing bias during the data processing stage.

Where an exposure is of sufficient extent, valuable additional information can be obtained by sampling discontinuity characteristics on an areal basis. In most cases the surface sample can be based upon a photographic print of the rock face which is then examined to determine the coordinates of the end points of each discontinuity trace. Although this is a laborious process, it provides valuable information on areal frequency, trace length and linear frequency in the plane of the rock face. Since three dimensional data cannot be obtained from a single photograph, it is usually necessary to carry out areal photographic surveys in conjunction with linear scanline surveys on the actual rock face. The procedure for scanline sampling together with copies of the associated coding sheets, used for recording the measurements, are presented in Appendix 1A.

A field trip to Pembrokeshire provided the necessary input data required to test and evaluate the statistical model. Six different sites were visited and over 30 scanlines were surveyed containing nearly 2000 discontinuity measurements. Photographs were taken at each scanline site, these gave additional information on a further 8000 discontinuities. Each site visited consisted of different rock types, including quartzites, limestones, slates and red sandstones, and covered a broad period in geological time. A more detailed geology of the sites visited can be found in the British Regional Geology - South Wales (1970). Descriptions, locations and names of the sites visited, as well as the data collected, are given in Appendix 1B.

3.1.3 Data processing

The computer programs SCANL and PHOCOM were developed in order to process data sampled by scanlines and photographs repectively. Firstly, the scanline data processing will be discussed. The raw field data are recorded in standarized coding sheets, as shown in Appendix 1A. The resulting data can be punched directly onto computing cards or typed in at a computer terminal. Some pre-processing is, however, needed in order to determine the number of discontinuity sets present at a specific survey site. This pre-processing consisted of plotting the normals of all the discontinuity planes onto a lower hemisphere projection, clusters of poles were then identified visually. Each cluster was delineated by an ellipse which represents the intersection of a cone with the hemisphere of projection. See Fig. 3.1 (a). The centre of the ellipse was located over the centre of the cluster, with typical cone angles ranging from 20° to 40°. Fig. 3.1 (b) shows a typical example containing 3 discontinuity sets. No contouring methods were used as they provide no measure of the degree to which the normals are clustered. Although the process of delineating clusters was usually straight forward, certain cases did produce some difficulties, particularly when two clusters were near to each other. In this case the two clusters were analysed first separately and then aggregated.

All of this information plus the scanline measurements are then fed into the SCANL program. User's instructions are included in the Appendix 1C. The SCANL program is capable of handling up to 15 scan-lines each one containing up to 500 discontinuities and can analyse up to four sets. The output of the program includes mean values and standard deviations for discontinuity spacing, orientation and semi-trace length for each discontinuity set. The Fisher's constant is calculated in order to evaluate the dispersion of the pole clusters. (See Section 2.2.3.). Theoretical distributions such as the log-normal and negative exponential are fitted to the observed frequency distributions of spacing and semi-trace length. The best fit is found by means of appropriate goodness of fit tests.

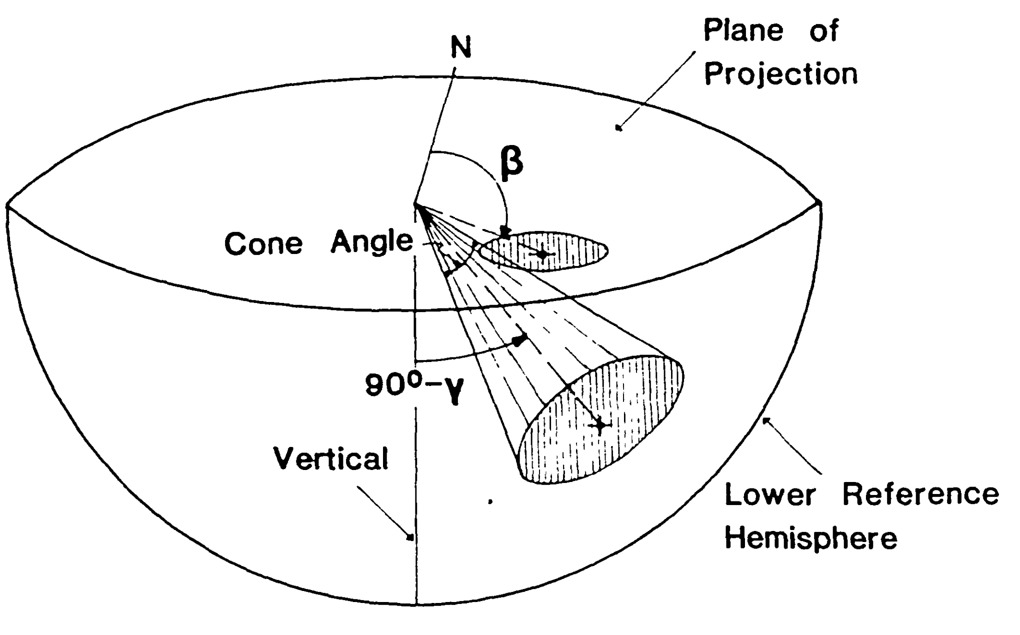

Fig. 3.1 Hemispherical projection of discontinuity normals

(a) Intersection of a cone with the hemisphere of projection

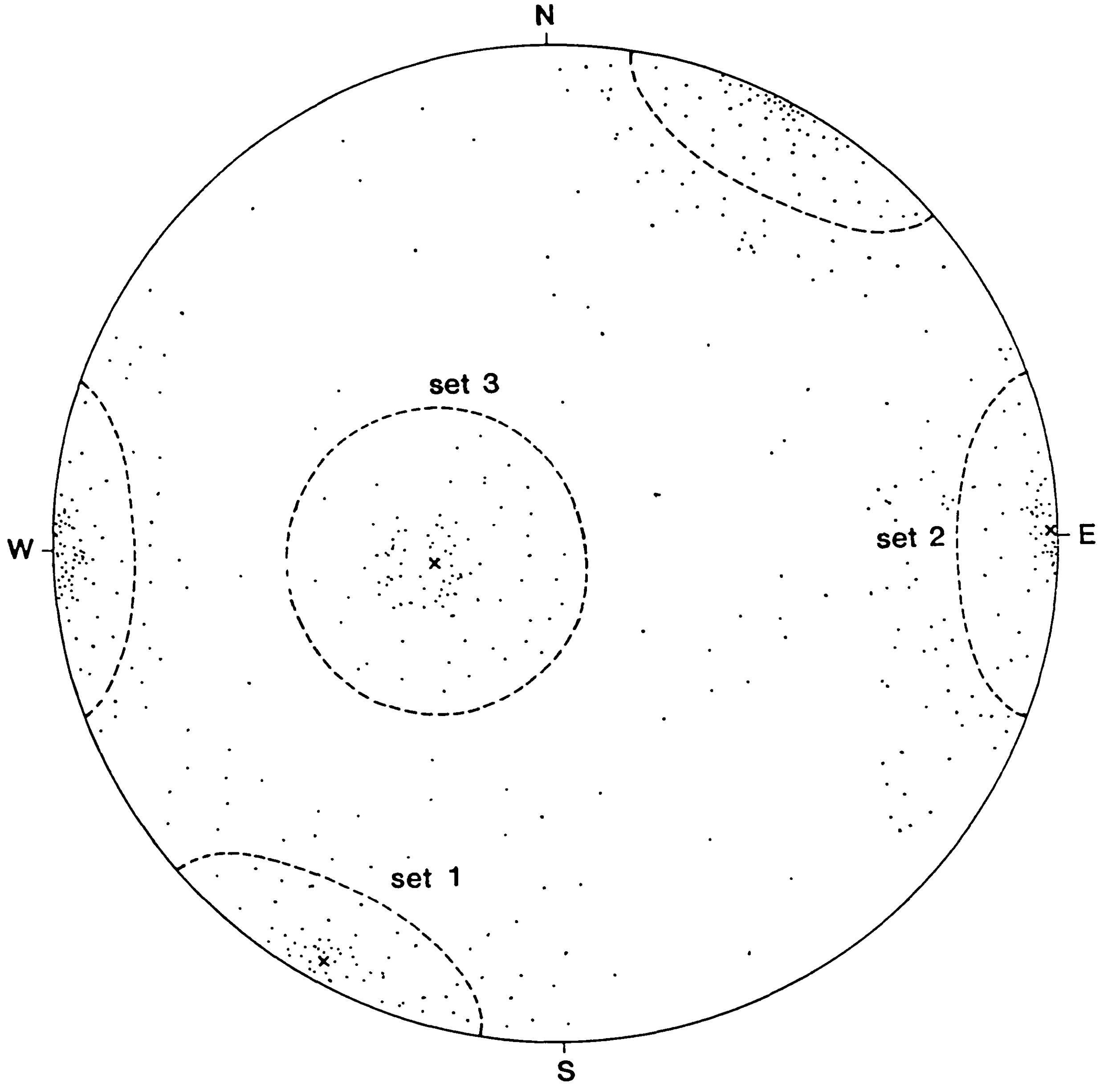

Fig. 3.1 (b) Typical example containing 3 discontinuity sets

The theory used in developing the SCANL program is outlined below. The mean orientation of a discontinuity set is calculated by vectorially averaging the discontinuity orientations of all those discontinuities whose normal lie within the elliptical boundaries, as specified in the pre-processing stage. The procedure is as follows: each discontinuity normal is represented by its unit vector $\vec{a}$. Fig 3.2 shows the cartesian coordinate used. The x, y and z cartesian components of unit vector $\vec{a}$ parallel to the ith discontinuity normal are given by a_{ix}, a_{iy}, a_{iz} as follows

$$a_{ix} = \text{Cos } \Theta_1 = \text{Cos } \gamma \text{ Cos } \beta$$

$$a_{iy} = \text{Cos } \Theta_2 = \text{Cos } \gamma \text{ Sin } \beta$$

$$a_{iz} = \text{Cos } \Theta_3 = \text{Sin } \gamma \tag{3.1}$$

Where β and γ are the trend and plunge of the discontinuity normal and $\text{Cos}\Theta_1$, $\text{Cos}\Theta_2$ and $\text{Cos}\Theta_3$ are its direction cosines. Assuming that there are N discontinuity normals and that the mean orientation is given by the resultant of their unit vectors, then the components of the resultant vector are:

$$R_x = \sum_{i=1}^{N} a_{ix}$$

$$R_y = \sum_{i=1}^{N} a_{iy} \tag{3.2}$$

$$R_z = \sum_{i=1}^{N} a_{iz}$$

and the magnitude of the resultant vector is:

$$R = \sqrt{R_x^2 + R_y^2 + R_z^2} \tag{3.3}$$

The components of its unit vector, $\vec{r}$, are:

$$r = (r_x, r_y, r_z) = (R_x/R, R_y/R, R_z/R) \tag{3.4}$$

The trend of the mean normal, β_m, and plunge of mean normal, γ_m, are given by:

$$\beta_m = \text{arc tan } (r_y/r_x) \tag{3.5}$$

$$\gamma_m = \text{arc tan } \; r_z/\sqrt{r_x^2 + r_y^2} \tag{3.6}$$

Caution should be taken to ensure that β_m lies in the correct quadrant and in the range of 0 to 360°. Priest (1984) shows ways how this problem should be tackled.

A measure of the clustering of poles is given by the Fisher's constant, K, where

$$K = \frac{N - 1}{N - R} \tag{3.7}$$

In this work a Fisher's constant greater than 5 is considered sufficient to form a discontinuity set.

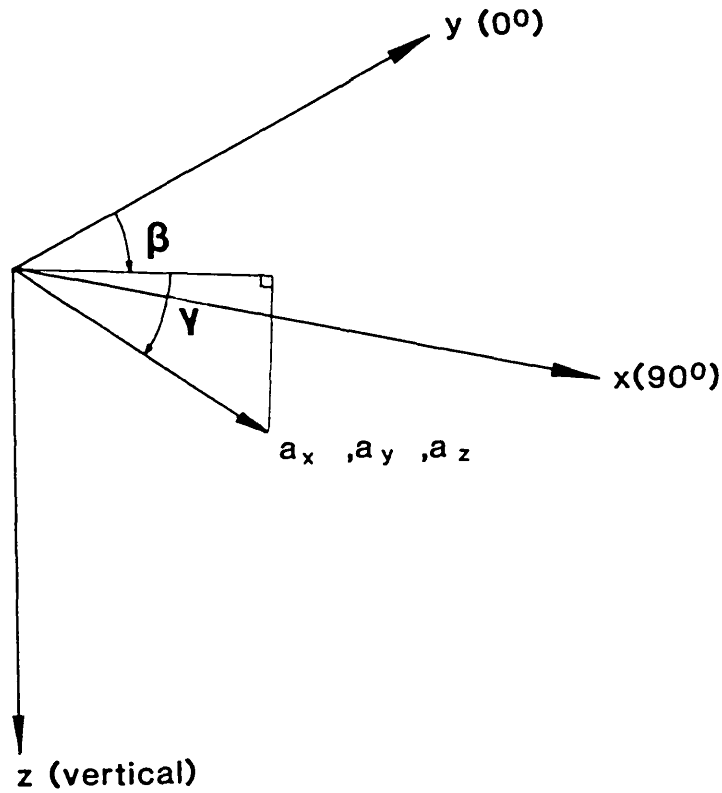

Fig. 3.2 Cartesian coordinates showing the components of the unit vector $\vec{a}$ parallel to a discontinuity normal

The mean discontinuity spacing is given by:

$$\bar{x} = \sum_{i=1}^{n} x_i/n \tag{3.8}$$

where x_i is the ith discontinuity spacing between two consecutive discontinuities that belong to the same set and is measured along a scanline of length L containing n values. Discontinuity frequency is the mean number of discontinuities encountered per unit length along a scanline. For a large sample $1/\bar{x} = n/L \approx \lambda s$ = discontinuity frequency.

Because discontinuity spacing and frequency are dependent on the orientation of the scanline they have been expressed in terms of their components in the direction normal to the mean discontinuity. Hudson and Priest (1983) suggested the following expression

$$\lambda_s = \lambda \ |\mathrm{Cos} \ \alpha \ | \tag{3.9}$$

where λ_s is the discontinuity frequency along a scanline, λ discontinuity frequency along a line normal to the discontinuities and α is the angle between the scanline and the normal to the discontinuities. The absolute value of cos α is taken because the resolved component of λ is always positive. The program SCANL outputs both types of means and frequencies for each discontinuity set, i.e. frequency along the scanlines and frequency along the normal to the discontinuity planes.

The mean trace length is calculated by two different approaches, the first formulated by Priest and Hudson (1981) and the second by Bray (1982). In the first approach it was assumed that the trace lengths followed a negative exponential distribution. A summary of the deduction of the relevant equations is presented here. If i(l) is the probability density distribution of the censored semi-traces lengths, its mean value, $1/\mu_i$, for a negative exponential distribution is given by

$$\frac{1}{\mu_i} = \frac{1}{\mu} - \frac{ce^{-\mu c}}{(1 - e^{-\mu c})} \tag{3.10}$$

where c is an arbitrary censoring level and $^1/_\mu$ is the mean of the population of trace lengths. Priest and Hudson (1981).

Two analytical expresions for estimating mean trace were derived by Priest and Hudson (1981). First, assuming that for a large sample, the numerical proportion of intersected discontinuities which have semi-trace lengths of less than c is estimated by r/n, where r is the number of discontinuities with a semi-trace length less than c and n is the total number in the sample. For a negative exponential distribution this can be expressed as:

$$\frac{r}{n} = 1 - e^{-\mu c} \quad \text{or} \quad \frac{n - r}{n} = e^{-\mu c} \tag{3.11}$$

and

$$\mu = \frac{\log_e((n-r)/n)}{c} \tag{3.12}$$

Equation (3.12) is the first analytical equation derived. If equation (3.10) is substituted using equations (3.11) and (3.12) and it is assumed that $\bar{\ell}_i$ is a good estimate of $\frac{1}{\mu_i}$, where $\bar{\ell}_i$ is the mean censored semi-trace length calculated from the measurements, the second analytical expression is given by:

$$\mu = \frac{1}{\bar{\ell}_i + c\,\frac{n-r}{r}} \tag{3.13}$$

The program SCANL estimates the mean semi-trace length in both ways, i.e. using equations (3.12) and (3.13).

The second approach developed by Bray (1983) is a distribution independent method and its deduction is given in appendix 1D. The expression to estimate mean trace length is given by:

$$\frac{1}{\mu} = \frac{nc}{r} \quad \text{(when } c \to o\text{)} \tag{3.14}$$

It was noticed that when c approaches zero $\frac{nc}{r}$ is subject to considerable statistical variation. Bray (1983) proposed a graphical approach to overcome this problem. From a sample of semi-traces, varying the value of c produces a series of values of $\frac{nc}{r}$. The results can be plotted with $\frac{nc}{r}$ as ordinates and c as abscissae. If enough points are plotted the region which is least affected by statistical variations can be indentified. Extrapolating from the curves in this region to the c = o axis, provides an estimate for $\frac{1}{\mu}$. This approach does not depend on the type of distribution that the trace lengths may have. The program SCANL calculates and plots the values of the function $\frac{nc}{r}$ vs c.

The complete set of processed data from scanline samples is presented in appendix 1E. A summary of these data is, however, given in Tables 3.I to 3.VII, each table corresponding to a different site. It can be seen that 68% of the total number of discontinuity sets had a negative exponential distribution for spacing, 16% lognormal and 16% were not identified. The discontinuity spacings quoted in these tables are the true values, measured along a line normal to the discontinuity planes.

In the case of semi-trace length 44% of the samples followed a negative exponential distribution, 28% lognormal and 28% were not identified. The mean trace length values are those calculated: in (a) by equation (3.13), and in (b) by the distribution independent method expressed in equation (3.14).

The type of termination is indicated in percentages and can be used as a measure of how accurate the estimates for mean trace length were. For example, a large percentage of censored trace lengths would indicate that the estimation of mean semi-trace length is poor. A high percentage of discontinuities ending in intact rock indicates that the assumption of equidimensional shape, i.e. discs, for the discontinuities is valid. The converse applies if it is found that a high percentage of discontinuities terminate at other discontinities. In this case it would be more appropriate to assume that the discontinuities shape is rectangular.

The program SCANL also produces a graphical output; one group of diagrams for each discontinuity set. Each group of diagrams contains a plot for the estimation of mean trace length by the distribution independent method and also histograms of semi-trace length and discontinuity spacing. A typical group of diagrams is shown in Fig. 3.3. The complete graphical output is included in Appendix 1F.

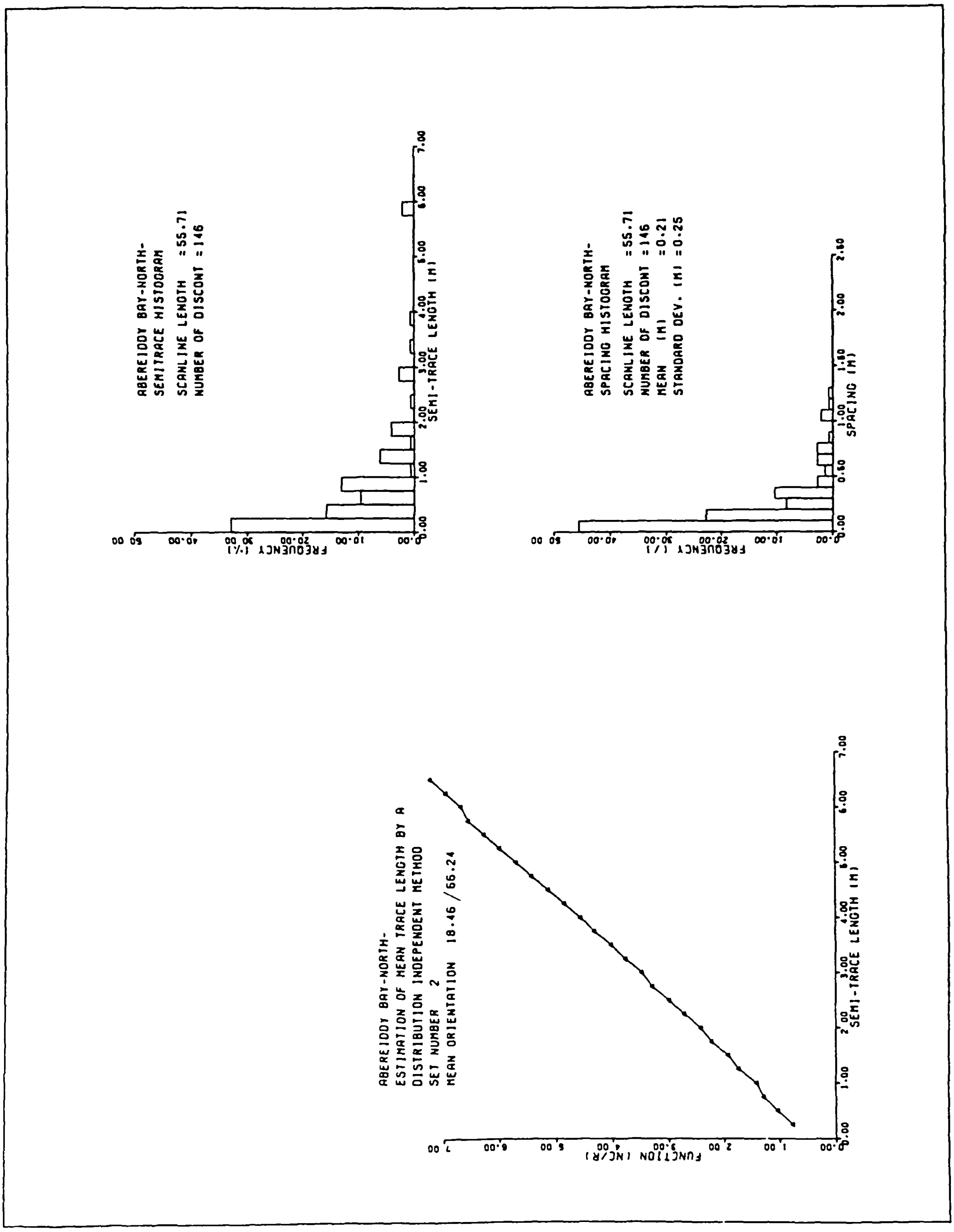

Fig. 3.3 Typical group of diagrams produced by the program SCANL

SCANLINE ANALYSIS

SITE NAME: ABEREIDDY BAY - NORTH

	SET 1	SET 2(*)	SET 3	SET 4(*)
(1) MEAN ORIENTATION °	40.7/326.8	18.5/066.2	57.9/043.3	19.3/272.9
FISHER'S CONSTANT	40.75	2.49	1.28	1.69
MEAN SPACING (m)	1.312	0.213	0.419	0.767
S.DEV OF SPACING	1.321	0.250	0.576	1.443
(2) TYPE OF DISTRIBUTION	NE	NE	NE	NE
(a) MEAN TRACE LENGTH (m)	-	0.59	0.54	0.40
(b) MEAN TRACE LENGTH (m)	-	0.55	0.40	0.35
(2) TYPE OF DISTRIBUTION	-	NE	NE	LN
No. OF DISCONT.	11	146	67	45
TERMINATION TYPE %				
- CENSORED	90	28.8	19.4	31.1
- INTACT ROCK	0	38.4	28.3	40.0
- ANOTHER DISCONT.	10	32.8	52.3	28.9

(1) ORIENTATION: dip/dip direction

(2) TYPE OF DISTRIBUTION: NE Negative exponential

LN Log-normal

\- Not identified

(*) Sets used in geometric validation

Table 3.I

SCANLINE ANALYSIS

SITE NAME: ABEREIDDY BAY - SOUTH

	SET 1	SET 2	SET 3	SET 4
(1) MEAN ORIENTATION °	39.7/336.7	23.4/27.7	10.6/61.0	68.6/46.9
FISHER'S CONSTANT	38.68	53.21	1.78	1.12
MEAN SPACING (m)	0.397	0.410	0.377	0.293
S.DEV OF SPACING	0.319	0.846	0.583	0.321
(2) TYPE OF DISTRIBUTION	-	-	-	NE
(a) MEAN TRACE LENGTH (m)	-	0.52	0.67	0.56
(b) MEAN TRACE LENGTH (m)	0.35	0.42	0.60	0.50
(2) TYPE OF DISTRIBUTION	-	NE	NE	NE
No. OF DISCONT.	18	28	37	51
TERMINATION TYPE %				
- CENSORED	5.5	28.6	13.5	29.4
- INTACT ROCK	5.5	39.3	56.7	39.2
- ANOTHER DISCONT.	89.0	32.1	29.8	31.4

Table 3.II

SCANLINE ANAYLSIS

SITE NAME: MIDDLE MILL QUARRY

	SET 1	SET 2	SET 3	SET 4
(1) MEAN ORIENTATION °	17.3/358.9	30.9/057.6	9.8/293.1	73.7/345.5
FISHER'S CONSTANT	2.42	1.65	1.53	38.92
MEAN SPACING (m)	0.371	0.404	0.614	0.439
S.DEV OF SPACING	0.425	0.398	0.379	0.558
(2) TYPE OF DISTRIBUTION	NE	NE	-	-
(a) MEAN TRACE LENGTH (m)	0.75	0.65	-	-
(b) MEAN TRACE LENGTH (m)	0.35	0.40	-	-
(2) TYPE OF DISTRIBUTION	NE	NE	-	-
No. OF DISCONT.	34	31	4	19
TERMINATION TYPE %				
- CENSORED	8.8	16.1	25.0	100.0
- INTACT ROCK	8.8	12.9	0.0	0.0
- ANOTHER DISCONT.	82.4	80.0	75.0	0.0

Table 3.III

SCANLINE ANALYSIS

SITE NAME: PYLLWGAEOD HEAD

	SET 1	SET 2	SET 3	SET 4
(1) MEAN ORIENTATION °	33.2/302.3	20.2/063.7	22.6/063.9	
FISHER'S CONSTANT	30.28	28.52	46.03	
MEAN SPACING (m)	0.460	0.246	0.644	
S.DEV OF SPACING	0.426	0.482	0.558	
(2) TYPE OF DISTRIBUTION	NE	NE	NE	
(a) MEAN TRACE LENGTH (m)	0.20	0.53	0.60	
(b) MEAN TRACE LENGTH (m)	0.20	0.55	0.35	
(2) TYPE OF DISTRIBUTION	-	NE	-	
No. OF DISCONT.	20	114	15	
TERMINATION TYPE %				
- CENSORED	25.0	39.5	73.4	
- INTACT ROCK	10.0	35.1	13.3	
- ANOTHER DISCONT.	65.0	25.4	13.3	

Table 3.IV

SCANLINE ANALYSIS

SITE NAME: TENBY BAY

	SET 1	SET 2	SET 3	SET 4
(1) MEAN ORIENTATION °	17.6/014.9	37.9/305.7	64.3/037.3	
FISHER'S CONSTANT	45.83	1.32	15.04	
MEAN SPACING (m)	0.409	0.186	0.863	
S.DEV OF SPACING	0.292	0.205	1.116	
(2) TYPE OF DISTRIBUTION	LN	LN	NE	
(a) MEAN TRACE LENGTH (m)	0.98	0.55	0.35	
(b) MEAN TRACE LENGTH (m)	1.0	0.52	0.20	
(2) TYPE OF DISTRIBUTION	LN	LN	NE	
No. OF DISCONT.	85	153	28	
TERMINATION TYPE %				
- CENSORED	44.7	13.1	10.7	
- INTACT ROCK	22.4	33.3	17.8	
- ANOTHER DISCONT.	32.9	53.6	71.5	

Table 3.V

SCANLINE ANALYSIS

SITE NAME: ST. BRIDES HAVEN

	SET 1	SET 2	SET 3	SET 4
(1) MEAN ORIENTATION °	61.4/013.8	39.5/018.2	17.8/314.8	
FISHER'S CONSTANT	30.83	1.45	2.05	
MEAN SPACING (m)	0.174	0.265	0.322	
S.DEV OF SPACING	0.254	0.380	0.680	
(2) TYPE OF DISTRIBUTION	NE	NE	NE	
(a) MEAN TRACE LENGTH (m)	0.46	0.23	0.47	
(b) MEAN TRACE LENGTH (m)	0.40	0.20	0.30	
(2) TYPE OF DISTRIBUTION	NE	LN	LN	
No. OF DISCONT.	68	79	89	
TERMINATION TYPE %				
- CENSORED	33.8	12.7	19.1	
- INTACT ROCK	13.2	19.0	20.2	
- ANOTHER DISCONT.	53.0	68.3	60.7	

Table 3.VI

SCANLINE ANALYSIS

SITE NAME: MARLOES SAND

	SET 1	SET 2	SET 3	SET 4
(1) MEAN ORIENTATION °	22.3/002.9	17.8/081.7	39.3/229.1	30.9/057.6
FISHER'S CONSTANT	6.44	1.71	16.05	30.46
MEAN SPACING (m)	0.158	0.131	0.109	0.156
S.DEV OF SPACING	0.384	0.153	0.161	0.165
(2) TYPE OF DISTRIBUTION	LN	NE	LN	NE
(a) MEAN TRACE LENGTH (m)	0.19	0.20	0.17	0.16
(b) MEAN TRACE LENGTH (m)	0.25	0.15	0.10	0.15
(2) TYPE OF DISTRIBUTION	NE	-	LN	LN
No. OF DISCONT.	32	91	93	52
TERMINATION TYPE %				
- CENSORED	37.5	6.6	1.1	9.6
- INTACT ROCK	12.5	39.6	45.2	46.2
- ANOTHER DISCONT.	50.0	53.8	53.7	44.2

Table 3.VII

In was mentioned earlier that photographic sampling was used at each face in conjunction with scanline sampling. Fine grained, 50 ASA, black and white film was used with a 35 mm SLR camera mounted on a tripod. The camera had both shutter and aperture priority and was equipped with 52 mm and 135 mm lenses. All photographs were taken perpendicular to the scanline and where possible the lens axis was kept perpendicular to the rock face in order to minimise distortion. Typical face dimensions were 6 x 4 m. Scaling of the photographs was achieved using surveying staffs, 2.4 to 4.0 metres long. These were placed at suitable locations on the rock surface; one horizontally and the other vertically. It was found that a good sharp photograph was obtained by keeping the aperture at around f5.6 with shutter speeds not less than 1/15 second. Several photographs were taken at each location; each with a slightly different exposure time and/or aperture value.

The photographic negatives were enlarged to produce 40 x 30 cm prints, which were then examined to determine the coordinates of the end points of each discontinuity trace. The measurement of the co-ordinates was done by hand in some cases and by means of a computerised digitiser in others. The latter method proved to be faster but required a correction for photographic distortion. With the hand method it was possible to make the measurements directly from a pre-distorted scale.

The program PHOCOM was developed to analyse the photographic data. The input data for the program are the end coordinates of the discontinuity traces, and the approximate orientations of the discontinuity sets. The angle of orientation was measured anti-clockwise from the horizontal axis. The program is capable of handling up to 1500 discontinuities per photograph. Up to 4 discontinuity sets can be analysed and up to 20 scanlines superimposed on the photographs. The program calculates the means and standard deviation of discontinuity orientation and trace length. Fitting of theoretical distributions and goodness of fit tests are performed to determine the distributions for the above parameters. The mean trace length and its standard deviation for each discontinuity set are calculated following Baecher's (1980) solution. The set of observations can be divided into three groups:

$x = \{x_2, \ldots\ldots\ldots\ldots x_n\}$ trace lengths with both ends observable

$y = \{y_2, \ldots\ldots\ldots\ldots y_m\}$ trace lengths with one end observable

$z = \{z_1, \ldots\ldots\ldots\ldots z_p\}$ trace lengths with no ends observable

By using likelihood theory density functions for trace length were determined by Baecher (1980). By assuming an exponential distribution for trace length he found that the maximum likelihood estimator can be expressed as:

$$\mu = n / \sum_1^n x_i + \sum_1^m y_j + \sum_1^p z_k \tag{3.15}$$

and that the variance is given by

$$V(\mu) = \mu^2/n \tag{3.16}$$

A difficulty with this method is that the sampling variance of μ becomes large as n, the number of two-ended observations, becomes small.

The program PHOCOM also calculates mean spacing and semi-trace length by simulating several scanlines across the photograph. The theory applicable in this case is similar to that presented for the program SCANL. This method provides an independent check on the data obtained from the actual scanlines since, the linear frequency, λ, measured along a given scanline in the field can be compared with the linear frequency calculated from scanlines superimposed on the photographs. Furthermore, this can be compared with the frequency obtained from the following approximate relationship presented by Priest and Samaniego (1983)

$$N = k\mu\lambda \tag{3.17}$$

The parameter k is a constant which is 1 for parallel discontinuities and $\pi/2$ for randomly orientated discontinuities, N is the areal frequency and $1/\mu$ is the trace length. This relationship provides an important link between the areal and linear frequency and will be discussed in more detail in Chapter 4.

The raw data of the photographic analysis are given in Appendix 1B; the complete processed data are included in Appendix 1G. Tables 3.VIII to 3.XVII, however, show a summary of the results obtained after processing the raw data. These tables show the mean orientation of each discontinuity set, standard deviations and the types of the distributions. It can be seen that in the great majority of cases the distribution of orientation was normal. The mean trace length was calculated according to equation (3.15) and the standard deviation using equation (3.16). For trace length, 64% of the sampled distributions were of negative exponential form, 32% were lognormal and 4% were not identified.

A number of numerical scanlines were superimposed over the photographs, and the results obtained are also shown in tables 3.VIII to 3.XVII. The discontinuity spacing mean values and standard deviations are those measured along scanlines perpendicular to the discontinuity sets. It was found that 60% of sets had negative exponential spacing distributions, 21% were lognormal and 19% were not indentified. The mean trace length was calculated by the same two methods used in the program SCANL. For trace length, 54% of the sampled distributions were of negative exponential form, 28% were lognormal and 18% were not identified. It can also be seen in these tables that the type of termination was predomintly non-censored, i.e. the percentage of discontinuities with visible terminations was never less than 70%. This, together with the fact that trace lengths generally followed the negative exponential distribution, gave some indication that the use of equation (3.15), in estimating mean trace length, was a valid approach.

A typical graphical output produced by the PHOCOM program is shown in fig. 3.4. The rest of the plots are included in Appendix 1H. In these plots the properties of each discontinuity set were summarised in the form of histograms for discontinuity orientation spacing, trace length and semi-trace length, together with the graph for the estimation of mean trace length by the distribution independent method.

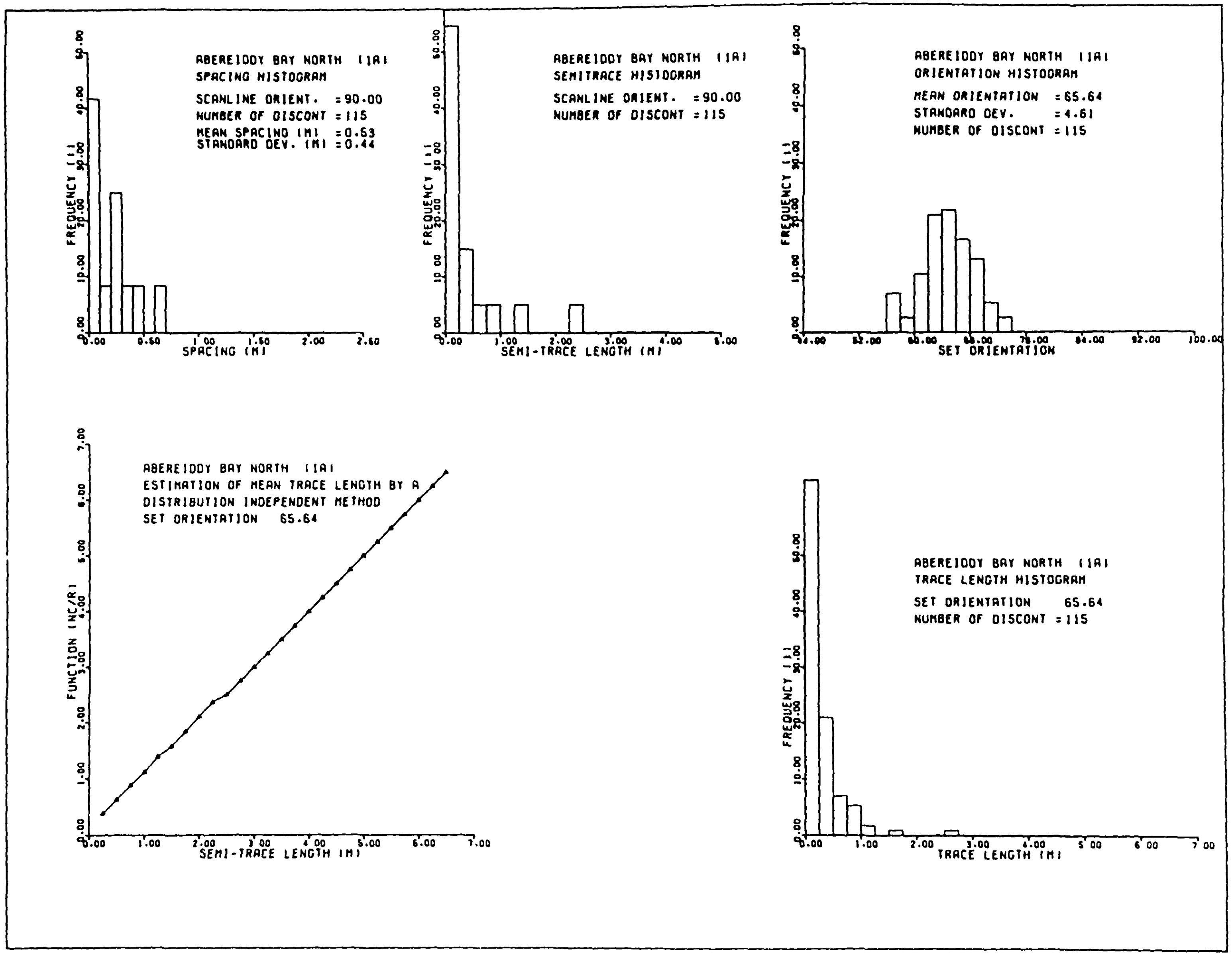

Fig. 3.4 Typical group of diagrams produced by the program PHOCOM

PHOTOGRAPH ANALYSIS

SITE NAME: ABEREIDDY BAY - NORTH   TOTAL No. OF DISCONT: 590

(1) FACE ORIENTATION: 50/338   (2) PHOTOGRAPH SIZE: (4.70, 3.40) m

	SET 1	SET 2(*)	SET 3(*)	SET 4
(3) MEAN ORIENTATION °	65.64	79.90	167.34	
S.DEV OF ORIENTATION	4.61	5.96	8.75	
(4) TYPE OF DISTRIBUTION	N	N	N	
MEAN TRACE LENGTH (m)	0.364	0.494	0.227	
S. DEV. OF TRACE LENGTH (m)	0.357	0.568	0.254	
(4) TYPE OF DISTRIBUTION	NE	NE	NE	
MEAN SPACING (m)	0.540	0.450	0.180	
S.DEV SPACING (m)	0.57	0.41	0.18	
(4) TYPE OF DISTRIBUTION	NE	LN	NE	
(a) MEAN TRACE LENGTH (m)	0.30	0.58	0.20	
(b) MEAN TRACE LENGTH (m)	0.30	0.52	0.20	
(4) TYPE OF DISTRIBUTION	NE	LN	NE	
DENSITY (m^{-2})	9.06	9.46	23.64	
TYPE OF TERMINATION %				
NON CENSORED	73.9	70.0	92.3	
ONE END CENSORED	24.3	22.5	7.7	
TWO ENDS CENSORED	1.8	7.5	0.0	

(1) FACE ORIENT: dip/dip direction (2) PHOTO SIZE (X-length, Y-length)

(3) ORIENTATION: is measured anti-clockwise from the horizontal axis

(4) TYPE OF DISTRIBUTION: N Normal, NE Negative Expontential, LN Log-normal, NI Not identified.

* Sets used in the Geometric Validation

TABLE 3.VIII

PHOTOGRAPH ANALYSIS

SITE NAME: MIDDLE MILL QUARRY 10   TOTAL No. OF DISCONT: 1040

(1) FACE ORIENTATION: 90/127   (2) PHOTOGRAPH SIZE: (9.88, 4.85) m

	SET 1	SET 2	SET 3	SET 4
(3) MEAN ORIENTATION °	180.31	92.27		
S.DEV OF ORIENTATION	5.35	9.26		
(4) TYPE OF DISTRIBUTION	N	N		
MEAN TRACE LENGTH (m)	0.507	0.346		
S. DEV. OF TRACE LENGTH (m)	0.706	0.353		
(4) TYPE OF DISTRIBUTION	LN	NE		
MEAN SPACING (m)	0.28	0.58		
S.DEV SPACING (m)	0.30	0.61		
(4) TYPE OF DISTRIBUTION	NE	NE		
(a) MEAN TRACE LENGTH (m)	0.80	0.30		
(b) MEAN TRACE LENGTH (m)	0.55	0.30		
(4) TYPE OF DISTRIBUTION	LN	LN		
DENSITY (m^{-2})	6.76	9.92		
TYPE OF TERMINATION %				
NON CENSORED	93.1	87.2		
ONE END CENSORED	6.3	12.6		
TWO ENDS CENSORED	0.6	0.2		

TABLE 3.IX

PHOTOGRAPH ANALYSIS

SITE NAME: MIDDLE MILL QUARRY 20 TOTAL No. OF DISCONT: 1343

(1) FACE ORIENTATION: 90/116 (2) PHOTOGRAPH SIZE: (3.50, 4.70) m

	SET 1	SET 2	SET 3	SET 4
(3) MEAN ORIENTATION °	88.63	178.57		
S.DEV OF ORIENTATION	8.69	5.77		
(4) TYPE OF DISTRIBUTION	N	N		
MEAN TRACE LENGTH (m)	0.243	0.291		
S. DEV. OF TRACE LENGTH (m)	0.284	0.457		
(4) TYPE OF DISTRIBUTION	NE	LN		
MEAN SPACING (m)	0.17	0.11		
S.DEV SPACING (m)	0.20	0.09		
(4) TYPE OF DISTRIBUTION	NE	NE		
(a) MEAN TRACE LENGTH (m)	0.26	-		
(b) MEAN TRACE LENGTH (m)	0.25	-		
(4) TYPE OF DISTRIBUTION	LN	-		
DENSITY (m^{-2})	31.98	32.83		
TYPE OF TERMINATION %				
NON CENSORED	90.1	90.4		
ONE END CENSORED	8.9	9.1		
TWO ENDS CENSORED	1.0	0.5		

TABLE 3.X

PHOTOGRAPH ANALYSIS

SITE NAME: TENBY (21E) TOTAL No. OF DISCONT: 653

(1) FACE ORIENTATION: 77/190 (2) PHOTOGRAPH SIZE: (5.20, 4.00) m

	SET 1	SET 2	SET 3	SET 4
(3) MEAN ORIENTATION °	88.75	178.68		
S.DEV OF ORIENTATION	6.20	6.62		
(4) TYPE OF DISTRIBUTION	N	N		
MEAN TRACE LENGTH (m)	0.697	0.236		
S. DEV. OF TRACE LENGTH (m)	0.617	0.272		
(4) TYPE OF DISTRIBUTION	LN	LN		
MEAN SPACING (m)	0.22	0.33		
S.DEV SPACING (m)	0.20	0.32		
(4) TYPE OF DISTRIBUTION	LN	NE		
(a) MEAN TRACE LENGTH (m)	0.52	0.27		
(b) MEAN TRACE LENGTH (m)	0.55	0.22		
(4) TYPE OF DISTRIBUTION	NE	NE		
DENSITY (m^{-2})	10.58	8.41		
TYPE OF TERMINATION %				
NON CENSORED	70.4	96.0		
ONE END CENSORED	25.0	3.4		
TWO ENDS CENSORED	4.6	0.6		

TABLE 3.XI

PHOTOGRAPH ANALYSIS

SITE NAME: TENBY (27E) TOTAL No. OF DISCONT: 869

(1) FACE ORIENTATION: 90/287 (2) PHOTOGRAPH SIZE: (8.70, 4.01) m

	SET 1	SET 2	SET 3	SET 4
(3) MEAN ORIENTATION °	73.87	149.46	175.54	
S.DEV OF ORIENTATION	5.12	2.86	9.59	
(4) TYPE OF DISTRIBUTION	N	N	-	
MEAN TRACE LENGTH (m)	0.591	0.212	0.271	
S. DEV. OF TRACE LENGTH (m)	0.505	0.189	0.465	
(4) TYPE OF DISTRIBUTION	LN	NE	-	
MEAN SPACING (m)	0.53	0.67	0.20	
S.DEV SPACING (m)	0.60	0.49	0.23	
(4) TYPE OF DISTRIBUTION	NE	-	NE	
(a) MEAN TRACE LENGTH (m)	0.62	-	0.33	
(b) MEAN TRACE LENGTH (m)	0.55	-	0.20	
(4) TYPE OF DISTRIBUTION	NE	-	-	
DENSITY (m^{-2})	8.88	2.69	13.95	
TYPE OF TERMINATION %				
NON CENSORED	75.7	96.7	96.5	
ONE END CENSORED	18.2	3.3	3.2	
TWO ENDS CENSORED	6.1	0.0	0.3	

TABLE 3.XII

PHOTOGRAPH ANALYSIS

SITE NAME: TENBY XE TOTAL No. OF DISCONT: 898

(1) FACE ORIENTATION: HORIZONTAL (2) PHOTOGRAPH SIZE:(2.65, 3.30) m

	SET 1	SET 2	SET 3	SET 4
(3) MEAN ORIENTATION °	86.41	179.69		
S.DEV OF ORIENTATION	8.37	6.18		
(4) TYPE OF DISTRIBUTION	N	N		
MEAN TRACE LENGTH (m)	0.172	0.204		
S. DEV. OF TRACE LENGTH (m)	0.189	0.206		
(4) TYPE OF DISTRIBUTION	NE	LN		
MEAN SPACING (m)	0.16	0.14		
S.DEV SPACING (m)	0.16	0.12		
(4) TYPE OF DISTRIBUTION	LN	NE		
(a) MEAN TRACE LENGTH (m)	0.18	0.31		
(b) MEAN TRACE LENGTH (m)	0.15	0.20		
(4) TYPE OF DISTRIBUTION	NE	LN		
DENSITY (m^{-2})	47.00	36.25		
TYPE OF TERMINATION %				
NON CENSORED	89.3	89.9		
ONE END CENSORED	9.9	9.5		
TWO ENDS CENSORED	0.8	0.6		

TABLE 3.XIII

PHOTOGRAPH ANALYSIS

SITE NAME: ST. BRIDES HAVEN (30F)   TOTAL No. OF DISCONT: 646

(1) FACE ORIENTATION: 90/227°   (2) PHOTOGRAPH SIZE: (3.28, 3.48) m

	SET 1	SET 2	SET 3	SET 4
(3) MEAN ORIENTATION °	179.37	79.02	125.67	
S.DEV OF ORIENTATION	6.49	7.63	8.42	
(4) TYPE OF DISTRIBUTION	N	N	N	
MEAN TRACE LENGTH (m)	0.331	0.334	0.122	
S. DEV. OF TRACE LENGTH (m)	0.378	0.359	0.095	
(4) TYPE OF DISTRIBUTION	NE	NE	LN	
MEAN SPACING (m)	0.11	0.47	0.70	
S.DEV SPACING (m)	0.09	0.43	0.57	
(4) TYPE OF DISTRIBUTION	LN	NE	-	
(a) MEAN TRACE LENGTH (m)	0.36	0.31	-	
(b) MEAN TRACE LENGTH (m)	0.30	0.35	-	
(4) TYPE OF DISTRIBUTION	LN	NE	-	
DENSITY (m^{-2})	28.71	9.57	6.29	
TYPE OF TERMINATION %				
NON CENSORED	87.3	78.7	94.4	
ONE END CENSORED	11.7	20.3	5.6	
TWO ENDS CENSORED	1.0	1.0	0.0	

TABLE 3.XIV

PHOTOGRAPH ANALYSIS

SITE NAME: ST. BRIDES HAVEN (31F)   TOTAL No. OF DISCONT: 827

(1) FACE ORIENTATION: 88/125   (2) PHOTOGRAPH SIZE: (4.60, 1.99) m

	SET 1	SET 2	SET 3	SET 4
(3) MEAN ORIENTATION °	117.69	91.83	176.79	
S.DEV OF ORIENTATION	8.03	8.06	8.16	
(4) TYPE OF DISTRIBUTION	N	N	-	
MEAN TRACE LENGTH (m)	0.163	0.173	0.265	
S. DEV. OF TRACE LENGTH (m)	0.128	0.166	0.385	
(4) TYPE OF DISTRIBUTION	LN	NE	LN	
MEAN SPACING (m)	0.51	0.40	0.09	
S.DEV SPACING (m)	0.60	0.48	0.09	
(4) TYPE OF DISTRIBUTION	NE	NE	NE	
(a) MEAN TRACE LENGTH (m)	0.13	0.12	0.17	
(b) MEAN TRACE LENGTH (m)	0.15	0.20	0.25	
(4) TYPE OF DISTRIBUTION	NE	NE	LN	
DENSITY (m^{-2})	16.39	16.71	39.87	
TYPE OF TERMINATION %				
NON CENSORED	92.7	86.9	94.0	
ONE END CENSORED	7.3	11.1	6.0	
TWO ENDS CENSORED	0.0	2.0	0.0	

TABLE 3.XV

PHOTOGRAPH ANALYSIS

SITE NAME: MARLOES SAND (35G)   TOTAL No. OF DISCONT: 569

(1) FACE ORIENTATION: 75/178   (2) PHOTOGRAPH SIZE: (1.0, 1.33) m

	SET 1	SET 2	SET 3	SET 4
(3) MEAN ORIENTATION °	65.07	108.32	138.39	181.84
S.DEV OF ORIENTATION	5.00	5.25	4.85	6.45
(4) TYPE OF DISTRIBUTION	N	N	N	N
MEAN TRACE LENGTH (m)	0.161	0.143	0.160	0.151
S. DEV. OF TRACE LENGTH (m)	0.158	0.128	0.164	0.149
(4) TYPE OF DISTRIBUTION	NE	NE	NE	NE
MEAN SPACING (m)	0.14	0.17	0.19	0.07
S.DEV SPACING (m)	0.11	0.13	0.17	0.07
(4) TYPE OF DISTRIBUTION	LN	NE	NE	NE
(a) MEAN TRACE LENGTH (m)	0.10	0.13	0.10	0.14
(b) MEAN TRACE LENGTH (m)	0.10	0.11	0.15	0.15
(4) TYPE OF DISTRIBUTION	NE	NE	NE	NE
DENSITY (m^{-2})	64.66	54.89	37.59	100.75
TYPE OF TERMINATION %				
NON CENSORED	73.3	82.2	82.0	79.8
ONE END CENSORED	24.4	17.8	14.0	19.4
TWO ENDS CENSORED	2.3	0.0	4.0	0.8

TABLE 3.XVI

PHOTOGRAPH ANALYSIS

SITE NAME: MARLOES SAND (36G) TOTAL No. OF DISCONT: 378

(1) FACE ORIENTATION: 75/178 (2) PHOTOGRAPH SIZE: (0.70, 0.99) m

	SET 1	SET 2	SET 3	SET 4
(3) MEAN ORIENTATION °	15.19	29.55	87.86	126.43
S.DEV OF ORIENTATION	5.39	3.25	6.89	6.71
(4) TYPE OF DISTRIBUTION	N	-	N	N
MEAN TRACE LENGTH (m)	0.117	0.092	0.097	0.094
S. DEV. OF TRACE LENGTH (m)	0.090	0.053	0.098	0.107
(4) TYPE OF DISTRIBUTION	NE	NE	NE	NE
MEAN SPACING (m)	0.09	0.11	0.06	0.34
S.DEV SPACING (m)	0.09	0.13	0.05	0.29
(4) TYPE OF DISTRIBUTION	NE	-	NE	-
(a) MEAN TRACE LENGTH (m)	0.10	-	0.06	-
(b) MEAN TRACE LENGTH (m)	0.10	1.10	1.10	-
(4) TYPE OF DISTRIBUTION	LN	NE	NE	-
DENSITY (m^{-2})	103.90	57.72	138.53	51.95
TYPE OF TERMINATION %				
NON CENSORED	73.6	80.0	79.2	88.9
ONE END CENSORED	25.0	17.5	20.8	11.1
TWO ENDS CENSORED	1.4	2.5	0.0	0.0

TABLE 3.XVII

3.2 Discontinuity Fabric Generator

A computer program, DICHA, was developed to generate, in two dimensions, a random discontinuity fabric using scanline and photographic data in the form explained above. The resulting fabrics, which can be presented both numerically and graphically, are similar to those presented by Hudson and La Pointe (1980), but differ in that they are interrogated numerically rather than by the electrical analogue methods adopted by Hudson and La Pointe. A fully numerical method has several advantages over the analogue method; the model is flexible, can be interrogated easily and can be extended to three dimensions.

The main assumptions of the program, additional to those listed earlier in this chapter, are as follows:

(i) The orientation of the lines representing each discontinuity set are assumed to be normally distributed about a given mean value.

(ii) The discontinuity trace lengths for each set are assumed to be one of the following probability density distributions:
   (a) negative exponential
   (b) uniform
   (c) log-normal

(iii) The apertures for each set are assumed to be either constant or to obey a log-normal distribution.

(iv) The number of discontinuities for each set is defined in terms of the discontinuity areal density, N: the number of discontinuity centres per unit area.

Random values from the appropriate probability density distributions are generated in order to produce randomly located discontinuities from each set within a given generation area. A more detailed explanation of the mathematics of the probability density distributions of the random generators is given in Appendix 2.

The process of generation is as follows: the location of each discontinuity centre is determined by two random numbers, generated from a uniform distribution, representing the cartesian coordinate of a discontinuity centre. The orientation of that discontinuity is determined by a random angle generated from a normal distribution. This angle is measured anti-clockwise from the horizontal axis. The trace length of the discontinuity is determined by the generation of a random length, from one of the three distributions listed earlier, as selected by the user. Finally the apertures are determined to be either constant or to take a random value generated from a log-normal distribution, again as specified by the user. The above explanation is summarised diagramatically in Fig. 3.5.

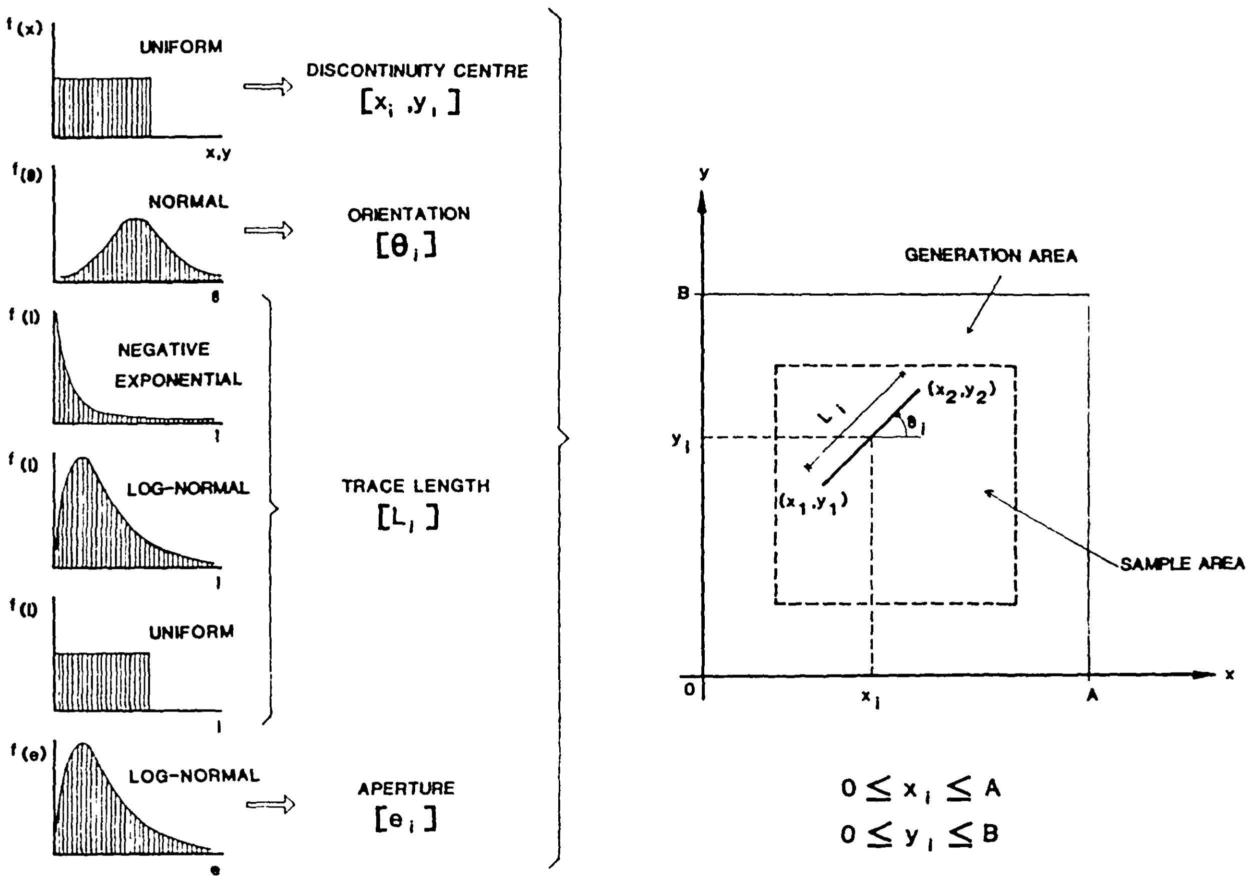

Fig. 3.5 The discontinuity mesh generation process

In this way all discontinuities belonging to a given set are generated consecutively. This is repeated for each set until all the sets have been generated. Although the program DICHA can handle up to 5 sets, each containing 2000 discontinuities, this maximum was rarely used because of restrictions imposed by the subsequent connectivity and flow analyses.

The program DICHA produces a numerical representation of a two-dimensional discontinuity mesh, recorded as the coordinates of the end points of each trace within a sample area, which, to minimise edge effect, is taken from only the central quarter of the generation area. The sample area can be interrogated using scanlines of any desired orientation. The following data can be obtained for the discontinuities intersected by each scanline:

(i) the mean semi-trace length, its standard deviation and type of frequency distribution for each set

(ii) the mean discontinuity spacing, its standard deviation and type of frequency distribution for each set and for all sets aggregated

(iii) analysis of censored semi-trace lengths for up to 20 censoring levels

(iv) actual mean and standard deviation values of discontinuity orientation, trace length and aperture.

A typical example of the graphical output is shown in Fig. 3.6.

Although the graphical output provides a visual impression of the discontinuity mesh, it is the numerical output that is of most value when studying the properties of this mesh. It is to this latter area that the remaining sections of this Chapter are devoted.

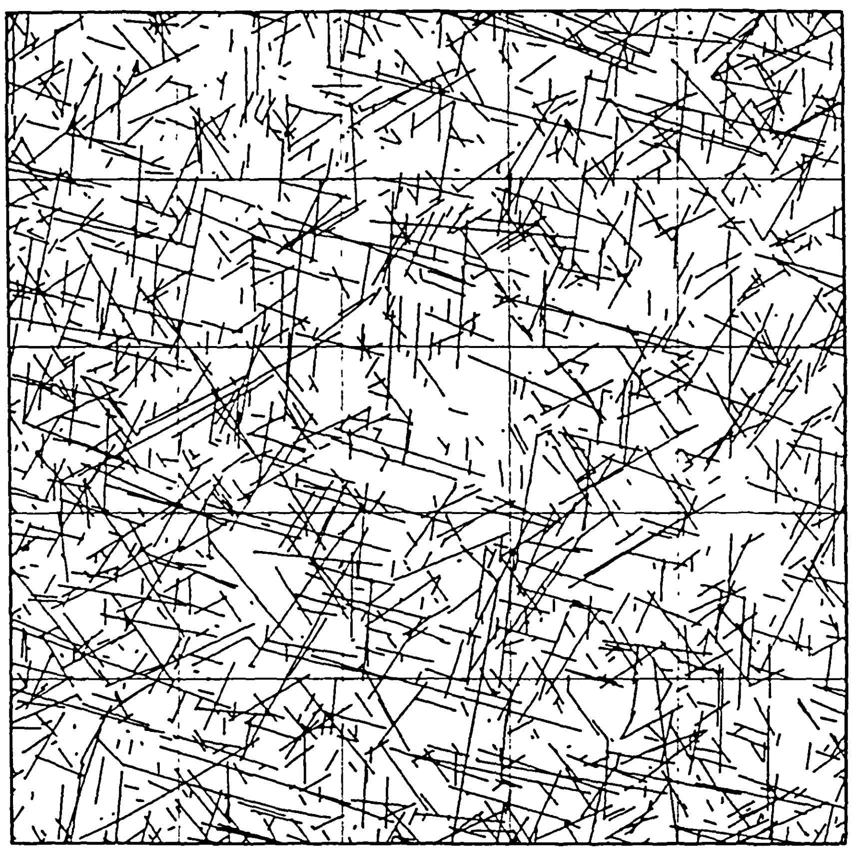

Fig. 3.6 Example of graphical output of mesh generator

3.3 The analysis of connectivity

The flow of water through the discontinuity mesh is controlled both by the connectivity and the conductance of the discontinuity traces. A program, DICONN, has been written to analyse the connectivity of the mesh generated by DICHA. The aim of this program is to identify the subset of discontinuities that are connected either directly, or through other discontinuities, to one or more of the geometrical boundary lines. This process, which is achieved by carrying out a systematic search of all discontinuities and all intersections points, greatly simplifies the subsequent flow calculations by removing all of the unconnected discontinuities. The user's instructions for the connectivity analysis program is given in Appendix 6 and the program listings in Appendix 7.

In order to begin an analysis of connectivity it is necessary to define the geometric boundary conditions of the zone under investigation. The approach used here is to define a square zone, known as the test area. This test area can cover any part, or alternatively the whole, of the sample area and can have any prescribed orientation. For the purposes of the search the four boundary lines are treated as discontinuities.

The search starts by numbering each of the m discontinuities present in the mesh and then finding all of the intersections of the ith discontinuity with any other discontinuity in the mesh, for i = 1 to m. This leads to the construction of a list of intersections, named JIN, and two other associated lists named JINQ and JINL described below. The list of intersections JIN is divided in blocks, each corresponding to the ith discontinuity. The contents of each block are the index numbers of the discontinuities intersected by the ith discontinuity. The list JINQ contains a pointer which indicates the initial position of each block within the list JIN. The other linked list JINL contains the length of each block, in other words the number of intersections made by the ith discontinuity, for i = 1 to m.

In order to speed the search for intersections, only those discontinuities with a higher index number than the ith discontinuity are analysed. In other words when the ith discontinuity is being analysed for intersections only the sub-set of discontinuities between i = i + 1 to m is considered. Simultaneously, a list of distances named SI, is being constructed. The SI list contains the distance from the lower end of the ith discontinuity to the intersection point, i = 1 to m,as shown in Figure 3.7(a). The SI list is also associated with the JINQ and JINL sets in the same way as the list of intersections JIN.

Any discontinuities that do not intersect any other, will automatically be excluded from the above lists. The "dead ends" that only intersect one discontinuity will also be excluded. Isolated discontinuity groups which form closed loops are, however, difficult to remove at this stage and are left to be dealt with later in the anaylsis.

(a)

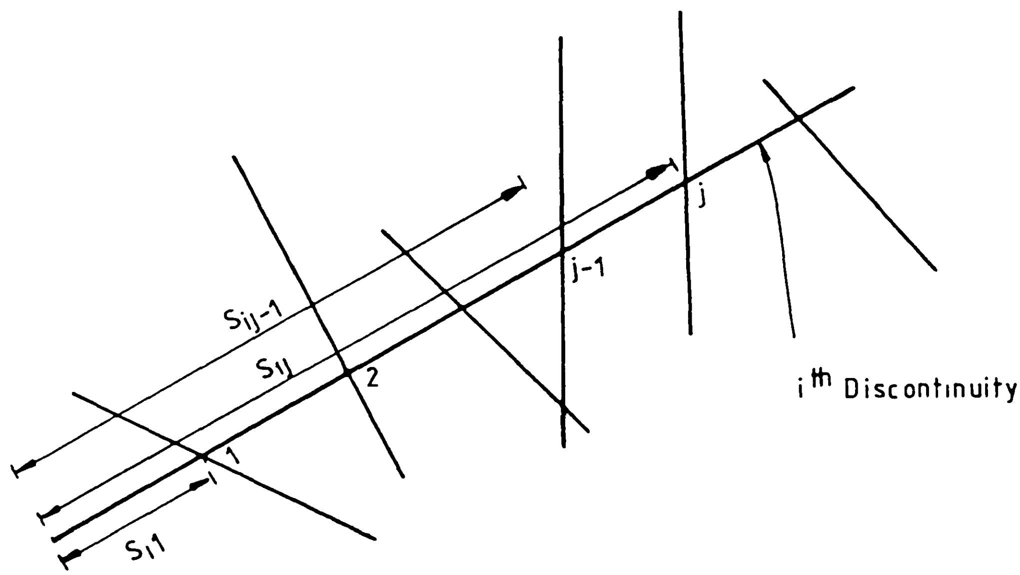

(b)

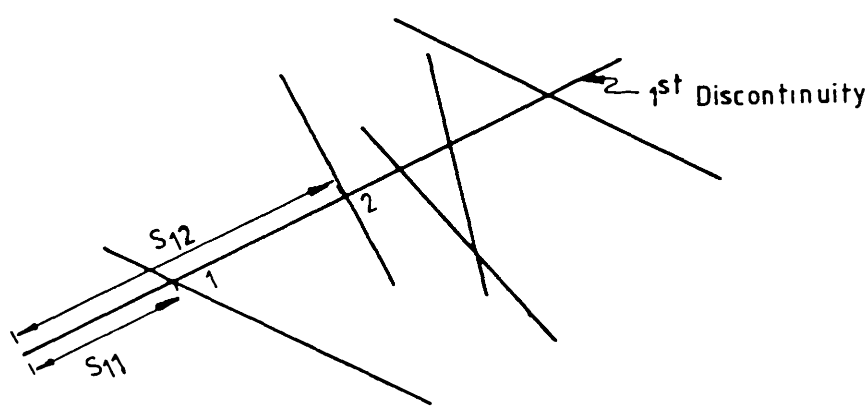

Fig. 3.7 Intersection distances and sorting of the distances

The next step is to sort the list of distances SI, into ascending order of length. Fig. 3.7(b) shows the form of SI after the sorting. The list of intersections must also be updated to allow for this re-ordering. Each of the intersection points is then assigned an index number, called the node number and stored in a list called KIN. The intersection between discontinuities i and k must, of course, have the same node number as the intersection between discontinuities k and i.

A path, or segment, is defined as the portion of a discontinuity that lies between two consecutive nodes. The sorted lists of intersections, distances and node numbers are then examined to determine the length of each segment. Each segment is then characterised by the node numbers at each end, the length of the segment, and the discontinuity on which it lies. This information is stored in lists named NODE, SL and JBL respectively. The list NODE is a two-dimensional array which contains the node numbers at each end of the segments. The lists of segments automatically exclude portions of single discontinuities terminating at a dead end.

The next step in the connectivity analysis is to examine the list NODE to construct lists of adjacent nodes and adjacent segments to the ith node, for i = 1, n; where n is the total number of nodes. This list of adjacent nodes, called NODCO, and the list of adjacent segments, called LINCO, are associated with two other lists called LINQ and LINL. The lists NODCO and LINCO are divided into blocks, each block corresponding to the ith node, for i = 1 to n. The contents of each block are the node numbers and segments numbers adjacent to the ith node. The list LINQ contains a pointer that indicates the initial position of each block within the lists NODCO and LINCO. The other list LINL contains the length of each block, i.e. the number of nodes or segments adjacent to the ith node, for i = 1 to n.

Isolated closed loops of discontinuities within the interconnected sample area are removed by tracing pathways from the boundary lines towards the centre of the sample area, each segment that is connected to any boundary is marked by a "flag" list. This procedure is continued towards the inner segments using the data on adjacent nodes and segments stored in the lists NODCO and LINCO. After completion of the search the only segments that are not marked by the 'flag' list are those that are isolated and therefore must be removed from the analysis. The resulting set of updated lists contains the necessary information to define the interconnected mesh. The analysis of connectivity is illustrated, using a simple example, in Fig. 3.8 which shows three discontinuity sets in an area 10 m square.

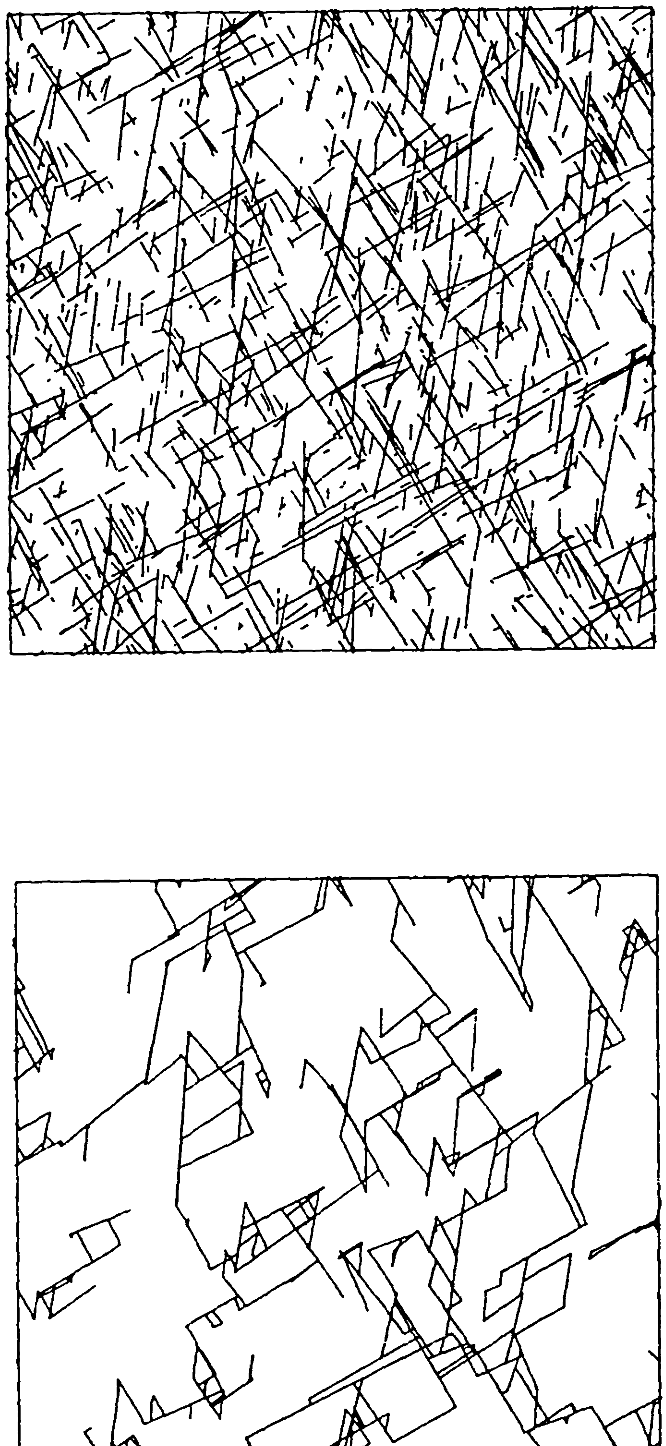

(a)

(b)

Fig. 3.8 An illustration of the connectivity analysis

3.4 The flow solution

A program DIFLOW was developed in order to analyse flow through the interconnected mesh. In the previous section the test area was defined by its geometric boundaries. To start the flow analysis it is necessary first to establish the hydraulic, or potential, boundary conditions. These should be such that the resultant average gradient is constant, in magnitude and direction, throughout the interconnected mesh. If this happens the behaviour of the mesh can be assumed to be similar to that of a homogeneous porous medium. Fig. 3.9 illustrates a typical potential distribution applied to the boundaries of a test area. Sides 1 and 4, which are the input and output lines respectively, carry constant potentials h_i and h_o respectively. The potentials on sides 2 and 3 are assumed to vary linearly between h_i and h_o. As the direction of the gradient is well controlled by the above hydraulic boundary conditions it is convenient to measure permeability in the direction of the gradient.

The flow of water through a mesh depends upon the conductance of the different discontinuities, which in turn is critically dependent upon their aperture. If it is assumed that discontinuities occur in a rigid, inert medium, then the conductance c of a smooth, parallel-walled, planar discontinuity of length ℓ, aperture e and width w is, for laminar flow, given by the standard equation:

$$c = \frac{ge^3 w}{12u\ell} \tag{3.18}$$

For the purposes of the flow analysis, the normal to each discontinuity is assumed to lie in the plane of the two-dimensional network. Although this approach ignores the three dimensional nature of the discontinuity fabric it does greatly simplify the calculations by effectively restricting the analysis to the plane of the network. In this case it is usually convenient to take the width, w, of each discontinuity as unity. The aperture of each discontinuity was generated by the method explained in Section 3.2. Equation (3.18) was then used to calculate the conductance of each discontinuity segment.

A fall in potential (or head loss) Δh over a length ℓ of a discontinuity segment of conductance c causes a quantity Q of fluid to flow per unit time, where Q is given by:

$$Q = c\,\Delta h \tag{3.19}$$

Assuming that there is no head loss due to turbulence at the nodes, and imposing the constraint that the flow into any given node should be equal to the flow out, it is possible to construct a series of linear simultaneous equations of the following form:

$$h_i = \frac{\sum c_{ij}\, h_j}{\sum c_{ij}} \tag{3.20}$$

where h_i and h_j are the potentials at nodes i and j, and c_{ij} is the conductance of the discontinuity segments linking these nodes. The subscript i indicates any internal node; the subscript j refers to any internal or boundary node. The potentials at the internal nodes form the unknowns; the potentials at the boundaries are fixed, as explained earlier.

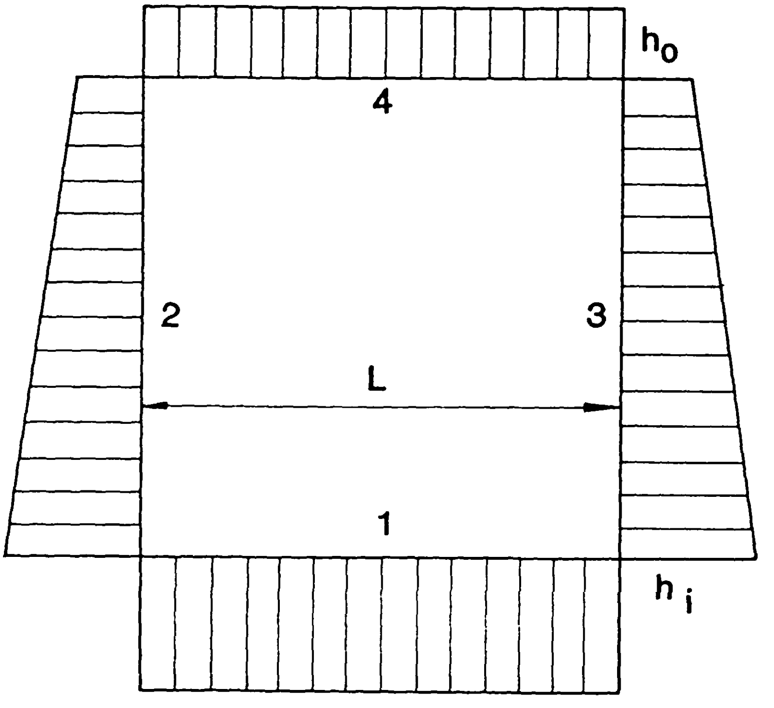

Fig. 3.9 Boundary potential distribution applied to a test area

Assuming that there are n internal nodes, then the n necessary equations are constructed, as shown in equation (3.20), with the assistance of the information passed by the connectivity analysis program DICONN. This information is provided on lists, NODCO, LINCO, LINQ and LINL. A list containing the discontinuity apertures, OPE, is also generated for this stage of the analysis.

The solution of the system of linear simultaneous equations was approached by two different methods; a relaxation method incorporating an over-relaxation factor and the bi-factorisation method.

The relaxation method is an iterative technique which can be applied in conjunction with an over-relaxation factor to accelerate the convergence. The iteration is carried out around each internal node by using the following equation:

$$h_i \cong \frac{\sum c_{ij}\, h_i}{\sum c_{ij}} F + (1-F)h_i \qquad (3.21)$$

where the summation is over all nodes and segments connected to node i, F is the over-relaxation factor and $\cong$ means "replaced by". Obviously, before starting the iteration some arbitrary initial values have to be assigned to all of the potentials at the internal nodes. The iterations are carried out until the residual, as calculated by equation (3.22), falls below a given value.

$$\text{Residual} = \sqrt{\frac{\sum(h_i - h_i^*)^2}{\sum(h_i^* - h_o)^2}} \qquad (3.22)$$

Here h_i^* is the potential at node i in the preceeding iteration and h_o is a fixed potential value, usually taken to be equal to the potential at the output boundary. This approach, although relatively slow, had the advantages of not necessitating the storage of the whole coefficient matrix at any one time in the core memory and also of allowing the solution of systems of non-linear equations in cases where the flow was non-laminar.

It was found that for small numbers of discontinuities (up to about 300), with an over-relaxation factor between 1.7 and 1.80, the relaxation method gave an acceptable solution, with a flow closing error of less than 0.1 mm^3/s. However, when a larger number of discontinuities was analysed it was found that the convergence slowed and the flow closing error increased significantly. This, together with a dramatic increase in computing time, hence cost, made the relaxation method unsatisfactory. In order to overcome this difficulty an alternative method of solution was sought.

A technique known as the bi-factorisation method was employed to increase the efficiency of equation solution. This method, which is fully explained by Zollenkopf (1971), is described in Appendix 3. The main characteristics of the method are summarized below:

(i) The method is appropriate for sparce coefficient matrices that have non-zero diagonal terms and that are either strictly symmetrical or alternatively asymmetrical in element value, but with a symmetrical sparscity structure. The matrix should be diagonally dominant.

(ii) Small memory requirements and short computation time can be achieved because only the non-zero terms of the matrix are stored and processed. This is possible because the method employs a single re-ordering strategy that requires comparatively little additional computation.

(iii) The method does not require any index renumbering or re-arrangement of the matrix terms. The method also allows repeated solutions for different load vectors without repeating the reduction process.

Analyses utilising the bi-factorisation solver typically cost approximately one third of those solved by the relaxation method.

When the potentials at the internal nodes have been solved, it is possible to calculate the flow volumes through each discontinuity in the interconnected network using equation (3.19) and also, to evaluate the total flow volumes accross each boundary line. A positive value of flow volume indicates that there is inflow into the test area; a negative flow volume is an outflow. The summation of the flow volumes accross all the boundaries should be zero. This provides a basis for checking the accuracy and precision of the numerical calculations; any deviation from zero is called the 'closing error'. The user's instructions of the program DIFLOW are given in Appendix 6 and the program listing in Appendix 7.

3.5 Equivalent Permeability Tensor

The permeability of a continuous medium that is hydraulically equivalent, on a macroscopic scale, to the discontinuity network can be determined by averaging the separate discontinuity flow volumes over some specified area covered by the network. One approach to this is to consider the total flow Q_i across a boundary, orientated parallel to the x_j direction, of area A_j. The macroscopic flow velocity is given by

$$V_i = Q_i / A_j \tag{3.23}$$

The relation between flow velocity and equivalent permeability can be expressed in terms of the generalised form of Darcy's Law, in tensor notation, as follows:

$$V_i = K_{ij} \frac{\delta h}{\delta x_j} \tag{3.24}$$

where K_{ij} is the permeability tensor, h is the hydraulic potential and the repeated subscript implies summation.

The sample area is a square of side length L, within the network, subjected to the boundary potentials h_i and h_o as shown in Fig. 3.9. If the potential is initially directed in the x_1 direction, then

$$\frac{\delta h}{\delta x_1} = \frac{(h_i - h_o)}{L} \quad \text{and} \quad \frac{\delta h}{\delta x_2} = 0 \tag{3.25}$$

From equations (3.230, (3.24) and (3.25)

$$K_{11} = \frac{Q_1}{(h_i - h_o)} \quad \text{and} \quad K_{21} = \frac{Q_2}{(h_i - h_o)} \tag{3.26}$$

The other terms of the permeability tensor, K_{22} and K_{12}, can be found in a similar way by applying a hydraulic gradient in the x_2 direction. Although this approach is appealing in its simplicity, the results obtained are highly sensitive to the location of the boundaries (Long, 1983). Indeed, boundaries on opposite sides of a network can give permeabilities which differ by one, or even two, orders of magnitude. This problem is illustrated in the simple example shown in Fig. 3.10.

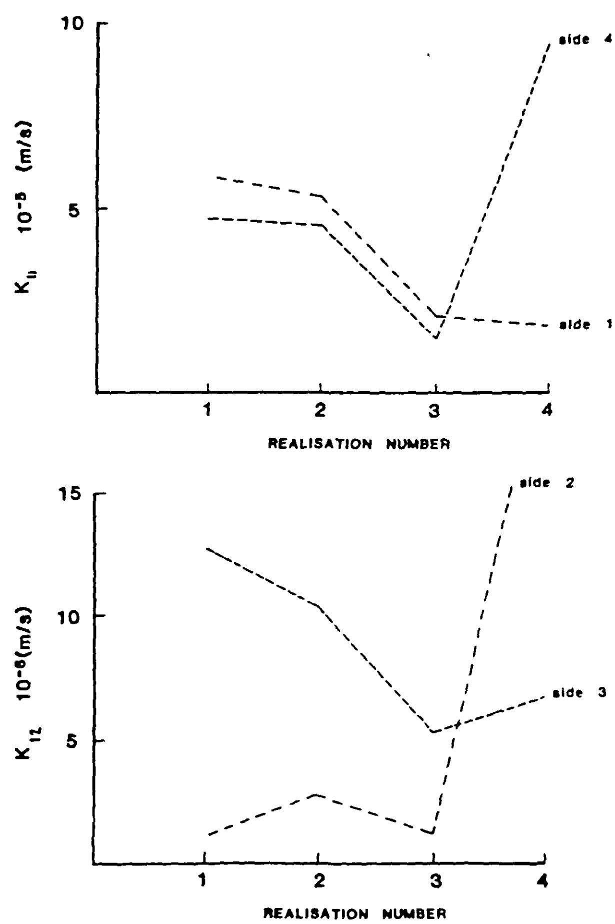

Fig. 3.10 Permeability tensor components, K_{11} and K_{12}, vs. realisation number for two opposite sides of a discontinuity network

A second approach to determining the equivalent permeability tensor is to consider instead the flow along the discontinuity segments between each of the nodal points within the network. If the flow velocity along the m^{th} discontinuity segment is V_m, the average macroscopic flow velocity V_i (here termed the specific discharge) in the direction x_i for a square sample area of side length L and unit width, containing n discontinuity segments is given by

$$\overline{V}_i = \frac{1}{L^2} \sum_{m=1}^{n} V_m \cos \Theta_{im} \, e_m \, \ell_m \qquad (3.27)$$

Where Θ_{im} is the angle between the m^{th} discontinuity segment and the x_i direction, e_m is the aperture of the discontinuity segment and ℓ_m its length. The cosine term simply gives the component of flow velocity in the direction x_i.

The quantity of flow q_m in the m^{th} discontinuity segment, per unit width, is given by

$$q_m = V_m \cdot e_m \qquad (3.28)$$

Using this expression to substitute for $V_m \cdot e_m$ in equation (3.27) gives

$$\overline{V}_i = \frac{1}{L^2} \sum_{m=1}^{n} q_m \cos \Theta_{im} \, \ell_m \qquad (3.29)$$

If the components of the specific discharge vector $\overline{V}_i$ are equated with V_i in equation 3.24, then the permeability tensor K_{ij} is determined by

$$K_{ij} = \frac{\overline{V}_i}{\delta h / \delta x_j} \qquad i,j = 1,2,3 \qquad (3.30)$$

The equivalent permeability tensor in two-dimensions, can be determined by carrying out two tests; the first with the hydraulic gradient in the x_1 direction; the second with the gradient in the x_2 direction. These are respectively:

$$K_{11} = \overline{V}_1 L/(h_i - h_o) \text{ and } K_{21} = \overline{V}_2 L/(h_i - h_o)$$

$$K_{22} = \overline{V}_2 L/(h_i - h_o) \text{ and } K_{12} = \overline{V}_1 L/(h_i - h_o) \qquad (3.31)$$

Since the results do not depend explicitly upon the locations of the boundaries of the test area, a better measure of equivalent permeability is obtained.

One of the constraints imposed upon the flow within the network is that there is no net loss or gain of fluid. Cundall (1983) has shown that, since this implies that the net flow into all internal nodes is zero, the flow quantities along all internal discontinuity segments can be omitted from the summation in equation (3.29). The summation is therefore limited to discontinuity segments that have at least one node on the boundary of the network. The following equation gives the same $\overline{V}_i$ as equation (3.29), by considering only the boundary flow volumes. A full derivation is given in Appendix 4.

$$\overline{V}_i = \frac{1}{L^2} \sum_{n=1}^{B} (x_i \; q) \qquad (3.32)$$

Where q is the flow volume across the boundary at the ith node of coordinates x_i and the summation is carried out over B, the total number of nodes at the boundaries. Computations on idealised and also random network geometries have shown that this simplification is entirely valid.

For complex networks, the permeability tensor found by equations (3.26) will differ from that based upon the summation of boundary discharge components (equation 3.31). However, for networks with extensive discontinuities the permeability tensor found by the two approaches will be equal and also symmetrical. Equation (3.26) does, however, ignore certain aspects of the flow regime. In particular, by assuming that a boundary is normal to a given discontinuity segment, any lateral component of fluid velocity is ignored. Since this makes equation (3.26) inaccurate permeability calculations in the remainder of this work will be based only upon the summation of boundary discharge components.

3.6 Validation of the model

A validation of the model by three different approaches was undertaken. The first, a geometrical validation, was undertaken to investigate how well the generated mesh represented the actual discontinuity characteristics in two-dimensions. The second, a numerical validation, was performed in order to verify the numerical algorithum used in calculating fluid flow and the permeability tensor. Finally a flow validation was undertaken to evaluate how well the predicted values of inflow, gradient distribution and permeability compared with values measured in the field. The geometrical and numerical validations are presented in the next two sections. The flow validation is presented in the form of a practical application of the model in Chapter 4. The above validations are summarized diagramatically in Fig. 3.11.

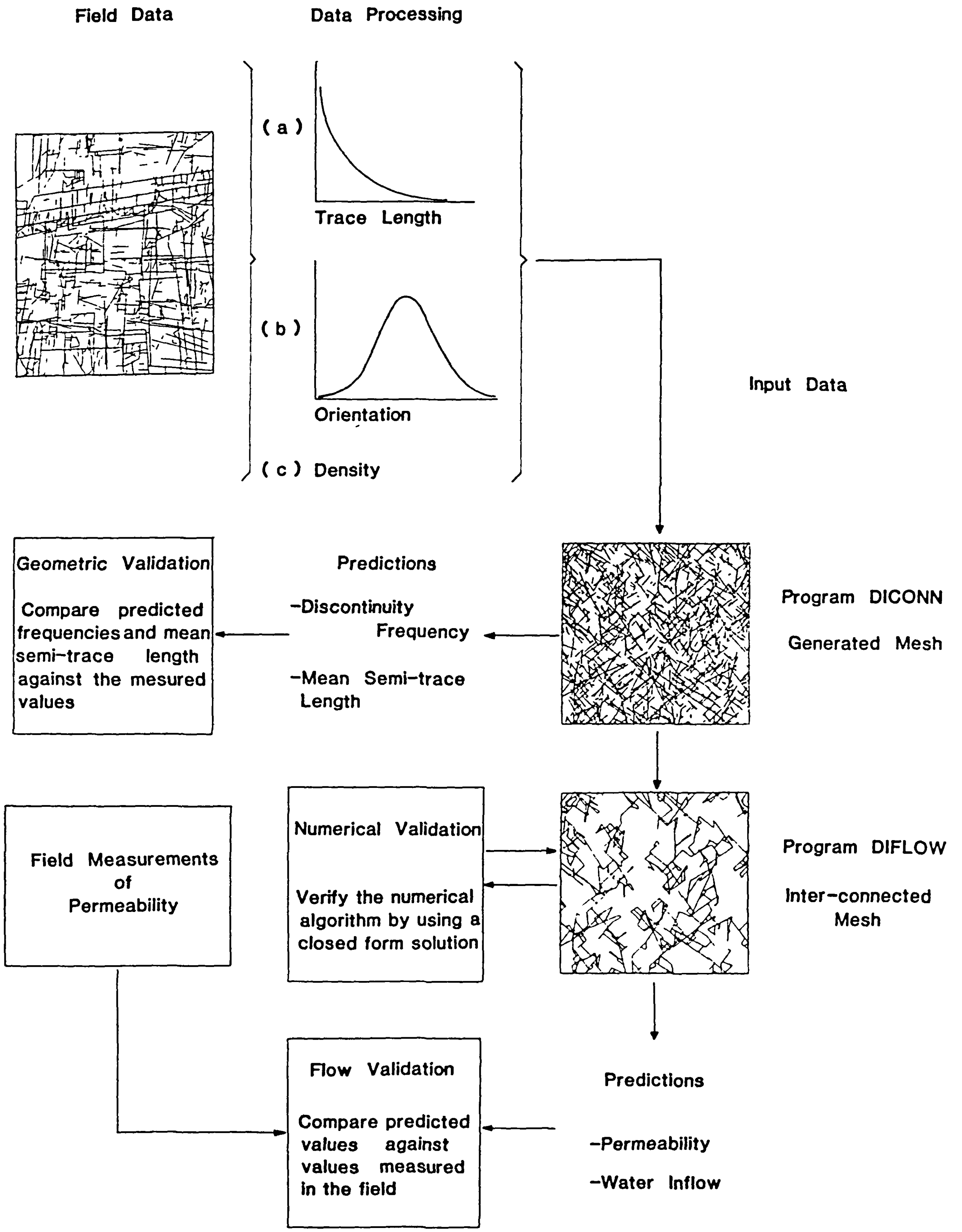

Fig. 3.11 Methodology for the validation of the model

3.6.1 Geometrical validation

In order to perform the geometrical validation discontinuity data from two of the sites in the Pembrokeshire area were selected. These comprised scanline and photographic data from Abereiddy Bay, which was an abandoned quarry, and Middle Mill, an operational quarry. The processed field measurements provided the necessary input data for the mesh generator program. For each site ten different mesh realisations were generated, and their mean values of orientation, trace length, semi-trace length and discontinuity frequency were calculated using several superimposed scanlines. These results were compared with those obtained from the networks traced from the photographs. Additionally the discontinuity frequency for each set, measured at the rock exposure by the scanline method, was first rotated to the plane of the rock face and then compared with the frequencies obtained from the photographic and numerically generated meshes. The results of these comparisons are shown in Tables 3.XVIII and 3.XIX.

It can be seen that agreement is not complete between the predicted and the measured discontinuity frequency values. The main reason for this is that the model generates an homogeneous density of discontinuity centres over the entire sample area that does not take account of the local variability of density of discontinuity centres on the actual rock face. This effect can clearly be seen in Figs 3.12, 3.13. There is, however, a reasonable agreement between the predicted and measured values of mean orientation and mean trace length. It is believed that a better agreement for discontinuity frequency would be achieved if the local variability of the intensity of discontinuity centres could be allowed for. Workers such as La Pointe and Hudson (1984) and Miller (1979) have proposed a promising geostatistical approach to this problem.

(a)

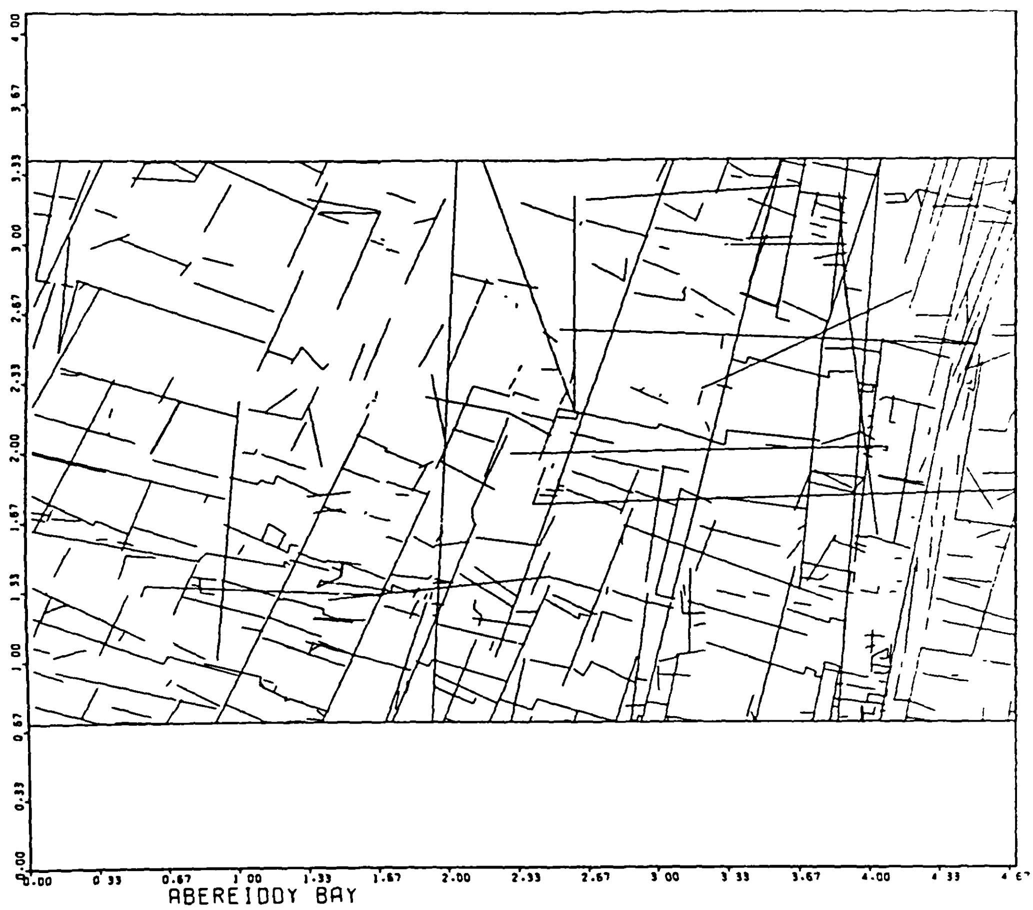

(b)

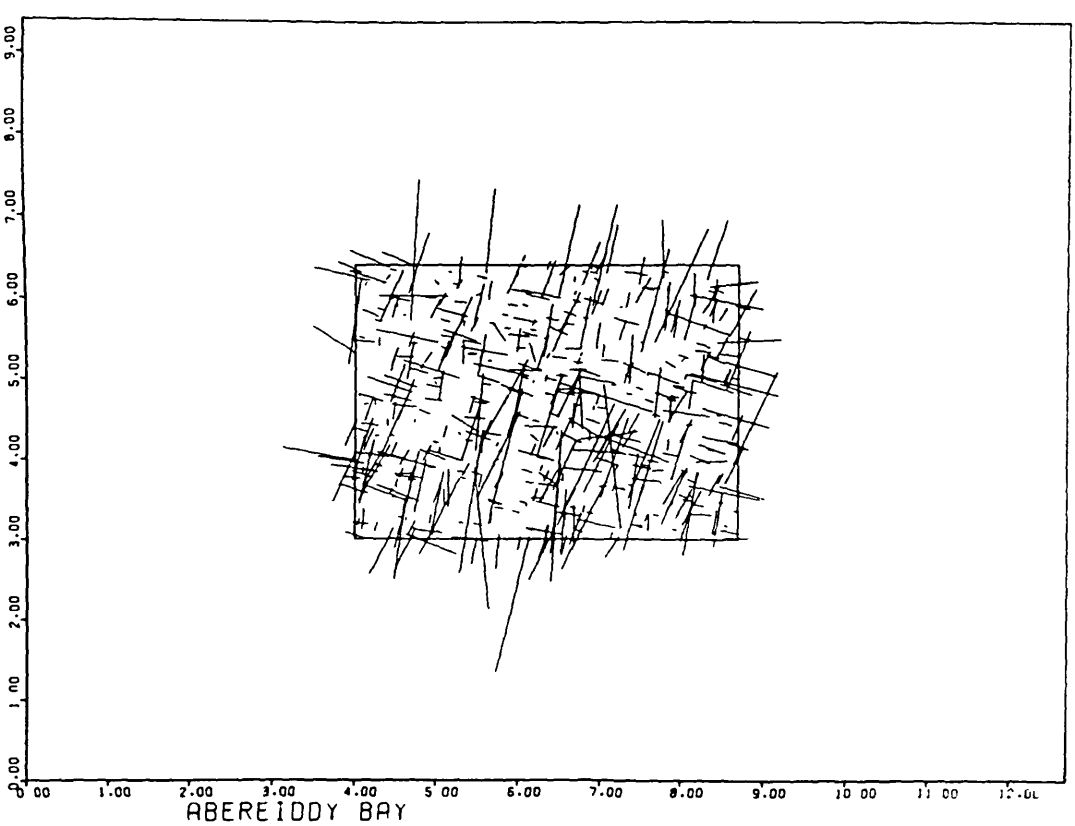

Fig. 3.12 (a) Photographic mesh and (b) generated mesh of a rock exposure in Abereiddv Bay-North, Pembrokeshire

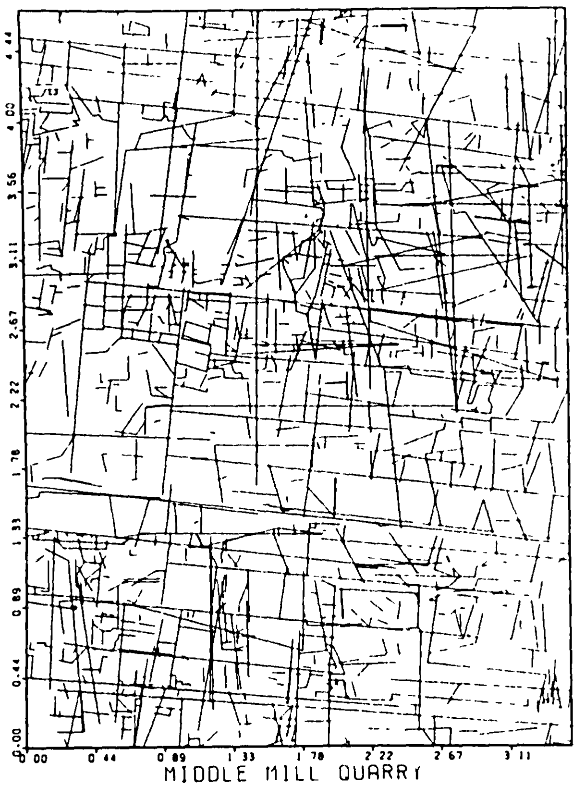

(a)

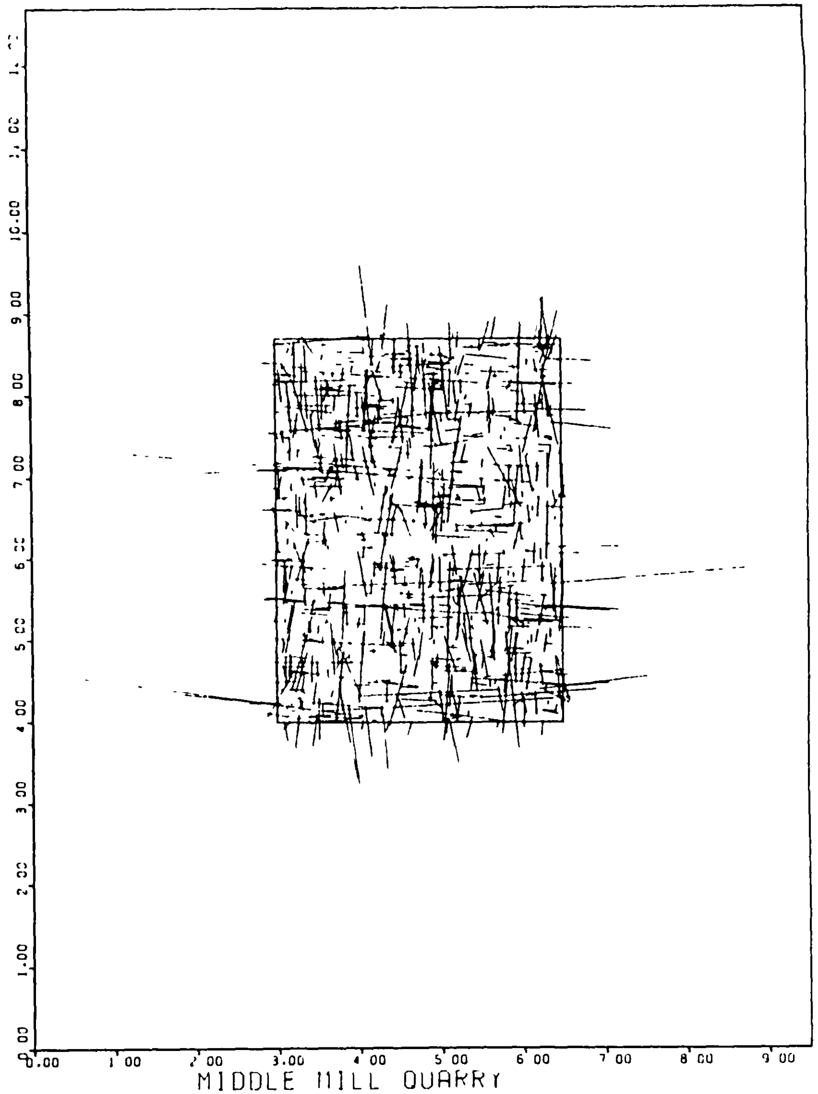

(b)

Fig. 3.13 (a) Photographic mesh and (b) generated mesh of a rock exposure in Middle Mill Quarry, Pembrokeshire

ABEREIDDY BAY NORTH (GEOMETRICAL VALIDATION)

		SET 1	SET 2	SET 3
MEAN ORIENTATION:	(a)	65.64°	79.90°	167.34°
	(b)	65.47°	79.90°	167.31°
MEAN TRACE LENGTH (m):	(a)	0.364	0.494	0.227
	(b)	0.348	0.502	0.213
DISCONTINUITY FREQUENCY (m^{-1})	(a)	1.85	2.22	5.55
	(b)	1.18	2.10	3.69
	(c)	1.22	4.70	-
DENSITY (m^{-2}):	(a)	9.06	9.46	23.64
	(b)	6.35	7.15	18.96

(a) measured along scanlines superimposed on the photographic mesh

(b) measured along scanlines superimposed on the generated meshes (mean value)

(c) measured along the field scanlines

Table 3.XVIII

MIDDLE MILL QUARRY (GEOMETRICAL VALIDATION)

		SET 1	SET 2
MEAN ORIENTATION:	(a)	83.63°	178.57°
	(b)	88.59°	178.55°
MEAN TRACE LENGTH (m):	(a)	0.243	0.291
	(b)	0.255	0.275
DISCONTINUITY FREQUENCY (m^{-1})	(a)	5.88	9.09
	(b)	3.58	7.51
	(c)	2.69	-
DENSITY (m^{-2}):	(a)	31.98	32.83
	(b)	30.50	33.94

Table 3.XIX

3.6.2 Numerical Validation

A validation process was applied to the program DIFLOW in order to verify that the numerical algorithums used to calculate fluid flow and the permeability tensor were correct. For this purpose geometrically regular meshes containing persistent discontinuity sets were analysed, Fig. 3.14. Although the theory for calculating the permeability of meshes of this type has been presented by workers such as Snow (1965), Parsons (1966) and Cundall (1983), a brief explanation of the analysis presented by Cundall (1983) is included here to provide some background.

In a preceding section, the following equation for the average flow velocity was formulated:

$$\overline{V}_i = \frac{1}{L^2} \sum_{m=1}^{n} q_m \cos \Theta_{im} \ell_m \tag{3.33}$$

Where Θ_{im} is the angle between the mth discontinuity segment and the x_i direction, e_m is the aperture of the discontinuity segment and ℓ_m its length. L is the side length of the sample area.

The flow in the mth discontinuity segment, q_m, can be expressed as

$$q_m = \Delta h c_m \tag{3.34}$$

Here Δh is the drop in potential head and c_m the conductance of the mth segment. The conductance is given by:

$$c_m = \frac{g\ e_m^3}{12\,\nu \ell_m} \tag{3.35}$$

For a persistent discontinuity it is assumed that the head drop is linearly proportional to the distance along the flow channel

$$\Delta h = \frac{\delta h}{dx_i} \ell_{im} \tag{3.36}$$

where ℓ_{im} is the component of the discontinuity segment in the direction x_i.

Using equations (3.35)and (3.36) to substitute for c_m and Δh in equation (3.34) and noting that $\ell_{im}/\ell_m = \cos\ \Theta_{im}$.

$$q_m = \frac{g\ e_m^3}{12\,\nu} \cos\ \Theta_{im} \frac{\delta h}{\delta x_i} \tag{3.37}$$

Substituting this expression for q_m into equation (3.33) gives

$$\overline{V}_i = \frac{g}{12\,\nu\,L^2} \frac{\delta h}{\delta x} \sum_{m=1}^{n} e_m^3 \operatorname{Cos}\ \Theta_{im} \operatorname{Cos}\ \Theta_{jm}\ \ell_m \tag{3.38}$$

But Darcy's Law

$$V_i = K_{ij} \frac{\delta h}{\delta x_j} \tag{3.39}$$

equating equations (3.38) and (3.39) gives

$$K_{ij} = \frac{g}{12\,\nu\,L^2} \sum_{m=1}^{n} e_m^3 \operatorname{Cos}\ \Theta_{im} \operatorname{Cos}\ \Theta_{jm}\ \ell_m \tag{3.40}$$

The contribution to permeability tensor of the mth discontinuity that transects the entire sample area is, according to equation (3.40), given by:

$$K_{ij}^{m} = \frac{g\ e_m^3}{12\,\nu L} \operatorname{Cos} \Theta_{im} \operatorname{Cos} \Theta_{jm} \tag{3.41}$$

If a discontinuity set comprises parallel extensive discontinuities of identical aperture, e, each with the same spacing, $1/\lambda$, then the number of discontinuities intersecting one side of the square sample area is given by λL. The contribution of such a discontinuity set to the overall permeability tensor is given by

$$K_{ij}^{s} = \frac{g\ e^3 \lambda}{12\,\nu} \operatorname{Cos} \Theta_i \operatorname{Cos} \Theta_j \tag{3.42}$$

When more than one discontinuity set is present, the contributions derived from equation (3.42) are summed for each set in order to obtain the overall permeability tensor.

A discontinuity of mesh containing two orthogonal sets, of parallel, evenly spaced, persistent discontinuities of equal aperture, shown in Fig. 3.14, was constructed for the numerical validation of the model. Table 3.XX summarises the characteristics of the two sets.

	SET 1	SET 2
Orientation	Arc tan ($^3/_1$)	Arc tan ($^1/_{-3}$)
Aperture (e)	1.0×10^{-6}m	2.0×10^{-6}m
Spacing ($1/_\lambda$)	0.949m	0.949m

Table 3.XX

The sample area was a square of 9.0m side length. From equation (3.42) the contributions of each set to the permeability tensor can be calculated as follows:

$$R_1 = \frac{g\ e_1^3\lambda_1}{12\nu} = 0.68125 \times 10^{-12} \text{ m/s}$$

$$R_2 = \frac{g\ e_2^3\lambda_2}{12\nu} = 5.45 \times 10^{-12} \text{ m/s}$$

Where $\nu = 1.2 \times 10^{-6}$ m^2/s and g = 9.81 m^2/s then

$$K_{11} = R_1 \left[\frac{1}{\sqrt{10}} \quad \frac{1}{\sqrt{10}}\right] + R_2\left[\frac{-3}{\sqrt{10}} \quad \frac{-3}{\sqrt{10}}\right]$$

$$K_{12} = R_1 \left[\frac{1}{\sqrt{10}} \quad \frac{3}{\sqrt{10}}\right] + R_2\left[\frac{-3}{\sqrt{10}} \quad \frac{1}{\sqrt{10}}\right]$$

$$K_{21} = R_1 \left[\frac{3}{\sqrt{10}} \quad \frac{1}{\sqrt{10}} \right] + R_2 \left[\frac{1}{\sqrt{10}} \quad \frac{-3}{\sqrt{10}} \right]$$

$$K_{22} = R_1 \left[\frac{3}{\sqrt{10}} \quad \frac{3}{\sqrt{10}} \right] + R_2 \left[\frac{1}{\sqrt{10}} \quad \frac{1}{\sqrt{10}} \right]$$

which gives

$$\begin{aligned} K_{11} &= 5.242134 \times 10^{-12} \\ K_{12} &= -1.508011 \times 10^{-12} \\ K_{21} &= -1.508011 \times 10^{-12} \\ K_{22} &= 1.220771 \times 10^{-12} \end{aligned} \qquad (3.43)$$

These four terms are the components of the theoretical permeability tensor for the mesh shown in Fig. 3.14.

The program DIFLOW was then applied to the network to calculate the flows across the boundaries and the permeability tensor. The hydraulic potentials applied to the boundaries were h_i = 10 m and h_o = 1 m.

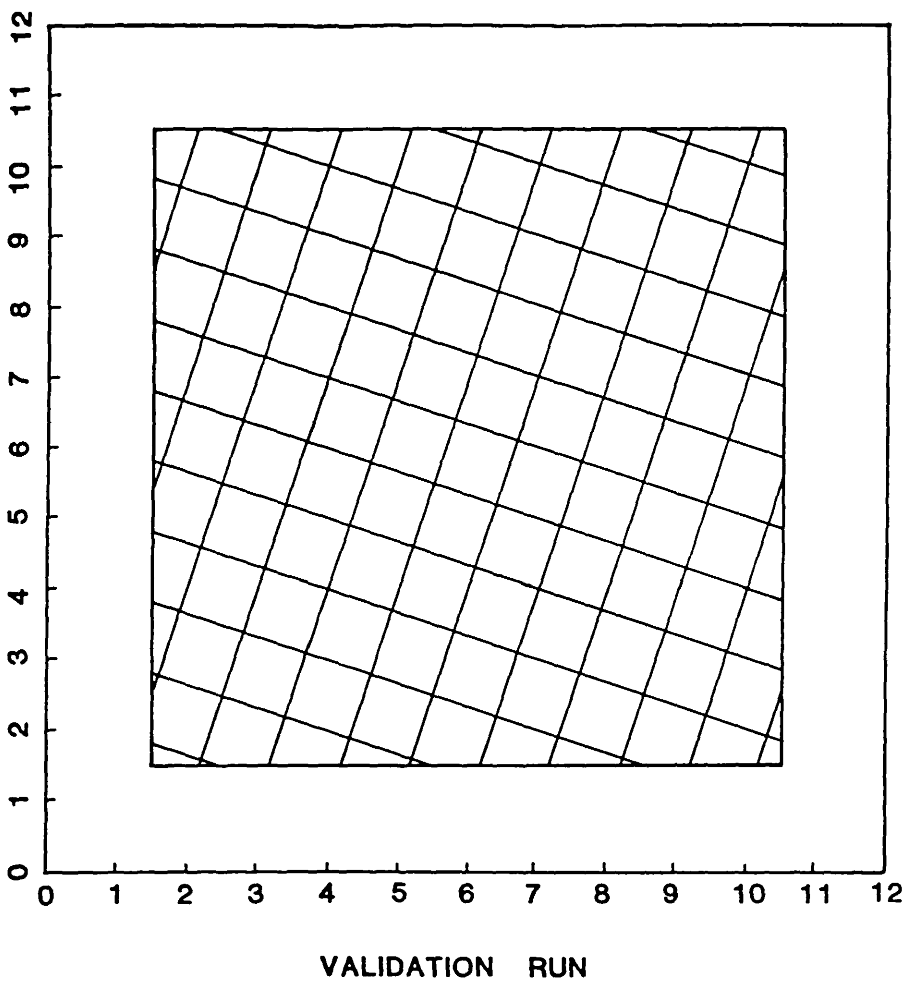

Fig. 3.14 Discontinuity mesh with two orthogonal persistent discontinuity sets for the numerical validation of the program DIFLOW

Two tests were carried out, the first with the gradient in the x_1 direction and the second with the gradient in the x_2 direction, as shown in Fig. 3.15. The results obtained are summarized in tables 3.XXI and 3.XXII.

Side	Flow rate $m^3/s \times 10^{-11}$	
	Gradient in x_1 direction	Gradient in x_2 direction
1	- 1.357210	1.098694
2	4.717921	- 1.357210
3	- 4.717921	1.357210
4	1.357210	- 1.098694

Table 3.XXI

Negative flow rates indicate that the flow is directed out of the test area

Component	Permeability tensor $m/s \times 10^{-12}$	
	Gradient in x_1 direction	Gradient in x_2 direction
K_{11}	5.242134	—
K_{12}	—	- 1.508011
K_{21}	- 1.508011	—
K_{22}	—	1.220771

Table 3.XXII

Comparing the results in table 3.XXII with those in equation (3.43) confirms that the permeability tensor components obtained by the program DIFLOW are equal to those calculated from standard theory. An additional check can be performed by assuming that a mesh containing persistent discontinuity sets behaves like an anisotropic continuous medium. This assumption has been made by many authors, such as Snow (1968), Parsons (1966) and Long (1983).

From Darcy's Law

$$V_i = K_{ij} \frac{\delta h}{\delta x_j} \tag{3.44}$$

Taking equations (3.25) and (3.26) and applying a hydraulic gradient first in the x_1 direction and then in the x_2 direction gives

$$\frac{\delta h}{\delta h_1} = h_i - h_o \,/_{L} = 1.0 \qquad \text{and} \qquad \frac{\delta h}{\delta x_2} = 0$$

$$\frac{\delta h}{\delta x_1} = 0 \quad \text{and} \quad \frac{\delta h}{\delta x_2} = h_i - h_o \,/_{L} \tag{3.45}$$

The flow quantity per unit thickness, Q_i, that passes across a boundary that is normal to x_1 is given by

$$Q_i = V_i \; L \tag{3.46}$$

Using equations (3.45) and (3.46) to substitute for $\frac{\delta h}{\delta x_j}$ and V_i in equation (3.44) gives

$$K_{ij} = Q_i/(h_i - h_o) \tag{3.47}$$

Combining equation (3.47) with the flow quantities listed in table 3.XXI gives the following values for the components of the permeability tensor

$$K_{11} = \quad 4.717921 \times 10^{-11}/(10-1) = \quad 5.242134 \times 10^{-12} \text{ m/s}$$

$$K_{21} = \quad 1.357210 \times 10^{-11}/(10-1) = - 1.508011 \times 10^{-12} \text{ m/s}$$

$$K_{12} = - 1.357210 \times 10^{-11}/(10-1) = - 1.508011 \times 10^{-12} \text{ m/s}$$

$$K_{22} = \quad 1.098694 \times 10^{-11}/(10-1) - \quad 1.220771 \times 10^{-12} \text{ m/s} \qquad (3.48)$$

These values again agree with those in Table 3.XXII and those given by equation (3.43). It can, therefore be concluded that the flow rates and associated permeability tensors, computed by DIFLOW, are free of numerical error.

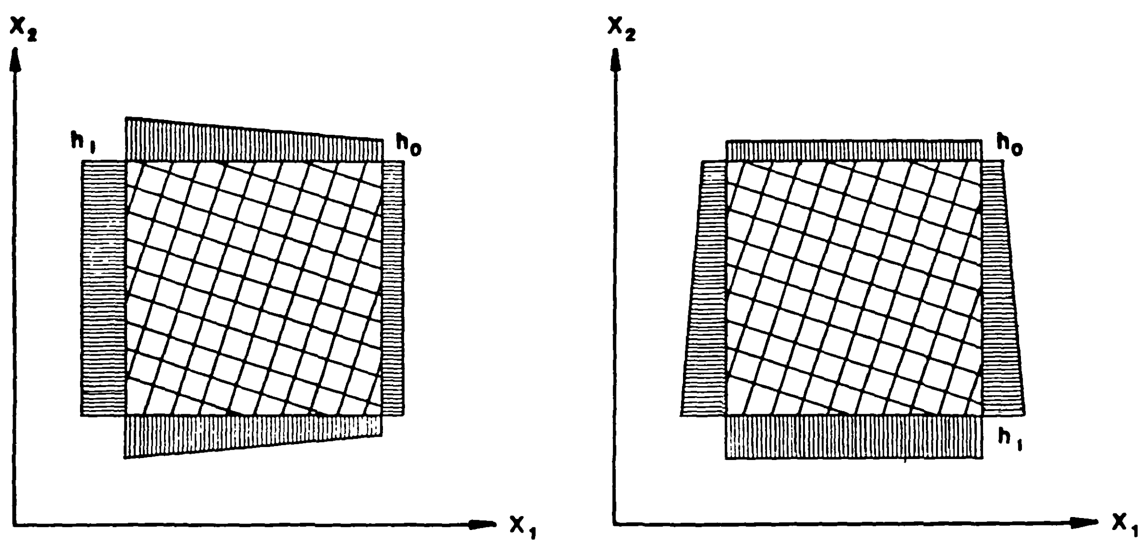

(a) (b)

Fig. 3.15 Tests carried out for numerical validation

(a) Gradient in the x_1 direction

(b) Gradient in the x_2 direction

CHAPTER 4 APPLICATIONS OF THE MODEL

In the preceding chapter the probabilistic model developed in this work was presented in the form of three separate computer programs; DICHA the mesh generator, DICONN the connectivity analysis program and DIFLOW the flow and equivalent permeability tensor program. In the first section of this chapter an application of the mesh generator program is presented, this includes the study of the relationship between discontinuity density, trace length and frequency as well as an analysis of the anisotropy of discontinuity frequency. This is followed by a Monte Carlo type study and an analysis of those geometric properties of a discontinuity mesh that are important in controlling its hydraulic characteristics. The latter includes: discontinuity trace length, density, aperture, orientation and size of the test area. This and the succeeding parts were carried out using the programs DICONN and DIFLOW, however, for practical reasons, such as computer file management, the above two programs were merged into a single program called DIFLOW A.

A study of the anisotropy of the permeability of discontinuity networks and its relation to the anisotropy of discontinuity frequency is presented in Section 4.3. Finally a study of water flow into an underground excavation is presented. The aim of this final section is to assess the factors that influence the quantity of water flow into an underground excavation. Two aspects are considered: firstly the effects of changing the size of the excavation and, secondly, a practical application involving the prediction of water flows into an underground tunnel.

4.1 Applications of the mesh generator

The discontinuity mesh generator program, DICHA, was used in order to study the following two properties of the discontinuity mesh: (1) the relation between discontinuity density, trace length and frequency and (2) the anisotropy of discontinuity frequency.

4.1.1 The relation between discontinuity density, trace length and frequency

Consider a single set of parallel discontinuities with a density of N discontinuity centres per unit area and a mean trace length $1/\mu$. Fig. 4.1(a) shows a rectangular sample area, of side lengths x by y orientated with the sides of length y normal to the discontinuity traces. It is assumed that x and y are both very large compared with $1/\mu$, such that edge effects are negligible. A scanline, of length y, across the sample area, normal to the discontinuity set will observe a discontinuity frequency λ. The aim of this analysis is to obtain the relation between N, μ and λ.

It is important to recognise that discontinuity frequency, unlike spacing, does not depend upon the actual location of each discontinuity, but simply upon the average number intersected. In view of this, it is possible to re-arrange the location (but <u>not</u> the orientation) of the discontinuities within the sample area without changing either λ, μ or N. This has been done in Fig. 4.1(b) so that all the discontinuities lie end to end, making complete traverses across the sample area. Each complete traverse will inevitably produce one, and only one, intersection with the scanline.

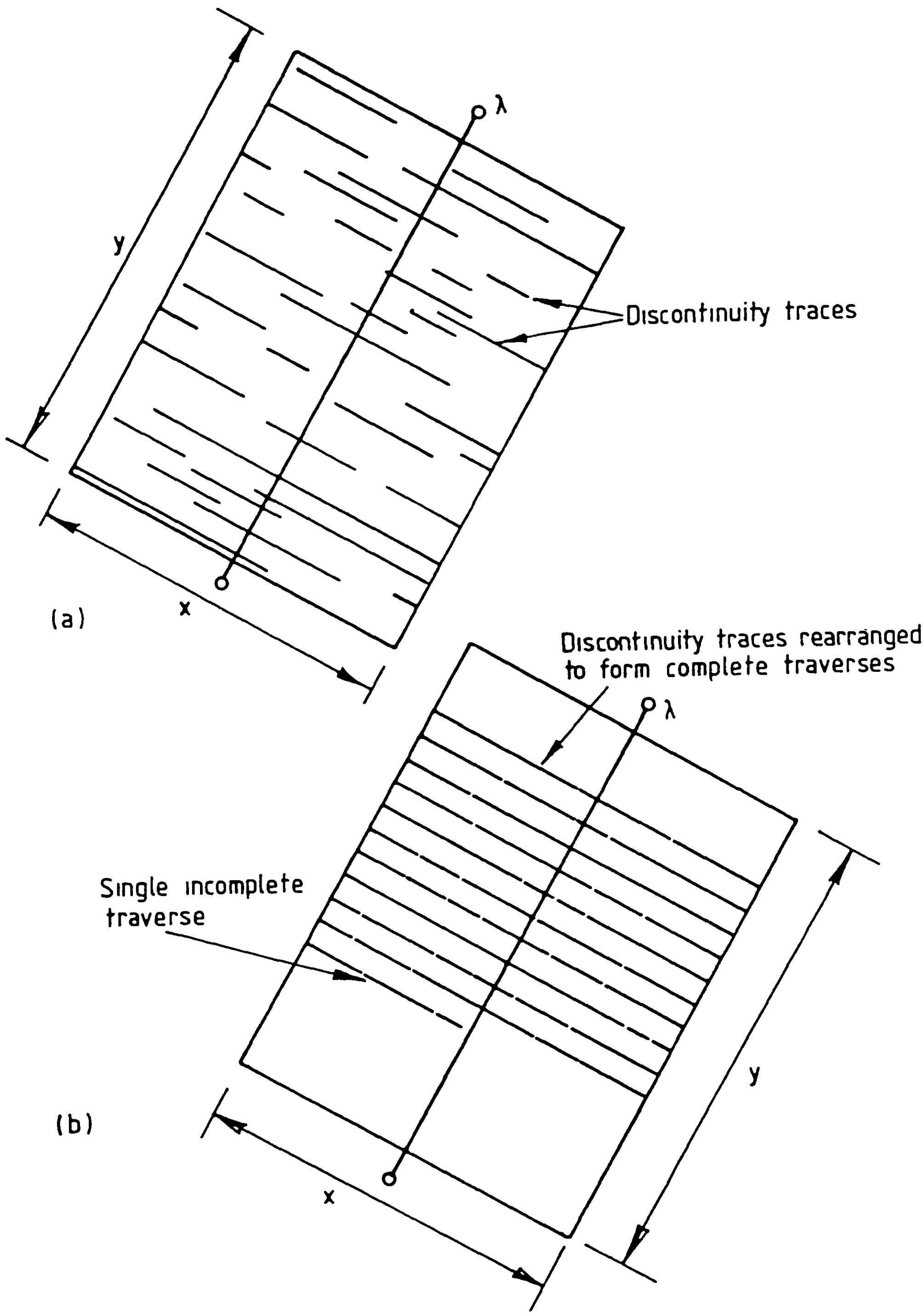

Fig. 4.1 Illustration of the geometrical analysis used to determine the relation between discontinuity density, trace length and frequency

Let T = number of complete traverses of length x

Hence $$\lambda = \frac{T}{y} + \frac{0.5}{y}$$

The error term $(\frac{0.5}{y})$ assumes that, on average, the scanline stands only a 50% change of intersecting the single incomplete traverse. For large values of T and y this term will have a negligible influence on λ and can be ignored.

Hence $$\lambda = \frac{T}{y}$$

Now, for a large sample area, the total number of discontinuities within the sample area approaches the value Nxy, and the total length of these is Nxy/μ. Hence the number of complete traverses of length x is given by

$$T = \frac{Nxy}{\mu x} = \frac{Ny}{\mu}$$

Hence $$\lambda = \frac{N}{\mu} \qquad (4.1)$$

The relation between the number of intersections and the average line length has been considered from a stereological point of view by Underwood (1967). He found that for a totally random line (i.e. discontinuity) orientation, an estimate of the average total length, L, of discontinuity traces per unit area is given by $\pi\lambda/2$.

Hence, for a large sample size $L = \frac{\pi\lambda}{2}$

but $$\mu = \frac{N}{L} \quad \text{hence} \quad \frac{N}{\mu} = \frac{\pi\lambda}{2}$$

or $$\lambda = \frac{2N}{\pi\mu} \qquad (4.2)$$

Equation (4.1) is applicable for perfectly parallel discontinuities, and equation (4.2) for totally random orientation. It is reasonable to expect, therefore, that discontinuities showing some variability about a preferred orientation will have a discontinuity frequency given by

$$\frac{2N}{\pi\mu} < \lambda < \frac{N}{\mu}$$

The hypotheses presented in equations (4.1) and (4.2) were tested by means of a series of numerical simulations, using the computer program referred to in the previous chapter. For each test, a given value of μ was selected and the discontinuities were generated, according to pre-defined distributions of discontinuity trace length and orientation, to achieve the required density, N. The resulting fabric was sampled, using a scanline orientated normal to the mean discontinuity orientation, to determine the discontinuity frequency λ. The process was repeated for different values of N and μ, and also different types of trace length distribution. Samples of the results, presented graphically as plots of N/μ against λ, are given in Figs. 4.2(a) to (c) for negative exponential, uniform and log-normal distributions of trace length respectively. Each figure contains data for a single, parallel discontinuity set and also for totally random discontinuity orientation. Where the hypothesis in equation (4.1) is applicable, the best straight line through the points in these figures should have a slope of unity, and zero intercept. Where equation (4.2) is applicable, the best staight line should have a slope of $\pi/2$ (i.e. 1.571) and also zero intercept. The complete set of simulation results indicate that, in all cases, there is an approximately linear relation between N/μ and λ. These results showed that for a single set of parallel discontinuities, the slope of the best straight line ranged between 0.812 and 1.415 with a mean of 1.113, and that the intercept ranged between $0.100m^{-1}$ and $0.469m^{-1}$ with a mean of $0.284m^{-1}$. For totally random discontinuity geometry the slope ranged between 1.064 and 1.779 with a mean of 1.421, while the intercept ranged between $0.114m^{-1}$ and $0.765m^{-1}$ with a mean of $0.439m^{-1}$. In all cases the slopes of the best straight lines tended to increase with increasing mean trace length.

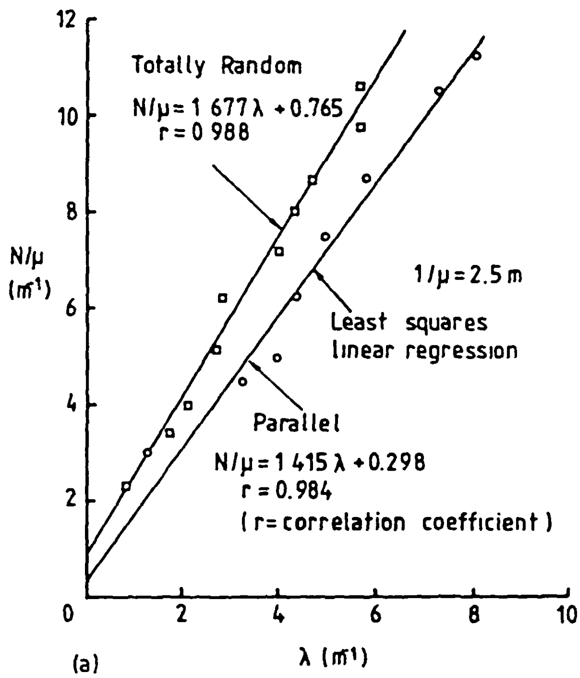

Fig. 4.2 The relation between discontinuity density, mean trace length and mean frequency for totally random and also parallel discontinuities with a mean trace length of 2.5m

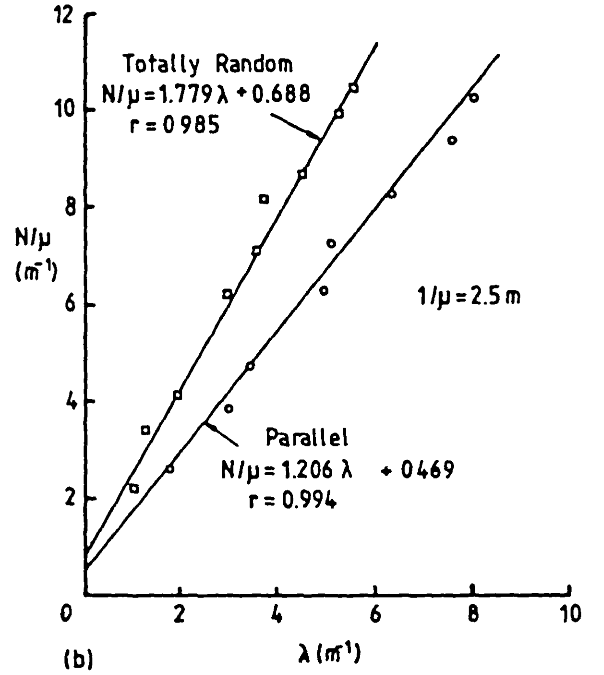

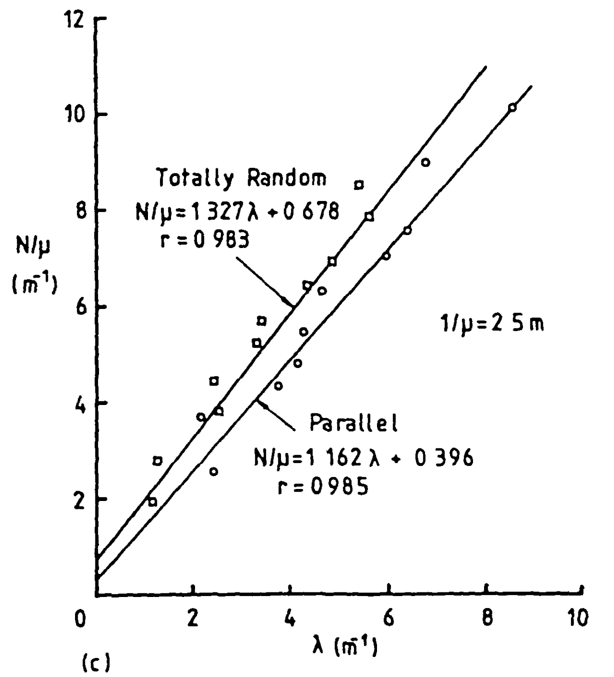

Fig. 4.2 Continued

Further tests were carried out using field data from the Pembrokeshire sites in order to assess the validity of equations (4.1) and (4.2). A photograph from each of ten rock exposures was interpreted using the Program PHOCOM. The discontinuity frequency was calculated for each discontinuity set by superimposing fictitious scanlines over the photographs. The discontinuity density was evaluated by sampling all discontinuities that occurred within a pre-defined window. The trace length values were calculated using the distribution independent method explained in Chapter 2.

Fig. 4.3 shows a plot of N/μ against λ for the aggregated data from all the photographs. Regression analysis indicated that the relationship between N/μ and λ was linear. On both the simulated mesh and the actual field mesh the ratio N/μ over-estimated the value of λ. This was due to the fact that the probability density disstribution of trace length was of negative exponential form in most of the cases. This means that a large proportion of the discontinuities are relatively small and the value of λ is, therefore, underestimated.

The results of this work have important implications for the measurement of discontinuity characteristics using linear surveys such as scanlines or boreholes. In particular, the simple linear relation between N/μ and λ provides a basis for analysing the complex relation between discontinuity freqency and discontinuity size in three dimensions.

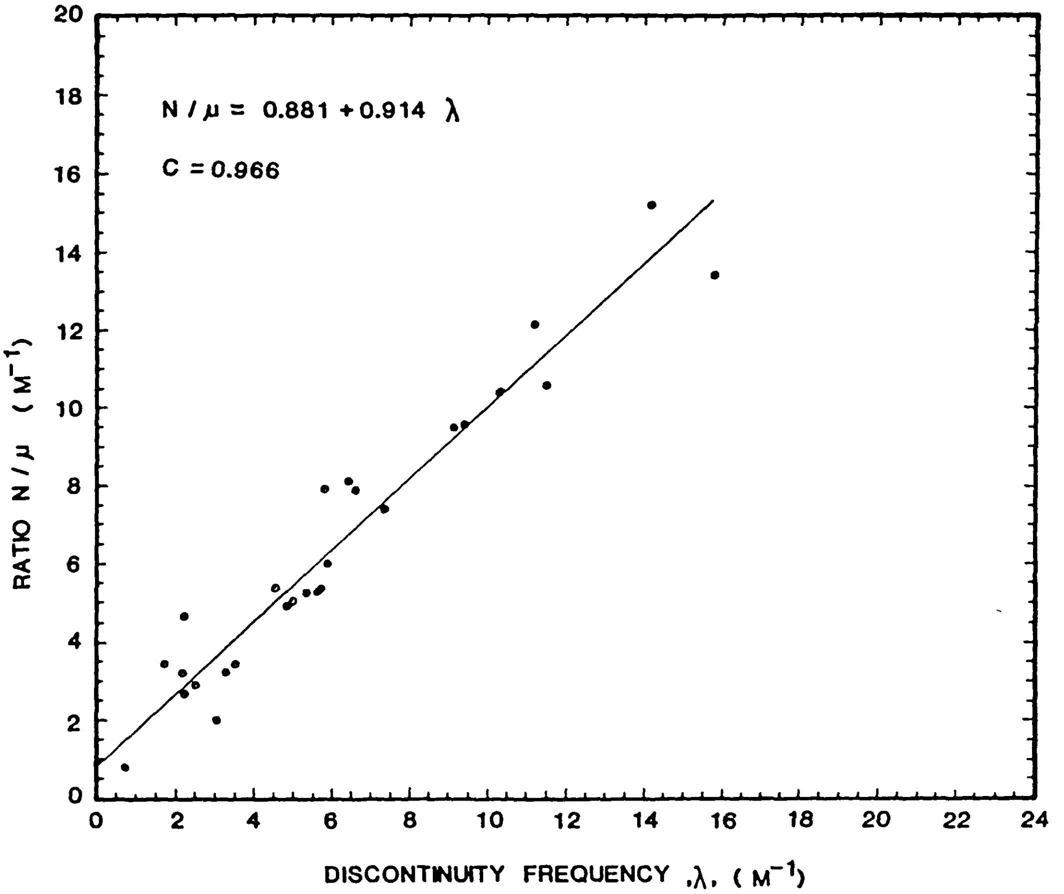

Fig. 4.3 The relation between discontinuity density, mean trace length and mean frequency for discontinuity data from the Pembrokeshire sites

4.1.2 Anisotropy of Discontinuity Frequency

Consider n sets of vertical, planar discontinuities intersecting a horizontal plane. Each set is assumed to consist of parallel, persistent discontinuities. The normal to the i^{th} discontinuity set has an azimuth direction α_i; the discontinuity frequency for the i^{th} set along this normal is λ_i. Hudson and Priest (1982) have shown that the total discontinuity frequency, λ_s, along a scanline of azimuth α, is given by

$$\lambda_s = \sum_{i=1}^{n} \lambda_i \cos|\alpha - \alpha_i| \qquad (4.3)$$

This equation can be used, by incrementing α in the range 0° to 360°, to generate the locus of λ_s in two dimensions. Hudson and Priest have shown that this locus is composed of 2n circular arcs that intersect to define cusps. In particular, there will be a direction of maximum frequency and also, but not necessarily at right angles to it, a direction of minimun frequency.

In practice, discontinuities are not persistent but have some finite value of mean trace length. Moreover, all the values of trace length will never be exactly the same but will follow a distribution of some form. Similarly, the discontinuities will never be perfectly parallel, but will be distributed about a mean orientation. The program DICHA was used to generate the λ_s locus for up to 3 sets of 4000 discontinuities having various distributions of trace length and orientation.

Each set was defined by the following characteristics:

1. The mean orientation of the set normal, α_i, relative to a horizontal axis and measured anti-clockwise.

2. The standard deviation of discontinuity orientation, SDα, assuming a normal distribution about the mean orientation, α_i.

3. The form of the trace length distribution (negative exponential or log-normal).

4. The mean trace length, $1/\mu$.

5. The number of discontinuity centres per unit area, N.

A sample of the results of this work is shown in Fig. 4.4(a) for one discontinuity set, and Fig. 4.4(b) for three sets of various orientations. In each case, the trace lengths were assumed to obey a negative exponential distribution. The solid line in each figure shows the theoretical variation of total discontinuity frequency, λ_s, with α as defined by equation (4.3), assuming there to be one or more sets of parallel persistent discontinuities. The broken lines in each figure give values of λ_s, measured, at 9° intervals of α, from a random discontinuity mesh generated by DICHA. The input frequency parameter(s) for each set λ_i, used in equation (4.3), were obtained from scanlines in the direction(s) αi across the generated mesh. This enabled the theoretical values, and each group of modelled values, of λ_s to be plotted at the same scale on the same diagram.

Figs 4.4(a) and (b) show that the theory presented in Equation (4.3) is valid even where the discontinuity traces have a finite mean length and follow a negative exponential distribution. The modelled variation of λ_s also agrees with the theory when there is some variability in discontinuity orientation. These results not only serve to validate the theory presented by Hudson and Priest (1982) but also suggest that the theory will be applicable to real rock masses containing impersistent discontinuities of variable orientation. Further in this chapter this analysis will be used to help develop a link between the anisotropy of discontinuity frequency and directional permeability.

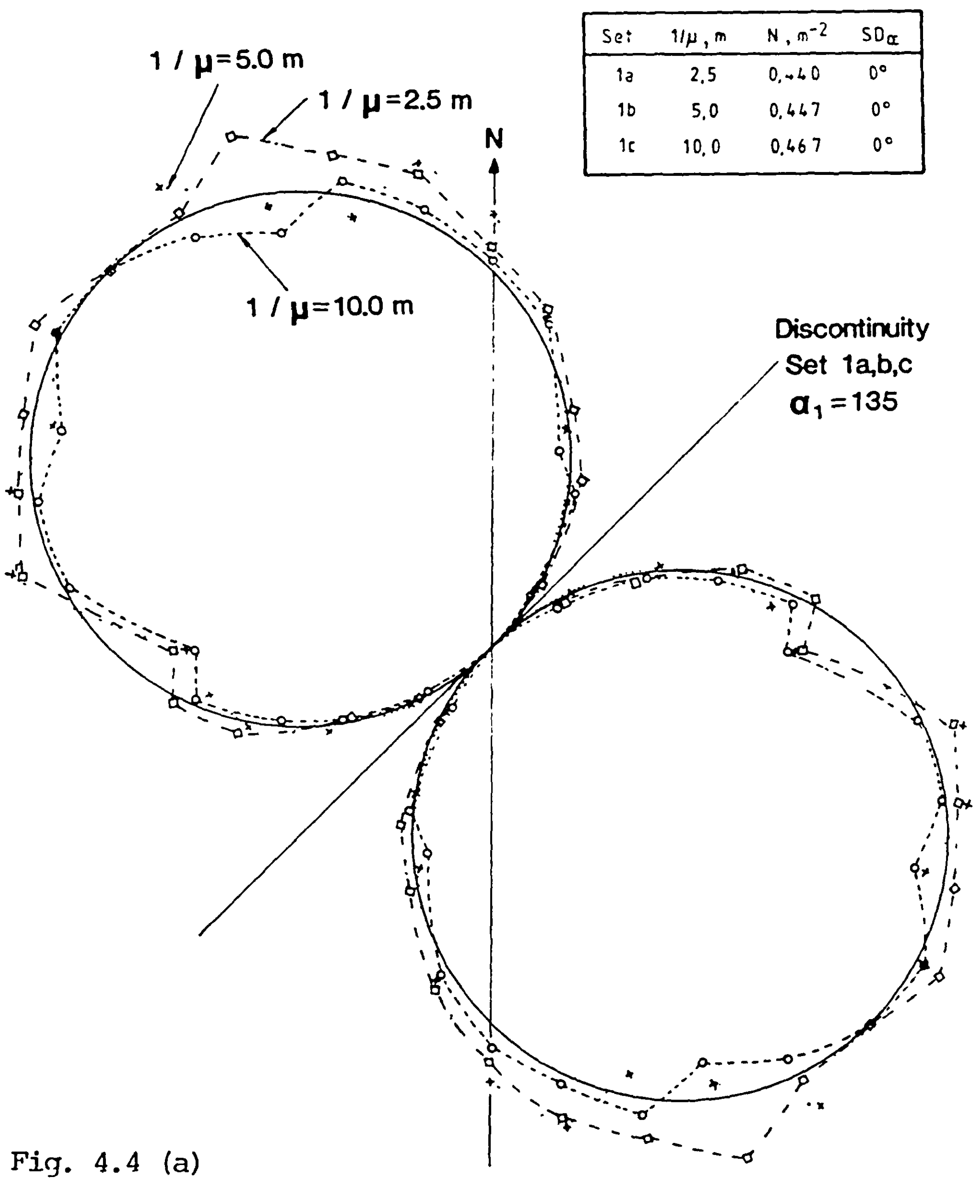

Set	$1/\mu$, m	N, m^{-2}	SD_α
1a	2,5	0,440	0°
1b	5,0	0,447	0°
1c	10,0	0,467	0°

Fig. 4.4 (a)

Set	1/u ,m	N, m^2	$\alpha°$
1	2.0	0 416	100
2	6.0	0 459	140
3	4.0	0 407	20

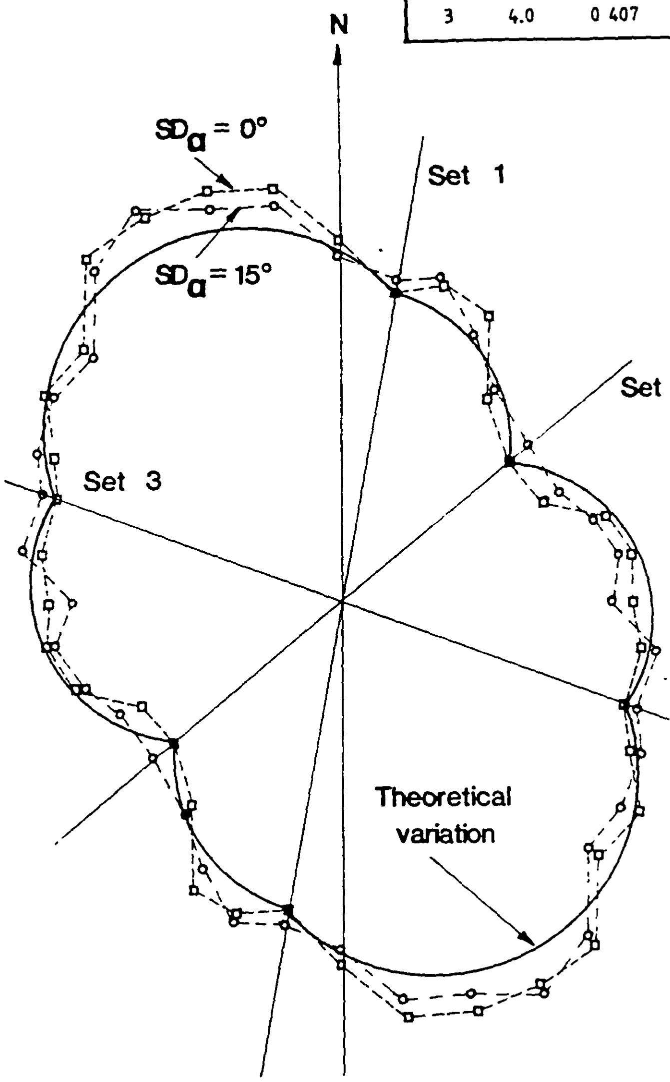

(b)

Fig. 4.4 Modelled and theoretical variation of total discontinuity frequency with changing sampling direction

(a) one discontinuity set, three different values of mean trace length

(b) three discontinuity sets, two different values of the variability in discontinuity orientation

4.2 Analysis of factors affecting permeability

The aim of this section is to study those geometric properties of discontinuity sets that are crucial in controlling the hydraulic characteristics of the mesh. The possibility of establishing an equivalent continuum permeability tensor is also analysed and its reliability is tested by calculating the expected flow across the boundaries and comparing it with the modelled flow values.

In the first part of this section a Monte Carlo type of analysis is carried out in order to study the variability in equivalent permeability produced by the random generation of different realisations of discontinuity meshes using identical input parameters values. This is followed by a study of the effects of changing the mean discontinuity trace length and density. The aim of this study is to establish when the discontinuity mesh starts to behave like a continuous medium. The effects of changing the aperture of the discontinuities are then analysed for constant and variable apertures within the discontinuity mesh. This is followed by a study of the effects on permeability of the relative orientation of the discontinuity sets. Finally a study of the effects on permeability of a given discontinuity mesh for a variable test area is presented. The aim of this analysis is to determine if it is valid, or even possible, to define a representative elementary volume, REV, as proposed by Long (1983).

4.2.1. Different realisations using identical input parameters

This series of tests was designed to study the variability of permeability produced when different realisations of discontinuity mesh are generated from the same input parameters. Table 4.I lists the input values used to generate 60 random realisations of the same fundamental rock structure in two dimensions. The generation area used was 20m by 20m; the sample area for the permeability calculations was taken from the central 10m by 10m area. Each realisation was processed by the connectivity program DICONN to determine the inter-connected mesh. One of the random realisations, and the associated inter-connected mesh is shown in Fig. 4.5. The information describing the inter-connected mesh was then passed to the program DIFLOW. Boundary potentials of h_i = 20m and h_o = 10m were first applied in the x_1 direction and then in the x_2 direction to permit calculation of the equivalent permeability tensor (EPT) as explained in section 3.4.

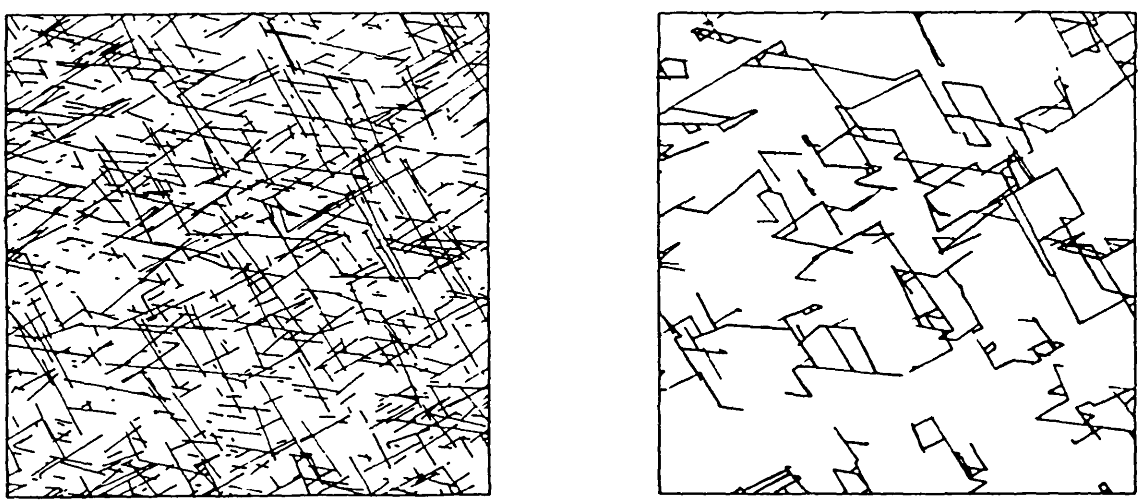

GENERATED MESH INTERCONNECTED MESH

Fig. 4.5 Example of one of the randomly generated and inter-connected discontinuity mesh

Property	Set 1	Set 2	Set 3
Orientation:			
mean	30°	80°	120°
standard deviation	5°	5°	5°
type of distribution	Normal	Normal	Normal
Trace length (m)			
mean	0.7	0.5	0.6
standard deviation	0.7	0.5	0.6
type of distribution	Neg. Exp.	Neg. Exp.	Neg. Exp.
Aperture (mm)			
mean	0.5	0.8	0.6
Standard deviation	0.05	0.05	0.05
type of distribution	Log-normal	Log-normal	Log-normal
Number of discontinuities	1000	1500	1500

Table 4.I   Input data for the analysis of random variability

Figure 4.6 shows histograms of the four terms of the EPT, together with the associated means, standard deviations (S.D.) and coefficient of variation (C) (defined as the ratio of the standard deviation/mean). A goodness of fit test indicated that all the terms followed a normal distribution, except K_{22} which appeared to follow a log-normal distribution. The numerical values for the permeability tensors are included in Appendix 5. For every realisation it was found that the permeability tensor was symmetric. In theory, therefore, the approximation to the continuum should apply. A comparison between the expected and measured flows across the boundaries, however, provides a better method for assessing the validity of the continuum aproximation. The expected flows were calculated from the permeability tensors for each of the 60 realisations as follows:

$$Q_i = K_{ij} \frac{\partial h}{\partial x_j} L \qquad (4.4)$$

These expected flows were compared with the flows calculated by the program DIFLOW. It was noted earlier that the net flows measured across two opposite sides of the sample area are not numerically equal. In order to avoid this difficulty, the measured flow across side 4 was arbitrarily chosen to represent the measured flow in each case. The relative error (R.E.) between the expected and measured flow was then calculated using the following expression:

$$\text{R.E.} = \frac{|\text{measured flow} - \text{expected flow}|}{\text{expected flow}} \qquad (4.5)$$

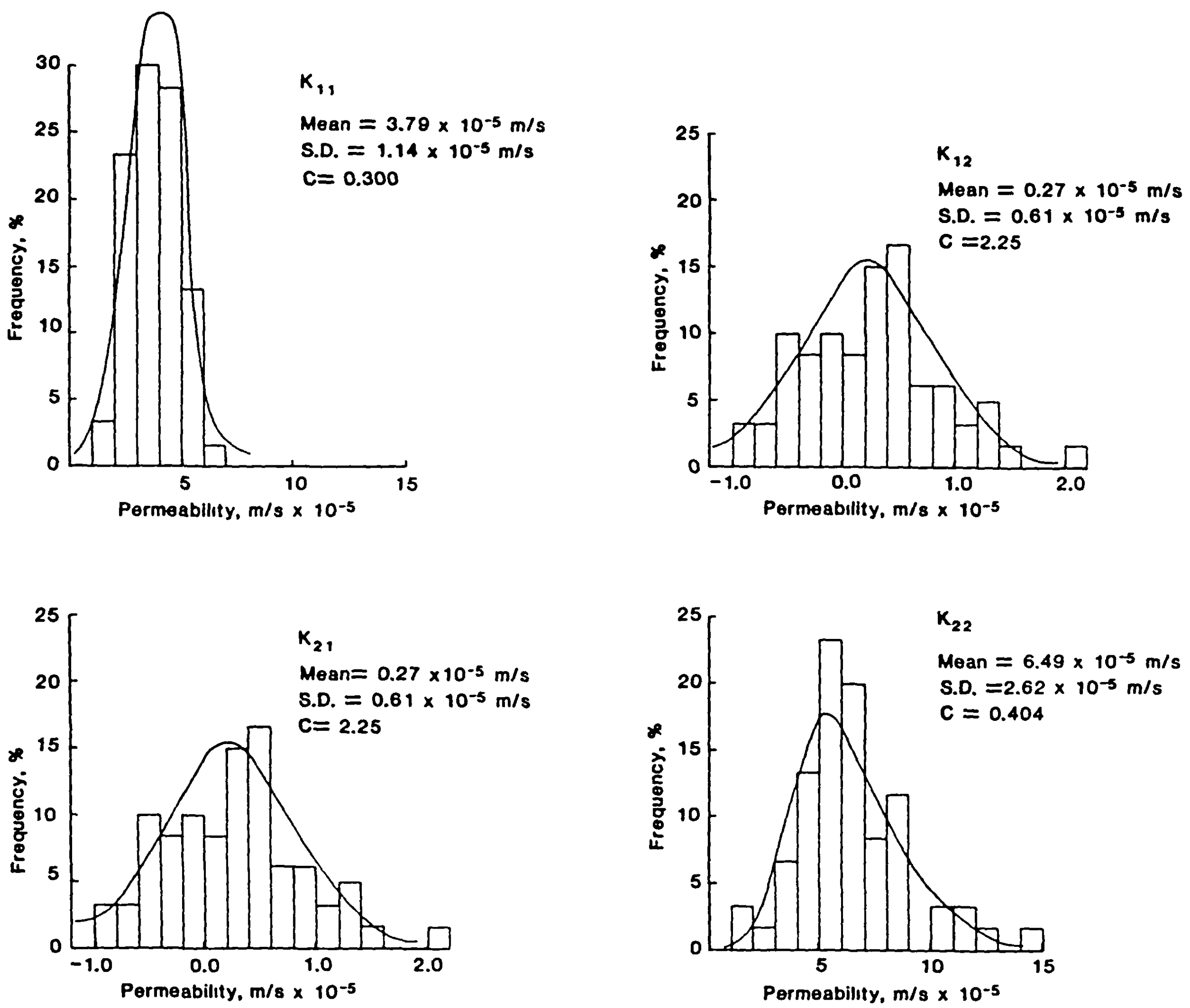

Fig. 4.6 Variability of the four components of the equivalent permeability tensor

Figure 4.7 shows a histogram of the distribution of frequencies of the relative error as calculated by equation (4.5). The flow errors were calculated in both, the x_1 and x_2 directions and the results combined to give a larger sample size. A normal distribution curve provided a good fit to the experimental data; consequently the central limit theorem can be applied in order to establish confidence limits as follows

$$\underline{\bar{u}} = \bar{e} \pm z \frac{s}{\sqrt{n}} \tag{4.6}$$

where $\underline{\bar{u}}$ represents the upper and lower confidence limits for the estimate of u, the true population mean flow error, $\bar{e}$ is the mean value of the sampled flow error, s is its standard deviation and z the associated confidence level. For a 95 percent confidence level the upper and lower limits are given by e ± 0.14. In the case of a 99 percent confidence level the limits are e ± 0.18. For the data presented in Figure 4.7 the confidence bandwidths are: 0.338 to 0.058 at the 95 percent level and 0.378 to 0.018 at the 99 percent level respectively. The central limit theorem concept is of particular importance when investigating flow through fractured media using probalistic models. This is because the flow or permeability will depend on many randomly generated discontinuity parameters, each of which exerts only a very small influence in the overall flow or permeability. The central limit theorem provides a method of determining a measure of the totality of these effects, irrespective of the nature or distribution of their individual components.

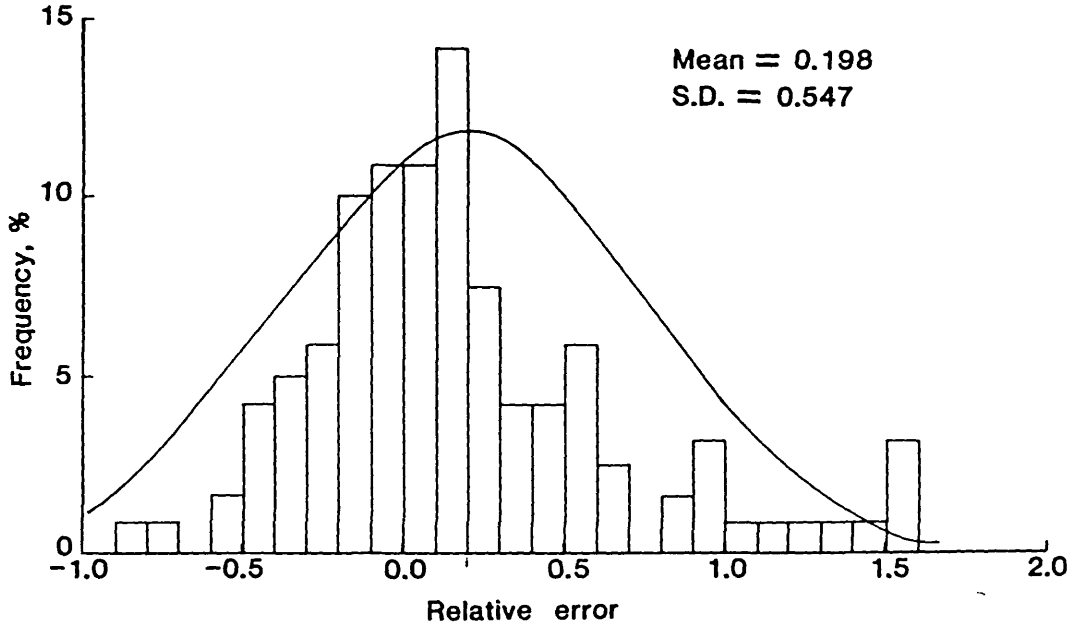

Fig. 4.7 Variability of the relative error between the expected and measured flows

The permeability tensor for each of the 60 realisations was found to be symmetric in an x_i coordinate system. This implies that their principal permeabilities can be found directly from the tensor. In Chapter 2 a general formulation for principal permeabilities was presented. However, for the sake of completeness a development of the formulation for the two-dimensional case is included here. Equation (2.14) represents a system of three linear homogeneous equations where the components of the principal directions, u_i are the unknowns

$$(K_{ij} - K\delta_{ij})\, u_i = 0 \qquad i,j = 1,2,3$$

Assuming that the trivial solution, $u_i = 0$, is ignored then for a solution to exist the determinant of the above equation must vanish, i.e.

$$|K_{ij} - K\delta_{ij}| = 0 \tag{4.7}$$

Development of equation (4.7) gives a quadratic equation known as the characteristic equation of the symmetric tensor K_{ij}.

$$K^2 + I_1 K + I_2 = 0 \tag{4.8}$$

where I_1 and I_2 are scalars independent of the coordinate system called the basic invariants of the symmetrical tensor K_{ij}, and are given by

$$\begin{aligned} I_1 &= K_{ii} = K_{11} + K_{22} \\ I_2 &= \tfrac{1}{2}(K_{ii}K_{jj} - K_{ij}K_{ji}) = K_{11}K_{22} - K_{12}{}^2 \end{aligned} \tag{4.9}$$

The roots, K_1 and K_2, of the characteristic equation are called principal values or eigenvalues of the symmetrical tensor K_{ij} and are given by:

$$K_1 = \frac{K_{11} + K_{22}}{2} + \sqrt{\left[\frac{K_{11} - K_{22}}{2}\right]^2 + K_{12}{}^2}$$

$$K_2 = \frac{K_{11} + K_{22}}{2} - \sqrt{\left[\frac{K_{11} - K_{22}}{2}\right]^2 + K_{12}{}^2} \tag{4.10}$$

The principal directions are found by solving the following equation

$$\tan 2\Theta = \frac{2\,K_{12}}{K_{11} - K_{22}} \tag{4.11}$$

where Θ is the angle between the system of coordinates x_i and the principal directions vector, u_i, as shown in Fig. 4.8.

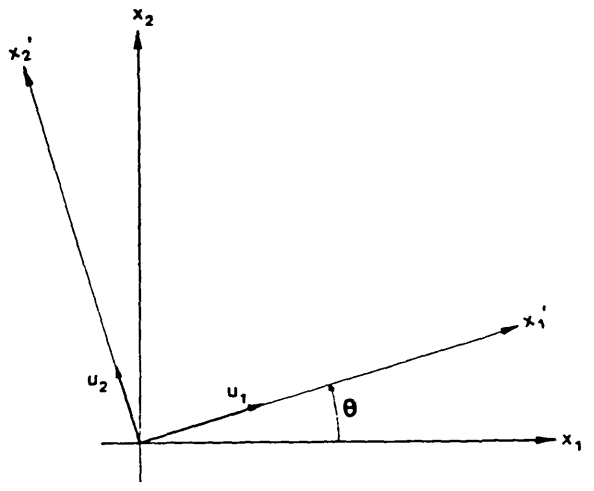

Fig. 4.8 Cartesian coordinates system showing the principal direction of the permeability tensor

The principal permeabilities, and their directions, for all 60 realisations are given in Appendix 5. Fig. 4.9 shows the frequency distribution of the eigenvalues of the permeability tensor. Their mean values, standard deviation and coefficients of variation are also shown. A goodness of fit test indicated that both principal permeabilities follow a normal distribution. Figure 4.10 shows a polar diagram of the principal directions where Θ is the angle between the direction of K_{11} and the direction of x_1.

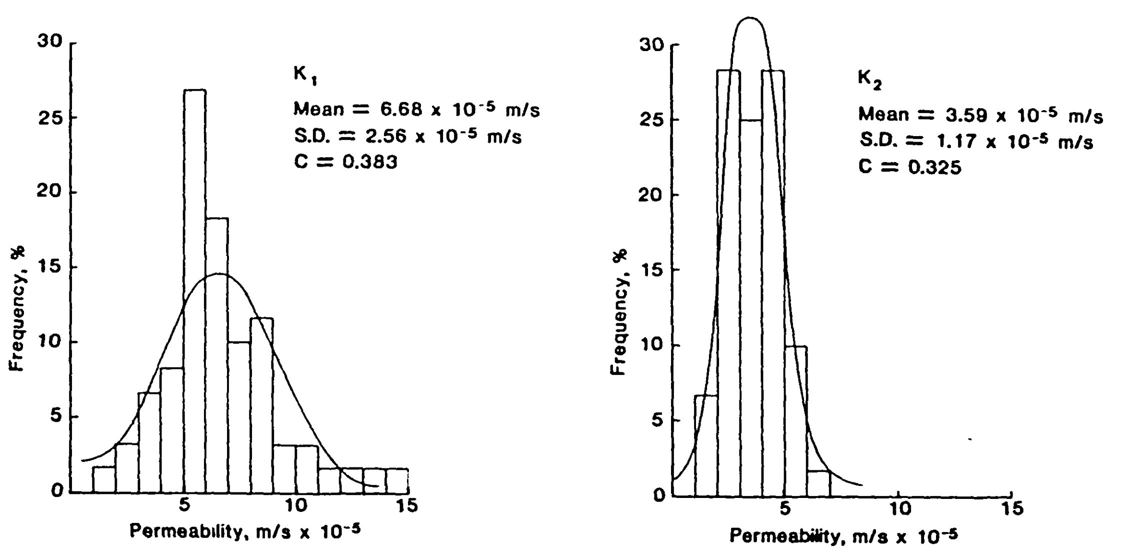

Fig. 4.9 Variability of the components of the principal permeability tensor

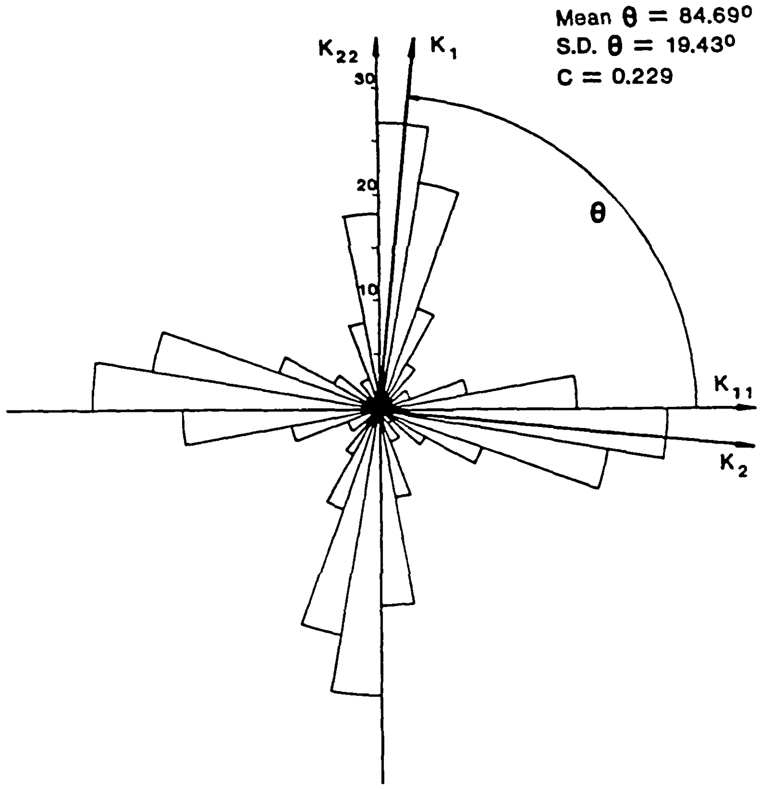

Fig. 4.10 Variability of the principal directions

From the above discussion it can be seen that, although the permeability tensor was found to be symmetric, the rather high values of the coefficient of variation for the EPT terms, the principal permeabilities and also the principal directions, emphasise that it is not appropriate to determine the permeability from a single realisation of a given discontinuity geometry. In general the variability of the results would depend upon several factors: particularly the areal distribution of the discontinuity centres, the aperture distribution and also the connectivity of the discontinuity mesh. For the purposes of this work, the areal distribution of discontinuity centres has been assumed to follow a Poisson process and will, therefore, be statistically homogeneous. The connectivity of the mesh is a function of the trace length distribution, the orientation distribution and the areal density. In order to quantify and study this latter effect, two indices of connectivity are proposed. The discontinuity index, I_D, is defined as

$$I_D = N_{DC}/N_{DT} \tag{4.12}$$

where N_{DC} is the number of discontinuities that form part of the interconnected network and N_{DT} is the total number of discontinuities in the test area. The node index, I_N, is defined as

$$I_N = N_{NC}/N_{NT} \tag{4.13}$$

where N_{NC} is the number of nodes in the interconnected mesh and N_{NT} is the total number of nodes in the test area.

Fig. 4.11 shows a plot of I_D against I_N for each realisation. It can be seen that the two quantities are strongly correlated and hence are both valid measures of inter-connectivity. It is also clear that the discontinuity index is greater than the node index. This is due to the fact that the probability density distribution of trace length is of a negative exponential form. This means that a large proportion of the discontinuities are relatively small and do not intersect others. If the discontinuity trace lengths had been less variable, there would have been a closer agreement between the values of the two indices. In cases where, for a given mesh the discontinuity density remains constant, if the discontinuity index approaches the node index it can be concluded that the discontinuity trace length values are relatively constant, and do not, for example obey the negative exponential distribution.

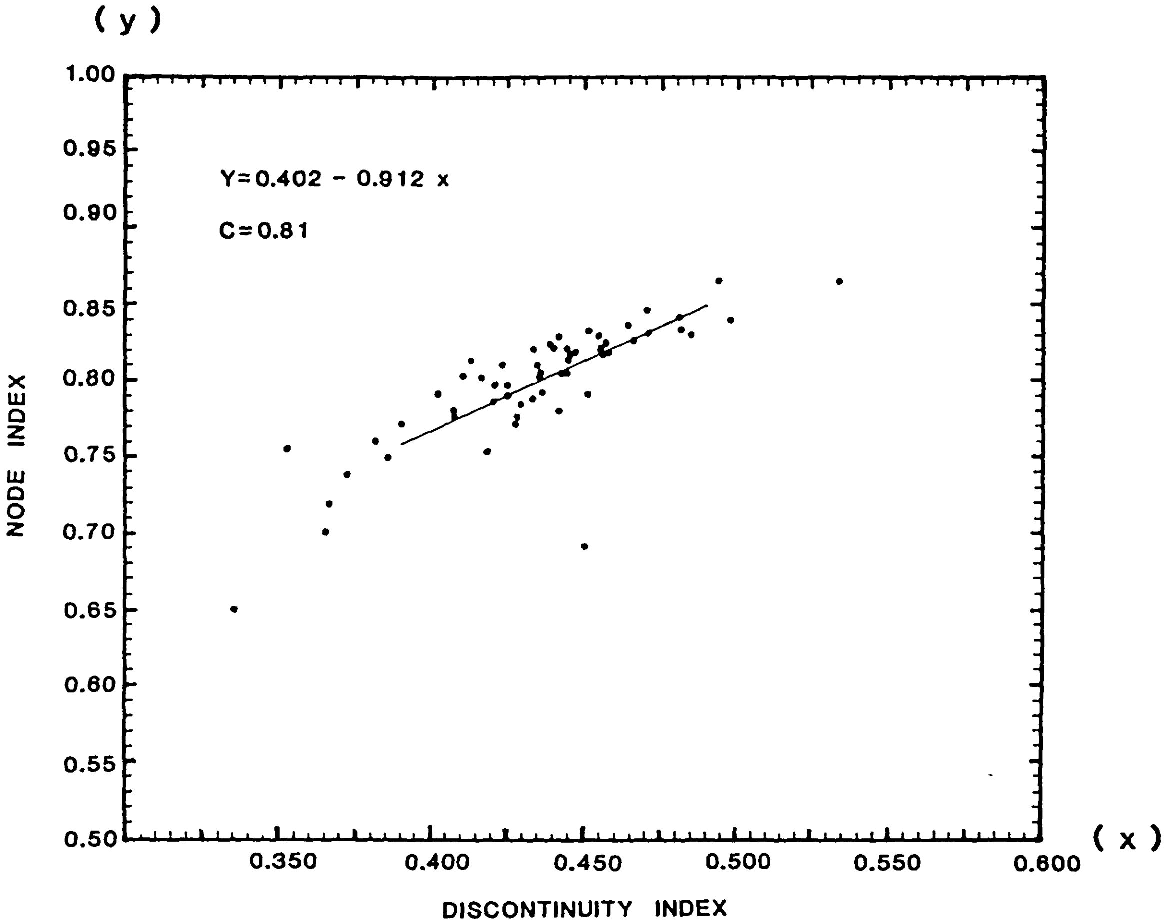

Fig. 4.11 Plot of the discontinuity index against the node index for each of the 60 realisations

Fig. 4.12 shows the frequency distributions of I_D and I_N; these have relatively small coefficients of variation of 0.083 and 0.050 respectively. It is, however, evident that variability in the permeability tensor is caused partly by variability in I_D and I_N, i.e. by variability in connectivity, and partly by variability in discontinuity aperture.

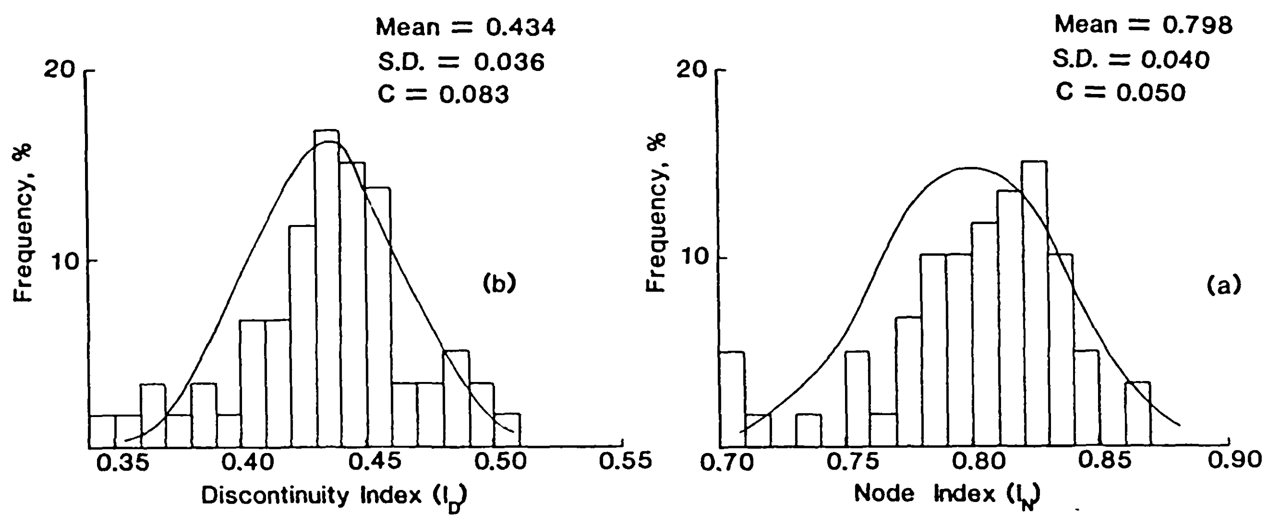

Fig. 4.12 Frequency distributions of the discontinuity index and node index

The diversity of results for the permeability tensor of realisations based on the same input parameters are consequences of randomness. In other words, a single permeability tensor represents only one of the many possible results that might have occurred. Occasionally permeabilities very much smaller or very much larger than the mean tendency are produced, as can be seen in Fig. 4.6. The ergodic hypothesis, which states that time plays no role in determining probabilities, is assumed here as a working hypothesis. This implies, however, that the tests must be conducted a large number of times.

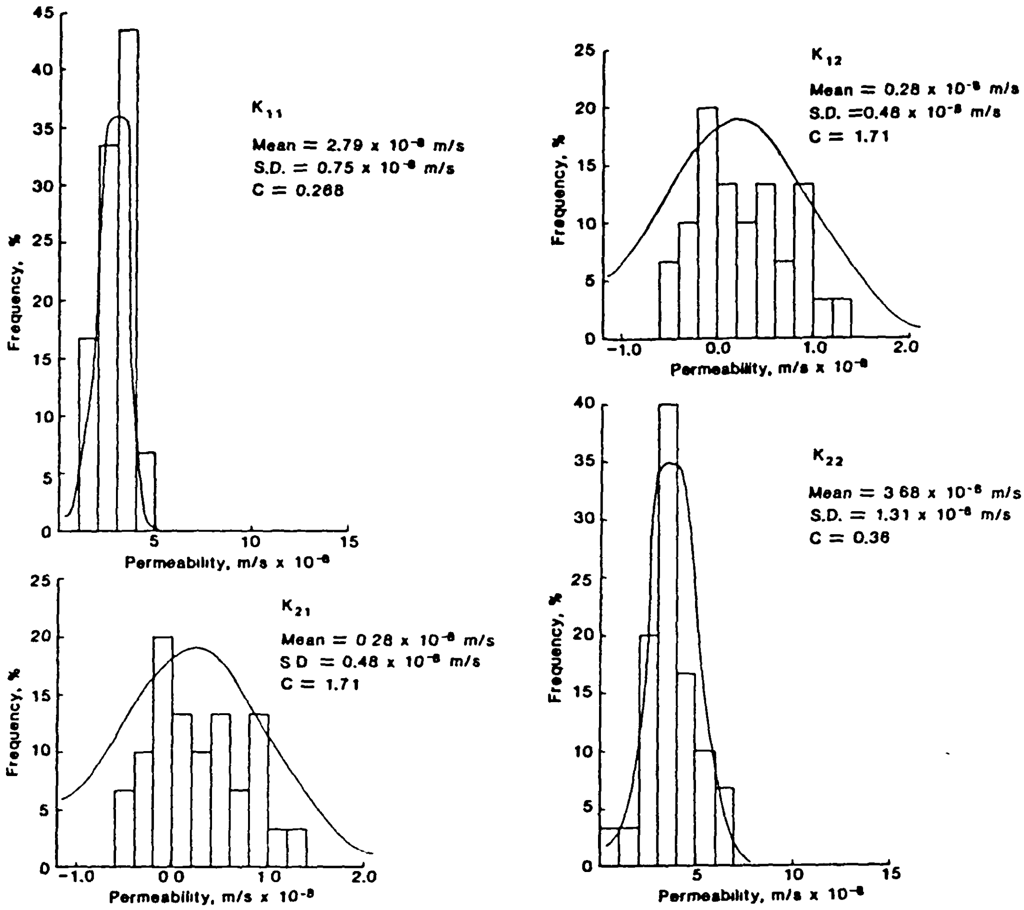

Fig. 4.13 Variability of the four components of equivalent permeability tensor when aperture of all discontinuities are constant

In order to study the effects of the variability in I_D or I_N on permeability, a second series of tests was conducted using 30 of the same 60 realisations. In this case discontinuity aperture assumed to be constant for all discontinuities in every mesh, and to take a value of 0.5mm. Fig. 4.13 shows the histograms of the four terms of the EPT when the apertures of all discontinuities are constant. In comparing the two sets of results, i.e. Figs. 4.6 and 4.13, it can be seen that the coefficients of variation of the EPT terms in the second test are reduced by approximately 4.4% for the diagonal terms and by up to 54% for the off diagonal terms. This reduction in variability shows, to some extent, the influence of variable discontinuity apeture on permeability. The histograms of the principal permeabilities are shown in Fig. 4.14. In this case, when compared with the results shown in Fig. 4.9, the reduction in variability is approximately 6%. Fig. 4.15 shows the polar diagram of the principal permeability directions. If this is compared with Fig. 4.10, it can be seen that the variability of the principal directions has increased. The reasons for this are examined in further studies in Section 4.2.3.

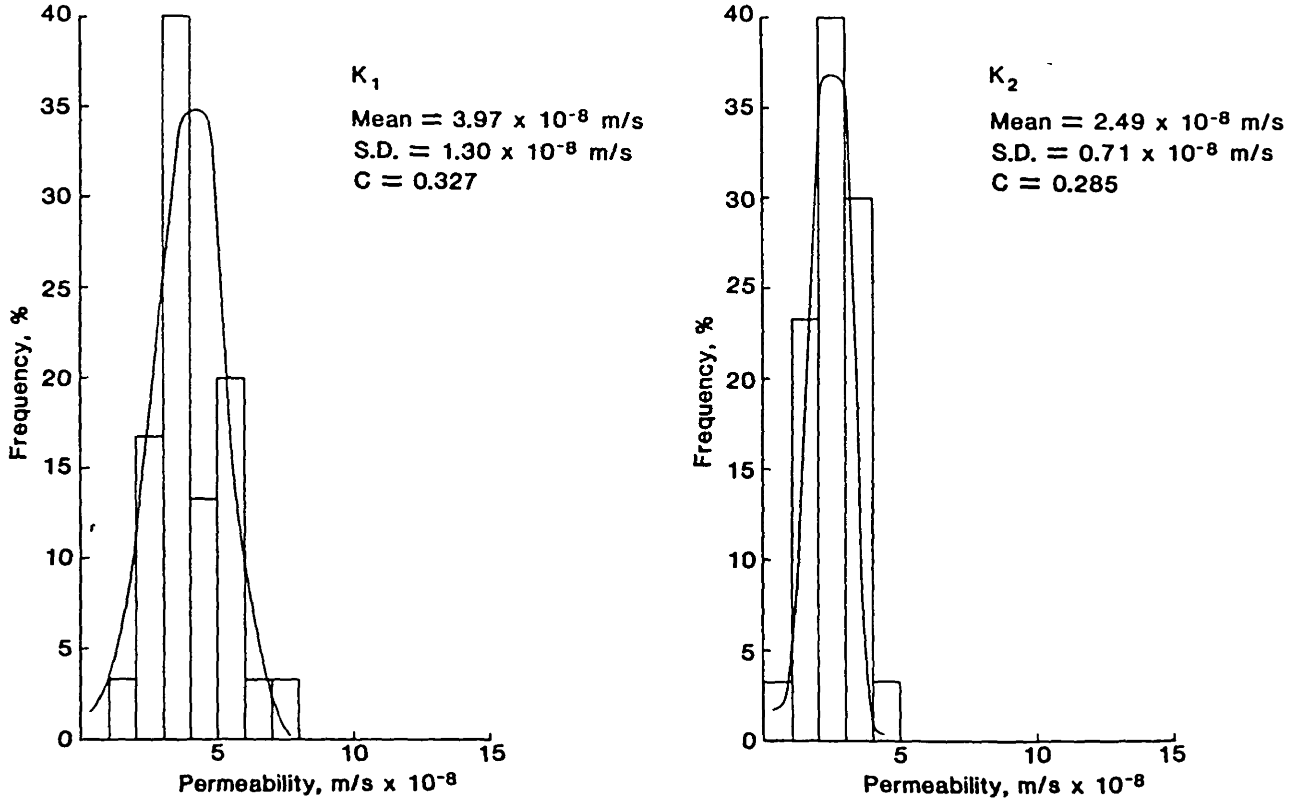

Fig. 4.14 Variability of the components of the principal permeability tensor when aperture of all discontinuities are constant

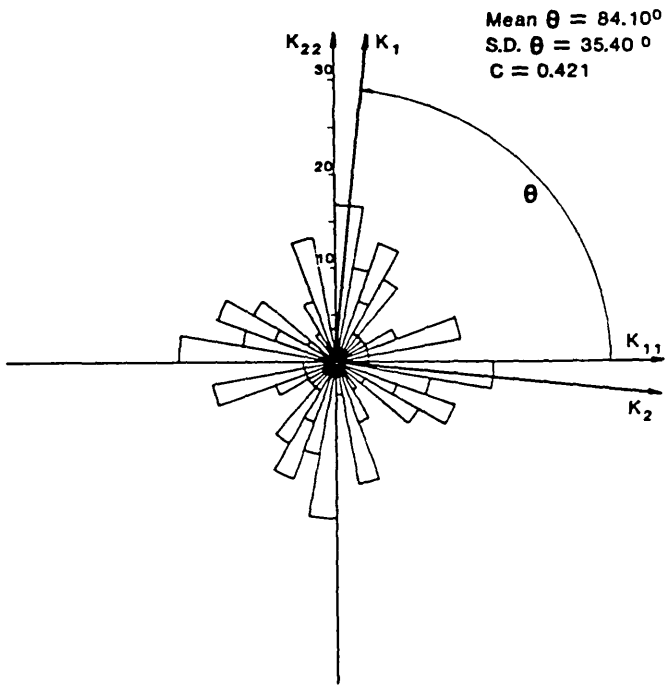

Fig. 4.15 Variability of the principal directions when the aperture of all discontinuities are constant

The relative errors between the expected and measured flows were calculated using equation 4.5; Figure 4.16 shows a histogram of the resulting values. A normal distribution provided a good fit, consequently the central limit theorem can again be used in order to establish confidence limits. For example, at a 95 percent confidence level the upper and lower limits are 0.398 and -0.001 respectively. When comparing these results with those in Fig. 4.7, it is clear that the limits for this second case are slightly wider; in other words a lower confidence level would have to be employed to give the same precision as in the former case.

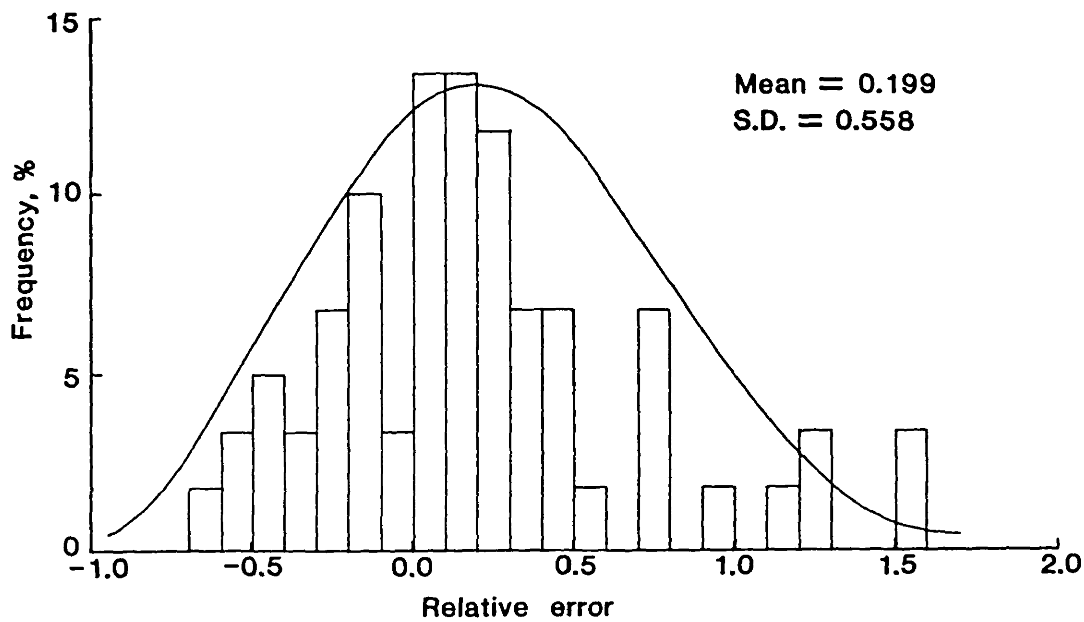

Fig. 4.16 Variability of the relative error between the expected and measured flows

In this section it has been shown that the variability of the EPT, the principal permeabilities and their directions are dependent on connectivity and discontinuity aperture. The precise nature of this dependancy is not, however, clear. Consequently further specific studies were carried out and are described in Sections 4.2.2 and 4.2.3. Having studied the effects of taking different random realisations based upon the same input parameters, in the remainder of this section, for the more specific parameter studies, and in order to economise on time and cost, only one mesh realisation for each set of input parameters will be considered.

4.2.2 Effects of changing the mean discontinuity trace length and density

The aim of this investigation is to asses the effects on permeability when the mean discontinuity trace length and density are changed. Equations 4.1 and 4.2, suggest that these two parameters need to be studied together; this is for the following two reasons. First it is possible to obtain the same discontinuity frequency from more than one combination of N and μ. Secondly, line surveys are the most commonly used method for obtaining discontinuity information; many times it is impossible to obtain from them any reliable information on trace length and/or density individually, this is specially true when the line sampling is a borehole.

In this series of tests, a number of meshes, each containing three sets of discontinuities, were constructed in a generation area of 20 m by 20 m, the sample area being taken from the central 10 m by 10 m area. The input data used are listed in Table 4.II. All possible combinations of different values of trace length (1) combined with three different values of discontinuity density (2) were tested. The generated meshes were first processed by the connectivity program so that the inter-connected meshes could be determined, as is shown in Fig. 4.17. The data describing the inter-connected mesh were then passed on to the program DIFLOW. Boundary potentials of h_i = 20 m and h_o = 10 m were applied first in the x_1 direction and then in the x_2 direction and the equivalent permeability tensor was calculated. Table 4.III shows the terms of the EPT together with the discontinuity and node indices of connectivity I_D and I_N. Tests 1 to 6 represent the six values of trace length; the letters A, B, C represent the three values of discontinuity density, according to Table 4.II.

It can be seen from Table 4.III that for test 1A down to test 3A the resultant permeability tensors, as calculated by equation (3.51), are not symmetrical as they should be. This is due to round-off errors occurring during the calculations. For practical purposes the off-diagonal terms would be considered to have zero value, however, in order to observe the effect of this error a plot of K_{12}/K_{21} against the node index was constructed; this is presented in Fig. 4.18. It can be seen that as the node index increases the ratio K_{12}/K_{21} approaches unity. A ratio of unity, of course, means that the resultant permeability tensor is symmetrical. For this series of tests, it can be seen that for a connectivity index I_N greater than about 0.41 the round-off errors become negligible and therefore the permeability tensors are in fact symmetrical.

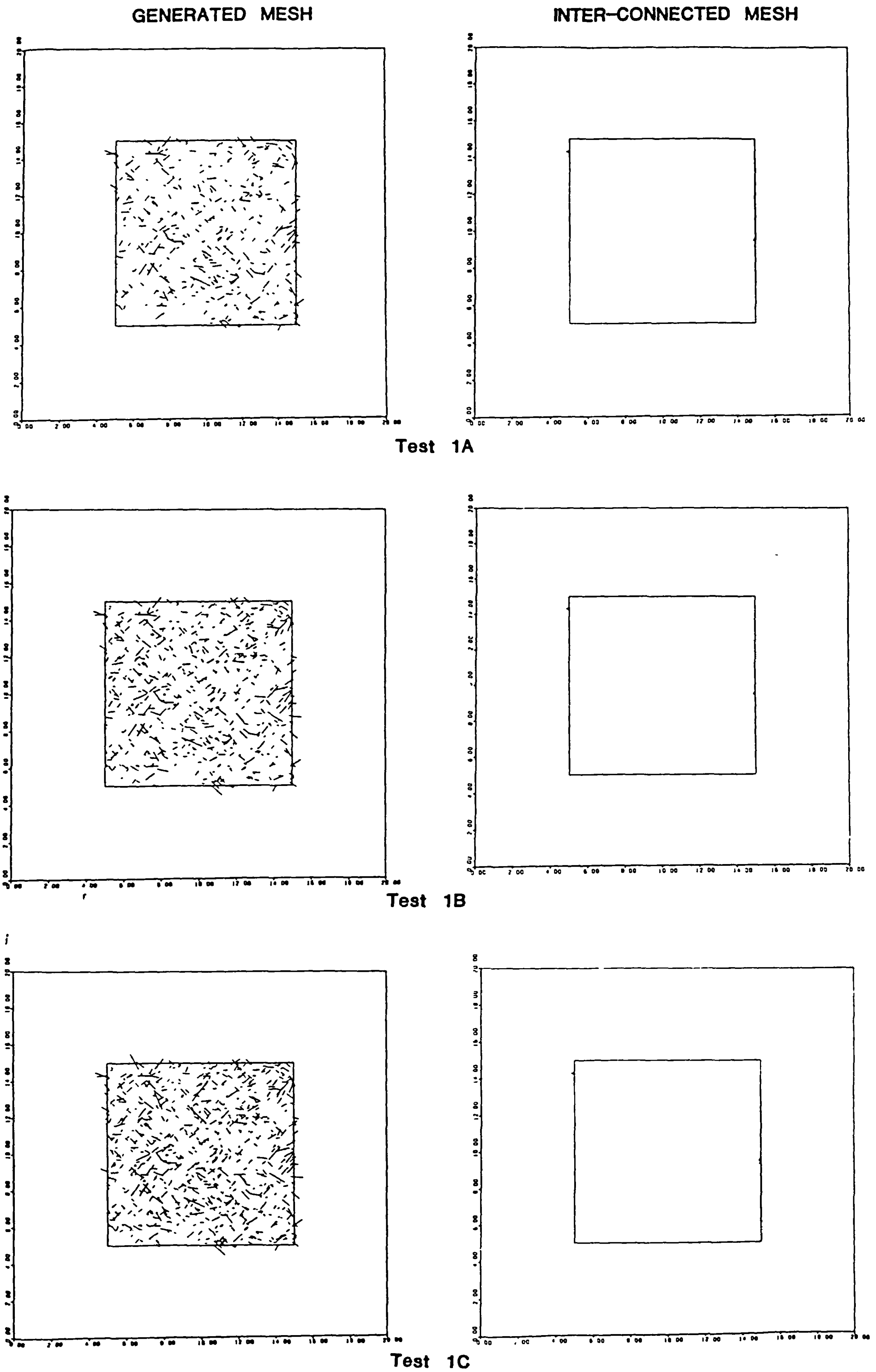

Fig. 4.17 The generated and inter-connected meshes for the discontinuity trace length and density analysis

GENERATED MESH INTER-CONNECTED MESH

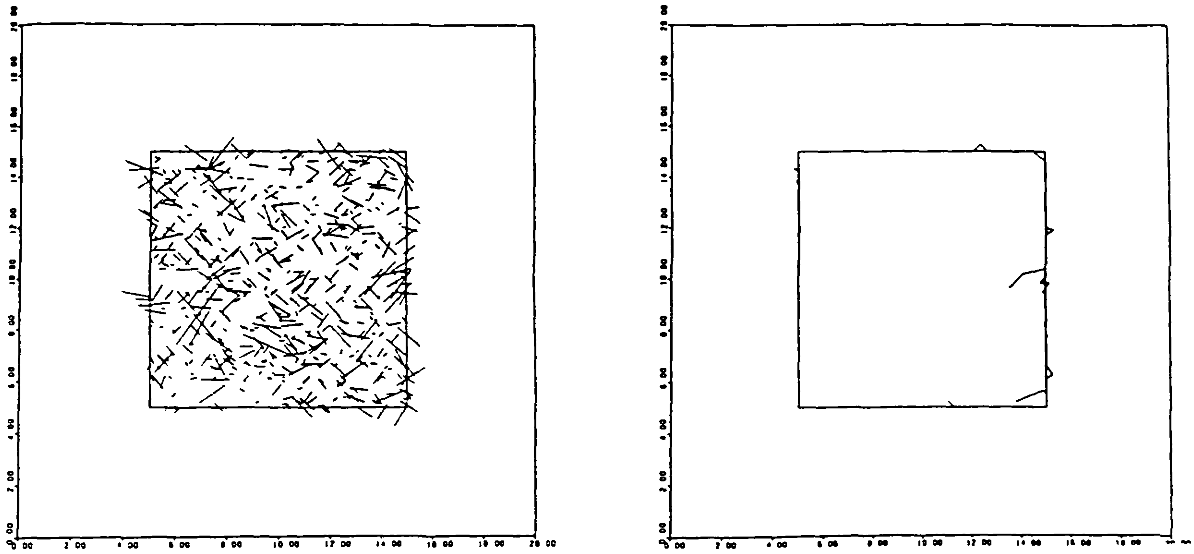

Test 2A

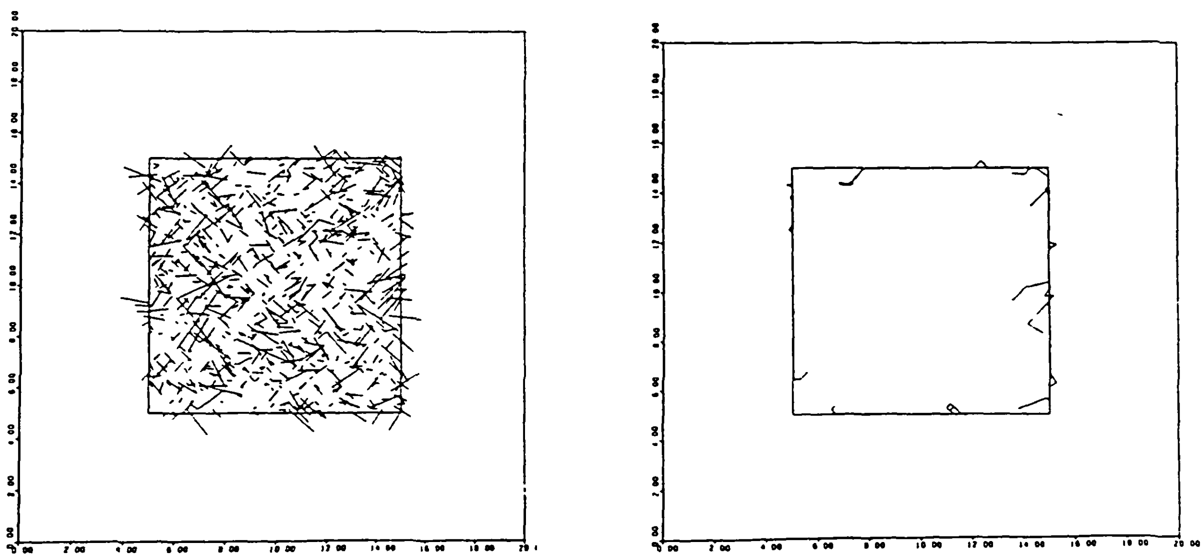

Test 2B

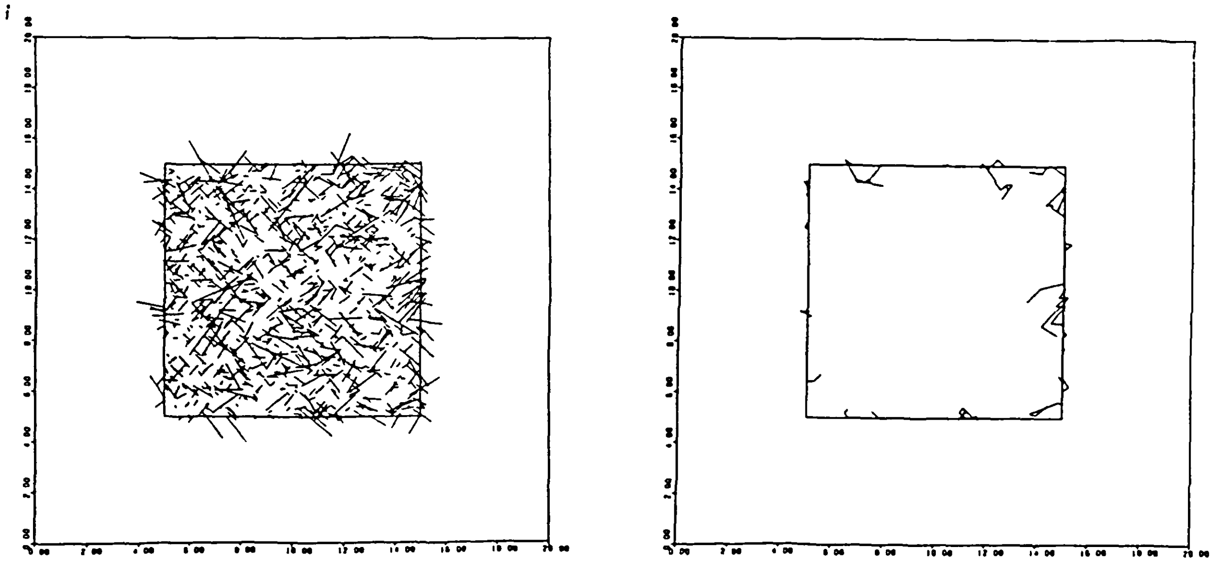

Test 2C

Fig. 4.17 Continued

GENERATED MESH INTER-CONNECTED MESH

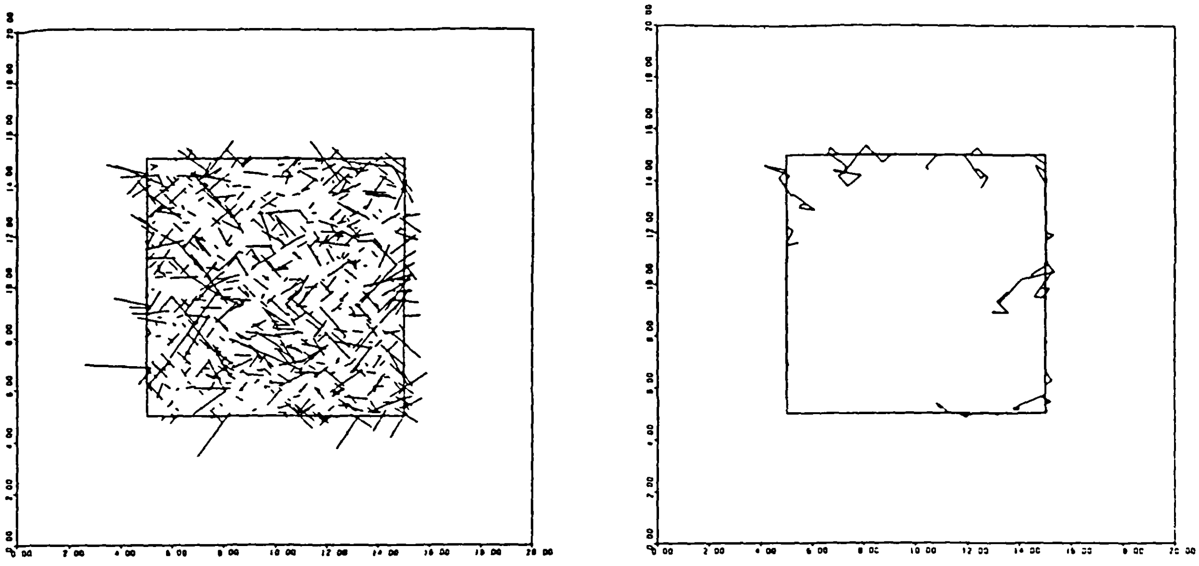

Test 3A

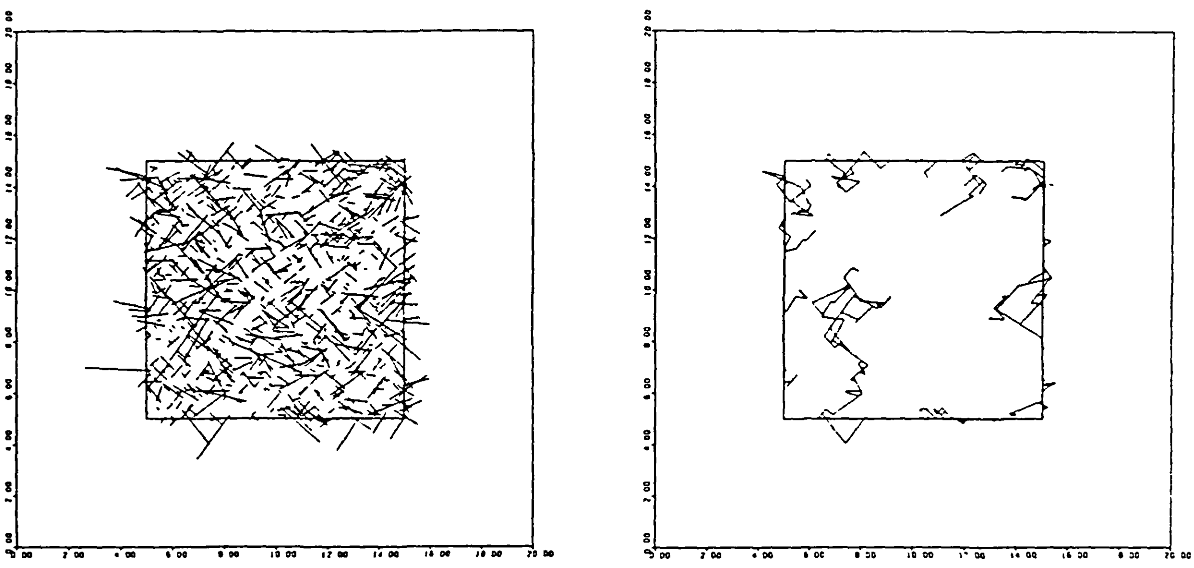

Test 3B

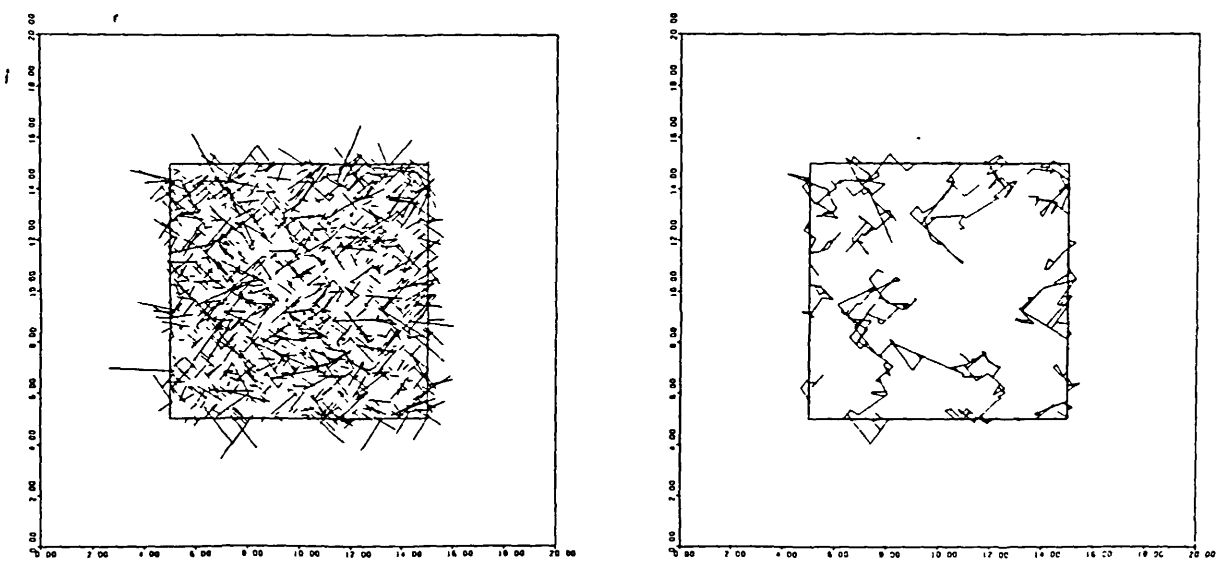

Test 3C

Fig. 4.17 Continued

GENERATED MESH INTER-CONNECTED MESH

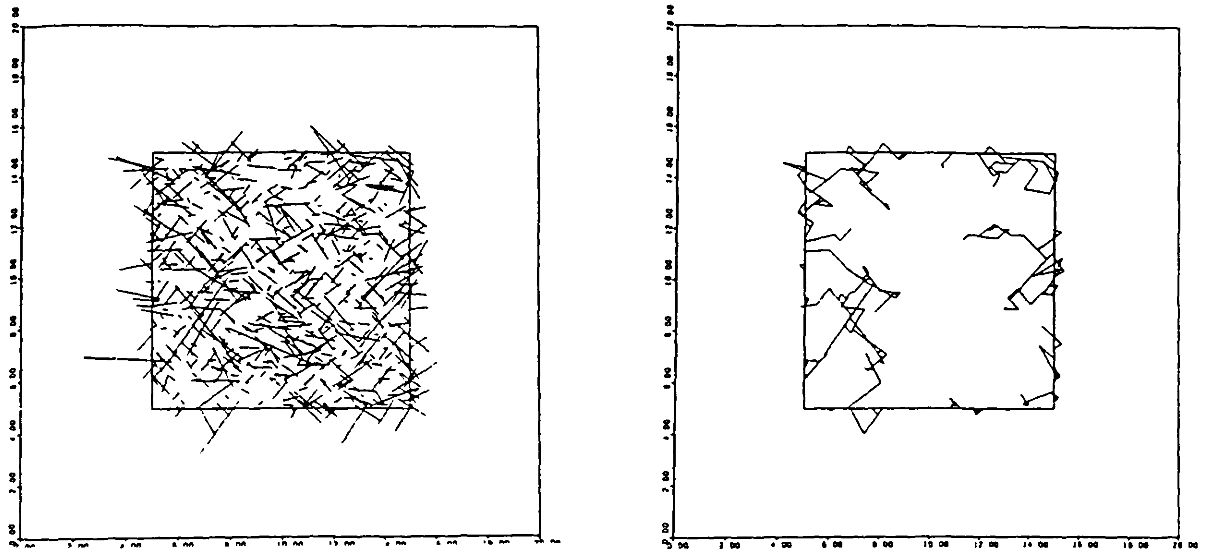

Test 4A

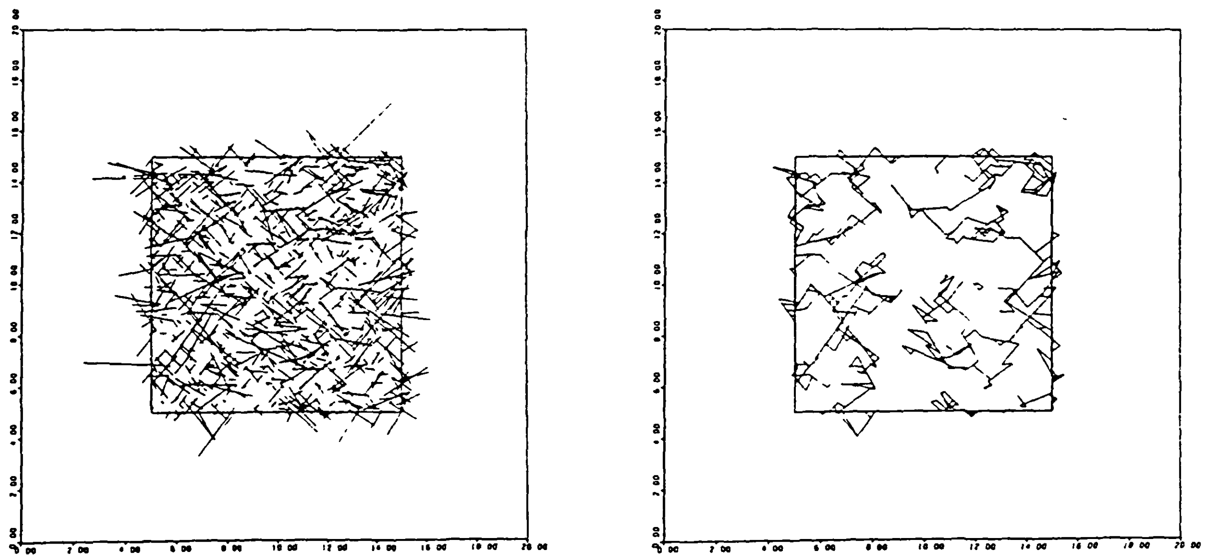

Test 4B

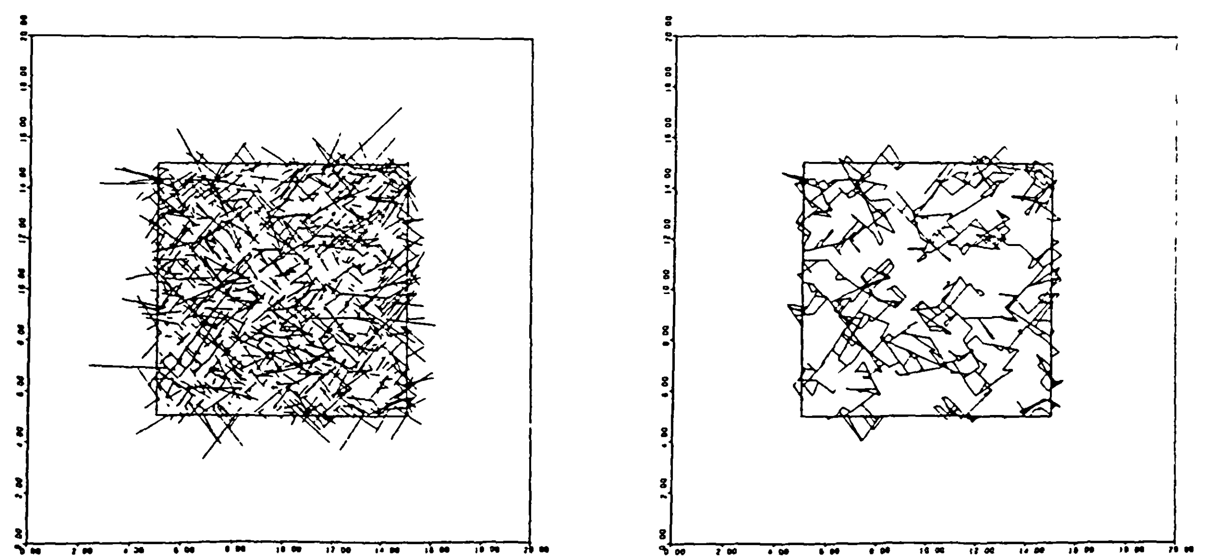

Test 4C

Fig. 4.17 Continued

GENERATED MESH   INTER-CONNECTED MESH

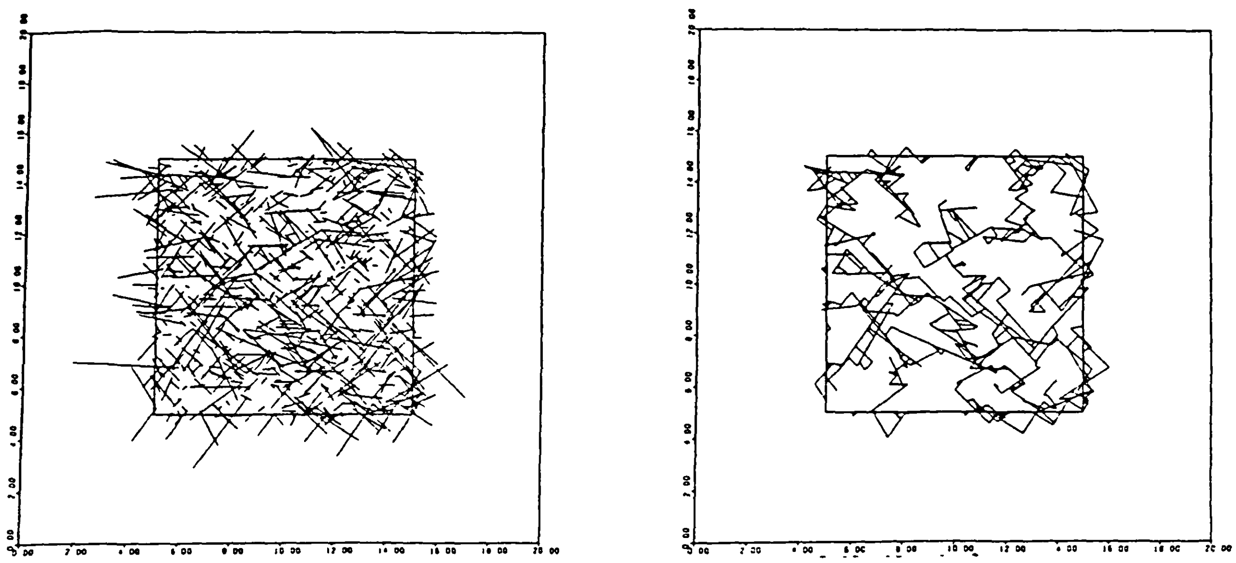

Test 5A

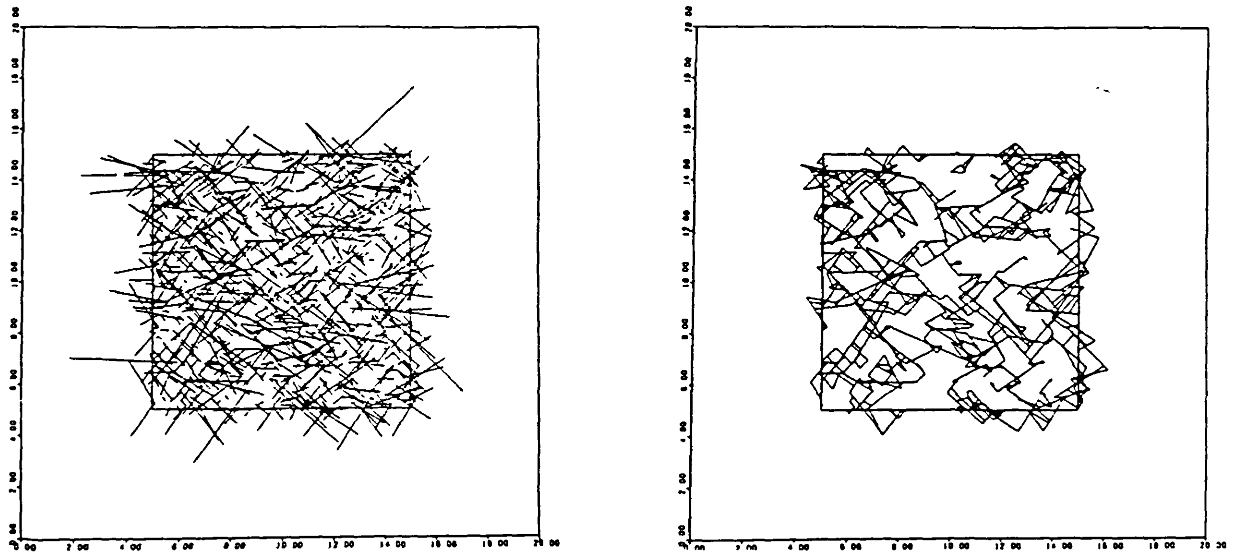

Test 5B

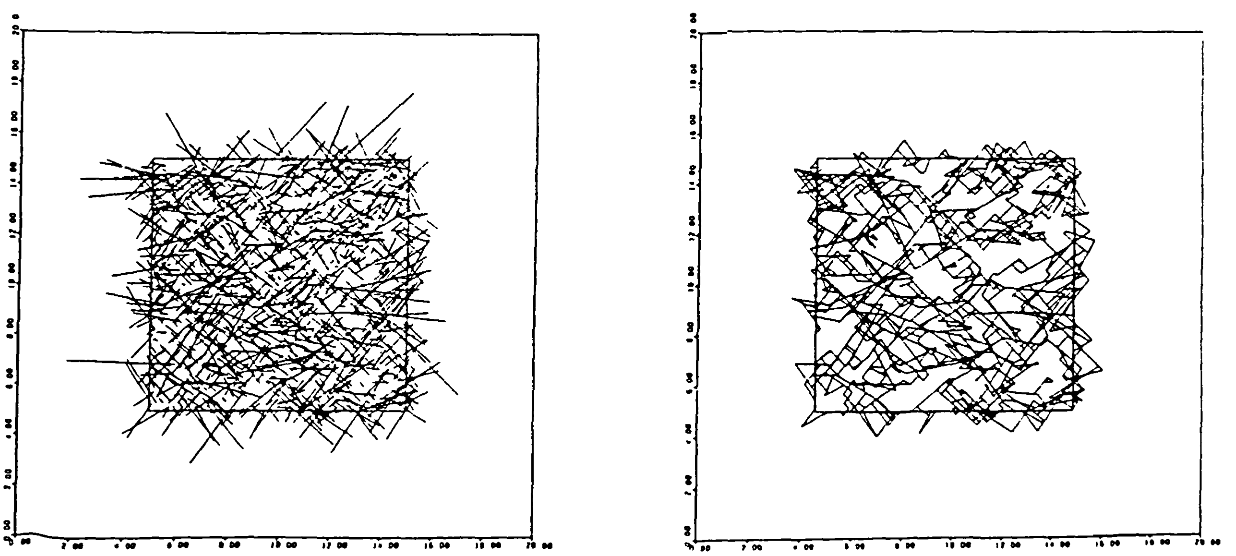

Test 5C

Fig. 4.17 Continued

GENERATED MESH INTER-CONNECTED MESH

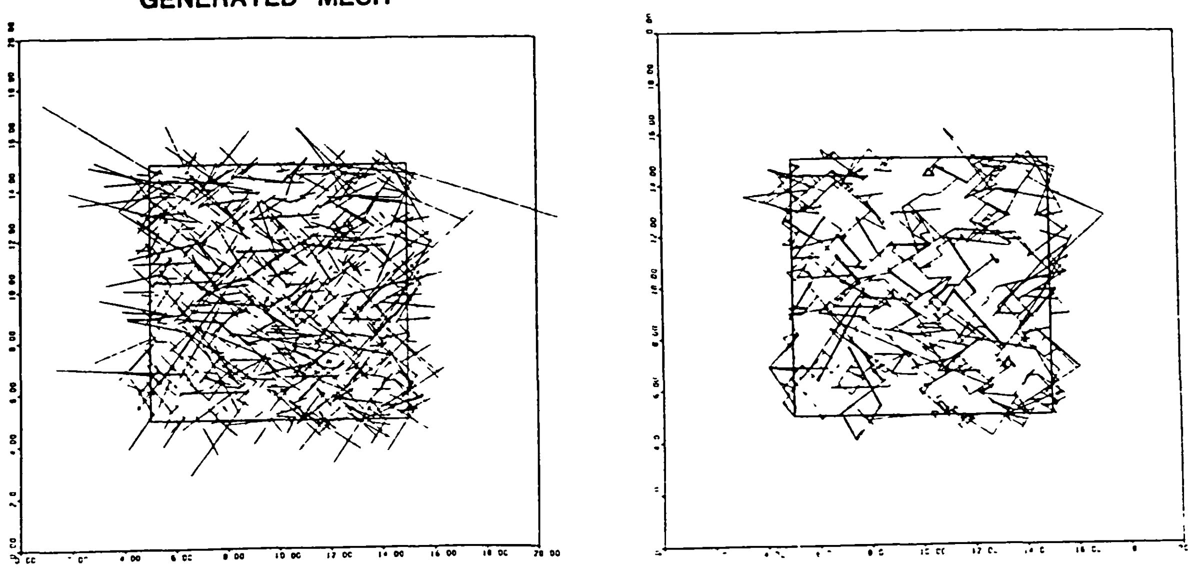

Test 6A

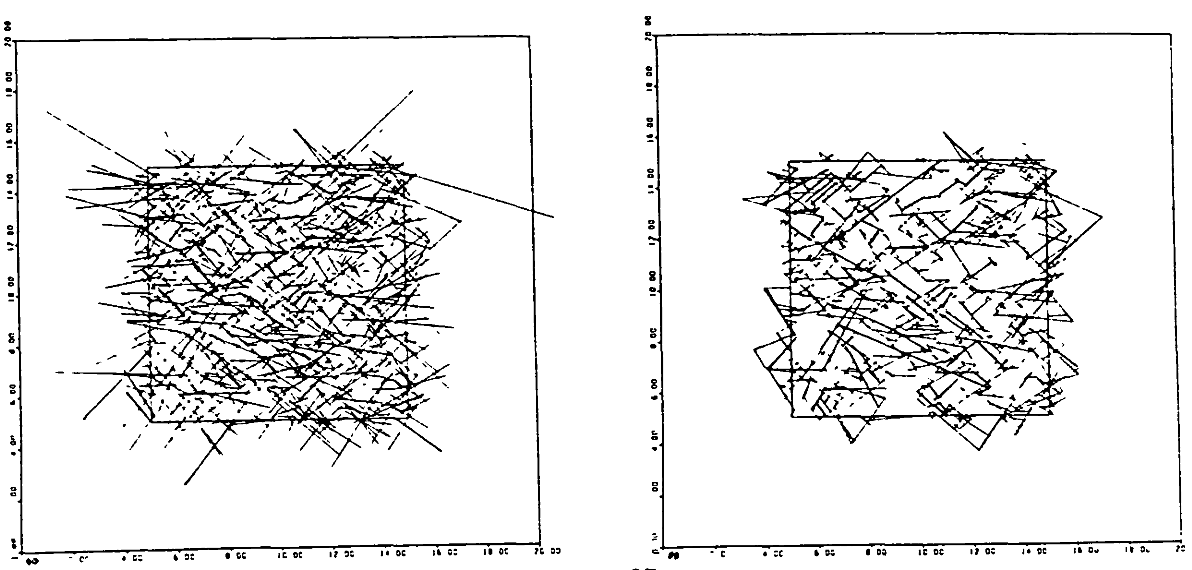

Test 6B

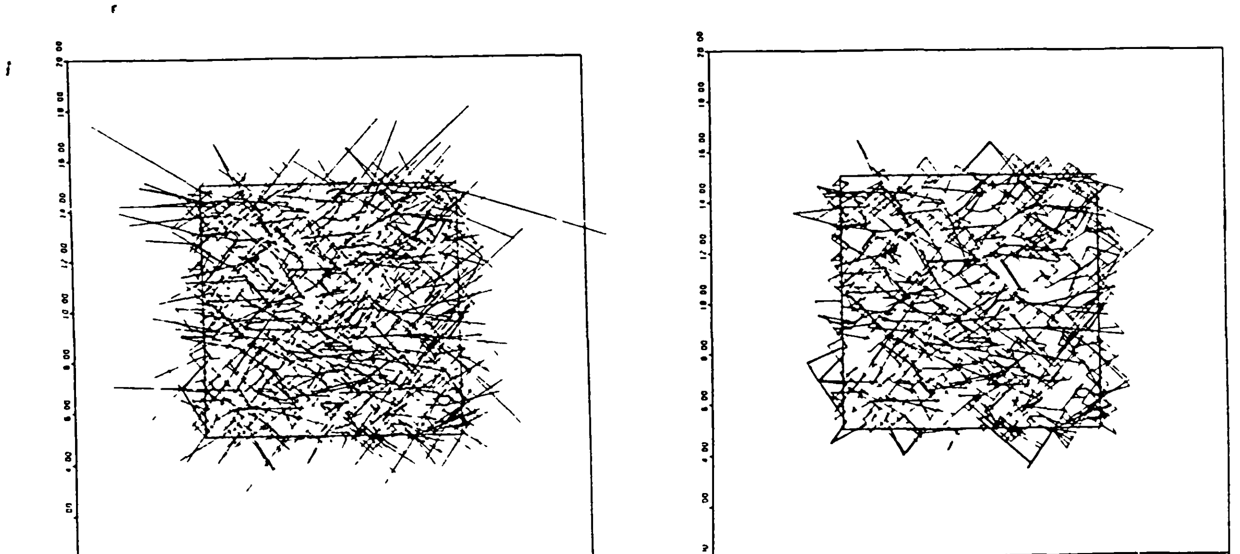

Test 6C

Fig. 4.17 Continued

Parameter	Set 1	Set 2	Set 3
Orientation:			
mean	0°	45°	135°
standard deviation	10°	10°	10°
type of distribution	Normal	Normal	Normal
(1) Trace length (m)			
mean 1	0.2	0.2	0.2
2	0.4	0.4	0.4
3	0.5	0.5	0.5
4	0.6	0.6	0.6
5	0.8	0.8	0.8
6	1.0	1.0	1.0
type of distribution	Neg. Exp.	Neg. Exp.	Neg. Exp.
(2) Number of discontinuities			
A	750	1125	1125
B	900	1550	1550
C	1000	2000	2000
Aperture (mm)	0.05	0.05	0.05

Table 4.II Input data for the trace length and density analysis

TEST	I_D	I_N	PERMEABILITY TENSOR m/s K_{11}	K_{12}	K_{21}	K_{22}
1A	0.019	0.234	1.115447E-11	-1.050673E-19	-2.265305E-19	1.038504E-10
1B	0.016	0.184	3.941379E-11	-1.386691E-19	-2.257173E-19	1.197469E-10
1C	0.017	0.171	3.941379E-11	-1.954542E-19	-3.353606E-19	1.254019E-10
2A	0.0625	0.266	3.355236E-10	-1.909128E-19	-2.745911E-19	1.074815E-09
2B	0.0805	0.269	5.163947E-10	-1.855993E-18	-1.689755E-18	1.569366E-09
2C	0.1010	0.291	2.333070E-09	6.029011E-18	4.210853E-18	3.490430E-09
3A	0.139	0.411	2.960936E-09	-5.979038E-19	-1.851606E-18	3.379891E-09
3B	0.221	0.529	5.966430E-09	-6.205168E-10	-6.205168E-10	6.342346E-09
3C	0.327	0.657	1.322815E-08	7.724549E-10	7.724549E-10	1.077330E-08
4A	0.284	0.620	1.062725E-08	-1.274360E-09	-1.274360E-09	1.392200E-08
4B	0.424	0.783	1.584270E-08	-1.370362E-09	-1.370362E-09	2.324113E-08
4C	0.514	0.849	6.247123E-08	1.470063E-11	1.470063E-11	3.898390E-08
5A	0.556	0.874	5.652949E-08	-5.650517E-09	-5.650517E-09	4.579821E-08
5B	0.637	0.919	1.195651E-07	2.839288E-09	2.839288E-09	8.336006E-08
5C	0.700	0.947	2.124980E-07	7.824750E-09	7.824750E-09	1.445009E-07
6A	0.701	0.947	1.443890E-07	-4.409059E-09	-4.409058E-09	1.084357E-07
6B	0.744	0.963	2.417367E-07	3.315741E-10	3.315741E-10	1.673324E-07
6C	0.789	0.976	3.560728E-07	8.249877E-09	8.249877E-09	2.584541E-07

Table 4.III Connectivity indices and permeability tensor for the trace length and density analysis.

In order to establish when the discontinuity mesh starts to behave like a continuous medium a criterion such as the one presented in the preceeding section is applied here. As before the expected flows were calculated from the permeability tensors using equation (4.4), then these expected flows were compared with those flows calculated by the program DIFLOW and the relative error calculated using equation (4.5). A plot of the flow relative error against the node index was constructed and is presented in Fig. 4.19. It can be seen that the relative error decreases exponentially as the node index increases. For values of node index greater than 0.90 the relative error is in the range 0.20 to 0.10. For low values of the node index(less than about 0.10) the relative error can be quite high and can even exceed 15.0. Since the results shown here correspond to only single mesh realisation for each group of input parameters, it is necessary to introduce at this point some results obtained earlier to account for the variability introduced by taking account of random effects. In Section 4.2.1, it was found that the relative error bandwidth for confidence levels of 95 percent and 99 percent were 0.14 and 0.18 respectively. Therefore, combining the results of both sections it is possible to conclude that:

For a node index greater than 0.50 there is 95 percent chance that the boundary flows can be predicted with a relative error lying within the range 1.14 and 0.86, and a 99 percent chance of predicting flow with a relative error lying in the range 1.18 and 0.82.

For a node index greater than 0.90 there is 95 percent chance that the boundary flows can be predicted with a relative error lying within the range 0.36 and 0.08, and a 99 percent chance of predicting flow with a relative error lying in the range 0.40 and 0.04.

The above approach is the only quantitative way to define when the continuum approach is a valid approximation for flow through a network. This is because the flows across the boundaries of the sample area are very much dependent on the actual location of the boundary; observed flows will always have some inherent variability due to this effect alone.

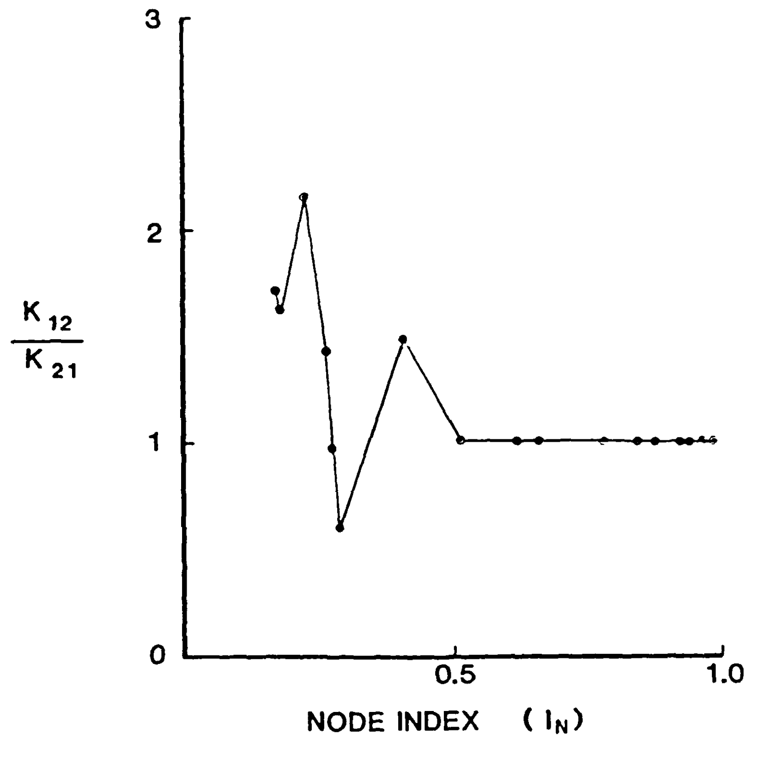

Fig. 4.18 Node index against the ratio K_{12}/K_{21} for the discontinuity trace length and density analysis

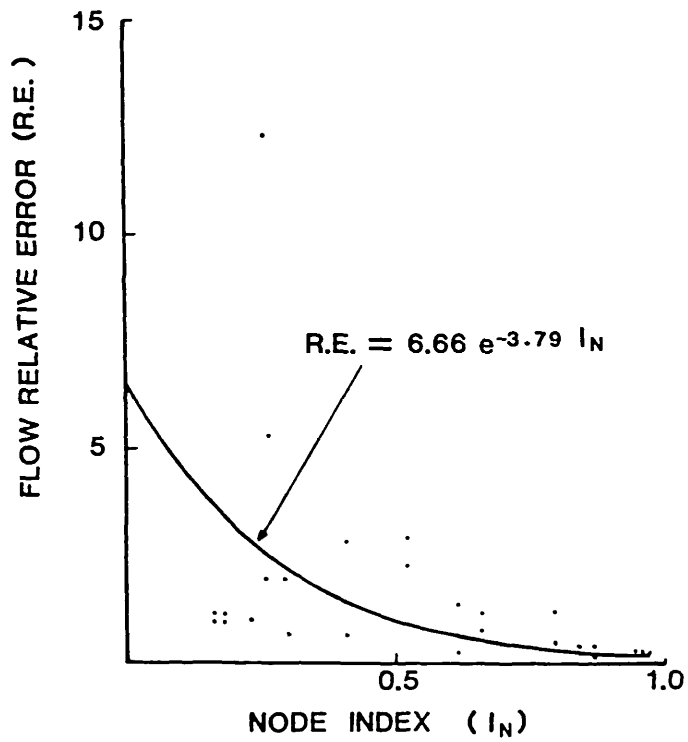

Fig. 4.19 Node index against the flow relative error for the discontinuity trace length and density analysis

Fig. 4.20 shows the plot of each of the two connectivity indices against the diagonal terms of the EPT. It was found that a cubic polynomial produced the best fit for the data points. Although a quadratic polynomial also produced a good fit, giving correlation coefficients ranging between 0.96 - 0.97, it was the cubic polynomial that produced the "S" shaped curve that most realistically represented the data points. It can be seen from the curves that for low values of connectivity index, i.e., node indices less than 0.3 and discontinuity indices

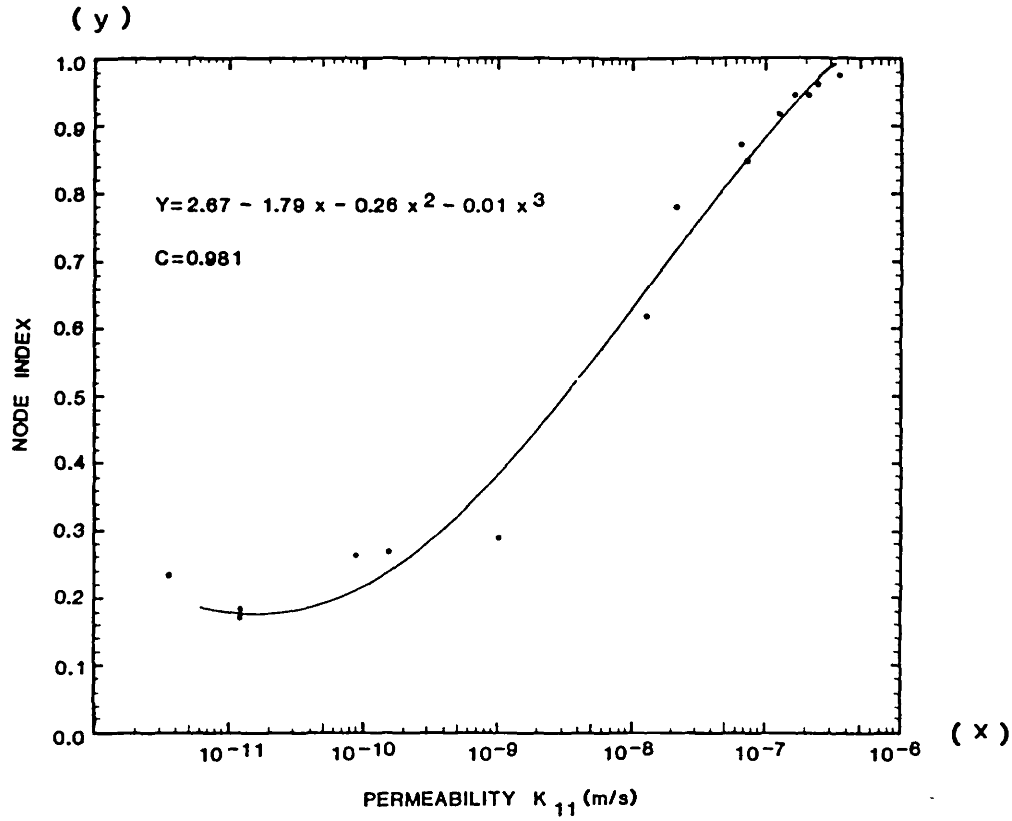

(a)

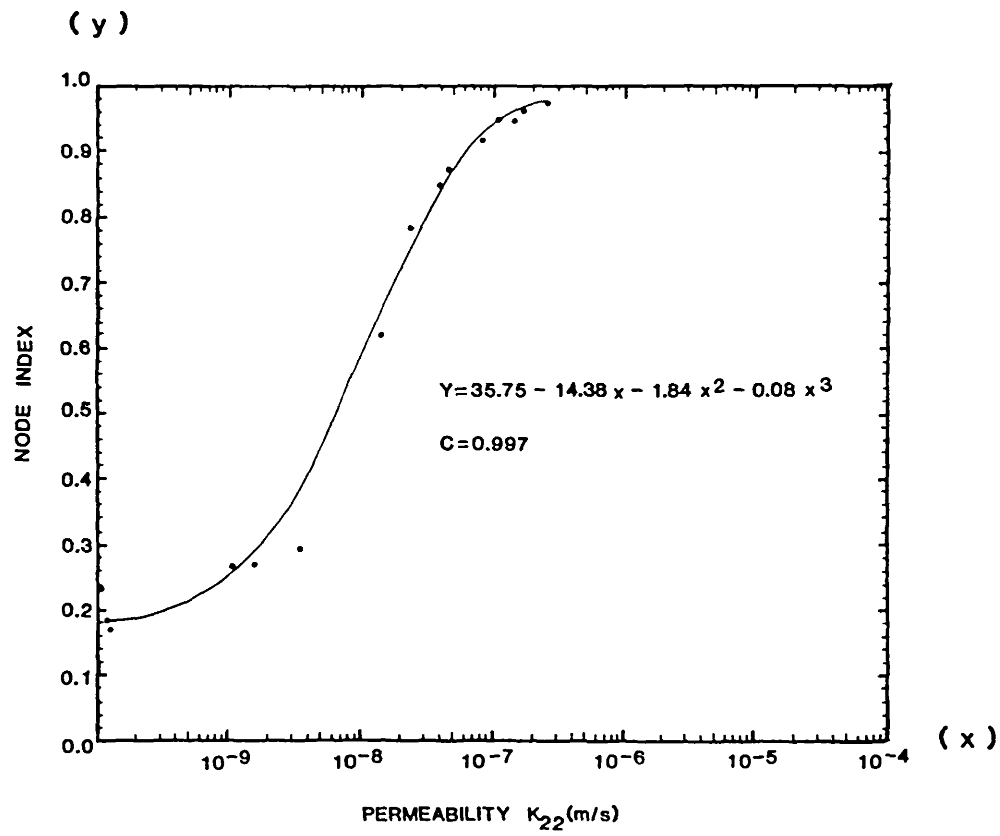

Fig. 4.20 Connectivity indices against diagonal terms of the EPT

(a) Node index

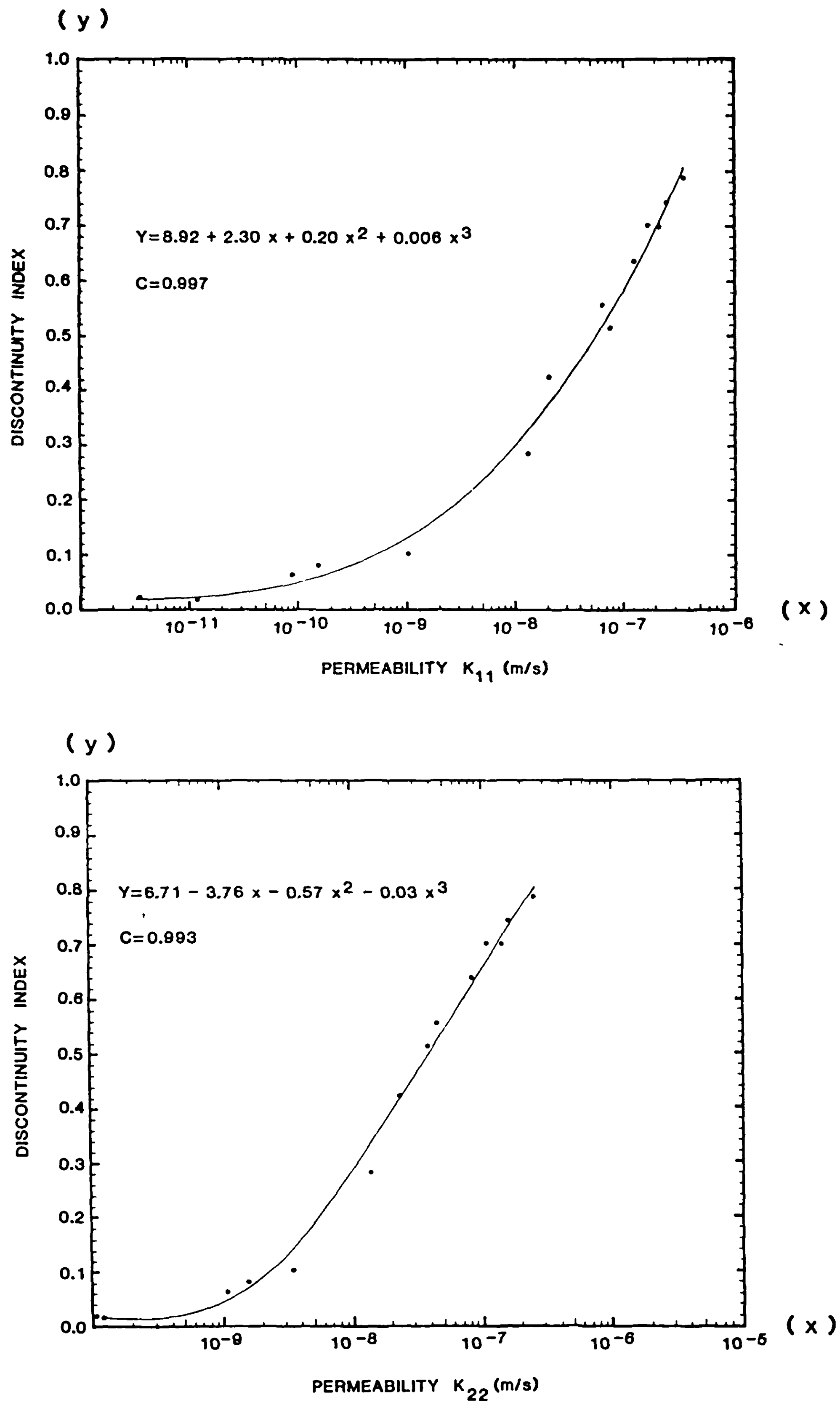

(b)

Fig. 4.20 (b) Discontinuitv index

less than 0.1 the slope of the curve is very low. Here the permeability is relatively insensitive to changes in the connectivity indices. As the connectivity indices increase, i.e. node index between 0.3 and 0.9 and the discontinuity index between 0.1 and 0.8, the permeability becomes very sensitive to small changes in connectivity index. Finally if the connectivity index increases further, i.e. node index greater than 0.9 and discontinuity index greater than 0.8, the slope of the curve becomes flatter and the permeability is again relatively insensitive to changes of connectivity index.

It was noted earlier in this chapter that the connectivity index is a function of several geometric properties of the discontinuity mesh. An attempt to link some of these properties with the concept of connectivity index is presented below. Fig. 4.21 shows the plot of discontinuity index against node index for values showed in Table 4.III. Here, again the node index overestimates the discontinuity index. The best fit this time was, however, obtained by a power curve in contrast to the straight line that best fitted the data of Section 4.2.1, shown in Fig. 4.11. The explanation for this is that the variability of the indices in the former case was only caused by the random variability of different realisations based upon identical input parameters; in the latter case the input data were actually changed for each mesh realisation. This has also meant that the range of values of the indices presented in Section 4.2.1 is small compared to the range of values presented here.

Even though the relation in Fig. 4.21 is non-linear, the correlation coefficient of 0.981 implies that there is a strong correlation between the two indices of connectivity.

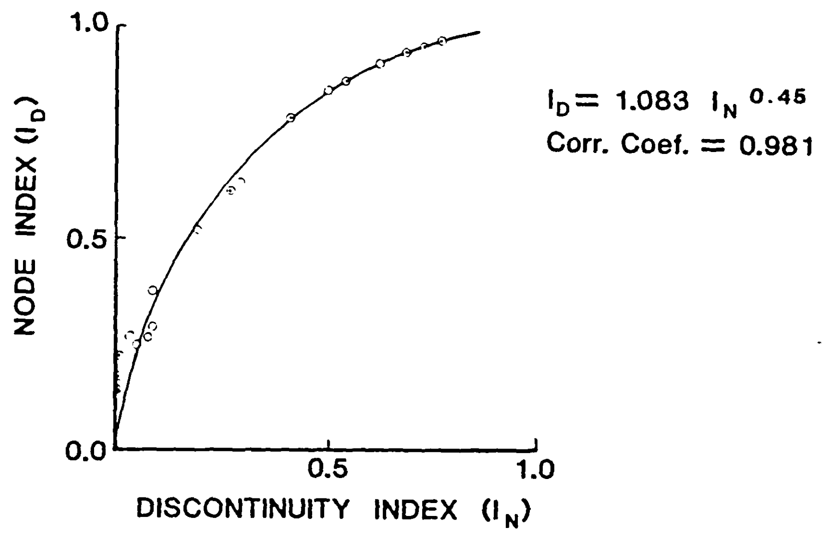

Fig. 4.21 Discontinuity index against node index for the discontinuity trace length and density analysis

The node and the discontinuity indices were plotted against the ratio of mean trace length, $\bar{\ell}$, to side the length, L, of the sample area, as shown in Fig. 4.22. Each curve corresponds to a particular discontinuity density. As this density increases, both of the connectivity indices increase, but at different rates. When the ratio $\ell/L < 0.02$ the change in connectivity is small and is almost un-affected by changes in density. As the ratio $\bar{\ell}/L$ increases to approximately 0.08 the connectivity begins to change dramatically. The curves become steeper as the discontinuity density increases, i.e, the rate of change of connectivity becomes more rapid. When $\bar{\ell}/L > 0.08$ the rate of change of the connectivity indices decreases rapidly and becomes less sensitive to changes in discontinuity density. In summary it can be said that connectivity is very sensitive to trace length for ratios $\bar{\ell}/L$ between 0.04 to 0.10 when the discontinuity index is used to measure connectivity and between 0.02 and 0.08 when the node index is considered.

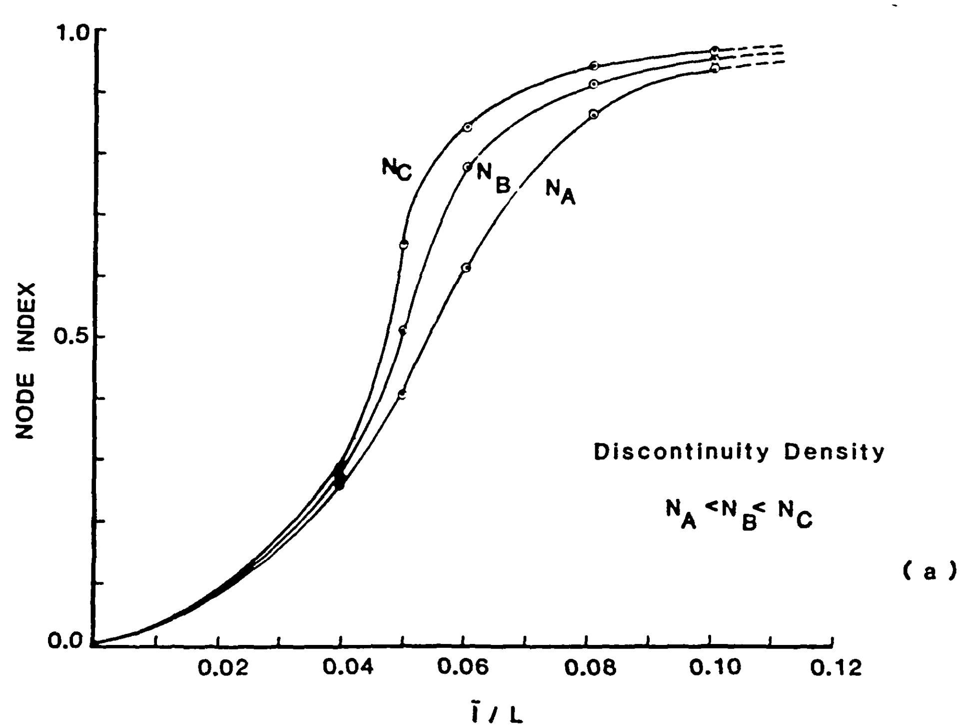

Fig. 4.22 Discontinuity index and node index against the ratio $\bar{\ell}/L$

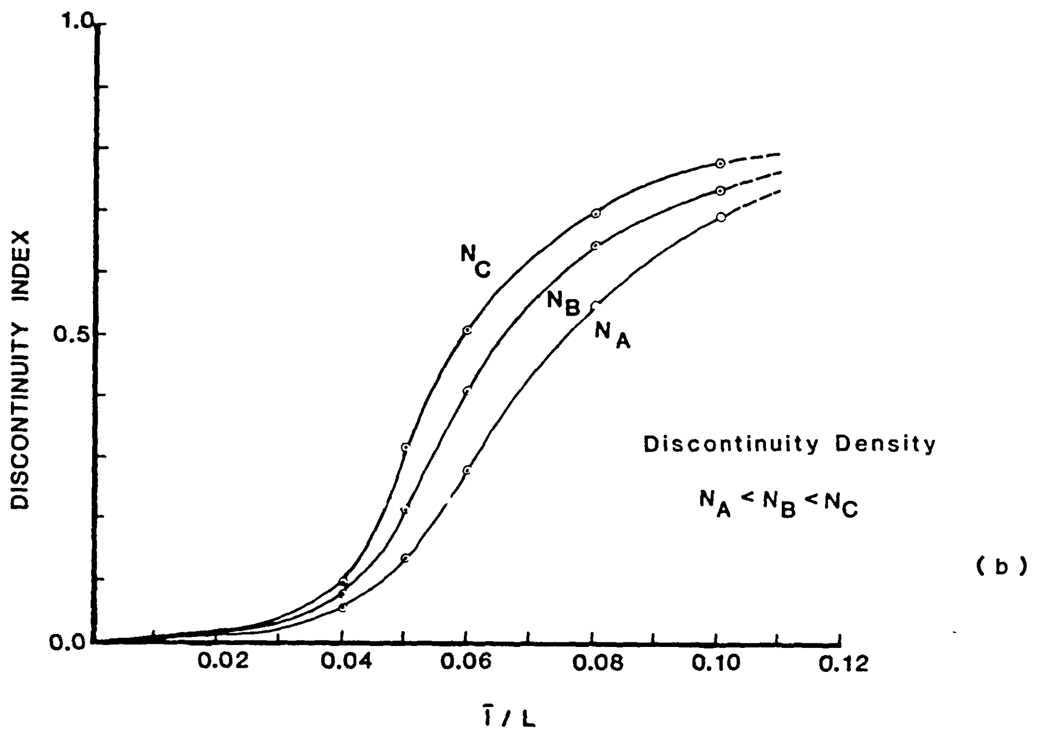

Fig. 4.22 Continued

An examination of the link between connectivity index and the discontinuity frequency of each discontinuity set is shown in Fig. 4.23. Each curve corresponds to a discontinuity set of a particular density for which the trace lengths have been varied according to Table 4.II. In total, there are three discontinuity sets and for each mesh, as before, the density has been incremented three times. Again in each case an "S" shaped curve is formed but contrary to the results shown in Fig. 4.22, this time the more dense the discontinuity set, the flatter the curves become, this is because as the density increases the changes in connectivity tend to be more gradual. The bottom tails of the curves for the sets of higher density do not pass through the origin. This is because the measurement of discontinuity frequency is conducted over the total number of discontinuities and not just the connected ones. It is, therefore, possible to have a finite discontinuity frequency and zero connectivity.

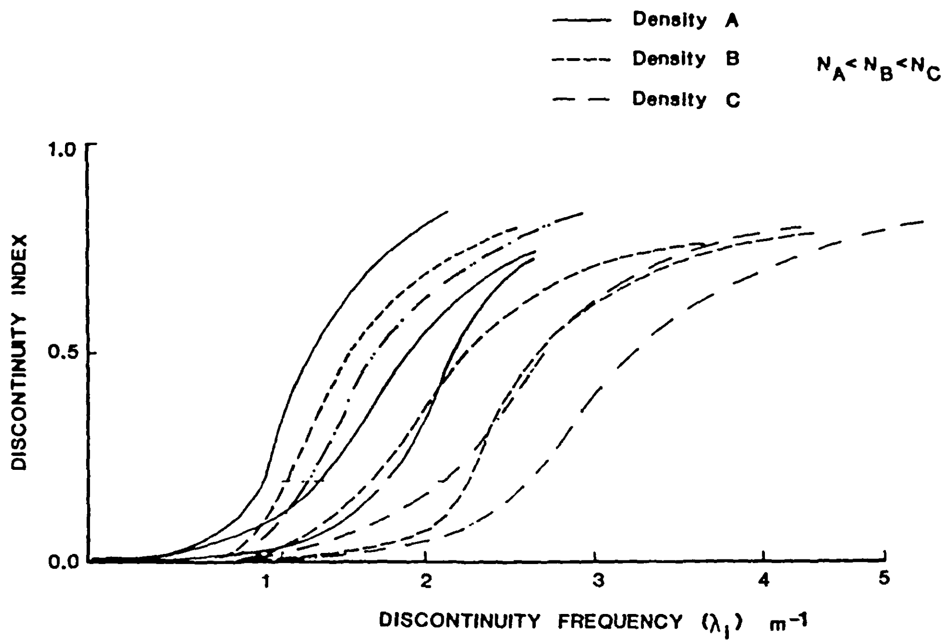

Fig. 4.23 Discontinuity index against discontinuity frequency for the discontinuity trace length and density analysis

4.2.3. Effects of changing the aperture of the discontinuities

This study is designed to analyse the effects on permeability of changes in discontinuity aperture. Two series of tests were performed. In the first series, discontinuity density and orientation were held constant, and the discontinuity trace length was varied in order to change the connectivity index. The discontinuity aperture was held constant throughout the mesh and was assumed to be represented by a parallel plate model. Four tests, each with different apertures were studied. In the second series of tests trace length was also held constant while two values of mean aperture were considered. In this latter series, aperture was assumed to follow a log-normal distribution.

The input data for the first series of tests are shown in Table 4.IV. The generation area used was 20 m by 20 m with the sample area in the central 10 m by 10 m square. The hydraulic gradient applied was h_i = 20 m and h_o = 10 m. As in previous examples, the connectivity analysis was carried out using the program DICONN. The information describing the interconnected meshes was then passed on to the DIFLOW program where the flow and the permeability tensor were calculated as in previous examples. Fig. 4.24 shows the resulting generated and interconnected meshes.

All combinations of the four trace lengths, from A to D, and four mean apertures, from 1 to 4, as listed in Table 4.IV, were used as input data; this gave 16 different meshes. For each mesh the hydraulic gradient was applied in two orthogonal directions; the x_1-direction and x_2-direction. The results of the permeability tensor calculations together with both indices of connectivity are shown in Table 4.V.

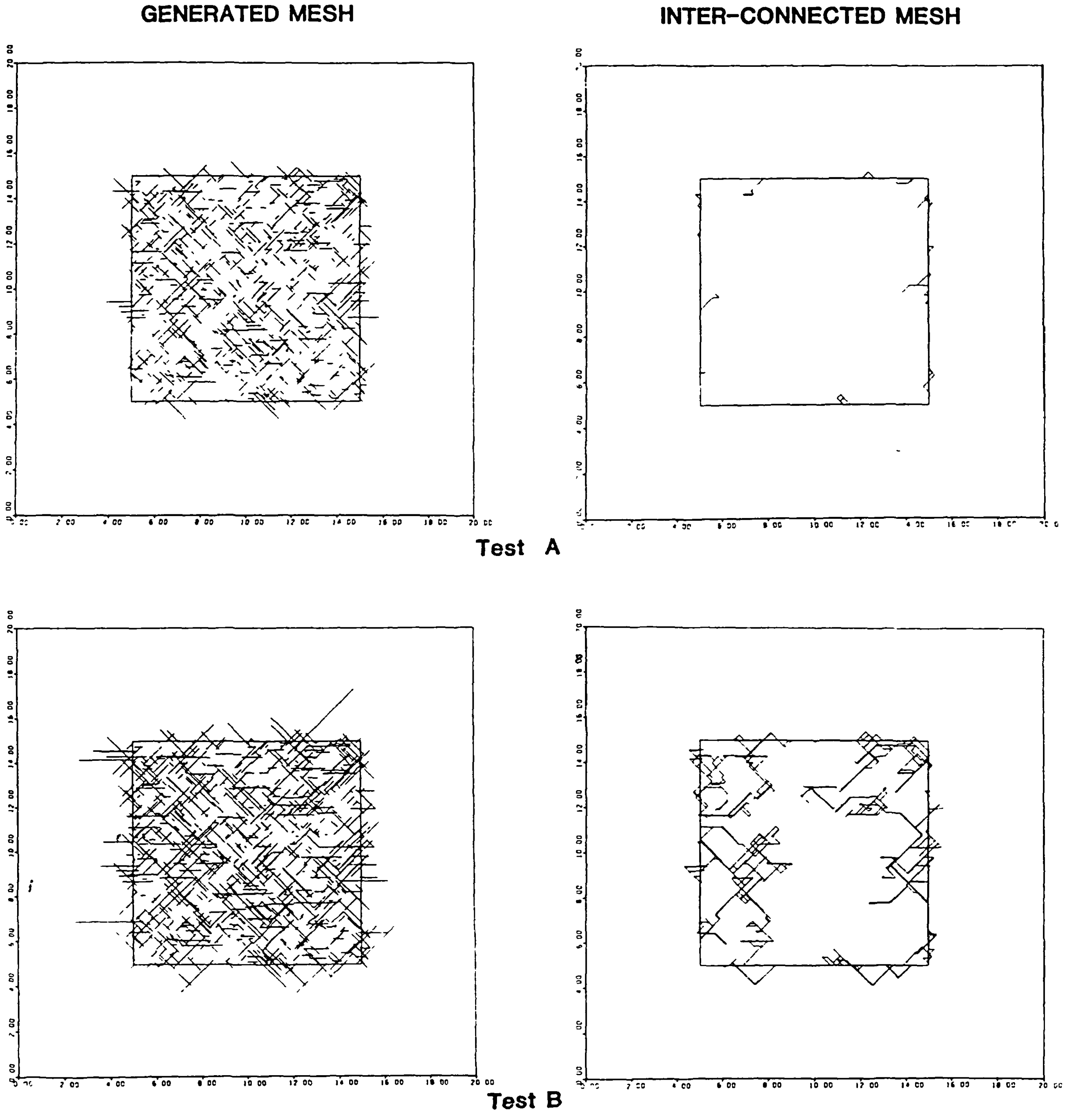

Fig. 4.24 The generated and inter-connected meshes for the discontinuity aperture analysis

GENERATED MESH

INTER-CONNECTED MESH

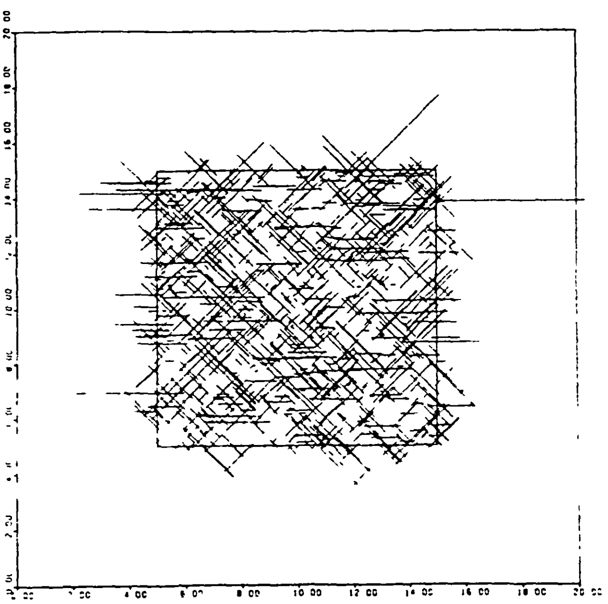

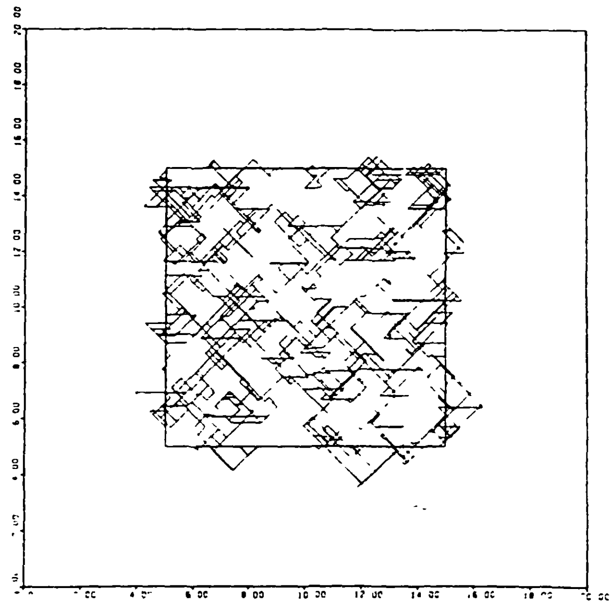

Test C

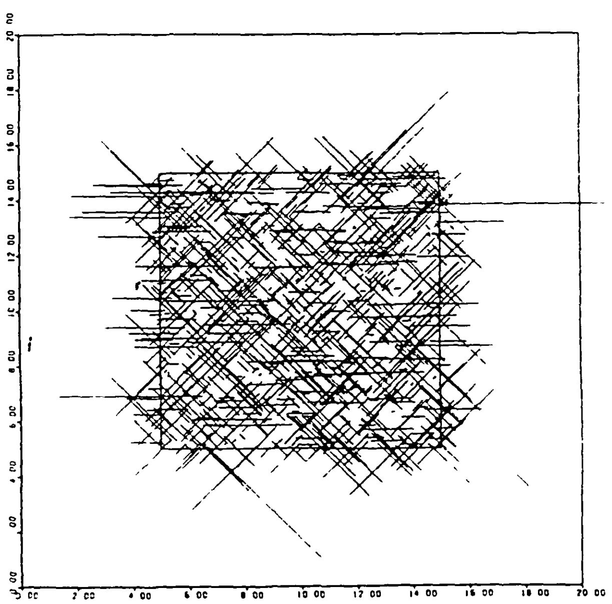

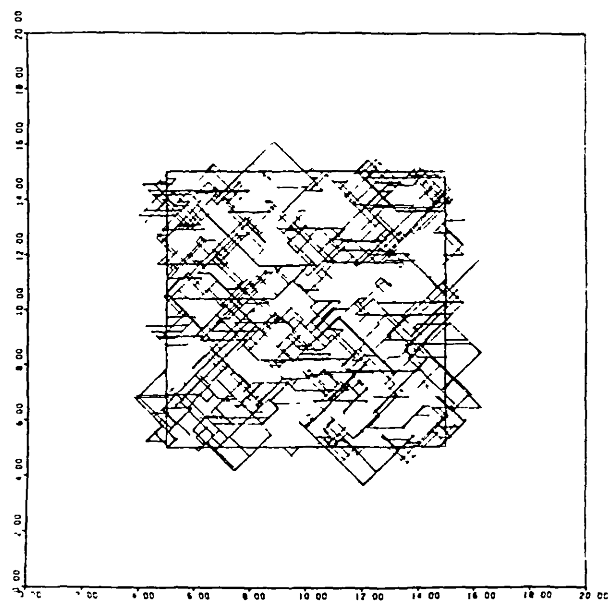

Test D

Fig. 4.24 Continued

Parameter	Set 1	Set 2	Set 3
Orientation:			
mean	0°	45°	135°
standard deviation	0°	0°	0°
type of distribution	Normal	Normal	Normal
(1) Trace length (m)			
mean A	0.4	0.4	0.4
B	0.6	0.6	0.6
C	0.8	0.8	0.8
D	1.0	1.0	1.0
type of distribution	Neg. Exp.	Neg. Exp.	Neg. Exp.
Number of discontinuities	900	1550	1550
(2) Aperture (mm)			
mean 1	0.01	0.01	0.01
2	0.05	0.05	0.05
3	0.10	0.10	0.10
4	0.50	0.50	0.50
S. deviation (mm)	0	0	0
(in all cases)			

Table 4.IV Input data for the discontinuity aperture analysis

TEST	I_N	I_D	PERMEABILITY TENSOR m/s			
			K_{11}	K_{12}	K_{21}	K_{22}
1A	0.266	0.077	4.157876E-12	-4.697384E-23	-1.229087E-22	1.981720E-11
1B	0.676	0.349	1.428515E-10	-3.095158E-12	-3.078812E-12	2.082424E-10
1C	0.906	0.605	9.437778E-10	2.132117E-11	2.132225E-11	6.934056E-10
1D	0.954	0.728	1.880048E-09	2.399680E-11	2.399755E-11	1.253962E-09
2A	0.266	0.077	5.198482E-10	6.373123E-21	2.595601E-20	2.477150E-09
2B	0.676	0.349	1.785794E-08	-3.861361E-10	-3.835182E-10	2.602998E-08
2C	0.906	0.605	1.179726E-07	2.665591E-09	2.665601E-09	8.667612E-08
2D	0.954	0.728	2.350060E-07	2.999703E-09	2.999670E-09	1.567453E-07
3A	0.266	0.077	4.158786E-09	5.098498E-20	2.076481E-19	1.981720E-08
3B	0.676	0.349	1.428635E-07	-3.089089E-09	-3.071931E-09	2.080092E-07
3C	0.906	0.605	9.437805E-07	-2.132473E-08	2.132481E-08	6.934089E-07
3D	0.954	0.728	1.880048E-06	2.399760E-08	2.399711E-08	1.253962E-06
4A	0.266	0.077	5.198482E-07	-6.420891E-18	-1.762777E-17	2.477150E-06
4B	0.676	0.349	1.785876E-05	-3.862111E-07	-3.835182E-07	2.602998E-05
4C	0.906	0.605	1.179722E-04	2.665090E-06	2.665241E-06	8.667565E-05
4D	0.954	0.728	2.350061E-04	2.999675E-06	2.999703E-06	1.567452E-04

Table 4.V Results of the permeability tensor for the discontinuity aperture analysis. Constant aperture.

The relation between trace length, discontinuity frequency and connectivity index are shown, for this first series of tests, in Fig. 4.25. It can be seen in Fig. 4.25(a) that the node index again exceeds the discontinuity index; for the same reasons given earlier. The "S" shaped curve is also obtained, with a best fit given by a cubic polynomial. Fig. 4.25(b) shows the plots of discontinuity frequency for each set against the node index. In this first series of tests the standard deviation of orientation was assumed to be zero and the density constant; consequently the connectivity index was mainly affected by changes in trace length. The curve for set 1 is the steepest since it has the lowest density of the three sets. As the discontinuity frequence increases the node index increases rapidly up to 0.90, from there the rate of change of the node index decreases drastically as the discontinuity frequency continues increasing.

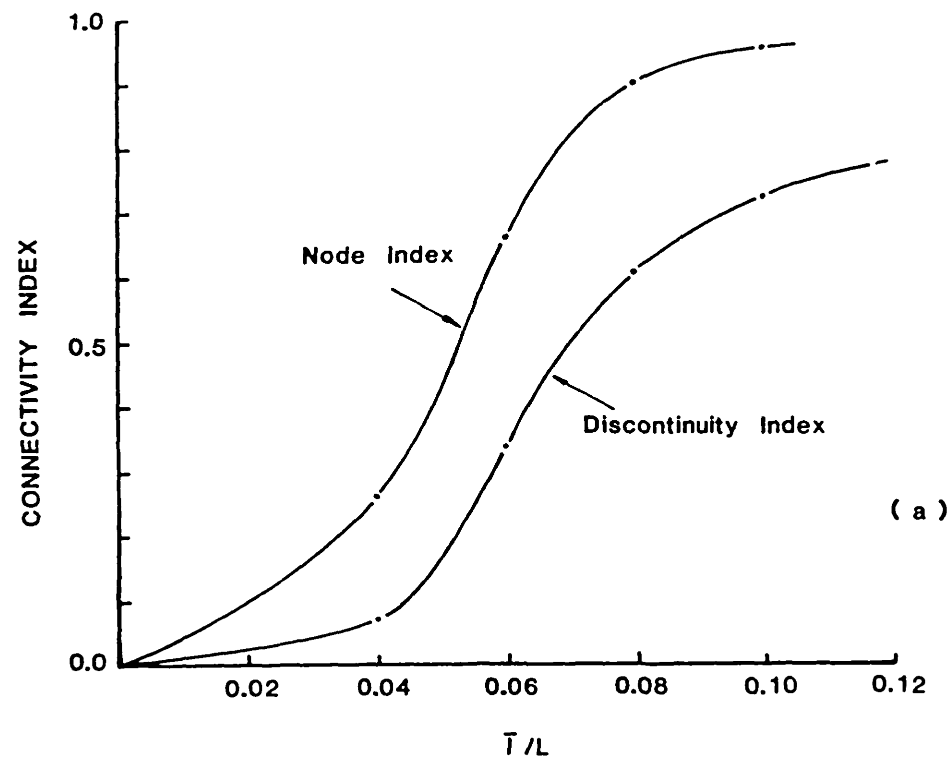

Fig. 4.25 (a) Connectivity index against ratio $\bar{\ell}/L$

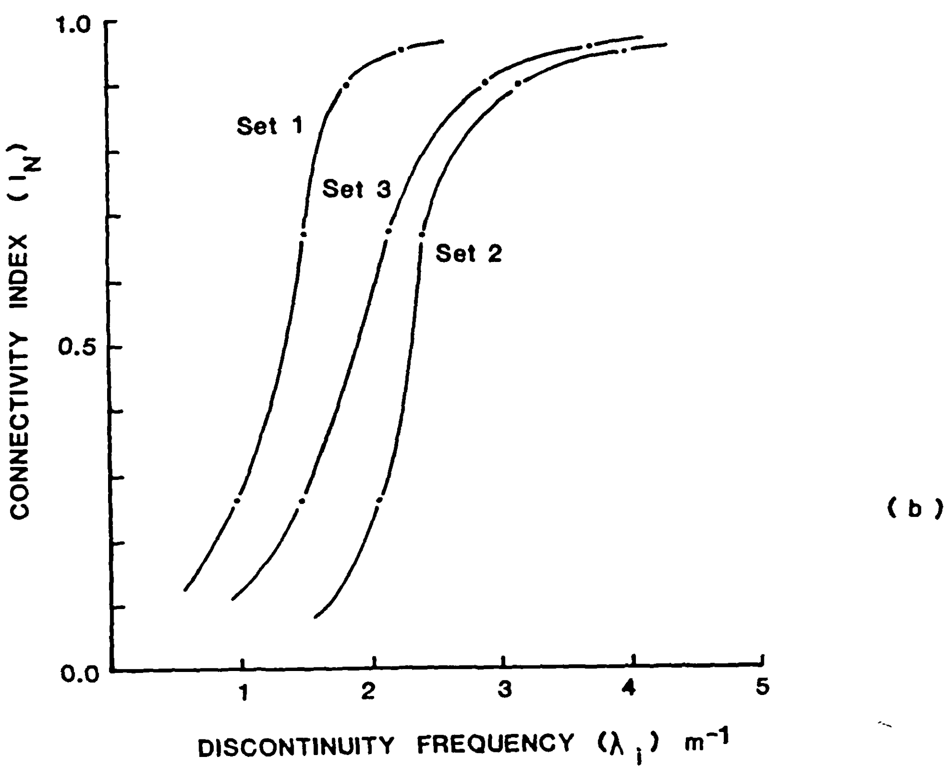

Fig. 4.25 (b) Connectivity index against the discontinuity frequency of each set

Fig. 4.26 shows a plot of the connectivity index (I_N) against each of the diagonal terms of the permeability tensor K_{11} and K_{22}. In each case the discontinuity aperture was assumed to be constant. Clearly, larger apertures lead to higher permeabilities. When connectivity is taken into consideration, however, it can be seen that for connectivity indices less than 0.4 and higher than 0.8, small changes of the connectivity index produce large changes in permeability. This was true for each of the four values of discontinuity aperture that were analysed.

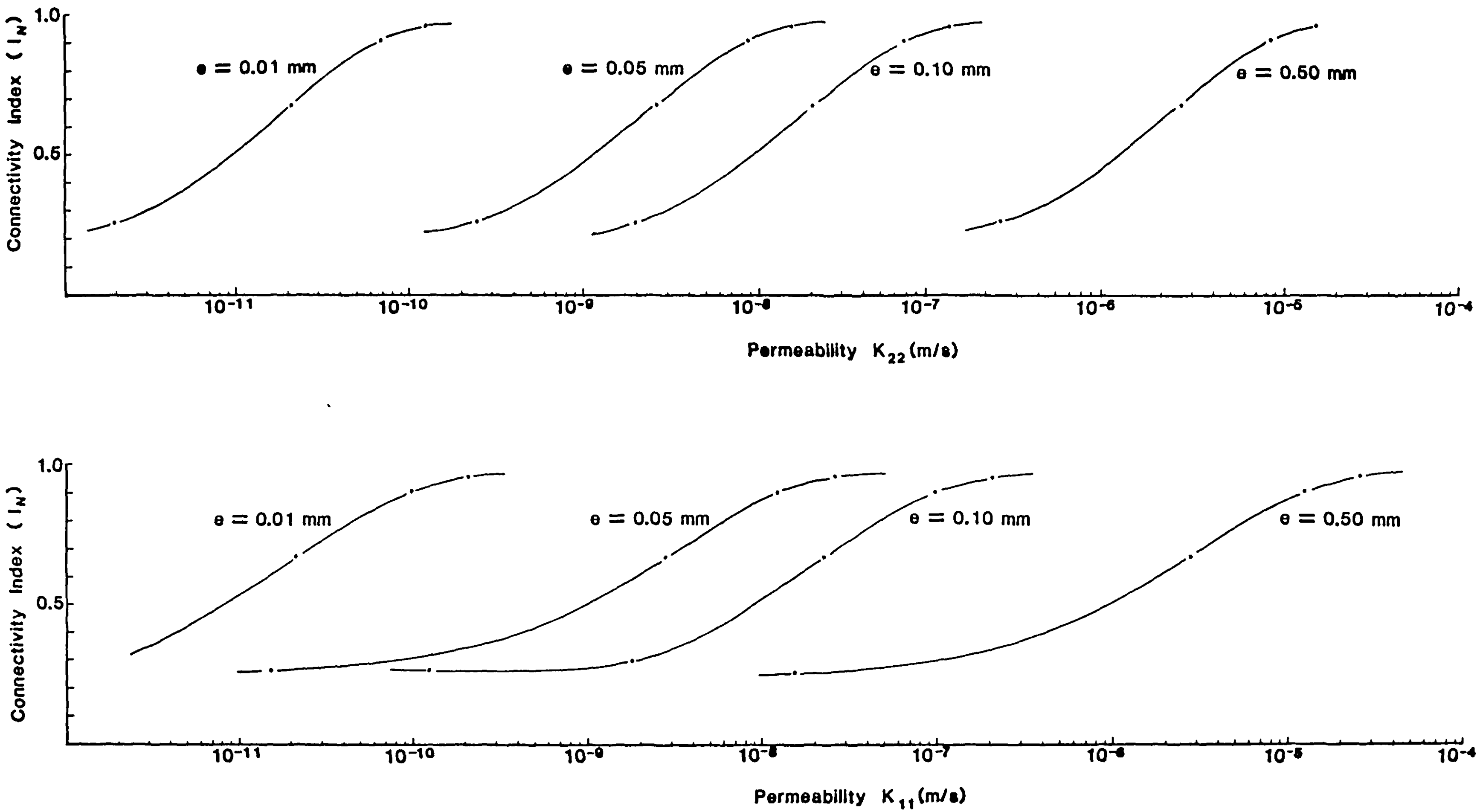

Fig. 4.26 Node index against the diagonal terms of the permeability tensor

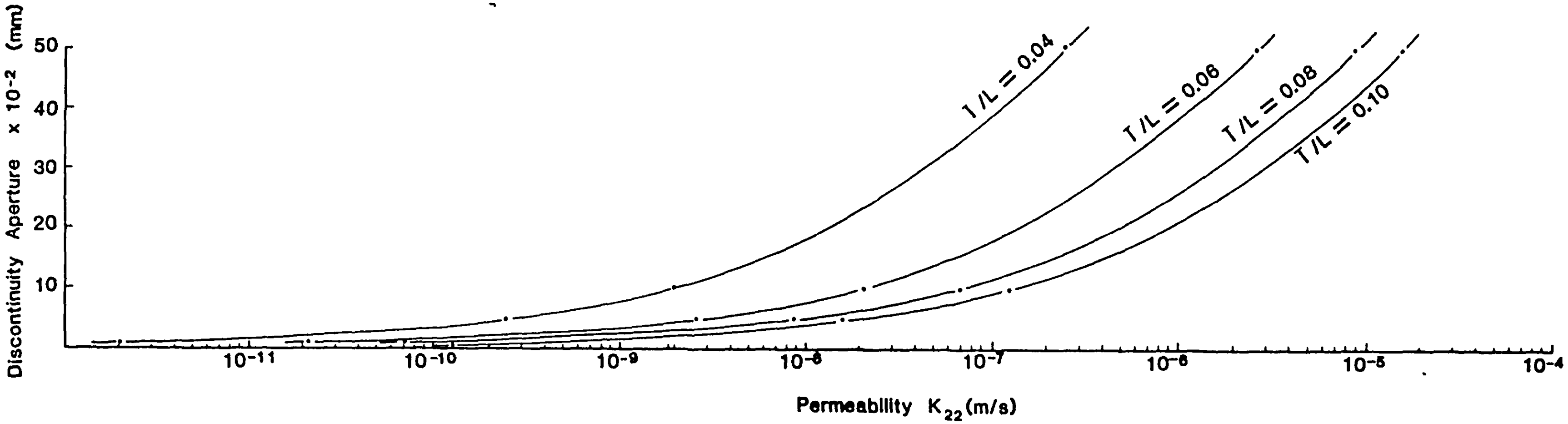

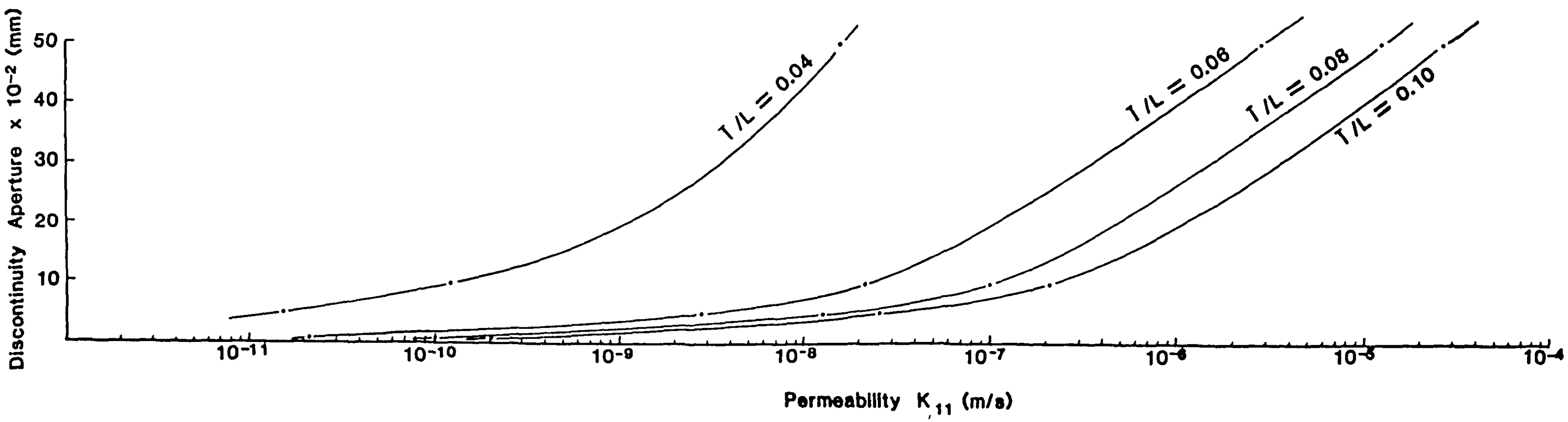

Fig. 4.27 Discontinuity aperture against the diagonal terms of the permeability tensor

The relation between the diagonal terms of the permeability tensor and the discontinuity aperture is shown in Fig. 4.27 for various values of the ratio of the input trace lenght, $\bar{\ell}$, to the size of the sample area, L. For a given ratio, $\bar{\ell}/L$, it can be seen that, if the aperture increases by Δe, each term of the permeability tensor increases by $(\Delta e)^3$. Although this result is expected it has previously only been proved on idealised discontinuity meshes containing discontinuities that transect the entire test area. As the ratio $\bar{\ell}/L$ increases, the curves of aperture versus permeability are shifted to the right, i.e. the overall permeability increases. The rate at which the permeability changes is, however, faster for the higher $\bar{\ell}/L$ ratios, especially when the aperture is less than 0.2 mm.

It can be seen from Table 4.V, that not all of the permeability tensors are symmetrical. In particular, tests numbers 1A, 2A, 3A and 4A have ratios for K_{12}/K_{21} of between 2 and 5. The remaining tests have a ratio K_{12}/K_{21} of between 0.995 and 1.0, however, for practical purposes they are considered to be symmetrical tensors by taking the average of K_{12} and K_{21}. The relative error in predicting flow across the boundaries was calculated, using equation 4.5, firstly for flows in the x_1 direction and then in the x_2 direction. It was found that the relative error in predicting flow in the x_1 direction varied between 2 and 6 percent, while in the x_2 direction it varied between 12 - 40 percent. The reason for this difference is the relative orientations of the discontinuity sets. Set 1 is orientated in the x_1 direction while the other two sets are at 45° and 135° repectively. It would, therefore, be expected that flow in the x_1 direction would be less variable and hence better represented by a continuum approximation.

The literature review presented in Chapter 2 shows that discontinuity aperture is one of the discontinuity parameters that is most difficult to measure. Several authors have suggested possible types of distributions that best describe observed aperture frequency distributions. In this work, based on the current knowledge of aperture distributions, it is assumed that apertures are log-normally distributed and that each discontinuity can be modelled by a smooth parallel plate.

The second series of tests was carried out using the input data from two of the tests presented earlier in this section; 2C and 4C. For this second series, however, the discontinuity apertures were allowed to follow a log normal distribution. The variability of aperture was described using the statistical concept of coefficient of variation i.e. (standard deviation/mean) x 100%. Five different coefficients of variation were selected, as shown in Table 4.VI. The generated meshes were first analysed by the connectivity program and then by the flow program. The results are shown in Table 4.VII, which includes values of the components of the permeability tensor and both of the connectivity indices.

Test	Discontinuity Aperture (mm)		
	Mean	S. Deviation	Coefficient of variability
A1	0.05	0.01	20 %
A2	0.05	0.02	40
A3	0.05	0.03	60
A4	0.05	0.04	80
A5	0.05	0.05	100
B1	0.50	0.10	20 %
B2	0.50	0.20	40
B3	0.50	0.30	60
B4	0.50	0.40	80
B5	0.50	0.50	100

Table 4.VI Variation of the discontinuity aperture

Test	Connectivity Index		PERMEABILITY TENSOR (m/s)			
	I_N	I_D	K_{11}	K_{12}	K_{21}	K_{22}
A1	0.906	0.605	1.149050E-07	4.901496E-09	4.901488E-09	8.742488E-08
A2	0.906	0.605	1.079336E-07	6.965968E-09	6.966069E-09	8.992891E-08
A3	0.906	0.605	1.043409E-07	1.274643E-08	1.274655E-08	9.832957E-08
A4	0.906	0.605	1.081210E-07	2.331609E-08	2.331609E-08	1.154738E-07
A5	0.906	0.605	1.214552E-07	4.143352E-08	4.143284E-08	1.418200E-07
B1	0.906	0.605	1.147620E-04	4.771334E-06	4.771467E-06	8.733794E-05
B2	0.906	0.605	1.081796E-04	7.209117E-06	7.209122E-06	8.989790E-05
B3	0.906	0.605	1.041242E-04	1.246706E-05	1.246700E-05	9.806569E-05
B4	0.906	0.605	1.079963E-04	2.315199E-05	2.315204E-05	1.153041E-04
B5	0.906	0.605	1.212755E-04	4.119887E-05	4.119889E-05	1.415102E-04

Table 4.VII Results of the permeability tensor for discontinuity aperture analysis. Variable aperture

Fig. 4.28 shows a plot of the aperture coefficient of variation against the relative change in permeability, (K-K*)/K*, where K is a diagonal terms of the permeability tensor for a mesh with variable aperture and K* the corresponding term of the permeability tensor for a mesh with constant aperture. It can be seen from this figure, and also Table 4.IV, that for both meshes the K_{11} term shows a negative change in permeability for aperture coefficients of variation of up to 60 percent; above this, changes in K_{11} become positive. For aperture coefficients of variation of up to 40 percent the change in the K_{22} term is almost negligible (only 3.75 percent). Beyond this point the change in permeability becomes positive, to give an overall change of almost 64 percent. The fact that K_{11} initially displays a negative change is caused by the randomness of the model. Although the input parameters were those specified in Table 4.VI, the actual mean values for the generated mesh were slightly different. In this particular example the mean trace length set 1 was underestimated by up to 6.0 percent, and the mean trace length of set 3 by up to 1 percent while the mean of trace length of set 2 was overestimated by up to 7.0 percent. Although it is difficult to make corrections to account for this, it is clear that the overall variability of K_{11} is less than that for K_{22}, for the same reasons already discussed in connection with the first series of runs. In summary the effect on permeability of variability in discontinuity aperture can be considered negligible for aperture coefficients of variation of up to 20 percent. For larger coefficients of variation, however, the effect on permeability increases rapidly depending on the anisotropy of the discontinuity mesh. The influence of the relative orientations of discontinuity sets as well as the relation between discontinuity frequency anisotropy and directional permeability will be discussed in the following section.

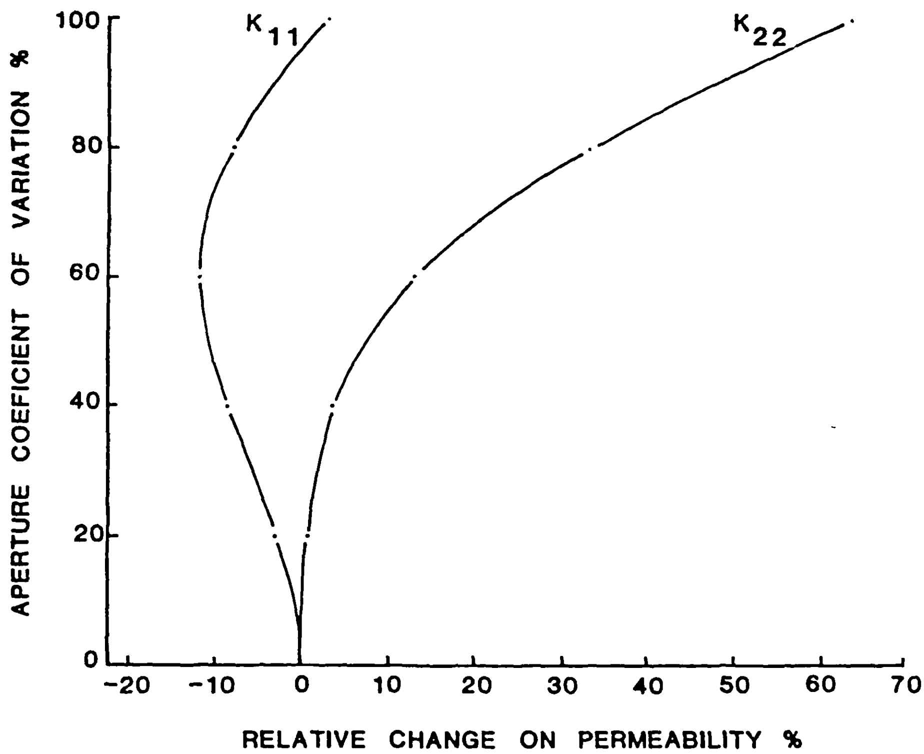

Fig. 4.28 Relative change in permeability against the aperture coefficient of variation

4.2.4 Effects of the relative orientation of the discontinuity sets

The object of this section is to study how connectivity and permeability change when the variability in the orientation of the discontinuity sets is increased. A group of tests was performed on discontinuity meshes generated according to the input data shown in Table 4.VIII. In all of the tests discontinuity density and aperture were held constant while mean trace lengths were increased in four equal stages, from 0.4 m to 1.0 m. The variability in orientation was achieved by increasing its standard deviation in 5 stages, from 0° to 60°.

As in the previous studies, the generation area used was 20 m by 20 m with a sample area in the central 10 m by 10 m square. The hydraulic gradient applied was h_i = 20 m and h_o = 10 m. The connectivity analysis was again done using the program DICONN and the flow and permeability analysis by the program DIFLOW. Fig. 4.29 shows the generated and interconnected meshes used in this work. Table 4.IX lists the connectivity indices and the components of the permeability tensors. Two plots, shown in Fig. 4.30, were constructed using the connectivity index and trace length data. In Fig. 4.30, as before, the connectivity indices increase as the ratio $\bar{\ell}/L$ increases. Again the typical "S" shaped curve was produced. It is not clear, however, how an increment in the orientation variability affects the connectivity index. It can be seen, for example, that when the standard deviation of the angle of orientation is increased from 0° through 10° to 20° the corresponding curves become increasingly steep. For values of

Parameter	Set 1	Set 2
Orientation:		
mean	0°	90°
S. deviation 1	0°	0°
2	10°	10°
3	20°	20°
4	40°	40°
5	60°	60°
type of distribution	Normal	Normal
Trace length (m)		
mean A	0.4	0.4
B	0.6	0.6
C	0.8	0.8
D	1.0	1.0
type of distribution	Neg. Exp.	Neg. Exp.
Number of discontinuities	2000	2000
Aperture (mm)		
mean	0.5	0.5
standard deviation	0.0	0.0
type of distribution	Log-normal	Log-normal

Table 4.VIII Input data for the orientation analysis

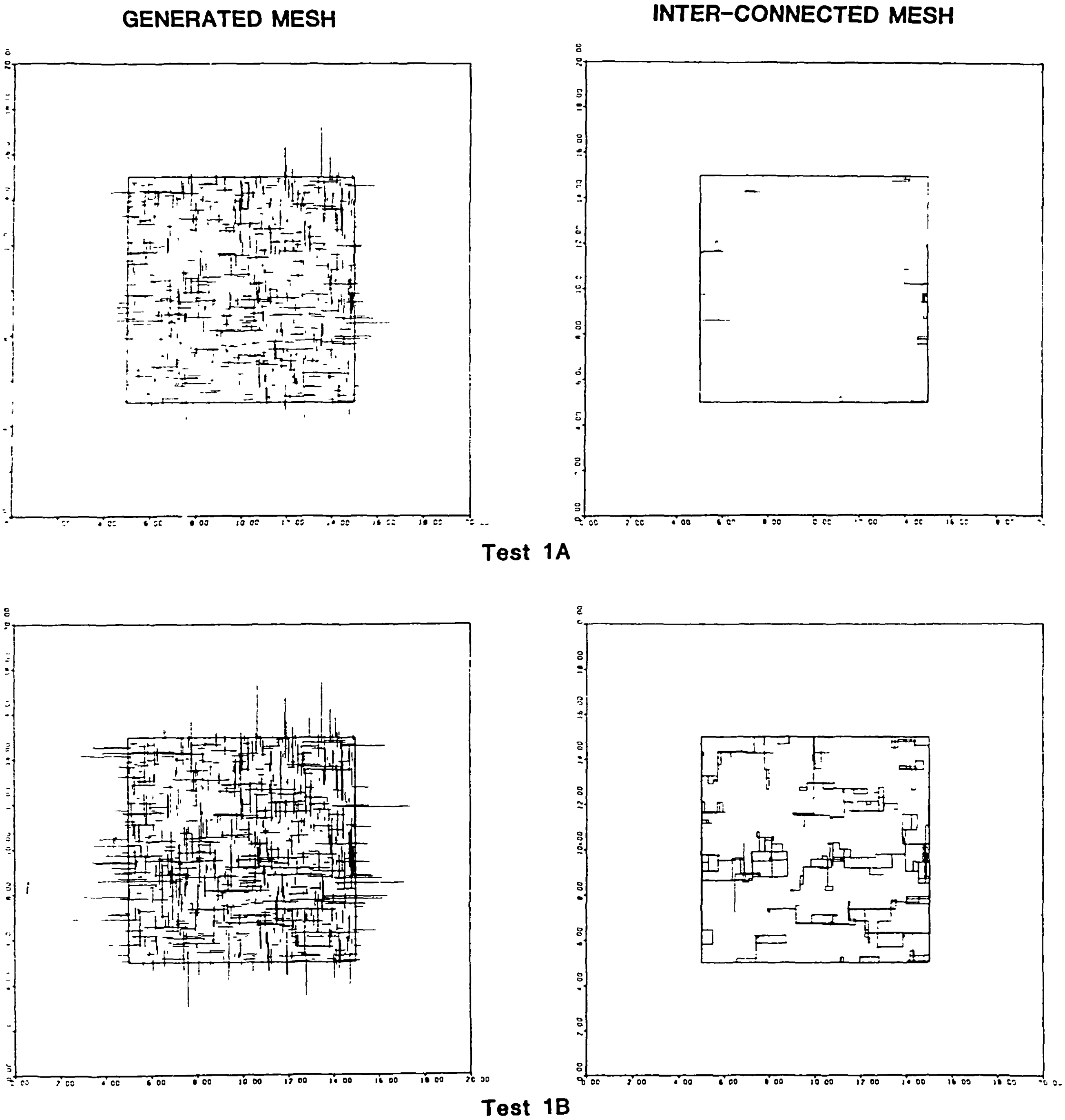

Fig. 4.29 The generated and inter-connected meshes for the discontinuitv set relative orientation analvsis

GENERATED MESH

INTER-CONNECTED MESH

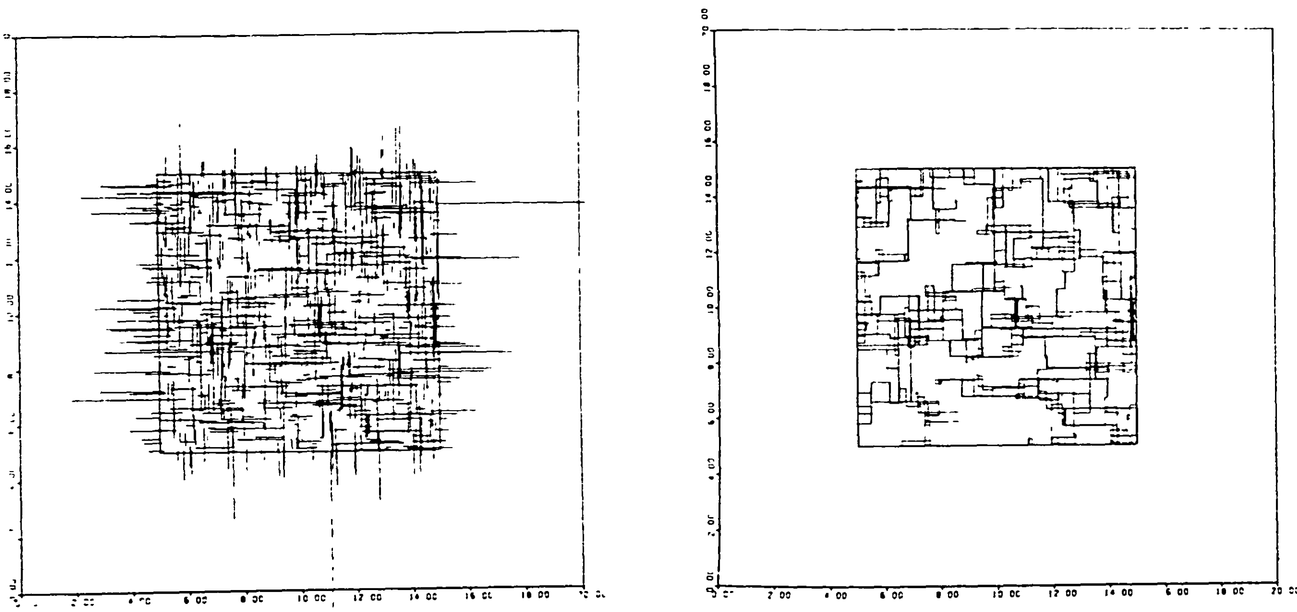

Test 1C

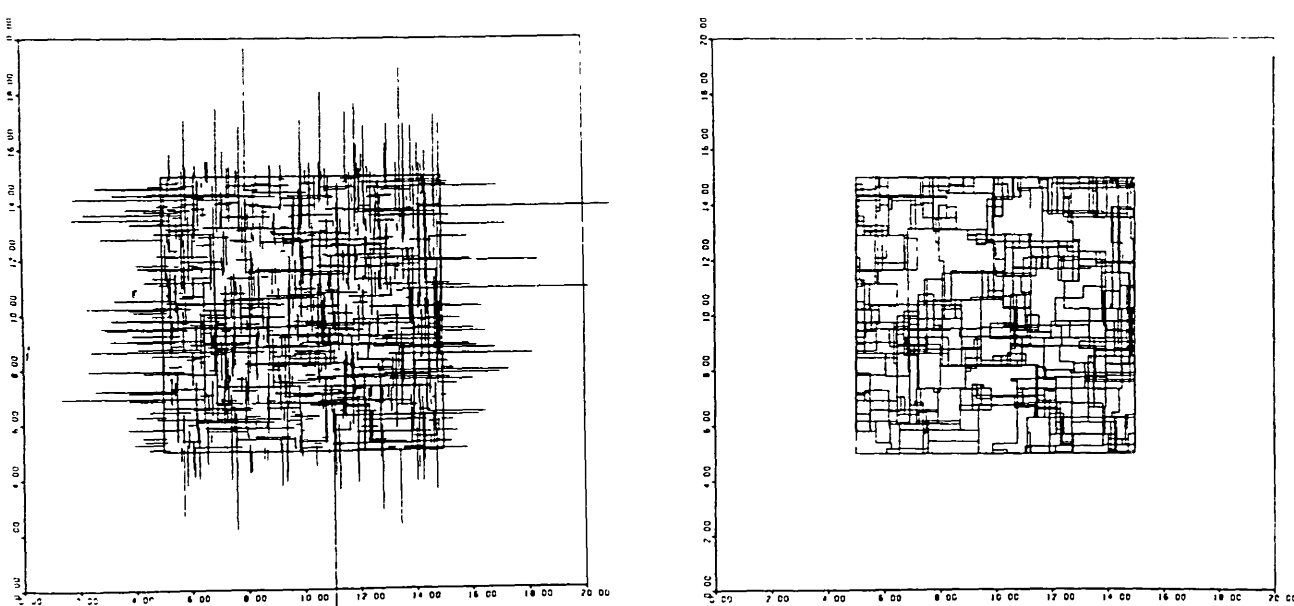

Test 1D

Fig. 4.29 Continued

GENERATED MESH　　　　INTER-CONNECTED MESH

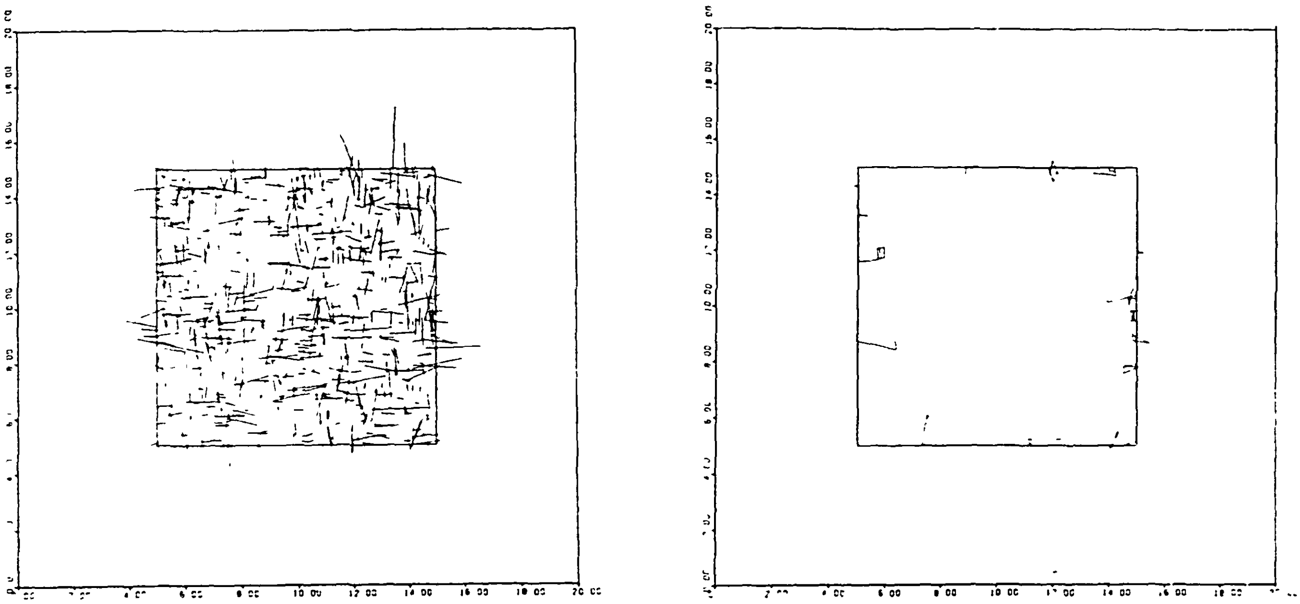

Test 2A

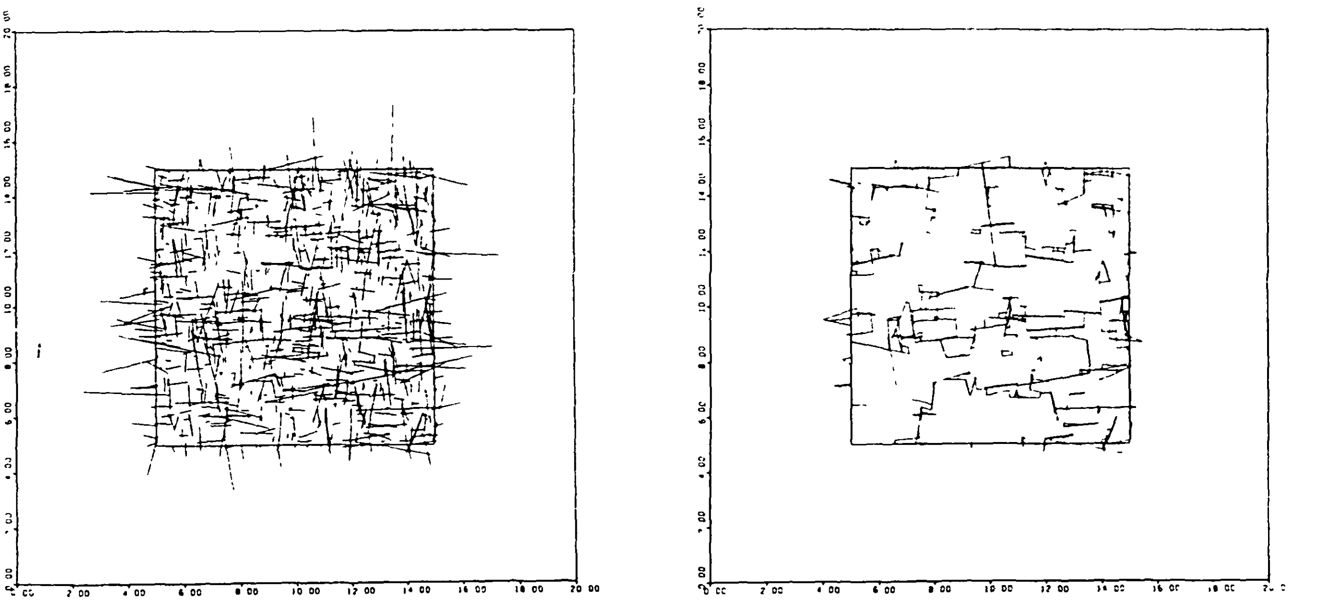

Test 2B

Fig. 4.29 Continued

GENERATED MESH

INTER-CONNECTED MESH

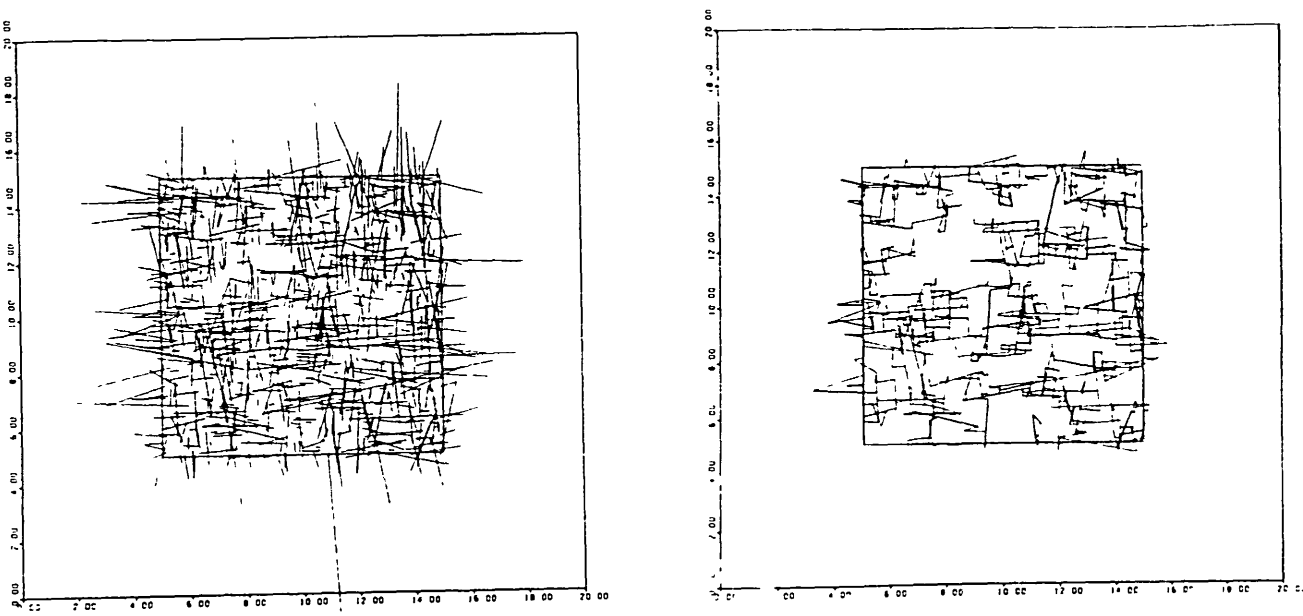

Test 2C

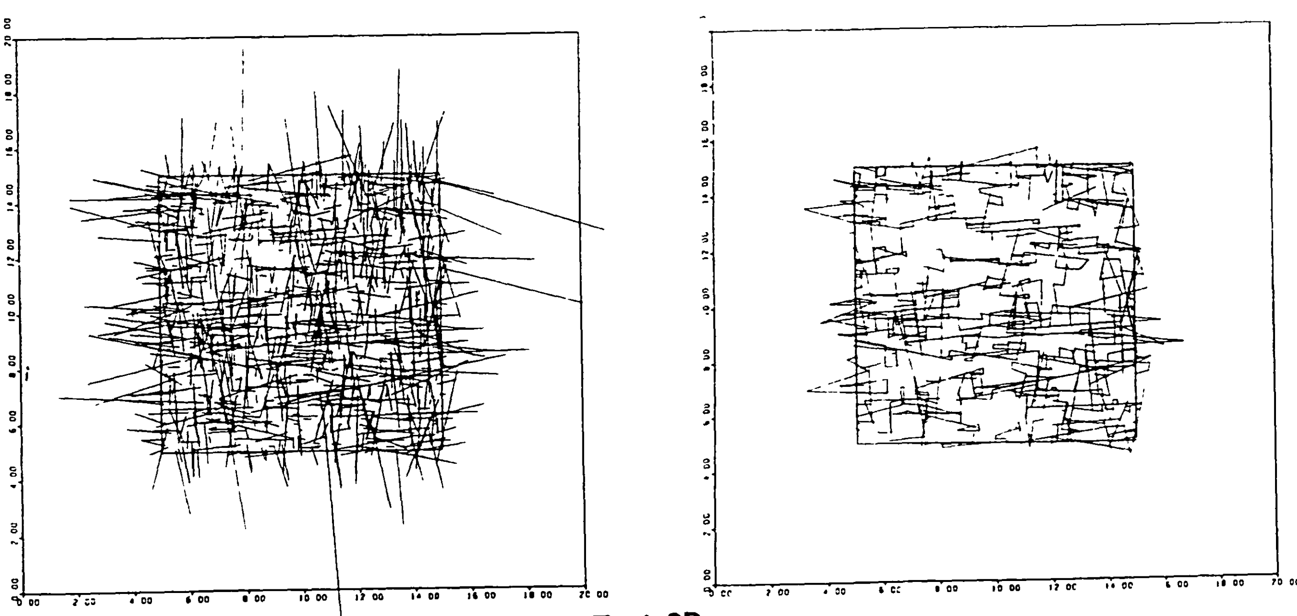

Test 2D

Fig. 4.29 Continued

GENERATED MESH INTER -CONNECTED MESH

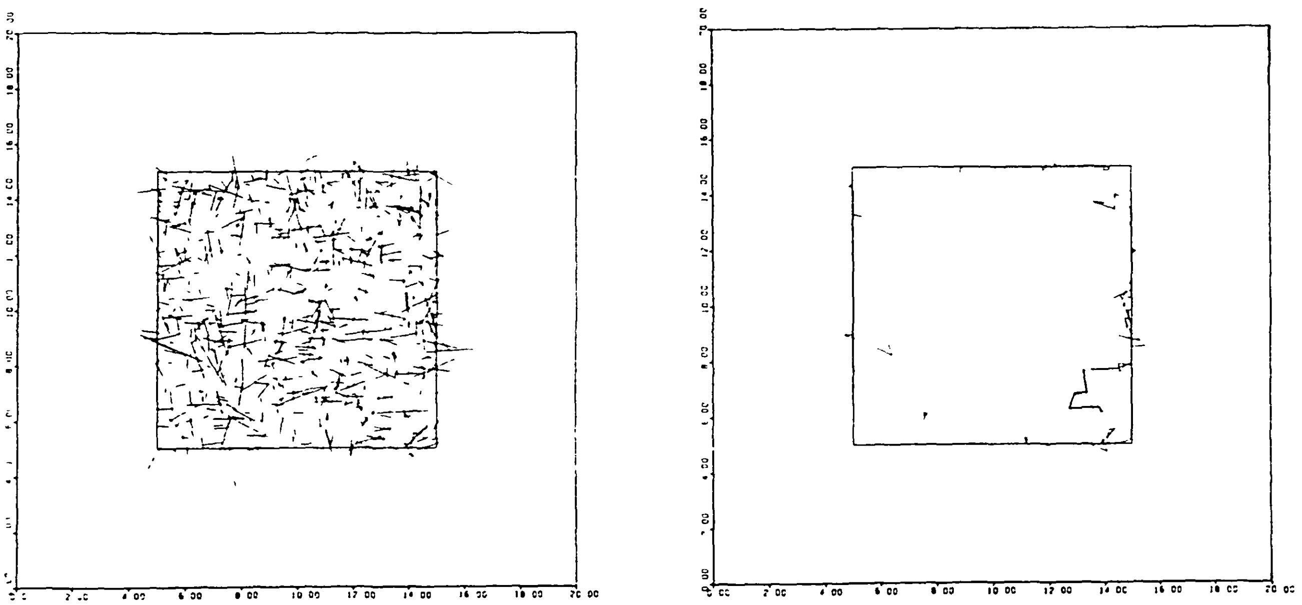

Test 3A

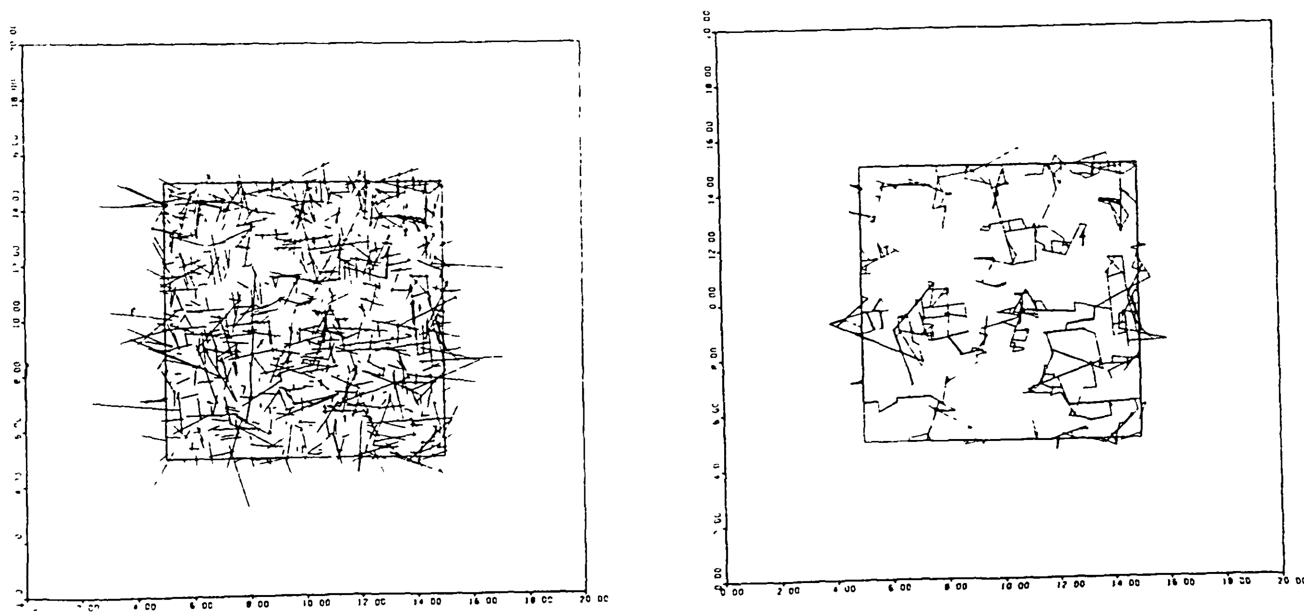

Test 3B

Fig. 4.29 Continued

GENERATED MESH　　　　INTER-CONNECTED MESH

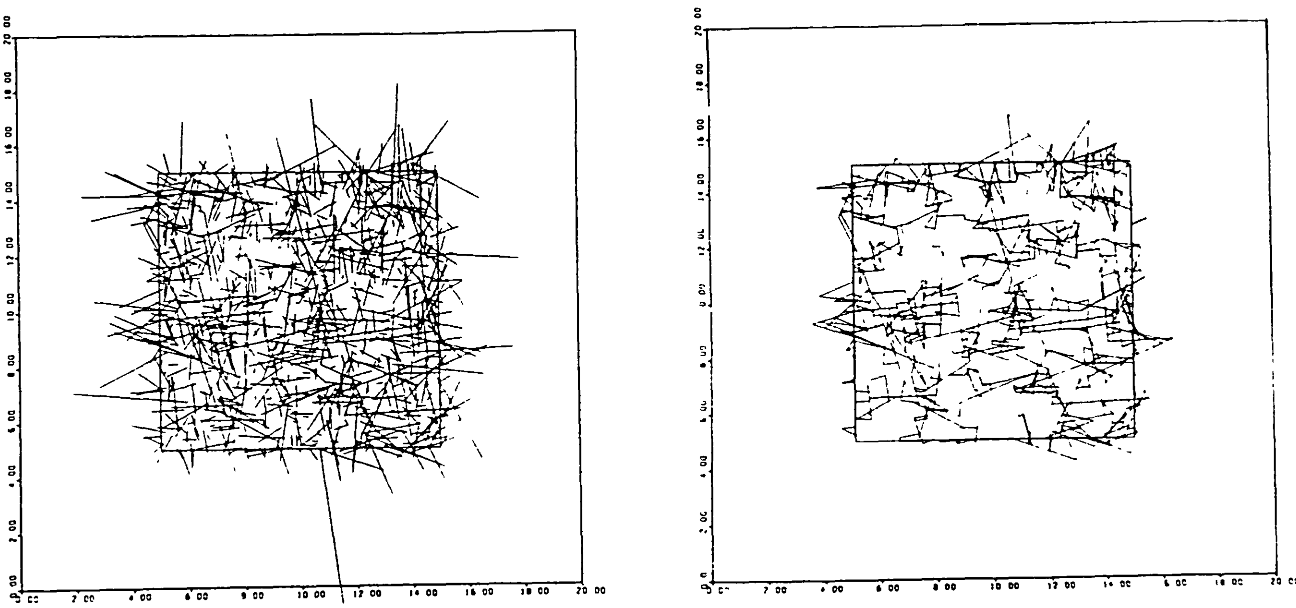

Test 3C

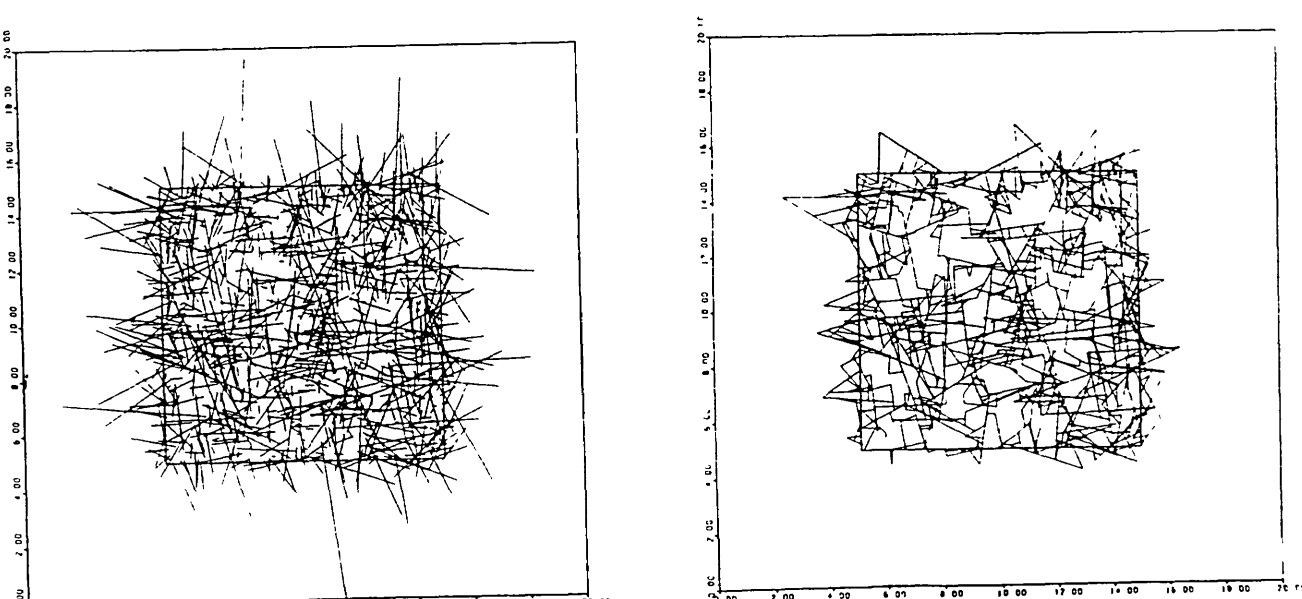

Test 3D

Fig. 4.29 Continued

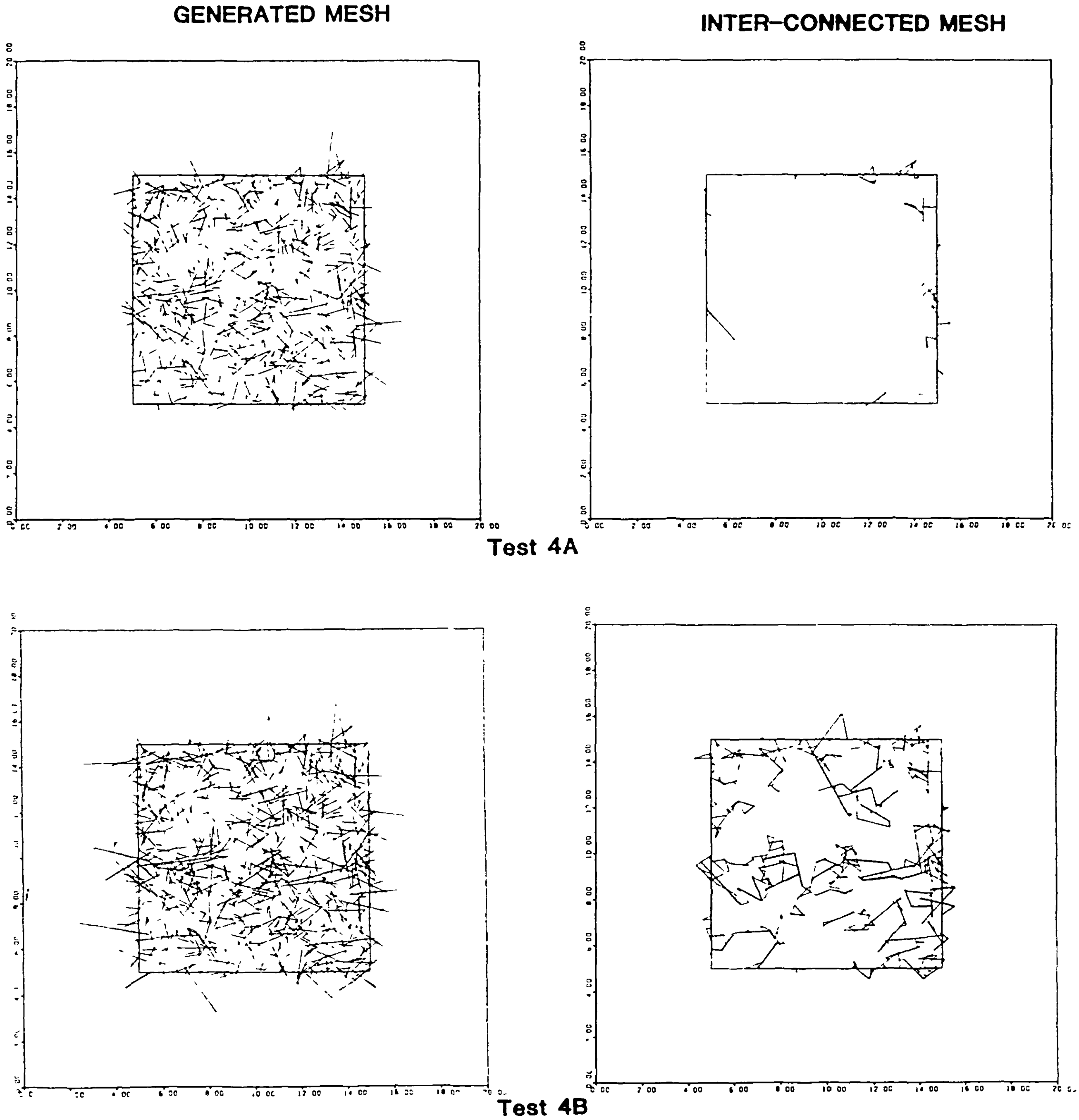

Fig. 4.29 Continued

GENERATED MESH INTER-CONNECTED MESH

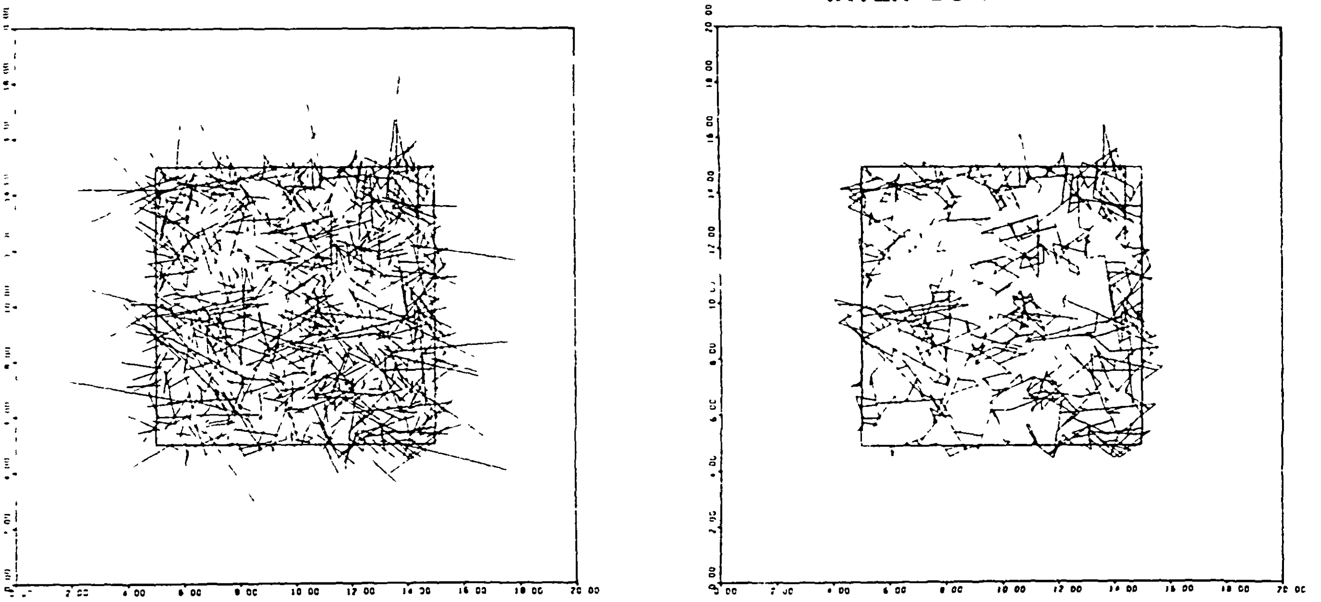

Test 4C

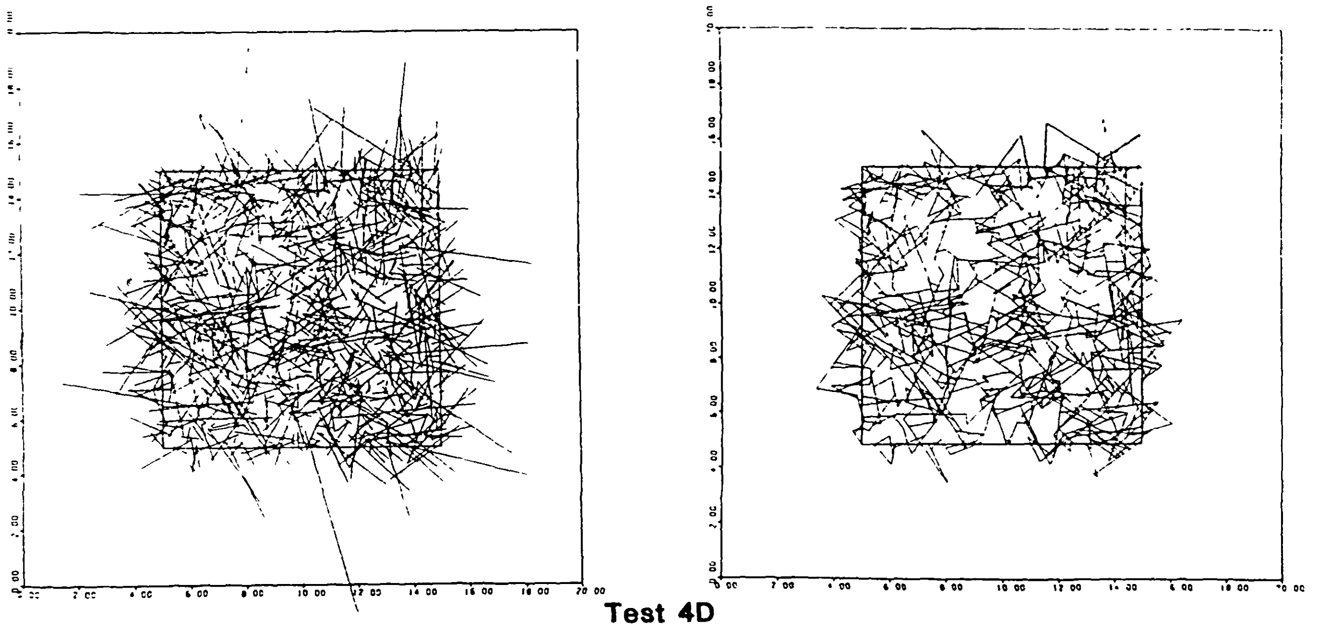

Test 4D

Fig. 4.29 Continued

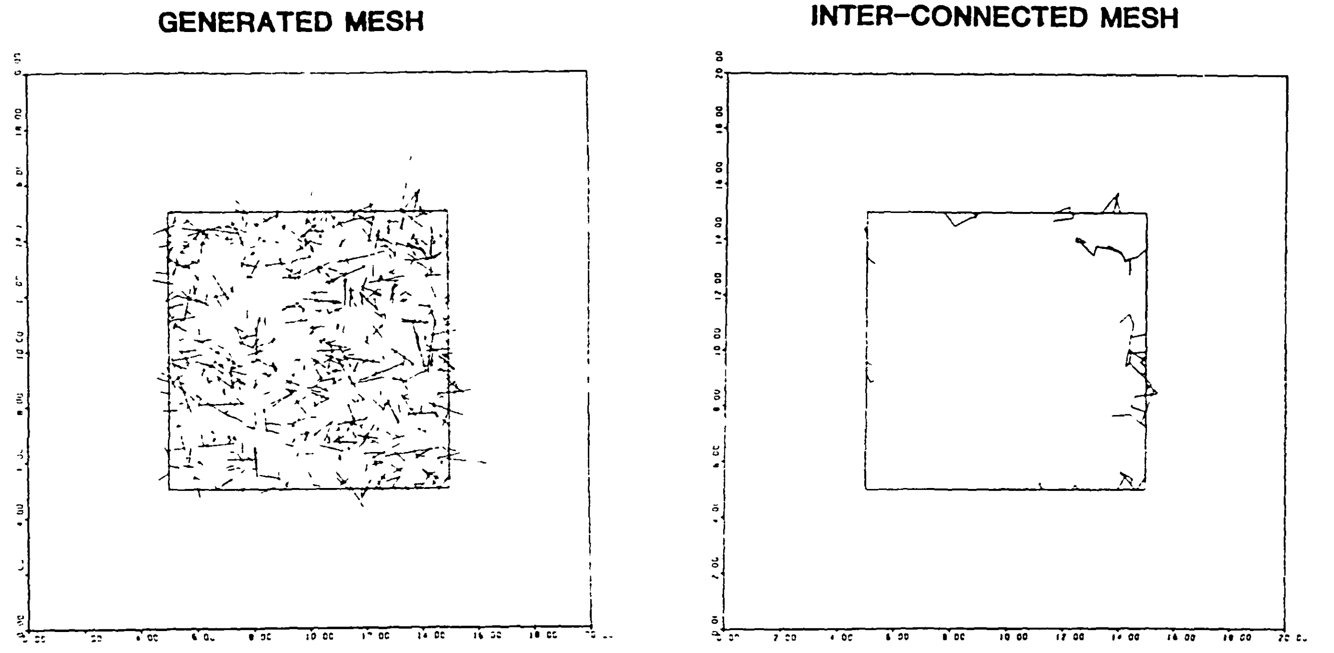

Test 5A

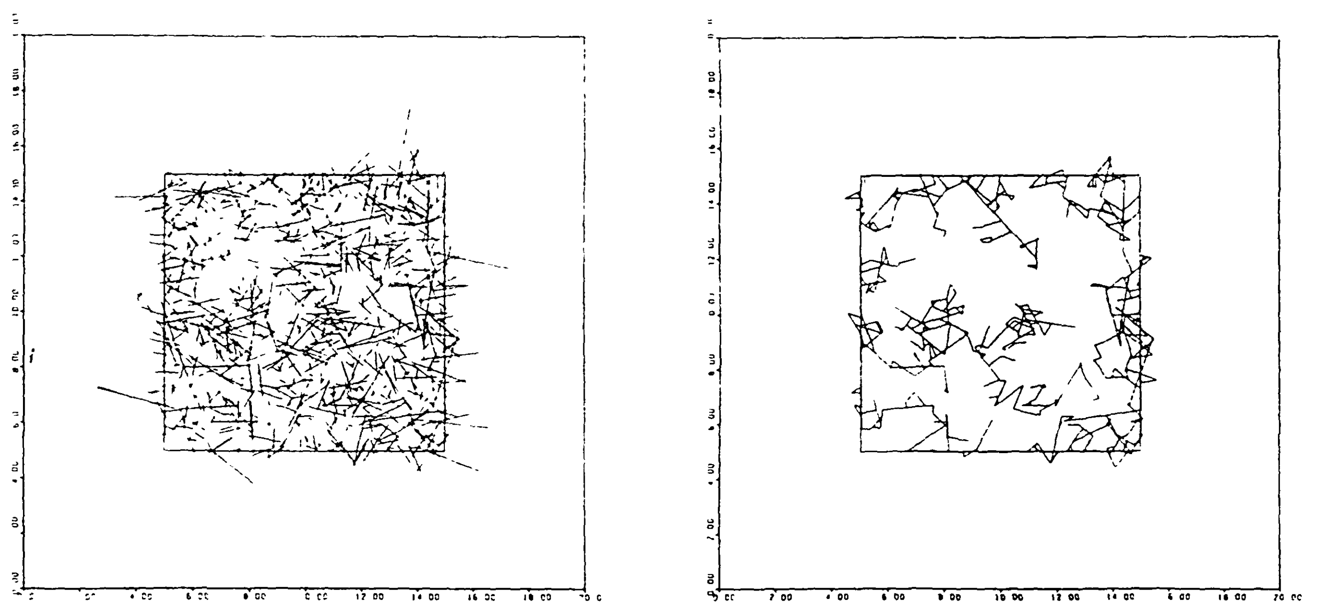

Test 5B

Fig. 4.29 Continued

GENERATED MESH INTER-CONNECTED MESH

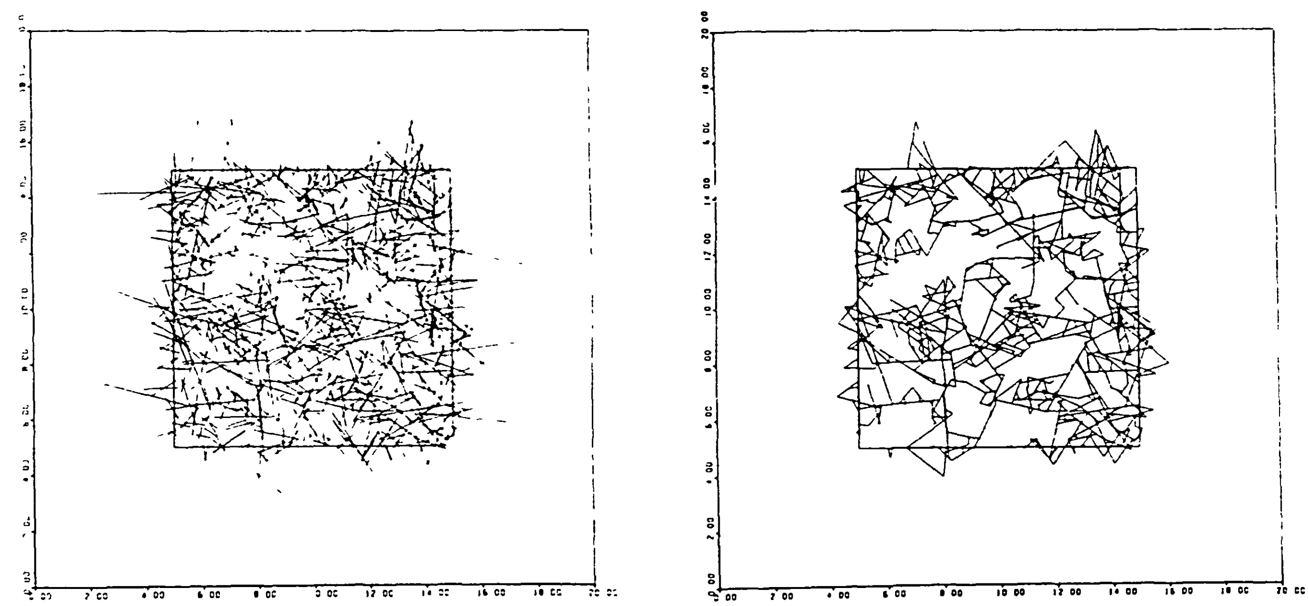

Test 5C

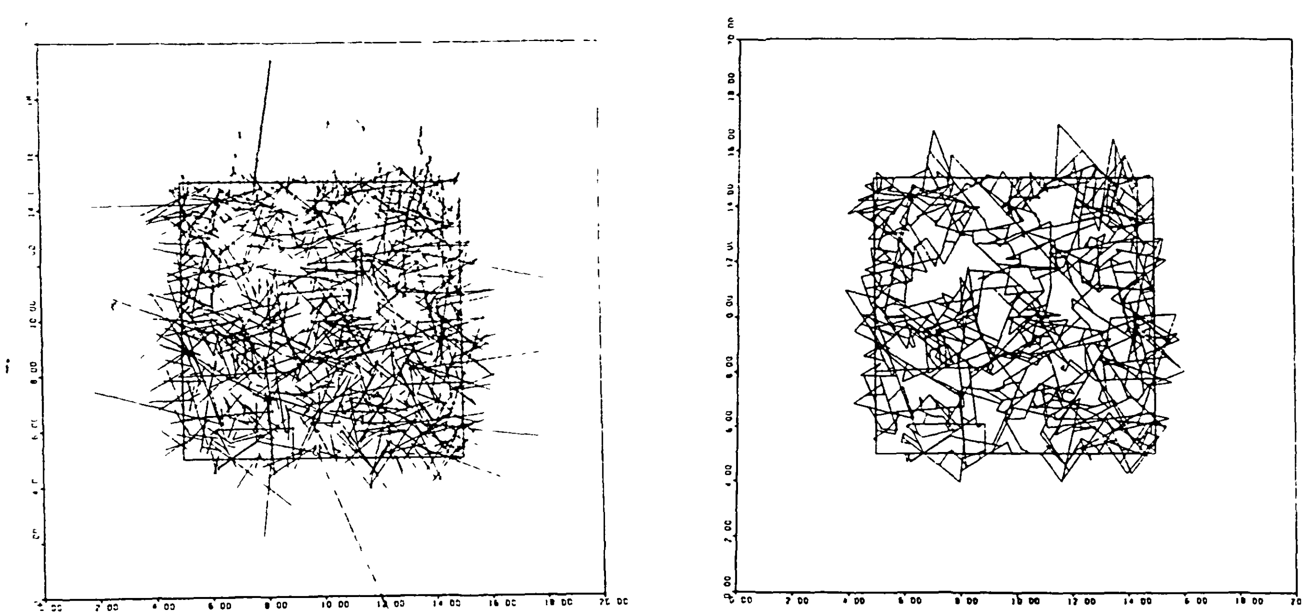

Test 5D

Fig. 4.29 Continued

standard deviation of 40° and 60°, however, this trend is no longer maintained, indeed the corresponding curves lie between the curves for standard deviations of 0° and 20°.

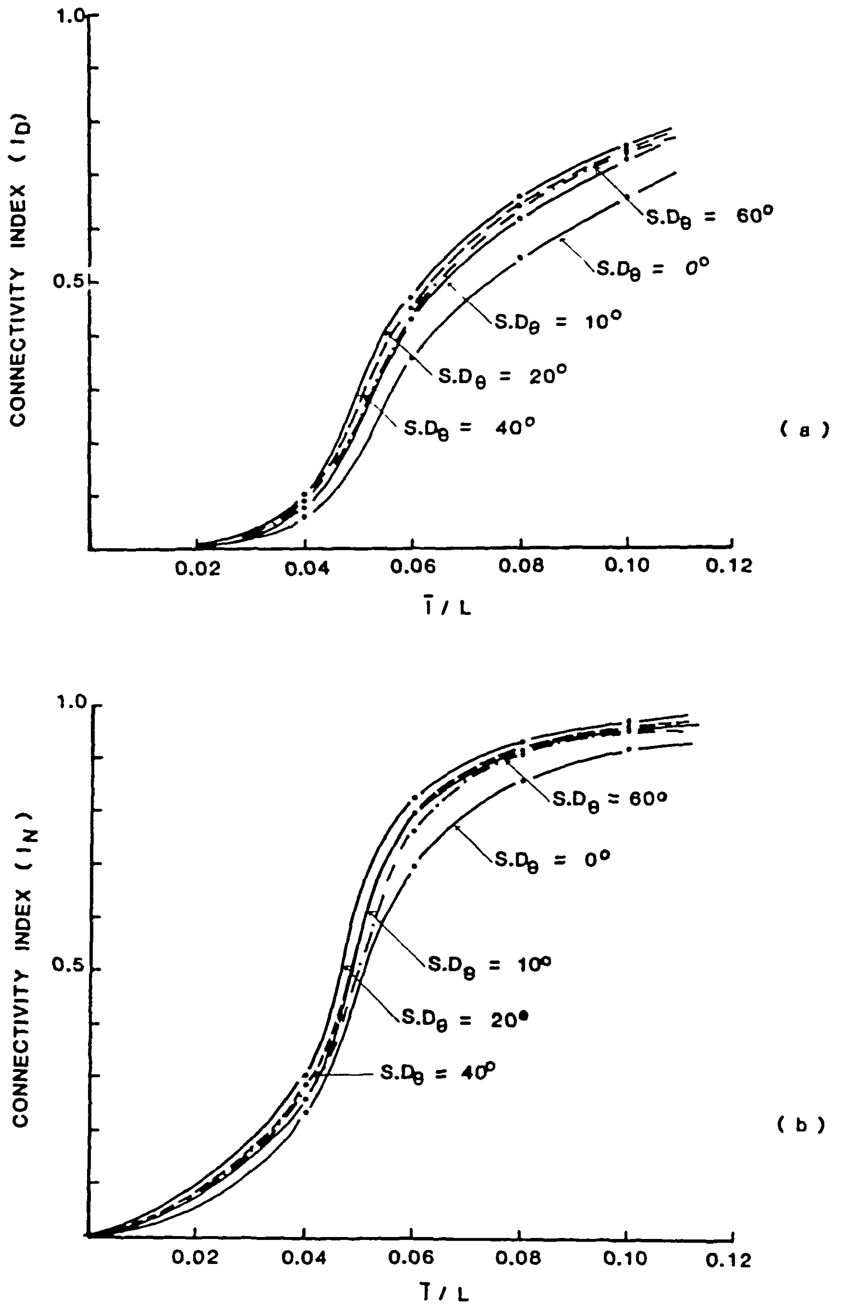

Fig. 4.30 Node index and discontinuity index against the ratio $\bar{\ell}$/L

TEST	CONNECTIVITY INDICES		PERMEABILITY TENSOR m/s			
	I_N	I_D	K_{11}	K_{12}	K_{21}	K_{22}
1A	0.233	0.069	7.157765E-10	6.202209E-11	6.202209E-11	2.620310E-09
1B	0.699	0.357	7.098481E-09	2.071478E-09	2.072442E-09	1.062915E-08
1C	0.861	0.541	9.751824E-08	4.612857E-09	4.612850E-09	8.631852E-08
1D	0.922	0.656	1.938062E-07	-2.260530E-10	-2.281065E-10	1.848712E-07
2A	0.256	0.080	4.151585E-10	7.982131E-11	7.982131E-11	2.616879E-09
2B	0.799	0.431	2.603365E-08	1.687972E-09	1.687972E-09	1.893840E-08
2C	0.917	0.616	1.138584E-07	2.735972E-09	2.735972E-09	9.741612E-08
2D	0.959	0.728	2.092325E-07	9.501765E-10	9.501765E-10	2.088648E-07
3A	0.312	0.094	1.371622E-09	1.300823E-10	1.300823E-10	4.003540E-09
3B	0.825	0.464	2.893431E-08	3.074010E-09	3.074010E-09	2.070888E-08
3C	0.930	0.642	1.337583E-07	4.626300E-09	4.626300E-09	1.193540E-07
3D	0.963	0.752	2.235784E-07	-4.070659E-10	-4.070659E-10	2.235860E-07
4A	0.311	0.102	1.338245E-09	-2.138906E-21	-3.907263E-20	2.795599E-09
4B	0.797	0.453	3.454881E-08	1.745932E-09	1.745932E-09	1.953768E-08
4C	0.917	0.652	1.276160E-07	2.046851E-09	2.046851-09	1.042367E-07
4D	0.956	0.749	2.402947E-07	-2.389969E-09	-2.389969E-09	2.166090E-07
5A	0.281	0.092	2.147546E-09	2.487157E-10	2.487157E-10	3.657716E-09
5B	0.766	0.426	2.164342E-08	1.451873E-09	1.451873E-09	2.351691E-08
5C	0.919	0.641	1.333087E-07	3.357493E-10	3.357493E-10	1.007937E-07
5D	0.960	0.747	2.363968E-07	-4.386356E-09	-4.386356E-09	1.985978E-07

Table 4.IX Results of the discontinuity orientation anaylsis

Fig. 4.31 shows a plot of connectivity index against the coefficient of variation of the angle of orientation, it can be seen that, for all $\bar{\ell}/L$ ratios, the connectivity index increases as the coefficient of variation increases up to approximately 30 percent. Above this figure as the coefficient of variation continues increasing the connectivity index either remains constant or decreases. This effect is more noticeable when the ratio $\bar{\ell}/L$ is small. As the $\ell/\bar{L}$ ratio increases the curves become flatter, i.e. connectivity is relatively insensitive to the variability of orientation.

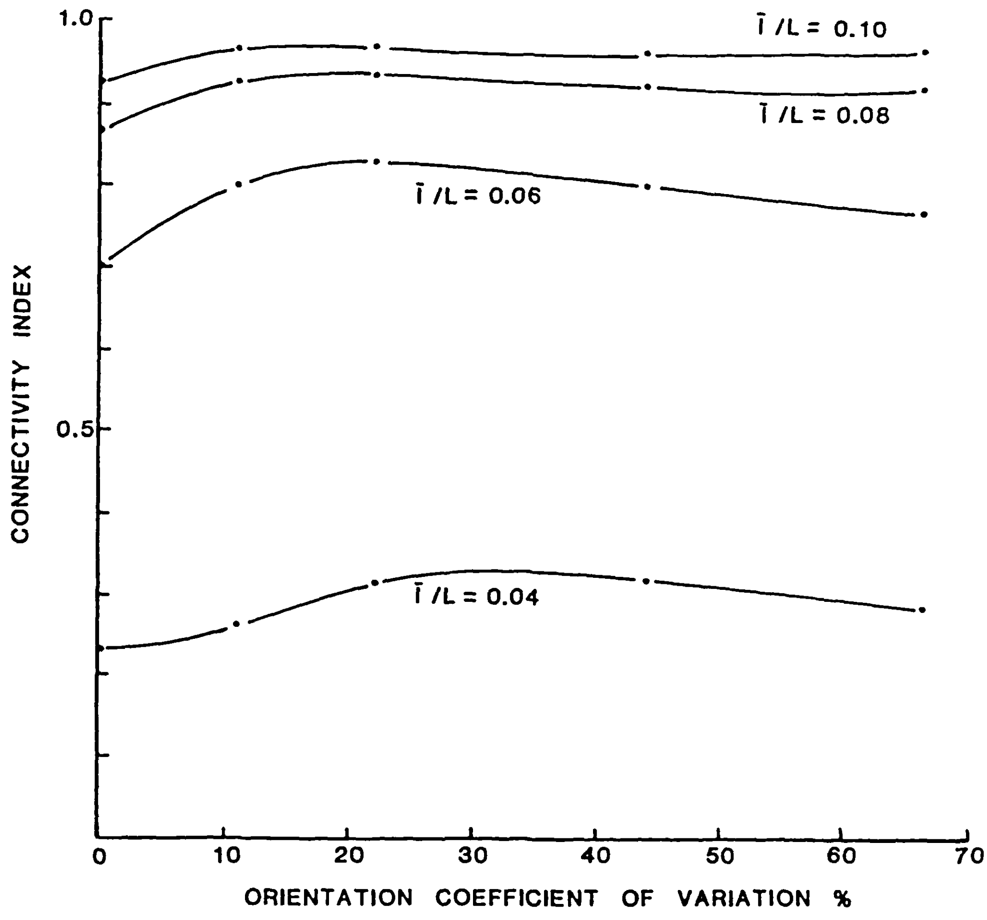

Fig. 4.31 Node Index against the coefficent of variation of the mean angle of orientation

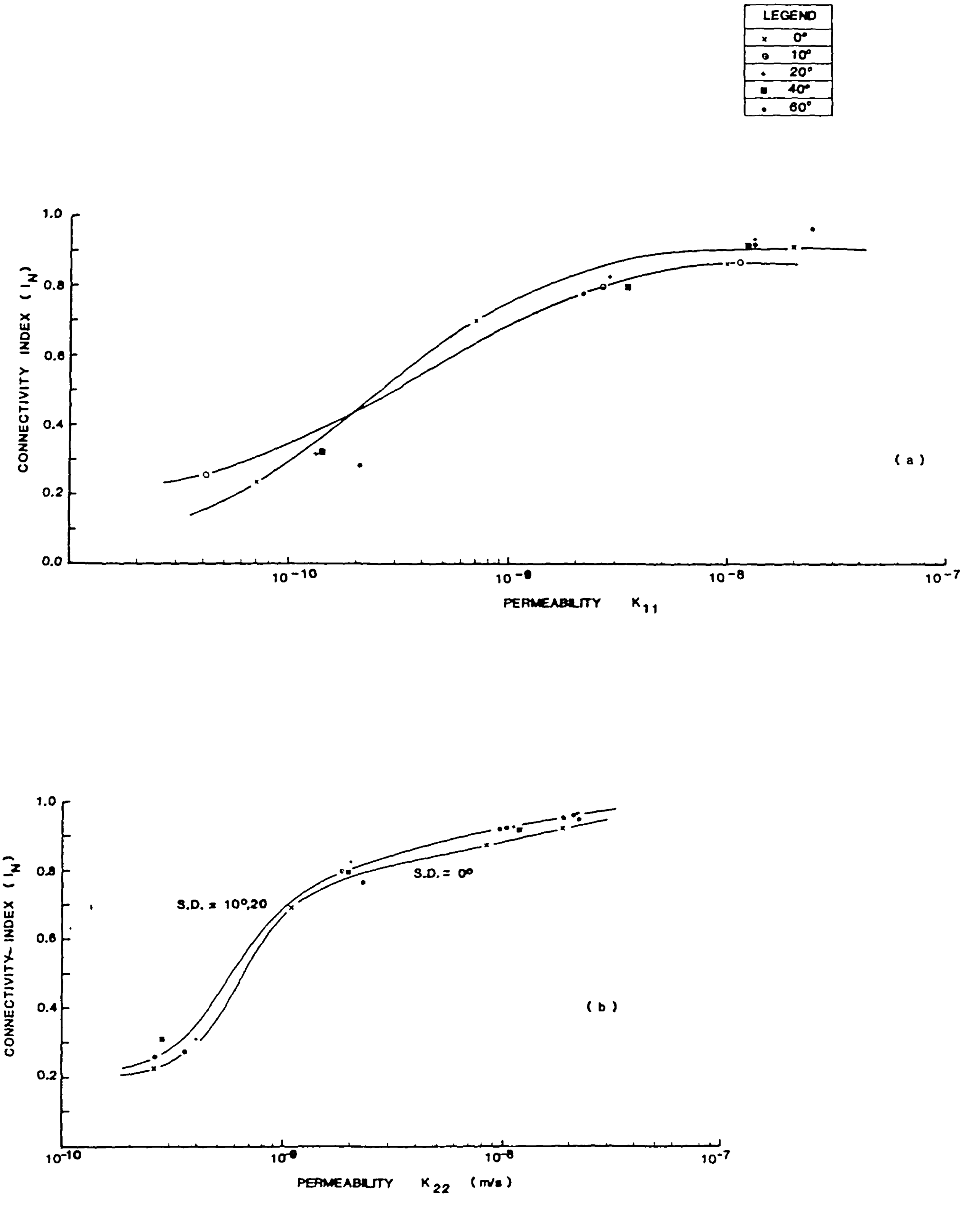

Fig. 4.32 Diagonal terms of the permeability tensor against the node index

A plot of the diagonal terms of the permeability tensor against the connectivity index is presented in Fig. 4.32. It can be seen that both diagonal terms of the permeability tensor increase as the connectivity index increases. It is not, however, clear how the change in orientation variability affects the permeability tensor terms. In Fig. 4.32(b) a clear pattern seems to emerge for standard deviations of 0°, 10° and 20°. However, as the standard deviation increases this pattern disappears completely. In Fig 4.32(a), which plots connectivity index against K_{11}, there was no evidence of any pattern developing. In order to understand how the ratios $\bar{\ell}/L$ affect permeability, a plot of permeability against the coefficient of variation of orientation was constructed. This is shown in Fig. 4.33. It can be seen that for a given coefficient of variation of orientation the permeability increases as the ratio $\bar{\ell}/L$ increases. This expected result has already been noted in previous sections. As the coefficient of variation is increased, however, it can be seen that for ratios of $\bar{\ell}/L$ less than 0.06, permeability oscillates within a range of 2 and 3 orders of magnitude. If the ratio $\bar{\ell}/L$ is greater than approximately 0.08, the permeability oscillation decreases significantly, to lie within a range of less than half an order of magnitude. Furthermore the permeability tensor becomes more isotropic when the ratio $\bar{\ell}/L$ is greater than 0.08. In summary, it has been shown that as the connectivity index increases permeability also increases. It has also been shown that an increment in the coefficient of variation of orientation has a greater effect on connectivity and permeability when the ratio $\bar{\ell}/L$ is less than approximately 0.06. As this ratio increases the effect is reduced considerably since the mesh starts to behave more like an isotropic continuum.

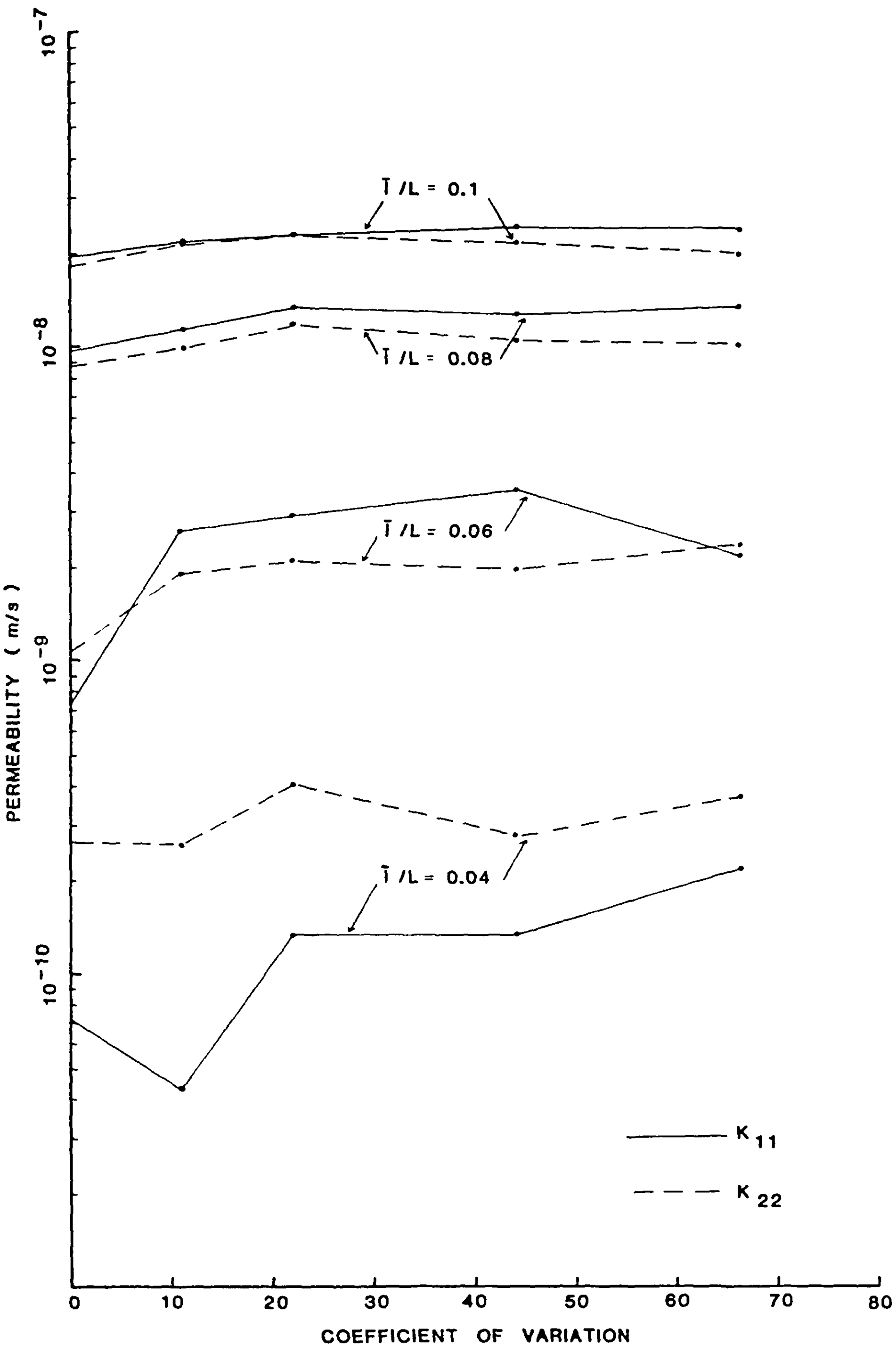

Fig. 4.33 Diagonal terms of the permeability tensor against the coefficient of variation of orientation

4.2.5 Effects of changing the size of the test area

The aims of this study are to analyse how the permeability of a given mesh behaves if the size of the test area is changed and also to see if it is possible to define a representative elementary volume, REV, or more appropriately a representative elementary area, REA, for the case of this two-dimensional model. The REV (REA), which is the volume (area) of rock, that contains a representative sample of fractures, above which the permeability ceases to vary, can be found by calculating the permeability tensor for increasing volumes (areas) of rock until the permeability tensor ceases to change significantly.

For this study a discontinuity mesh containing three sets was generated using the DICHA program. The input data used for the generation of the mesh are shown in Table 4.X. The generation area was 150 m by 150 m; the test zones were twenty-three different areas taken from the central portion of the generation area as shown in Fig. 4.34. The boundary potentials applied to each test area were such that a hydraulic gradient of 1.0 in both the x_1 and x_2 directions was produced. As before, the connectivity analysis was carried out by using the program DICONN and the flow analysis by using the program DIFLOW. The first ten of these tests had to be run on the Amdahl computer at London University, because of the large computer memory requirements. For example, for the largest test area (100 m by 100 m), the program had to handle 4137 discontinuities which in turn produced 5647 conducting nodes; consequently this number of simultaneous linear equations had to be solved. A typical running time for the largest test area was 4 minutes and 50 seconds of CPU time. For these reasons it was too expensive to perform more than one realisation for each mesh.

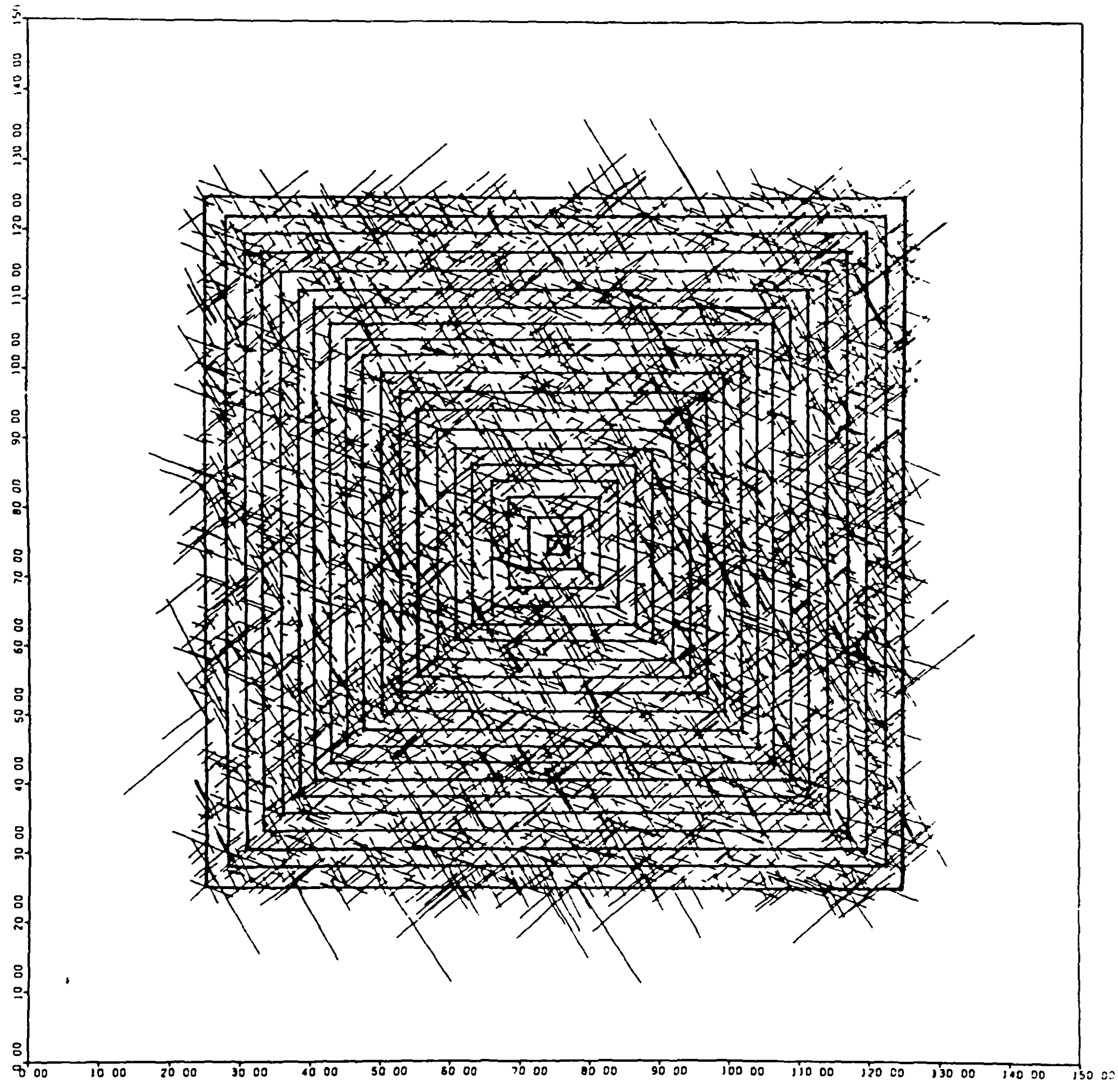

Fig. 4.34 The generated mesh used in the study of the effects of changing the size of the test area

Parameter	Set 1	Set 2	Set 3
Orientation:			
mean	40°	120°	160°
standard deviation	2°	2°	2°
type of distribution	Normal	Normal	Normal
Trace length (m)			
mean	4.0	4.0	3.0
standard deviation	3.0	3.0	2.0
type of distribution	log-normal	log-normal	log-normal
Number of discontinuities	3000	3000	3000
Aperture (mm)			
mean	0.5	0.5	0.3
standard deviation	0.0	0.0	0.0
type of distribution	log-normal	log-normal	log-normal

Table 4.X Input data for study of changing the size of the test area

Table 4.XI shows the side length, L, of each test area, the connectivity indices and the components of the permeability tensor. Fig. 4.35 shows the inter-connected meshes for the different sizes of test area studied. A plot of side L against discontinuity density is shown in Fig. 4.36 and a plot of side length L against connectivity index in Fig. 4.37. It can be seen that the changes in discontinuity density for test area side lengths of up to 10 m are very large and exhibit some oscillations. When the side length of the test area lies between 10 m and 20 m there is a smooth change towards a more constant value of density. When the length of the test area exceeds 20 m the changes in discontinuity density are almost negligible. A similar phenomenon can be seen for the plot of connectivity index shown in Fig. 4.37. In this case, however, the connectivity index converges to an almost constant value more rapidly, demonstrating negligible variation for test area side lengths above 15 m.

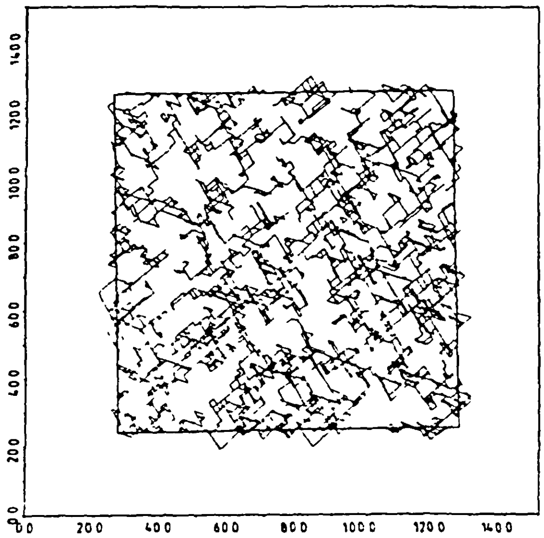

Test 1 (100 x 100) m

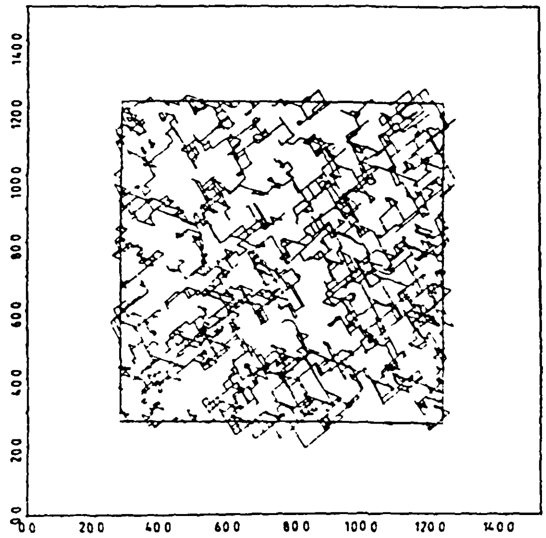

Test 2 (95 x 95) m

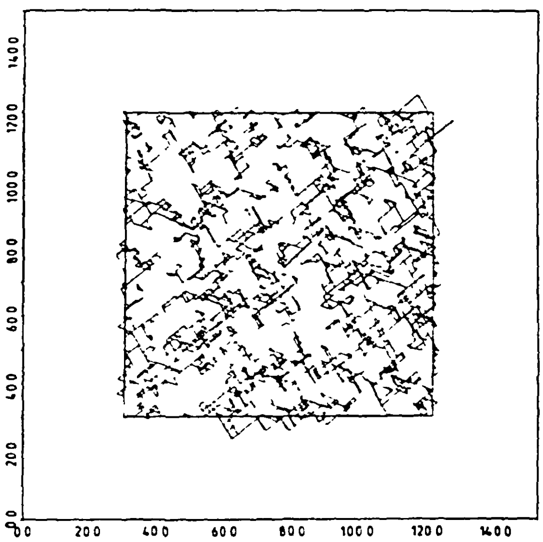

Test 3 (90 x 90) m

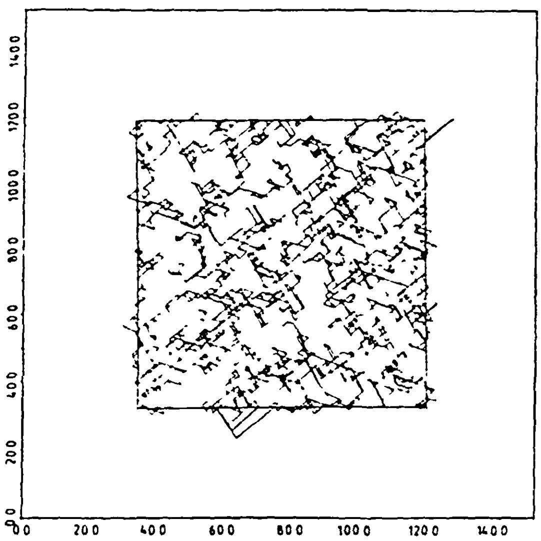

Test 4 (85 x 85) m

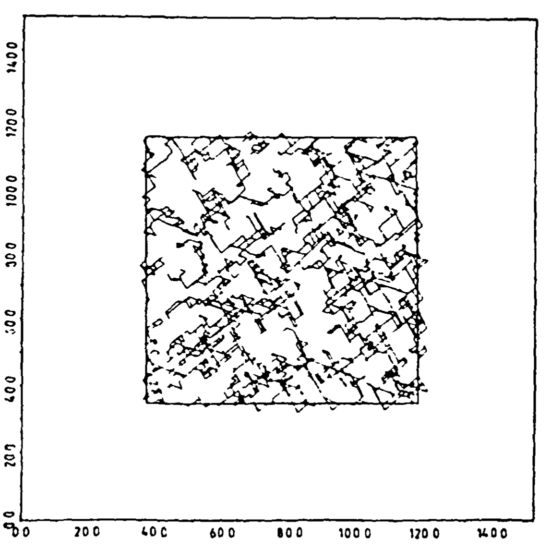

Test 5 (80 x 80) m

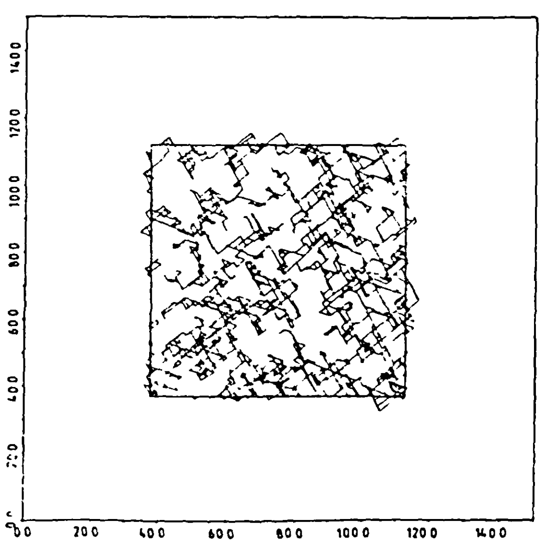

Test 6 (75 x 75) m

Fig. 4.35

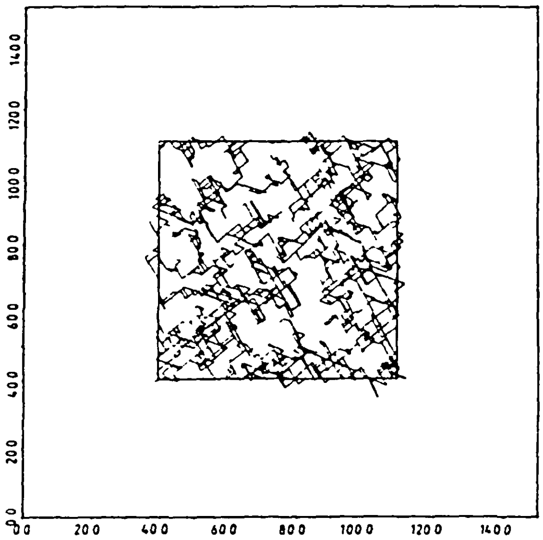

Test 7 (70 x 70) m

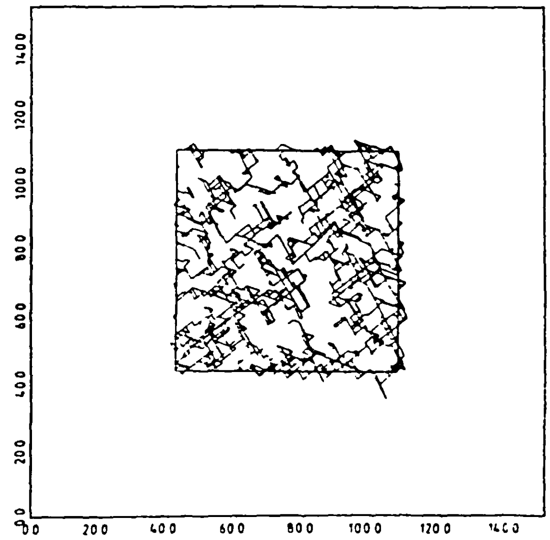

Test 8 (65 x 65) m

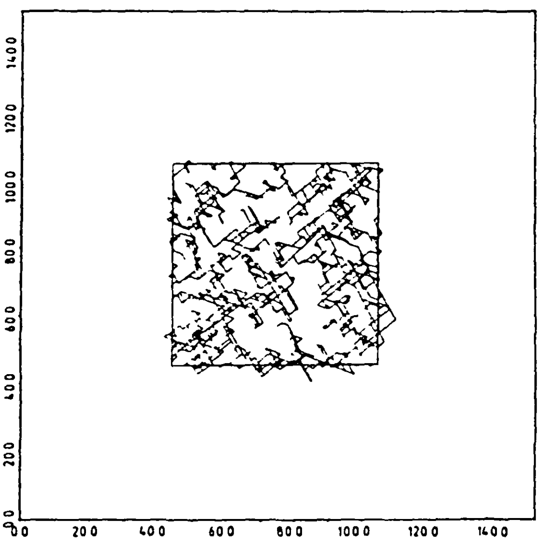

Test 9 (60 x 60) m

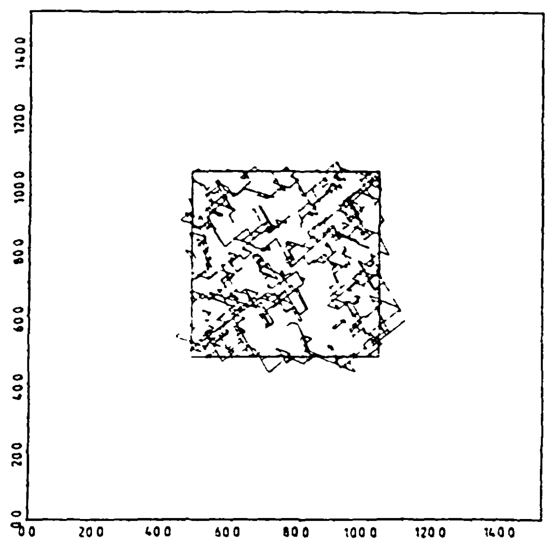

Test 10 (55 x 55) m

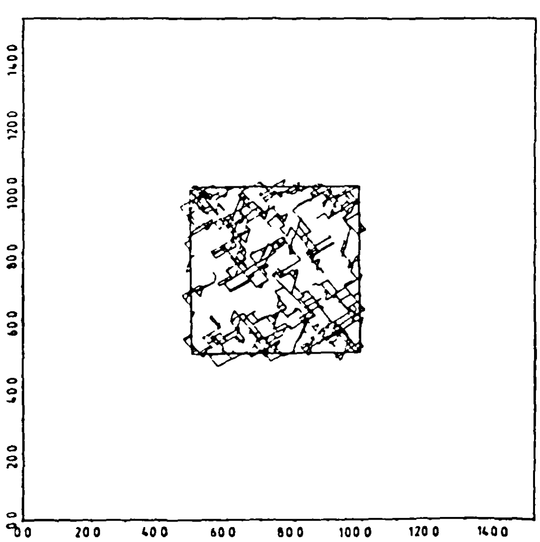

Test 11 (50 x 50) m

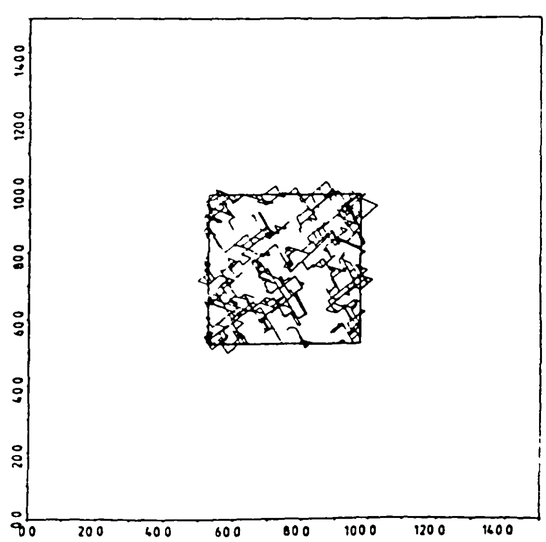

Test 12 (45 x 45) m

Fig. 4.35 Continued

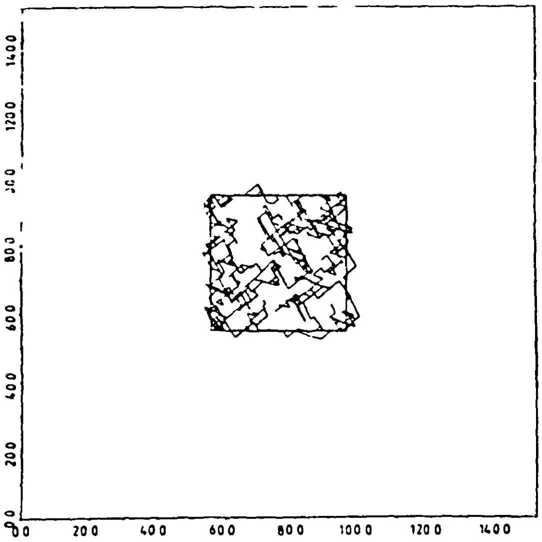

Test 13 (40 x 40) m

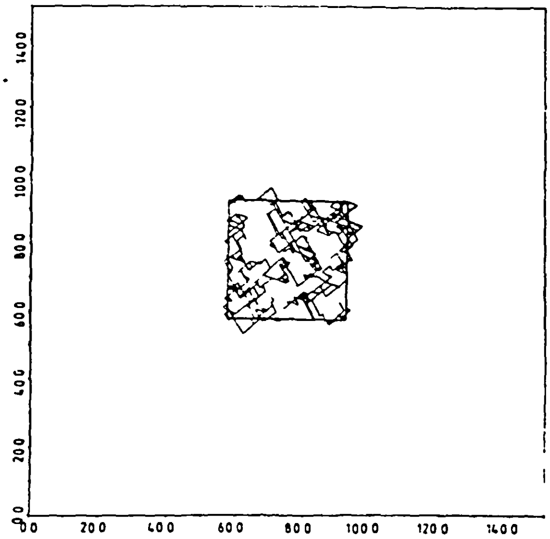

Test 14 (35 x 35) m

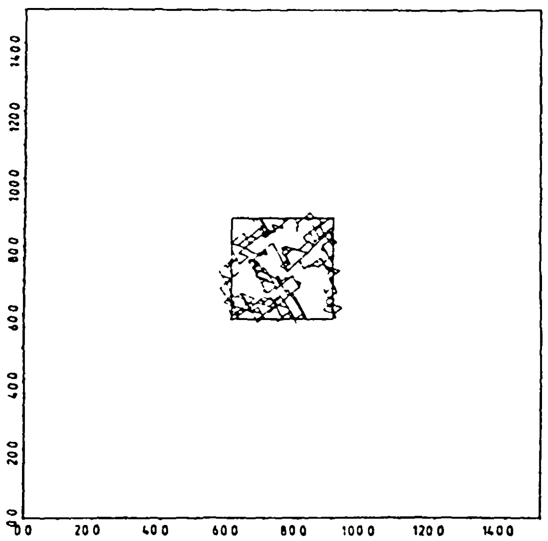

Test 15 (30 x 30) m

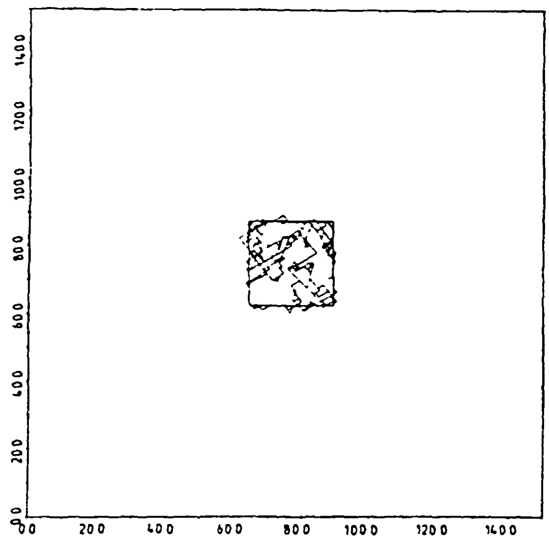

Test 16 (25 x 25) m

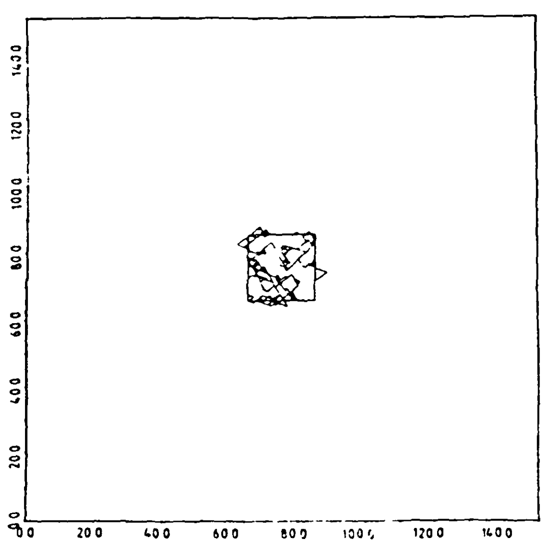

Test 17 (20 x 20) m

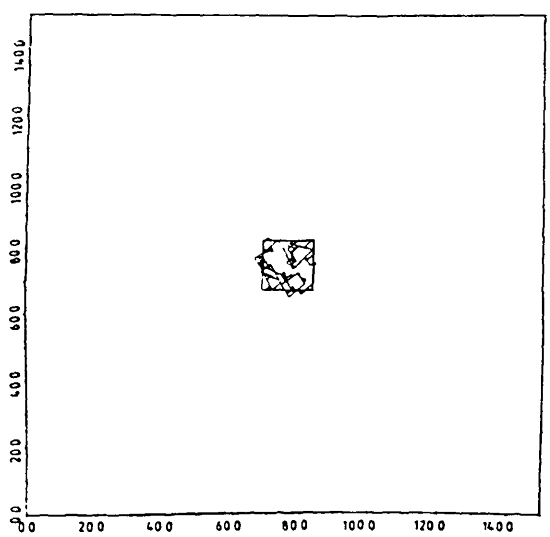

Test 18 (15 x 15) m

Fig. 4.35 Continued

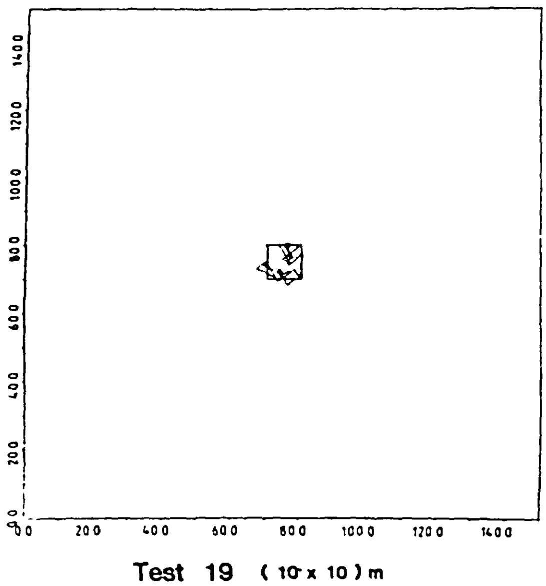

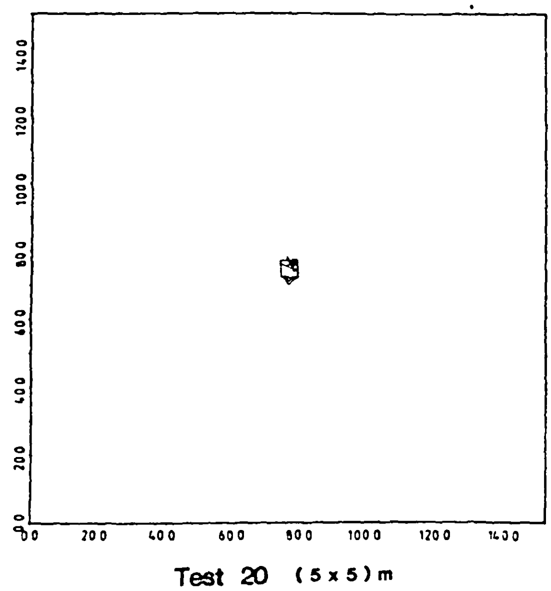

Fig. 4.35 The inter-connected meshes used in the study of the effects of changing the size of the test area

TEST	L(m)	I_N	I_D	PERMEABILITY TENSOR m/s			
				K_{11}	K_{12}	K_{21}	K_{22}
1	100	0.873	0.643	6.529338E-06	4.973046E-07	4.973046E-07	7.103099E-06
2	95	0.875	0.647	6.576272E-06	4.281437E-07	4.281437E-07	7.372333E-06
3	90	0.876	0.684	6.669518E-06	4.394417E-07	4.394417E-07	7.892517E-06
4	85	0.879	0.657	7.076687E-06	4.993832E-07	4.993832E-07	8.344920E-06
5	80	0.876	0.649	6.587721E-06	2.441388E-07	2.441388E-07	8.558782E-06
6	75	0.881	0.658	7.221741E-06	1.771538E-07	1.771538E-07	8.446740E-06
7	70	0.882	0.663	7.673601E-06	-3.539089E-07	-3.539089E-07	8.537232E-06
8	65	0.888	0.673	7.844054E-06	-4.222999E-07	-4.222999E-07	8.547521E-06
9	60	0.886	0.673	6.975489E-06	-5.299950E-07	-5.299950E-07	8.638278E-06
10	55	0.895	0.688	7.732815E-06	-8.466433E-07	-8.466433E-07	9.886608E-06
11	50	0.894	0.683	7.553642E-06	-7.387707E-07	-7.387707E-07	1.144566E-05
12	45	0.899	0.688	8.319020E-06	-9.901158E-07	-9.901158E-07	1.178786E-05
13	40	0.892	0.678	7.237870E-06	-8.586530E-07	-8.586530E-07	1.213788E-05
14	35	0.894	0.686	8.924998E-06	-1.018326E-06	-1.018326E-06	1.166620E-05
15	30	0.893	0.690	9.898947E-06	-1.654905E-07	-1.654905E-07	1.203915E-05
16	25	0.922	0.725	1.172641E-05	5.660479E-07	5.660479E-07	1.065364E-05
17	20	0.904	0.706	1.508675E-05	-2.880385E-06	-2.880385E-06	8.005983E-06
18	15	0.898	0.724	1.335713E-05	-3.358252E-06	-3.358252E-06	1.269570E-05
19	10	0.940	0.836	1.998357E-05	-3.655950E-06	-3.655950E-06	9.144698E-06
20	5	0.981	0.957	5.152571E-05	4.752549E-06	4.752549E-06	2.974857E-05
21	4	0.956	0.894	7.125219E-05	7.415681E-06	7.415681E-06	2.022562E-05
22	3	0.920	0.833	1.381842E-07	-8.764500E-07	-8.764500E-07	4.294725E-06
23	2	0.875	0.800	8.419671E-07	2.407001E-07	2.407001E-07	1.666612E-06

Table 4.XI Geometric properties of the mesh and permeability tensor for the representative elementary volume study

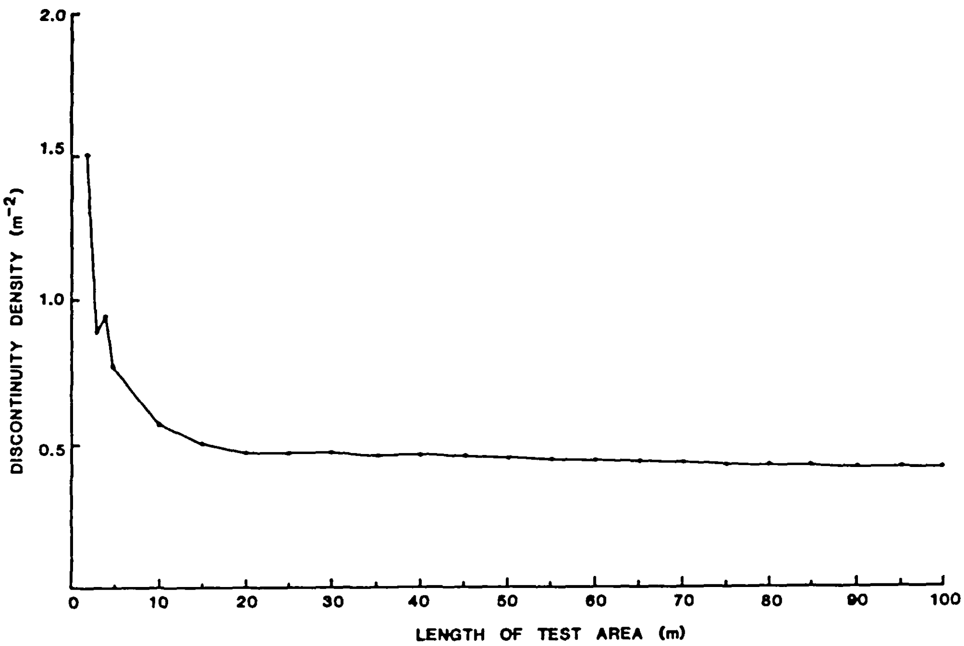

Fig. 4.36 Length of test area against discontinuity density

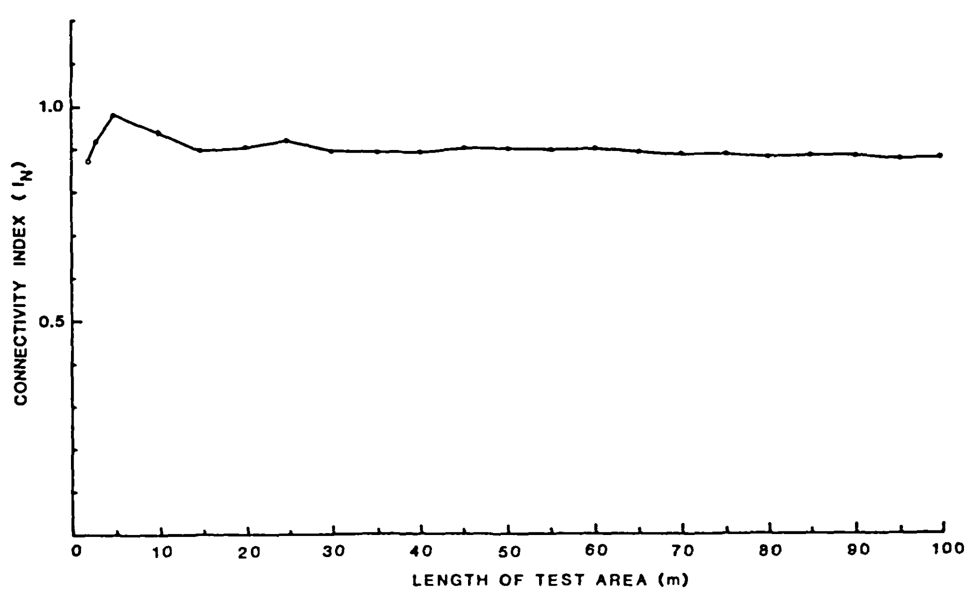

Fig. 4.37 Length of the test area against connectivity index

Fig. 4.38 shows a plot of L against the trace length ratio ℓ/L, where is the mean trace length of all the discontinuities in the generated mesh. In this figure it can be seen that for test area side lengths of up to 10 m, the ratio ℓ/L is very sensitive to small increments in the L. When L becomes greater than 10 m, however, the change in ℓ/L becomes less, and for values of L greater than about 25 m the change in the ℓ/L ratio is almost negligible. The above analysis shows that the geometric characteristics of a given discontinuity mesh, such as the density, the connectivity and the trace length ratio, ℓ/L, can exhibit some degree of variability as the size of the test area is increased. This variability is high for test area side lengths of less than 20 . For larger test areas this variability reduces considerably, and becomes almost negligible at side lengths above about 25 m. It can be expected, therefore, that when the size of the test area exceeds some critical value the permeability tensor will remain constant as the test area is allowed to increase further. Fig. 4.39 (a) shows a plot of K_{11} and K_{22} against the side length of the test area. It can be seen that the variability, in both K_{11} and K_{22}, decreases rapidly as the side length of the test area increases, and for side lengths exceeding 60 m the change in permeability becomes almost negligible. Fig. 4.39 (b) shows a plot of K_{12} and K_{21} against the side length of the test area. Again there is great variability of K_{12} and K_{21} for test areas side lengths of less than 10 m. Although the permeability tensor is symmetric, the variability of K_{12} and K_{21} remains high until it begins to stabilise at side lengths of about 75 m.

The principal permeabilities and principal directions were calculated, for each of the test areas, using equations (4.10) and (4.11). Fig. 4.40 shows a plot of the principal permeabilities K_1 and K_2 against the side length of the test area. As before, it can be seen that the principal permeabilities tend to a constant value as the side length of the test area increases above 20 m. Fig. 4.41 shows a polar plot of the major principal directions referred to the angle Θ, where Θ describes the major principal direction with respect to horizontal axis, x_1. It can be seen that there is also some variability in the values of the angle Θ.

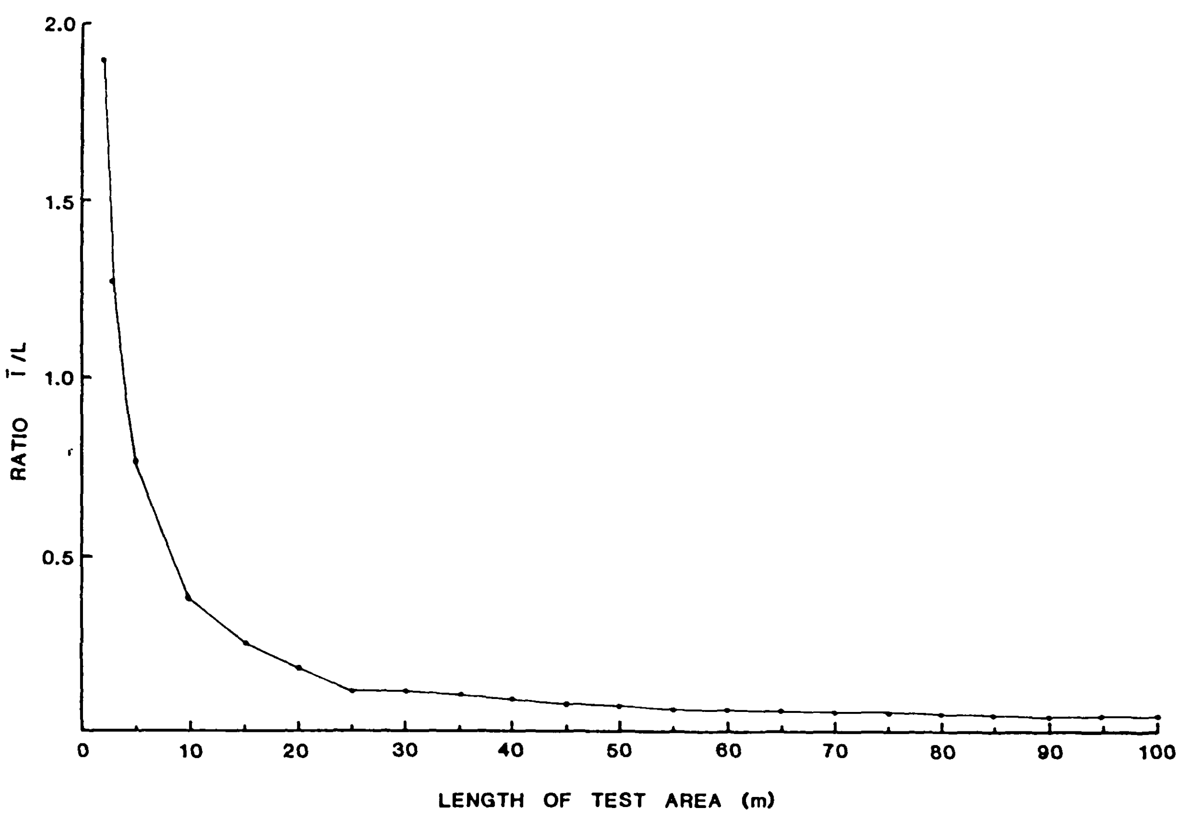

Fig. 4.38 Length of the test area against the ratio $\bar{\ell}/L$

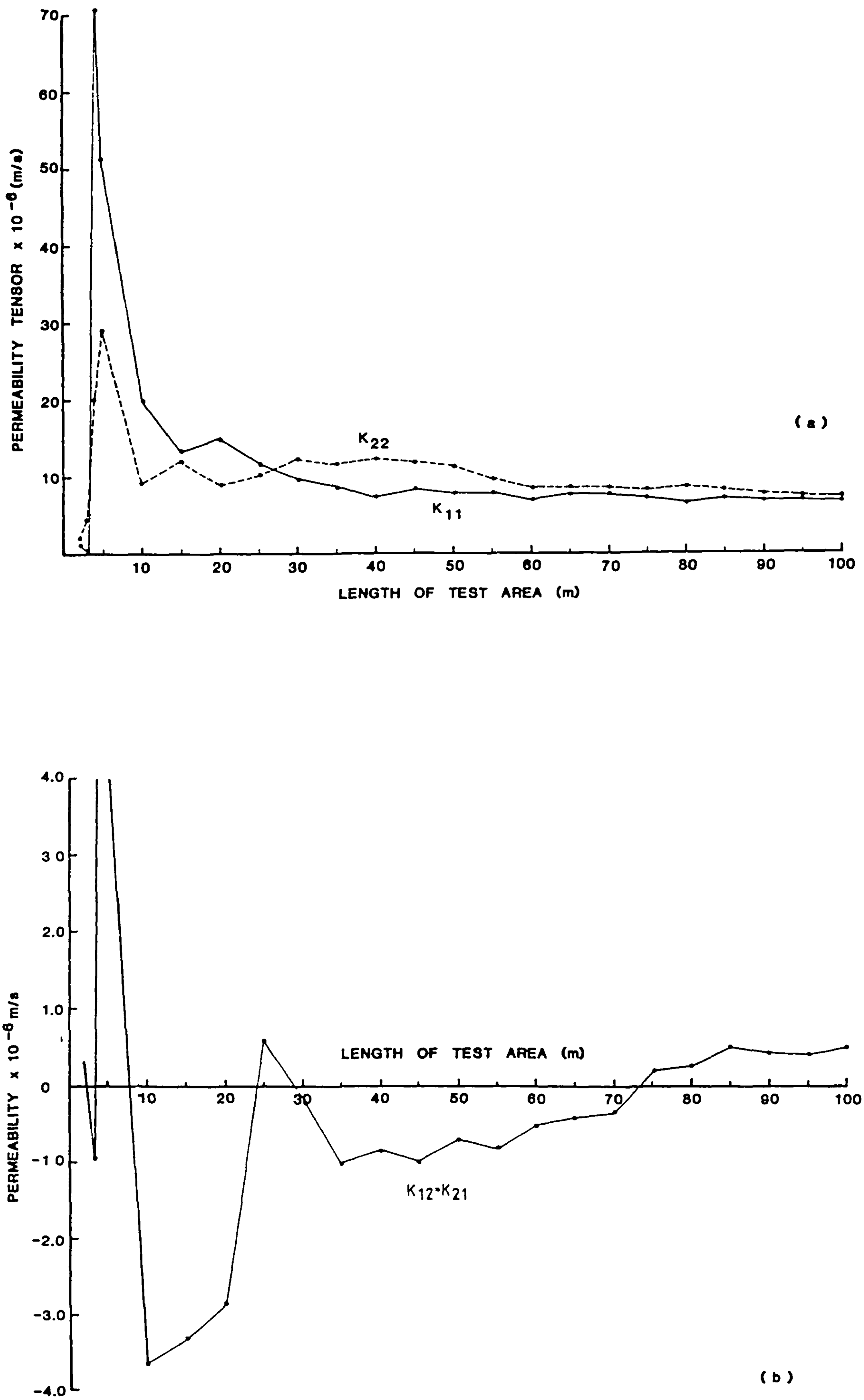

Fig. 4.39 Length of the test area against the components of the permeability tensor

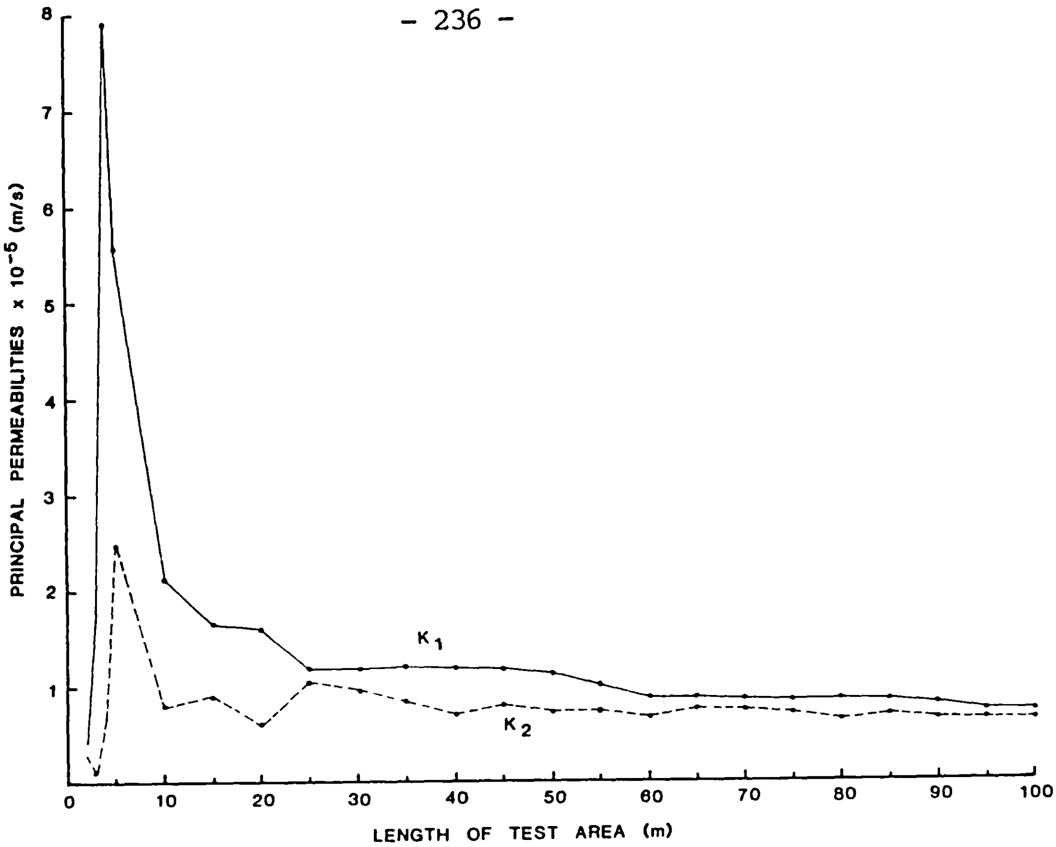

Fig. 4.40 Length of the test area against the principal permeabilities

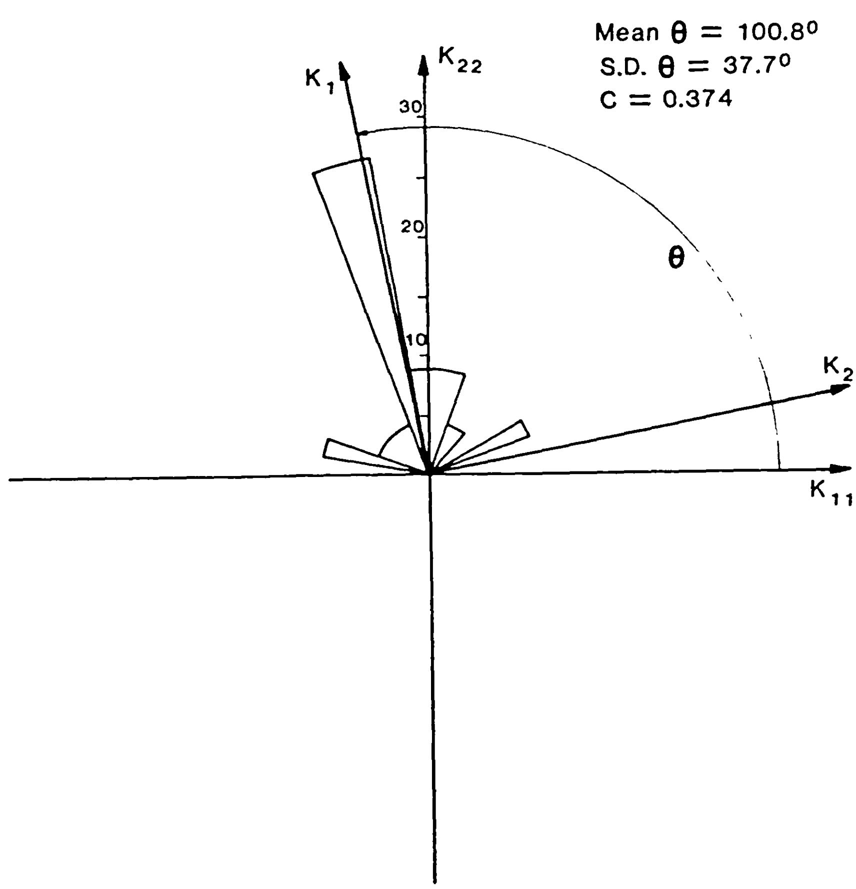

Fig. 4.41 Polar diagram of the principal directions permeability

The measured flow across the boundaries, first in the x_1 direction and then in the x_2 direction were compared with the flows calculated using the permeability tensor, assuming a continuous equivalent medium. A plot of the relative error of each observation, calculated using equation 4.5, against the side length of the test area is shown in Fig. 4.42. It can be seen that, RE_{11}, the relative error of flow in the x_1 direction, has greater variability than, RE_{22}, the relative error in the x_2 direction. This is due to the anisotropy of the mesh. Although there are exceptions, in general, both of the relative errors tend to decrease as the sample size increases. Above a test area side length of 55 m, the relative errors in both cases are less than 0.2, but still display some variability.

In order to define the REV it is necessary first to establish the acceptable level for the relative error in flow, bearing in mind that a better estimate of flow can be obtained as the size of the test area increases. Since the geometric characteristics of the mesh, such as discontinuity density, connectivity index and the trace length ratio, $\bar{\ell}/L$, also change as the size of the test area increases, it is necessary to define a size of test area beyond which these changes are negligible. For example in the mesh shown in Fig. 4.34, if a relative error of 0.2 is permissible, then the REV can be accepted at a side length of 55 m; if, however, a relative error of 0.45 is considered permissible then the REV can now be accepted at a side length of 45 m.

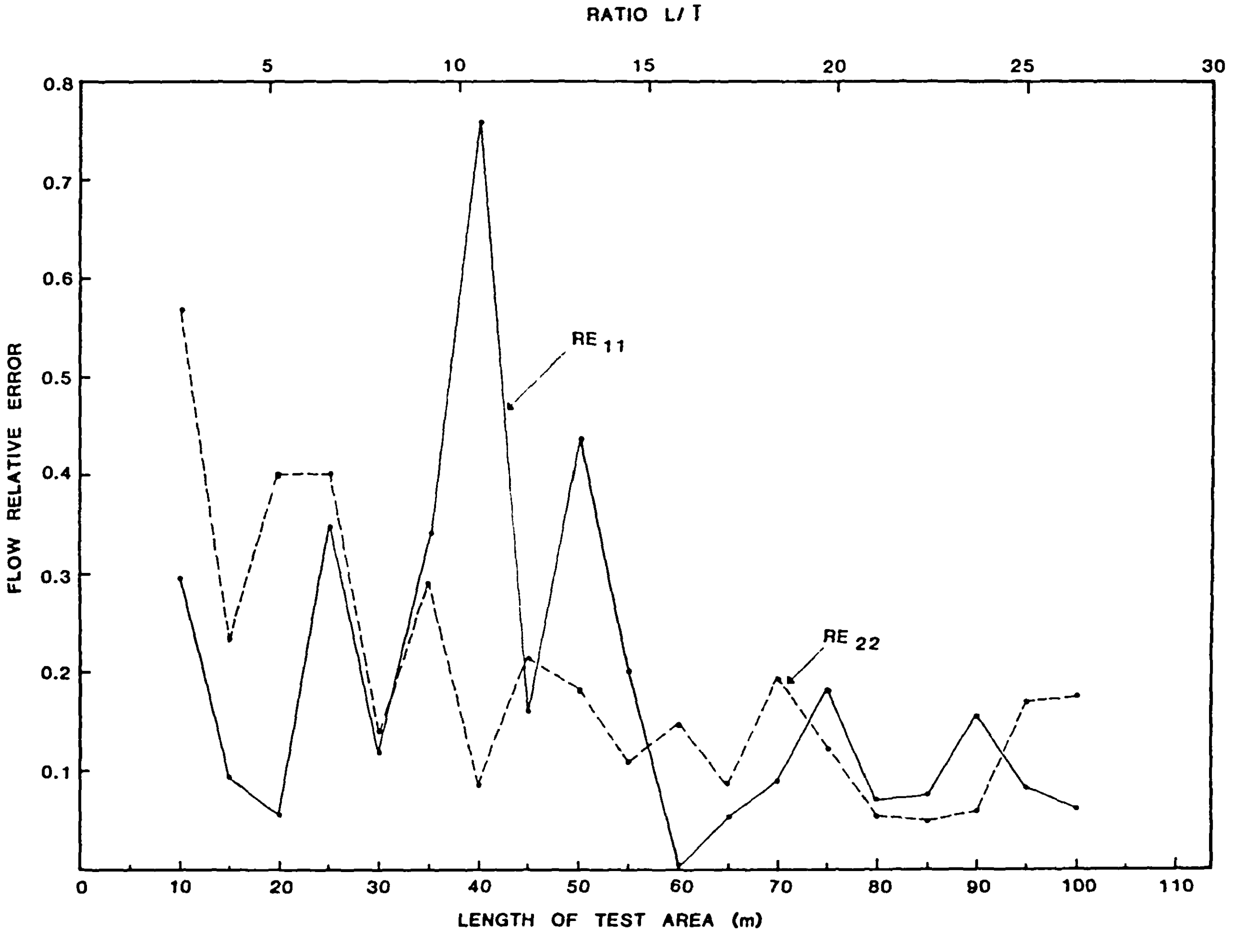

Fig. 4.42 Length of the test area against the flow relative error

4.3 Anisotropy of permeability in discontinuity networks

The aim of this study is to analyse the behaviour of discontinuity meshes when the direction of the applied potential gradient is changed by means of rotating the test area. In general, for an homogeneous anisotropic porous medium, if the gradient is rotated by an angle α and the directional permeability, Kg, is calculated, the relation between $1/\sqrt{Kg}$ against α will produce an ellipse when plotted in polar coordinates. For randomly generated discontinuity networks, however, $1/\sqrt{Kg}$ may not plot as an ellipse, indeed the plot can exhibit considerable variability. In some cases the shape of this plot provides a means of evaluating whether or not the given discontinuity mesh can be approximated as an homogeneous anisotropic porous medium.

Figure 4.43 illustrates the rotation of the test area, from $\alpha = 0°$ to $\alpha = 360°$, in increments of 15°. Two series of tests were carried out; the first was done on a discontinuity mesh containing 2 orthogonal sets and the second on a mesh with 3 discontinuity sets. The input values for the two series of tests are shown in Tables 4.XII and 4.XIII respectively. In both cases the generation area was 20 m by 20 m; the test area for the permeability calculations was taken from the central $10\sqrt{2}$ m by $10\sqrt{2}$ m square area; the actual dimensions of an individual test area were, as before, 10 m by 10 m. Since each test area of a different orientation must contain slightly different parts of the generated mesh (as can be seen in Fig. 4.43) the samples cannot be identical. It was assumed, however, that the error introduced was negligible. This assumption was supported by the measured values of

Parameter	Set 1	Set 2
Orientation:		
mean	45°	135°
standard deviation	5°	5°
type of distribution	Normal	Normal
Trace length (m)		
mean	0.60	0.60
standard deviation	0.60	0.60
type of distribution	Neg. Exp.	Neg. Exp.
Number of discontinuities	2000	2000
Aperture (mm)		
mean	0.2	0.2
standard deviation	0.0	0.0
type of distribution	Log-normal	Log-normal

Table 4.XII Input data for the anisotropy of permeability analysis. Two orthogonal sets

Parameter	Set 1	Set 2	Set 3
Orientation:			
mean	20°	100°	160°
standard deviation	5°	5°	5°
type of distribution	Normal	Normal	Normal
Trace length (m)			
mean	0.60	0.60	0.40
standard deviation	0.60	0.60	0.40
type of distribution	Neg. Exp.	Neg. Exp.	Neg. Exp.
Number of discontinuities	2000	2000	1500
Aperture (mm)			
mean	0.2	0.2	0.2
standard deviation (mm)	0.0	0.0	0.0
type of distribution	log-normal	log-normal	log-normal

Table 4.XIII Input data for the anisotropy of permeability analysis.
Three discontinuity sets

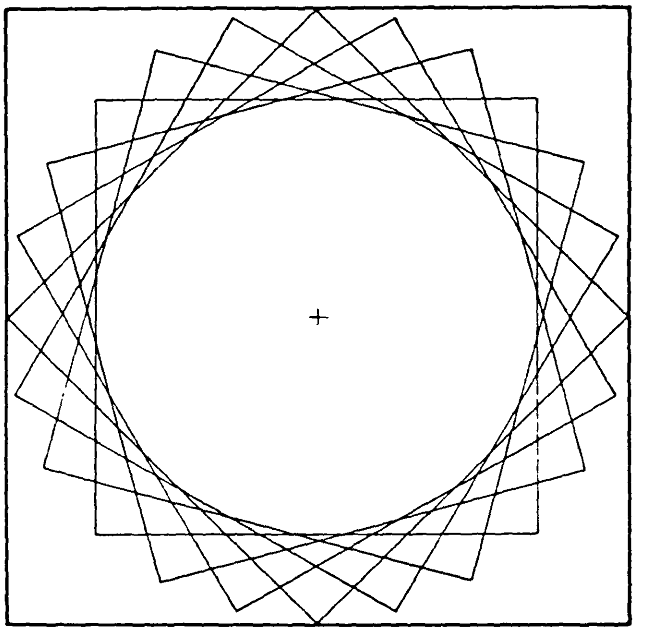

Fig. 4.43 Rotations of the test area from $\alpha = 0$ to $\alpha = 360°$ in increments of 15°

node index, which never varied by more than 2 percent. Fig. 4.44 shows the generated and inter-connected meshes used in this series of tests. The boundary potentials applied for all cases were h_i = 20 m and h_o = 10 m. As before, the programs DICONN and DIFLOW were used to calculate the mesh connectivity, the equivalent permeability tensor and the actual flow quantities across the boundaries.

Table 4.XIV shows the components of the equivalent permeability tensor for the two series of tests that were obtained when the potential gradient was in the x_1 and x_2 directions respectively.

Permeability Tensor (m/s)	(1) TEST A	(2) TEST B
K_{11}	2.454553E-06	3.952924E-06
$K_{12} = K_{21}$	2.176498E-07	6.466809E-08
K_{22}	2.043048E-06	2.350093E-06

TABLE 4.XIV Permeability tensors for test A and test B

(1) TEST A = 2 orthogonal discontinuity sets

(2) TEST B = 3 discontinuity sets.

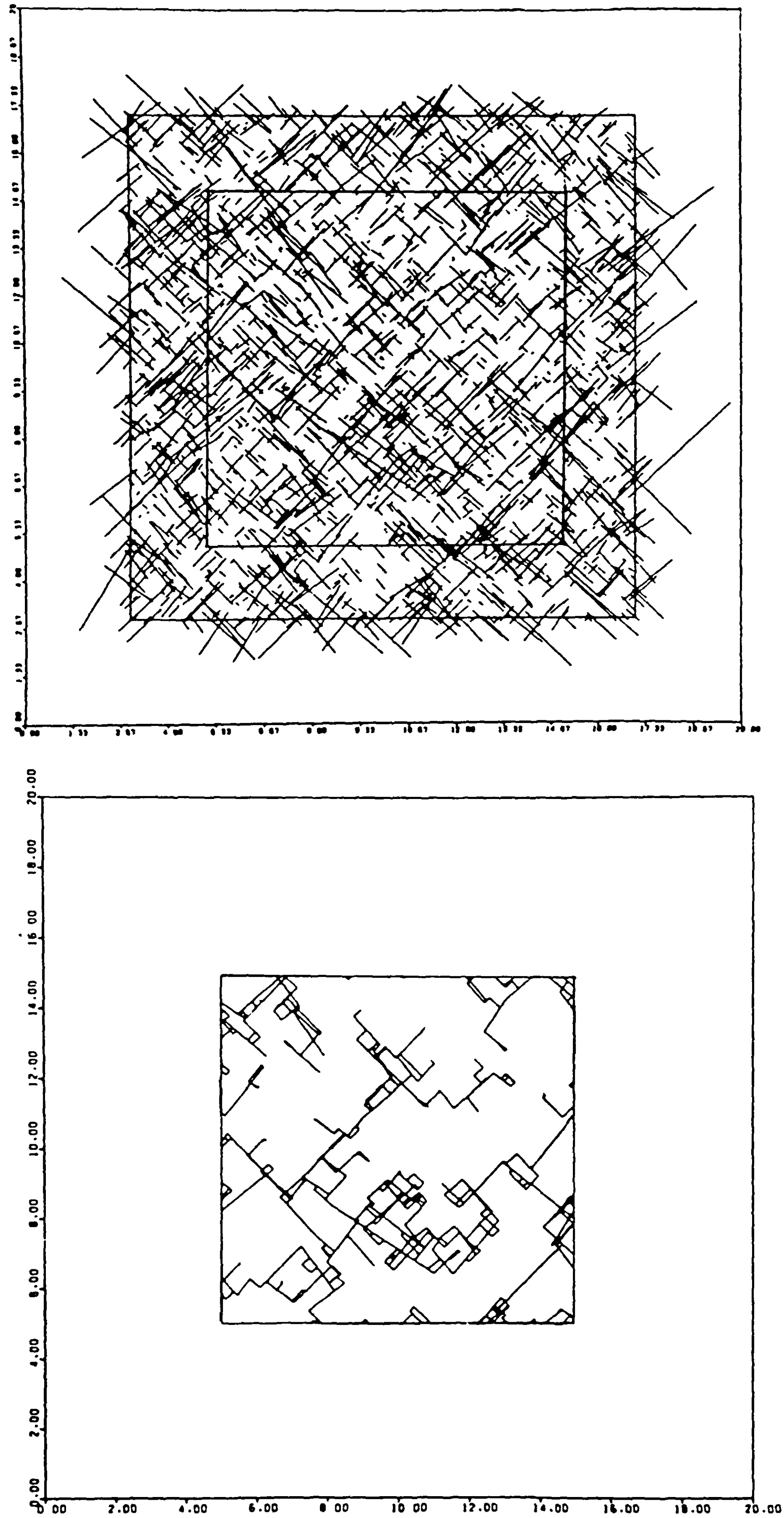

(a)

Fig. 4.44 Generated and inter-connected meshes for angle of rotation $\alpha = 0$

(a) Two discontinuity sets, test A

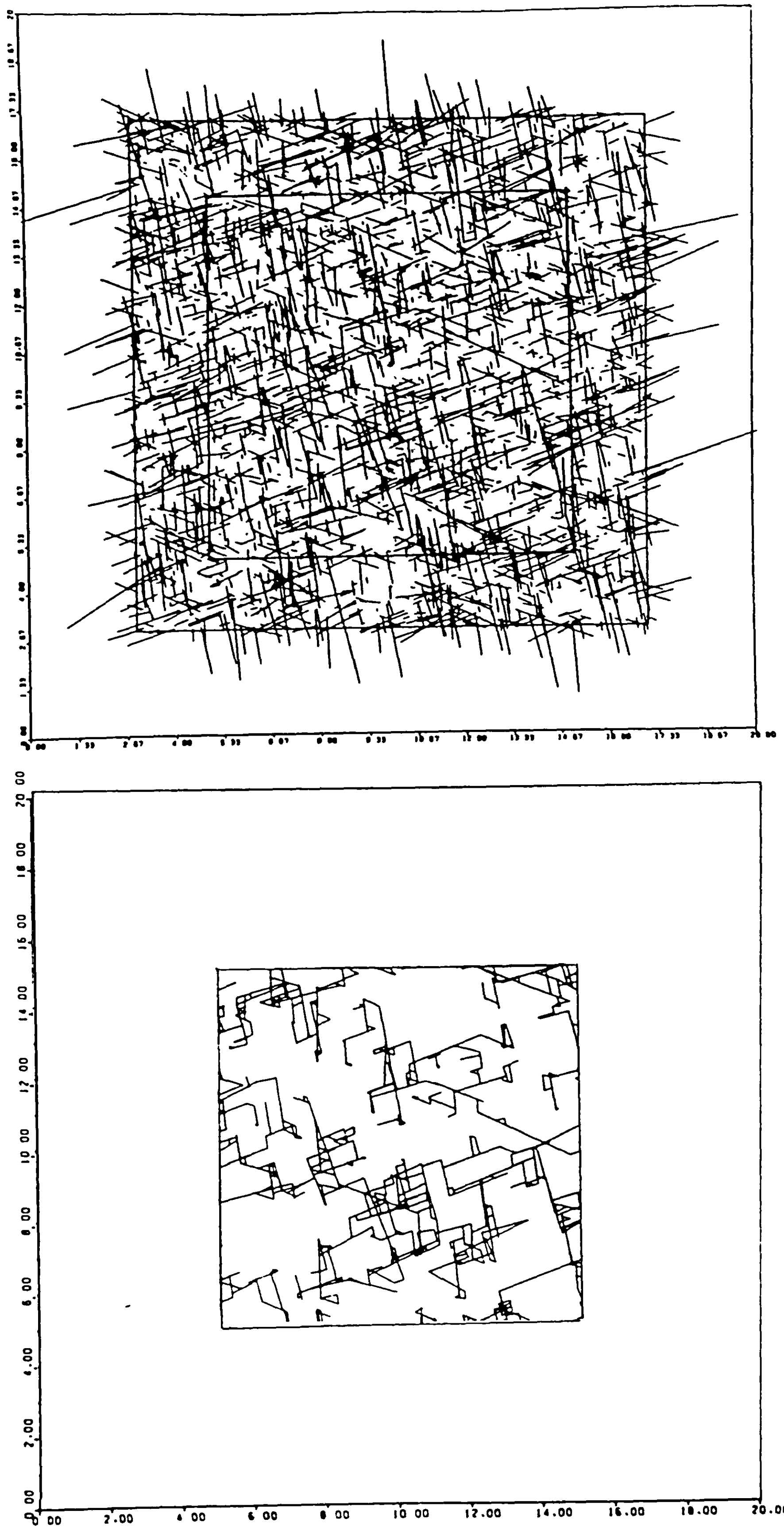

(b)

Fig. 4.44 (b) Three discontinuity sets, test B

It can be seen from Table 4.XIV that both permeability tensors are symmetric; this implies that the continuum approximation may be valid for these two meshes. Figures 4.45 (a) and (b) show the polar plots of $1/\sqrt{Kg}$. These figures show that the plots are ellipses, as the theory discussed in Chapter 2, predicts. The principal permeabilities and the principal directions are also shown in these figures. It can be seen that the minor axis of the ellipse corresponds to the major principal permeability, i.e. K_1, and that the major axis of the ellipse corresponds to the minor principal permeability, i.e K_2.

The permeability tensors shown in Table 4.XIV were used to predict the flow in the direction of the applied gradient. In each case, the actual flow across the two boundaries normal to the gradient orientation were calculated. These two flows are, however, rarely equal. In order to avoid this difficulty, side 1 was arbitrarily selected for the calculation of flow. Figures 4.46 (a) and (b) show the comparison between the predicted flows and the flows for each test area of different orientation. Although, in some cases, the measured flow is under-estimated by as much as one order of magnitude, in most cases the relative error is less than 0.6. Figure 4.45 shows that the permeability plot for the mesh with 3 discontinuity sets has a higher degree of anisotropy than the plot for the mesh with 2 discontinuity sets.

(a)

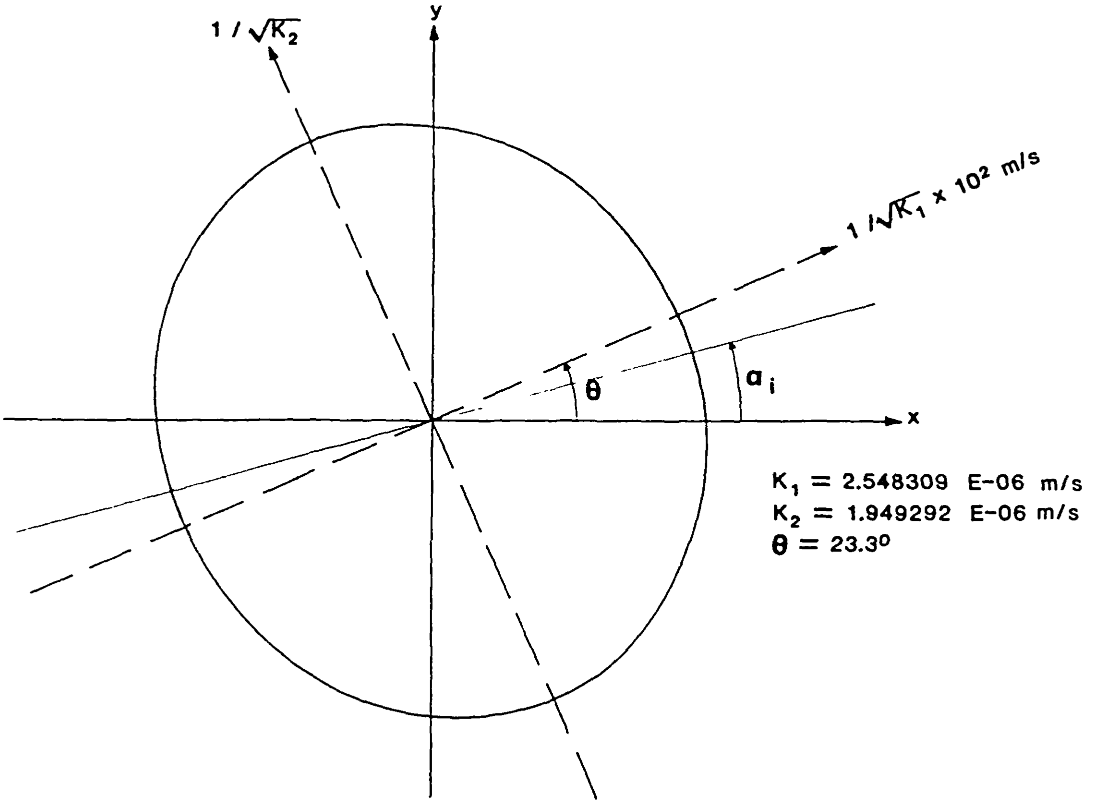

(b)

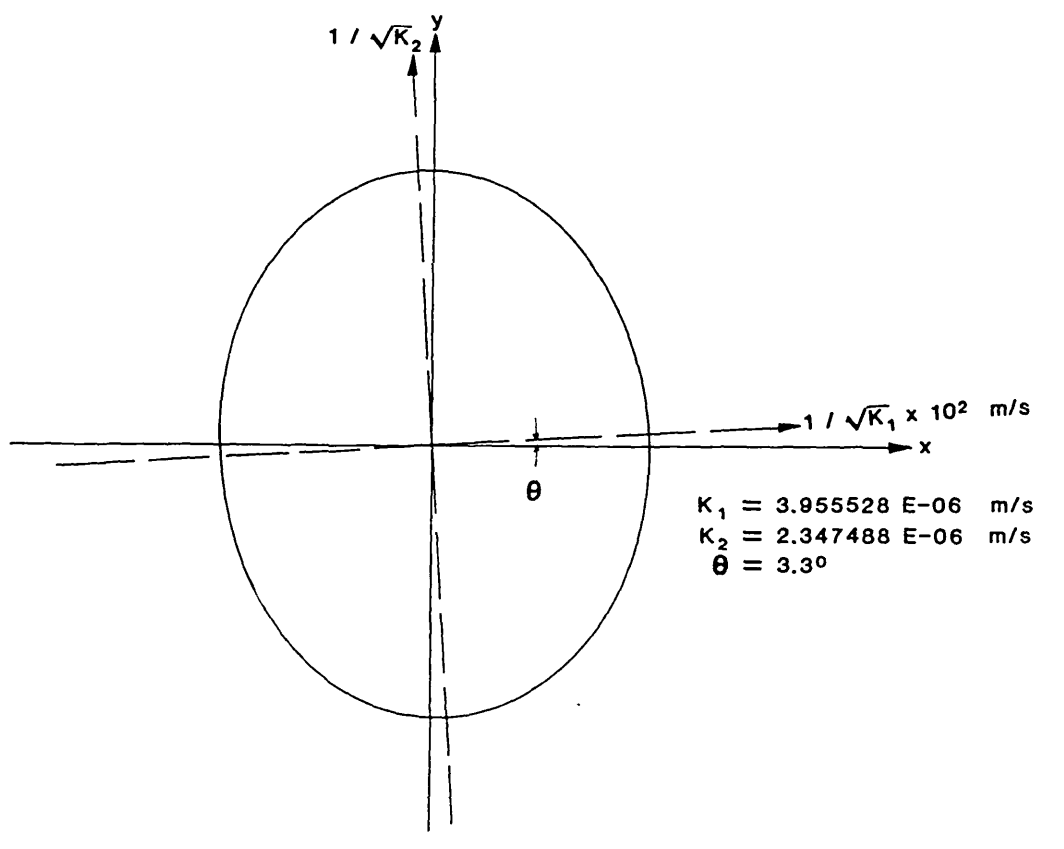

Fig. 4.45 Polar plot of $1/\sqrt{kg}$ against α

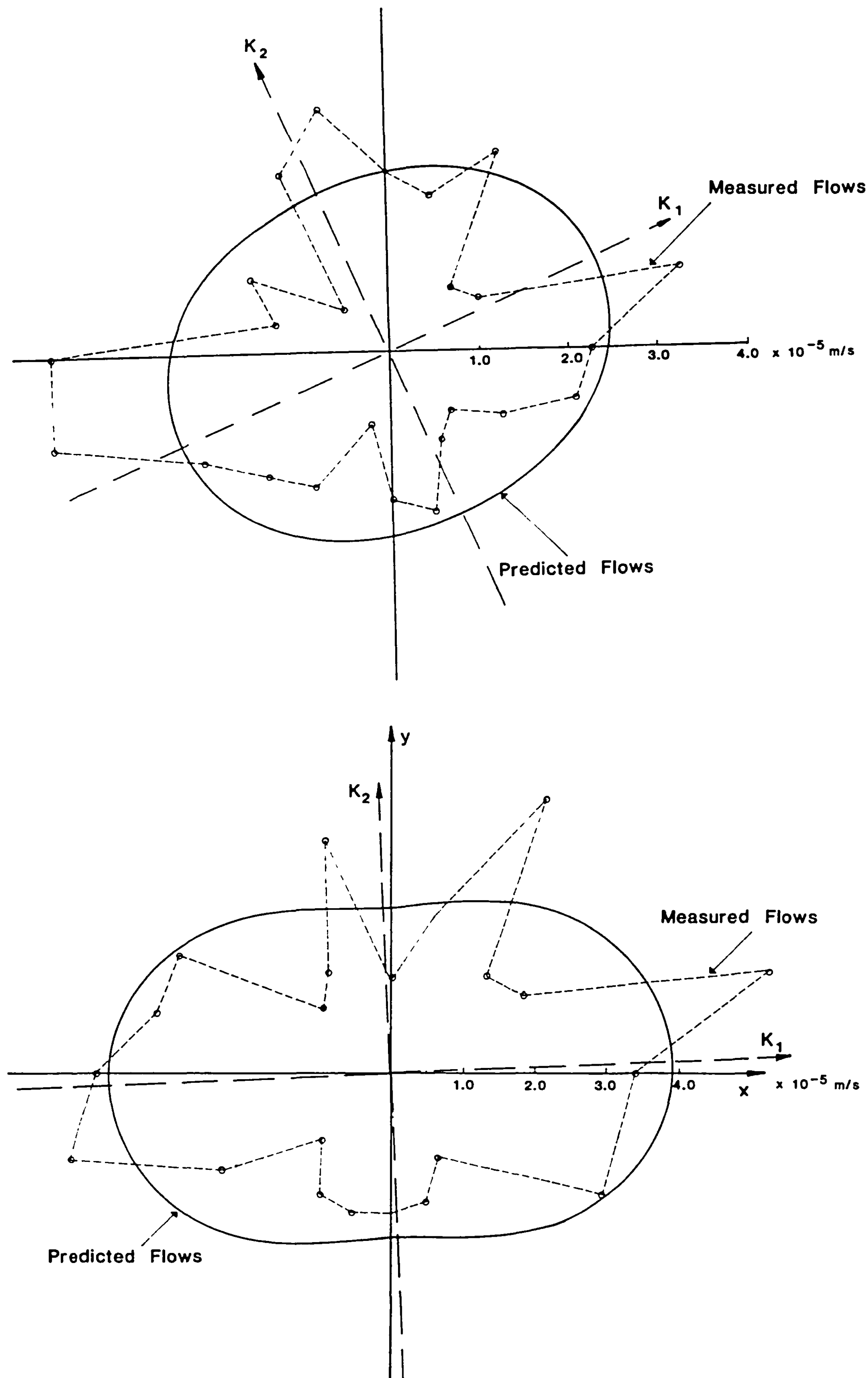

Fig. 4.46 Polar plot of measured and predicted flows against α

An analysis of the link between the geometric characteristics of a discontinuity mesh, such as the anisotropy of the discontinuity frequency, and the anisotropy of permeability is presented below. Discontinuity frequency rosettes were constructed by superimposing, onto the generated discontinuity meshes, a number of scanlines having the same orientations as the gradient potentials. The resulting discontinuity frequency rosettes are shown in Figure 4.47 (a) and (b).

In the case of the two orthogonal discontinuity sets, shown in Figure 4.47 (a) it can be seen that, although the theoretical frequency, as defined by equation (4.3), is symmetric, but anisotropic, the actual frequency measured by the rotating scanlines is slightly asymmetric. The actual frequencies for angles of α close to 90° overestimate the corresponding theoretical frequencies while for α values close to 0° the theoretical frequencies overestimate the actual frequencies. This variation is to be expected and is due to the random character of the model. Comparing Figure 4.45 (a) which contains the polar plot of $1/\sqrt{Kg}$ with the corresponding plot of discontinuity frequency (Fig. 4.47 (a)) shows that the orientation of the major axis of the permeability ellipse, i.e. the principal direction of permeability, coincides approximately with the orientation of the maximum discontinuity frequency. The minor axis of the permeability ellipse and the direction of minimum discontinuity frequency are also approximately parallel. Comparison between the appropriate plots of flow quantities (Fig. 4.47 (a)) and the plot of discontinuity frequency shows that the direction of maximum flow coincides approximately with

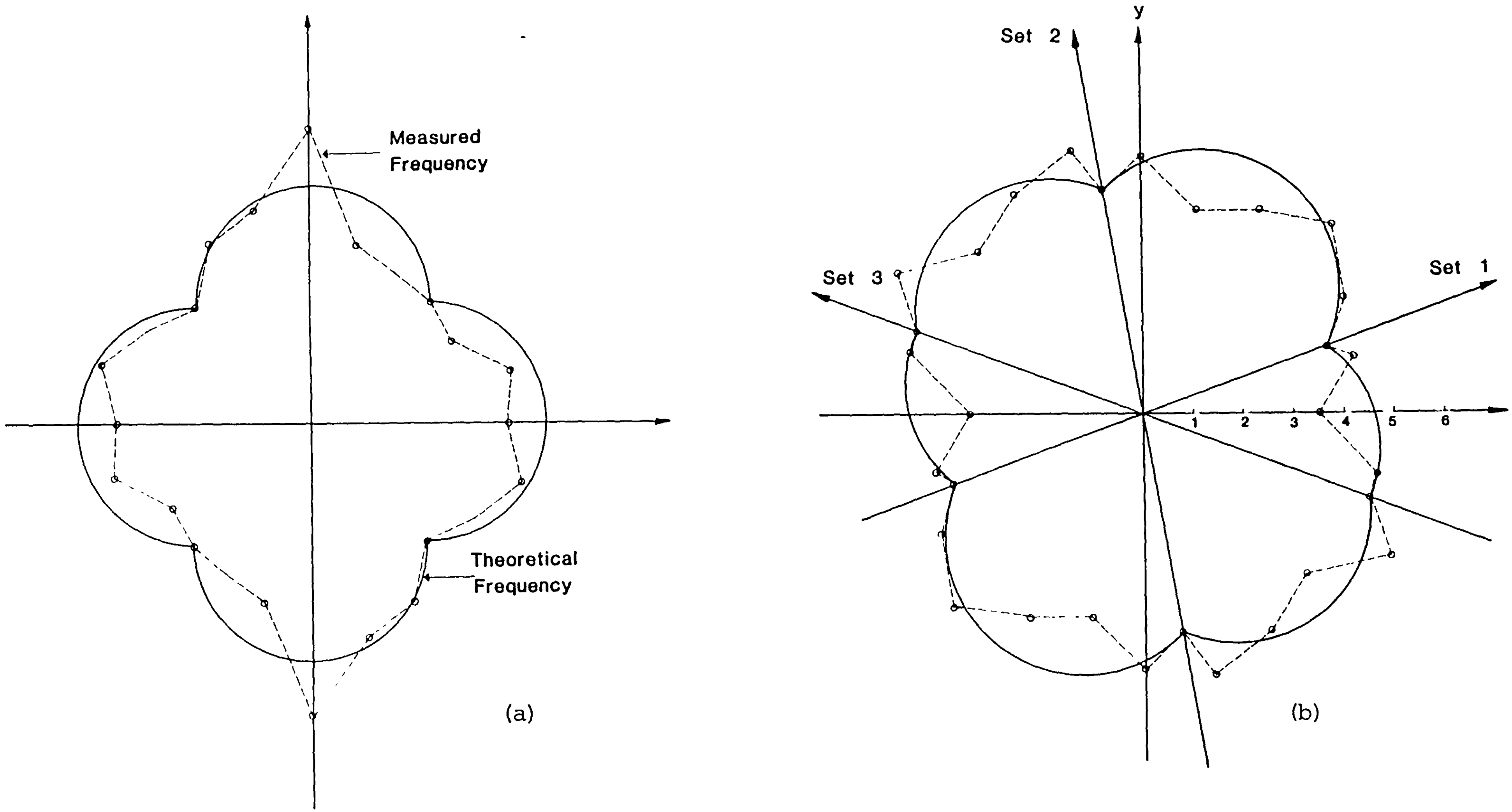

Fig. 4.47 Polar plot of the theoretical and modelled discontinuitv frequencv

(a) Two discontinuitv sets

(b) Three discontinuitv sets

the direction of minimum discontinuity frequency, while the direction of the minimum flow coincides approximately with the direction of the maximum discontinuity frequency.

For the second series of tests, Figure 4.47 (b) shows that the theoretical discontinuity frequency rosette and the measured frequencies are again anisotropic but show better agreement than in the previous case. The increased isotropy of the discontinuity frequency is due to the increased number of sets. Comparing the plot of $1/\sqrt{Kg}$ in Figure 4.45 (b) with the discontinuity frequency rosette of Figure 4.47 (b) it can be seen that, as in the case of the first series of tests, the orientation of the minor axis of the ellipse approximately coincides with the orientation of the minimum discontinuity frequency, and that the orientation of the major axis of the ellipse approximately coincides with the orientation of the maximum discontinuity frequency. The predicted and measured flow quantities when compared with the discontinuity frequency rosette showed the same characteristics as in the first series of tests. In this second series of tests, however, the overall agreement between the theoretical and the measured values for flow and the theoretical and measured discontinuity frequencies has improved, largely as a consequence of the more isotropic behaviour of the mesh.

In summary, it has been shown that, although there is not a clear relation between the discontinuity frequency rosette, the permeability ellipse and the polar diagram of flow quantities, there is an approximate correlation between the orientation of their minimum and maximum values. By constructing the discontinuity frequency rosette for a given mesh it is, therefore, possible to infer, approximately, the permeability anisotropy and the orientations of the principal permeability directions. From this it is possible to make a preliminary assessment of to what degree the given discontinuity mesh can be approximated by an homogeneous anisotropic porous medium.

4.4 Water flow into an Underground Excavation

The aim of this section is to assess the factors that influence the quantity of water flow into an underground excavation. To achieve this, the program DIFLOW was modified to permit the specification of the geometry and boundary potentials for an excavation of an elliptical or rectangular shape located anywhere within the network.

4.4.1 Effects of Changing the Size of the Excavation

Table 4.XV summarises the discontinuity input data that were used to generate 15 different realisations with a sample area of 50 m by 50 m. Circular tunnels were created at the centre of each realisation, with radii of 1, 2, 5, 7 and 10 m and a uniform potential of 10 m was appied to each of the boundaries of the sample area. Fig. 4.48 shows a typical example of a mesh realisation containing a tunnel of 10 m diameter. Although the specific flow characteristics of each network are dependent upon the input data listed in Table 4.XV, it is possible to draw some general conclusions concerning the influence of excavation size on water flow. Fig. 4.49 shows a plot of the total inflow against tunnel radius for the 15 realisations, together with the values of mean flow, the standard deviation (S.D.) of flow and the coefficient of variation (C) for each radius. It is clear from this figure that mean inflow tends to increase with increasing tunnel radius. This expected result is related to the fact that a larger tunnel tends to intersect more discontinuities. Fig. 4.49 also includes a plot of the mean number of interconnected discontinuities

Parameter	Set 1	Set 2
Orientation:		
mean	40°	120°
S. deviation	7°	8°
type of distribution	Normal	Normal
Trace length (m)		
mean	1.7	2.1
S. deviation	1.7	2.1
type of distribution	Neg. Exp.	Neg. Exp.
Aperture (mm)		
mean	0.05	0.05
standard deviation	0.0	0.0
type of distribution	Log-normal	Log-normal
Number of discontinuities	4000	4000

Table 4.XV Input data for the study of the effects of changing the size of the excavation

intersected by the tunnels at each radius; this is referred to as the "mean intersection frequency" (M.I.F.). The mean inflow rises at approximately the rate that could be expected from the increasing numbers of discontinuities intersected by the larger tunnels. In other words the mean flow rate per discontinuity intersected is independent of the tunnel radius. This result is, however, complicated by the fact that there is considerable variability in total inflow at all radii. This variability, as measured by the standard deviation of total inflow, tends to decrease significantly with increasing tunnel radius. This reflects the averaging effect produced by the larger number of discontinuities intersected by the larger tunnels.

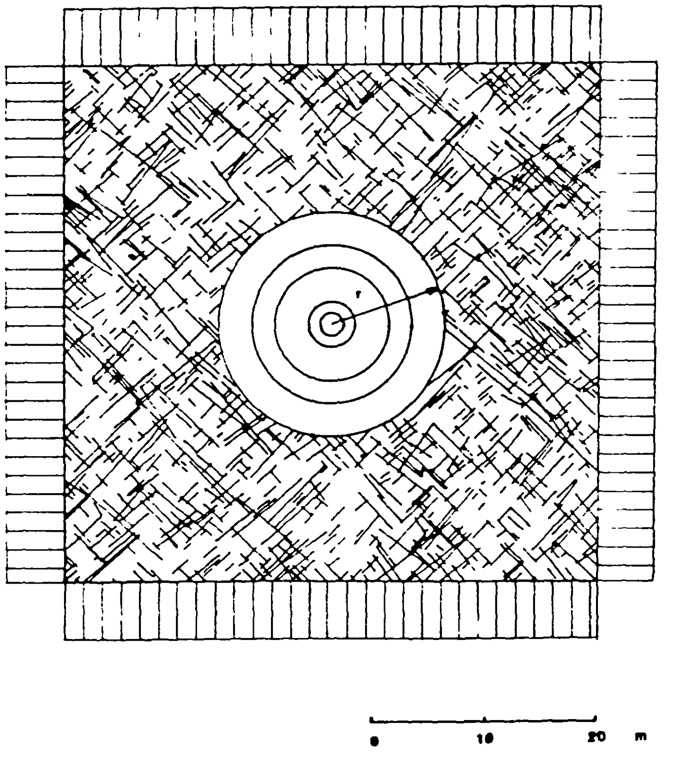

Fig. 4.48 Example of one random realisation of a discontinuity mesh containing a tunnel of 10 m diameter

Inflow, l/min x10⁻⁶					
Mean	0.70	0.77	1.66	2.31	4.02
S. D.	0.76	0.85	1.16	1.25	2.22
C.	1.09	1.10	0.70	0.54	0.55
M. I. F.	3.80	6.53	13.00	21.13	33.60

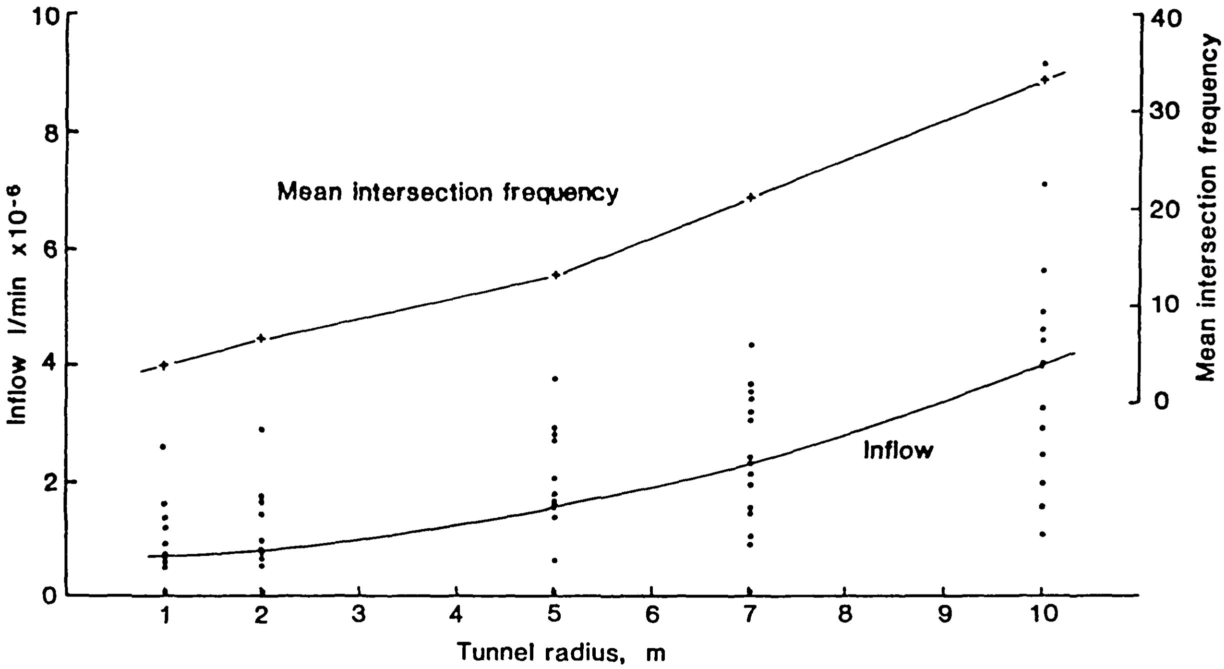

Fig. 4.49 Influence of the excavation size on inflow

4.4.2 A Case Study Involving the Prediction of Water Flow into a Tunnel

A tunnelling site in the Derbyshire area of England was selected to provide a case study for the testing and validation of the flow model. The tunnel length selected for study is currently being excavated along a line of trend 066° and plunge 01° to a diameter of 2.8 m at a depth of approximately 100 m through fractured sandstones, grits and mudstones of the Millstone Grit Series in the Carboniferous System. Since the tunnel is fully lined it was necessary to study a length of tunnel that had not yet been excavated to ensure that water inflow measurements were sufficiently detailed to justify a validation of the model; previous inflow assessments were of a largely qualitative nature.

The first task was to determine the discontinuity characteristics of the rock mass surrounding the tunnel. Since access to the tunnel face was restricted by operational constraints, and available exposures at the face were of limited extent, it was necessary to examine surface exposures. These comprised a natural cliff exposure and three abandoned quarries. The data were collected by linear and sampling, using scanlines, and by areal sampling using photographs as described in Chapter 3. The scanline data were processed by the computer program SCANL, described earlier, which analyses discontinuity trace length, spacing and orientation to produce histograms with associated mean values and standard deviations. An example of typical graphical output is shown in Fig. 4.50. The photographs of each face were first enlarged to a size of 300 by 400 mm then the coordinates of the end points of each

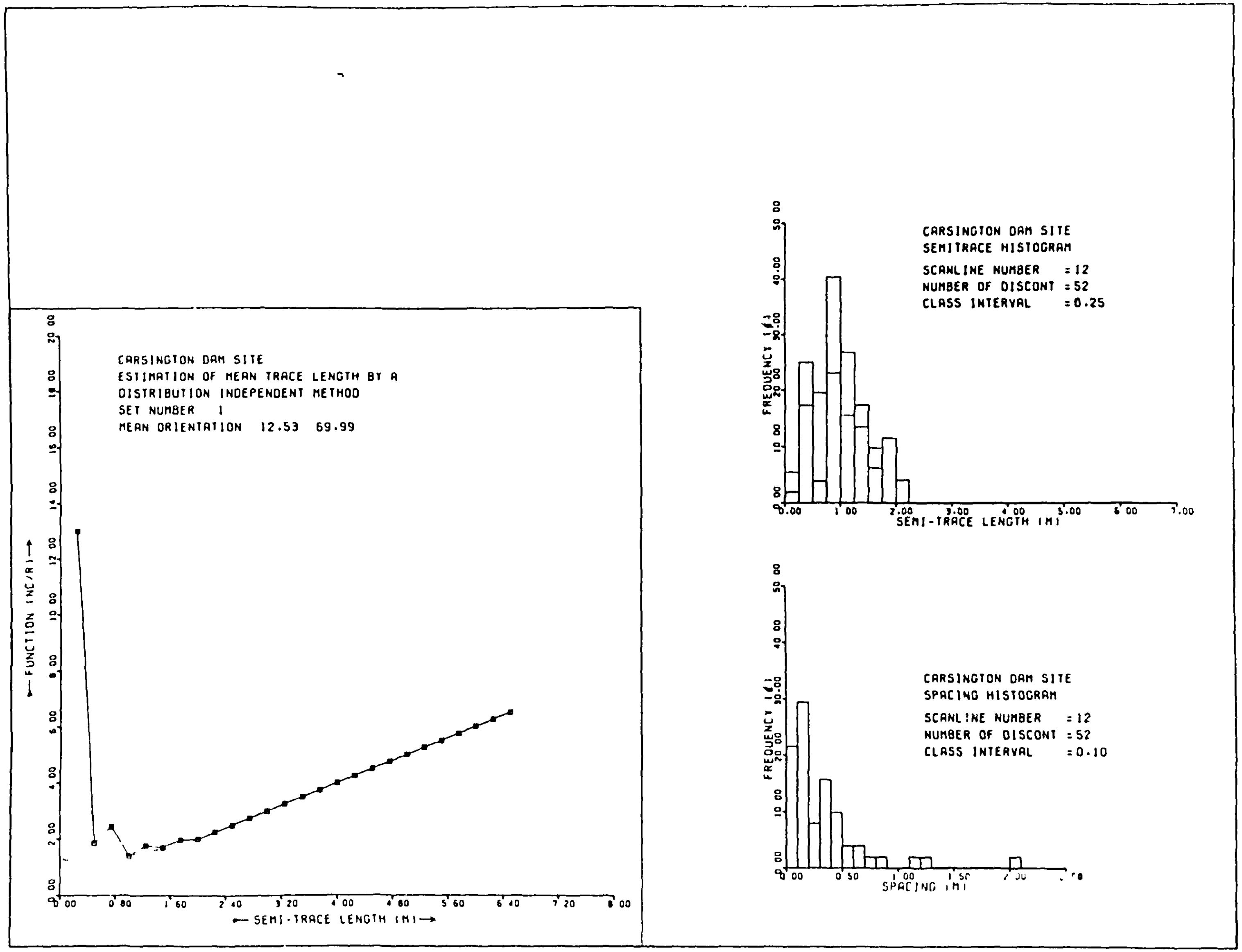

Fig. 4.50 Graphical output of the scanline discontinuity data processed by the SCANL program

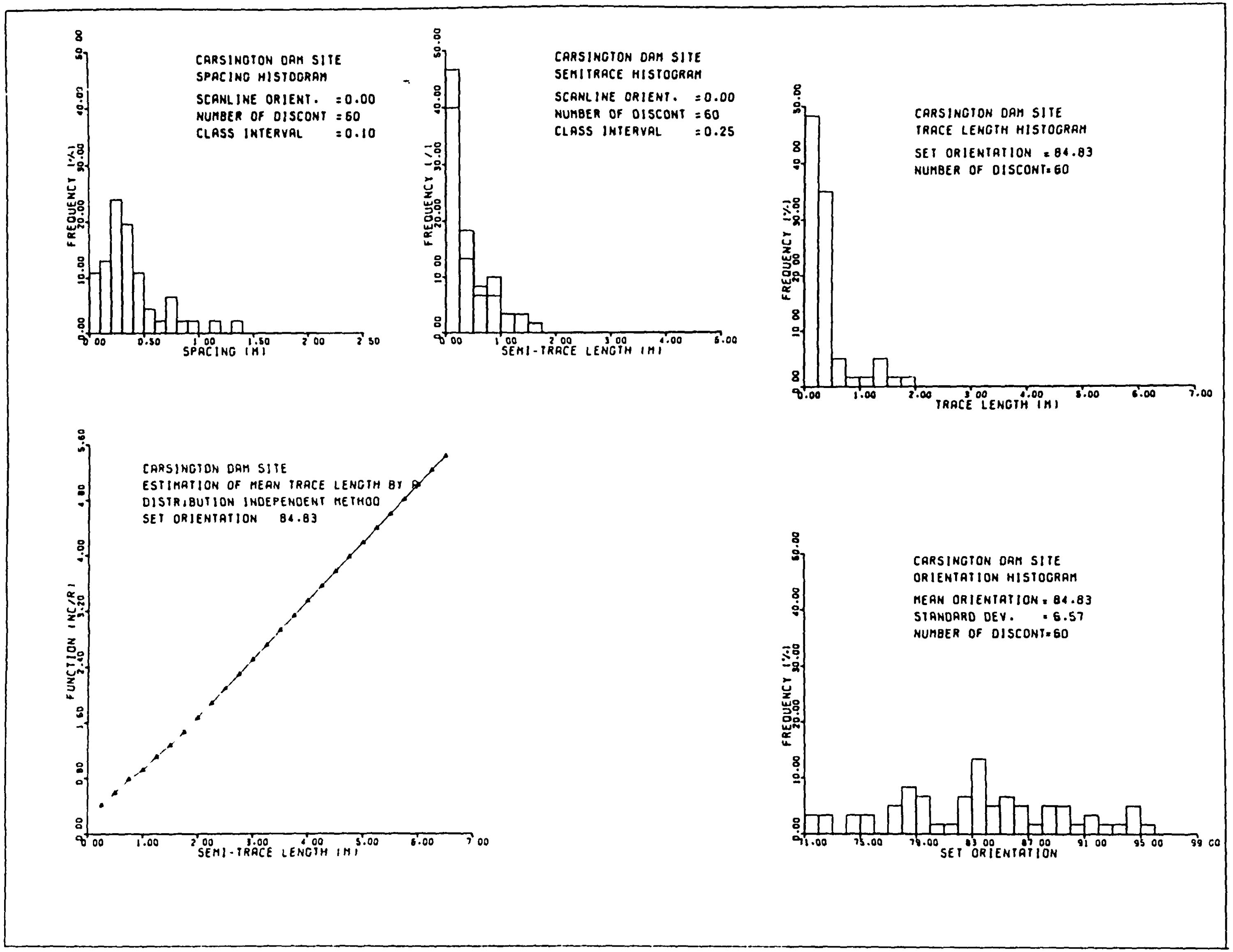

Fig. 4.51 Graphical output of the photographic discontinuity data processed by the PHOCOM program

discontinuity trace within the specified sample area were recorded by means of a scale designed to compensate for any photographic distortion. These data were then passed to a second program PHOCOM, described earlier, which analyses discontinuity trace length, areal density and orientation to produce histograms with associated mean values and standard deviations. As noted earlier, the program PHOCOM also has the facility to construct scanlines through the discontinuity traces to generate data equivalent to those collected by physical scanline sampling, and thereby provide independent checks on the results. Fig. 4.51 shows a typical graphical output of the program PHOCOM. The programs SCANL and PHOCOM also carry out curve fitting and goodness of fit tests to determine which probability density distributions provide the best fit for the observed data.

Analysis of the data showed that the discontinuity characteristics at each of the sites were remarkably consistent, despite the varying lithology. Analysis of the orientation data showed that there were two steeply dipping sets together with a third set, associated with bedding, dipping at an angle of about 45°, as plotted on the lower hemisphere projection in Fig. 4.52 (a). This figure, which also contains the tunnel drive direction, shows that the normals to discontinuity set 1 and the bedding planes lie, very nearly, in a vertical plane through the tunnel axis. In order to justify one of the important assumptions for the two-dimensional network analysis - that the discontinuity normals lie in the plane of the realisation - it was necessary to carry out this analysis in a vertical plane through the

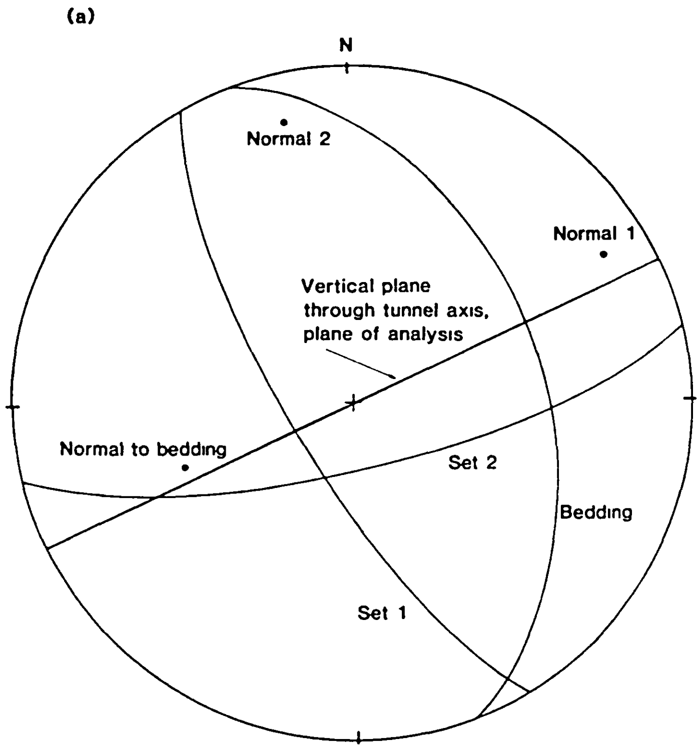

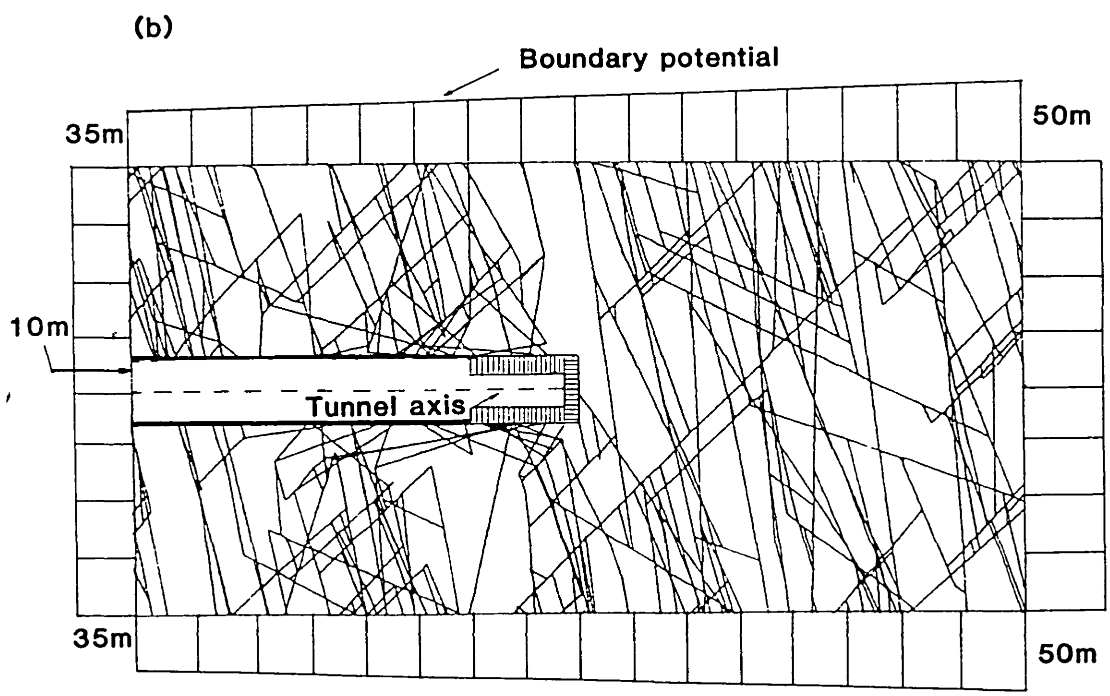

Fig. 4.52 (a) Equal area projection of orientation data

(b) Case study inter-connected mesh and boundary conditions for test area tunnel axis. This meant, unfortunately, that discontinuity set 2 would be almost parallel to the plane of the analysis and would, therefore, violate one of the assumptions of the two-dimensional model. This is one of the inevitable difficulties that can arise when trying to represent a three-dimensional structure by a two-dimensional model.

Additional geotechnical data were obtained from 4 boreholes, each of which was sunk to below the tunnel invert level in the zone of interest. The borehole logs were used to verify that the discontinuity data, obtained by examining surface exposures, were applicable to the zone of rock around the tunnel. In general the borehole logs, and also brief surveys at the tunnel face, confirmed the surface exposure data. In some cases, however, it was necessary to modify orientation and frequency values slightly to allow for surface weathering effects and regional variability.

Mass permeability values obtained from borehole packer tests at the tunnelling level were used, in conjunction with discontinuity frequency and orientation data, to estimate the mean apertures for each of the discontinuity sets. The calculations were based upon an approach presented by Rissler (1978). The choice of probabilitity density distribution for the discontinuity apertures and also the values for standard deviation, were based upon typical experimental data in the literature (Bianchi and Snow 1968). The formulations and methodology used in calculating aperture are given in Appendix 8. The complete set of input data, defining the discontinuity characteristics for the case study, is summarised in Table 4.XVI.

Parameter	Set 1	Set 2	Set 3
Orientation:			
mean	45°	105°	154°
standard deviation	2°	7°	8°
type of distribution	Normal	Normal	Normal
Trace length (m)			
mean	10.0	7.5	5.0
S. deviation	8.0	7.5	5.0
type of distribution			
Aperture (mm)			
mean	0.15	0.20	0.18
S. deviation (mm)	0.05	0.05	0.05
type of distribution	log-normal	log-normal	log-normal
Number of discontinuities	250	1500	200

Table 4.XVI Input data for the case study

Each realisation was generated in a vertical plane through the tunnel axis, to give a rectangular sample area 40 m wide and 20 m high. A 20 m length of the 2.8 m diameter tunnel was created at the mid-height of the sample area by specifying the hydraulic boundary conditions on the tunnel surface. All of the tunnel, except a 5 m length at the face, was assumed to be lined with an impermeable membrane. This was simulated by assigning a negligible conductance to those discontinuities that intersected the tunnel in the lined section. Ten different random realisations were generated; one of these is shown in Fig. 4.52 (b). The boundary potentials on the margins of the test area were determined from the piezometric readings monitored in four boreholes within the zone under study. Water table levels determined from readings taken between March 1982 and October 1983 indicated that the tunnel had tended to draw down the water table level during this period. Fig. 4.53 shows a tentative flow net, which was constructed on the basis of this piezometric data, and which was used to establish the distribution of hydraulic potentials on the four boundaries of the sample area. The resulting potential distributions are shown also in Fig. 4.52 (b).

Table 4.XVII lists, for each of the realisations, the number of interconnected discontinuities intersected by the tunnel face and the 5 m unlined length (the "intersection frequency") together with the predicted total inflow for this length, and the associated means and standard deviations. The two-dimensional nature of the model means that the inflow values refer to a tunnel with a 2.8 m square cross-section. The perimeter of the actual tunnel is circular, and therefore

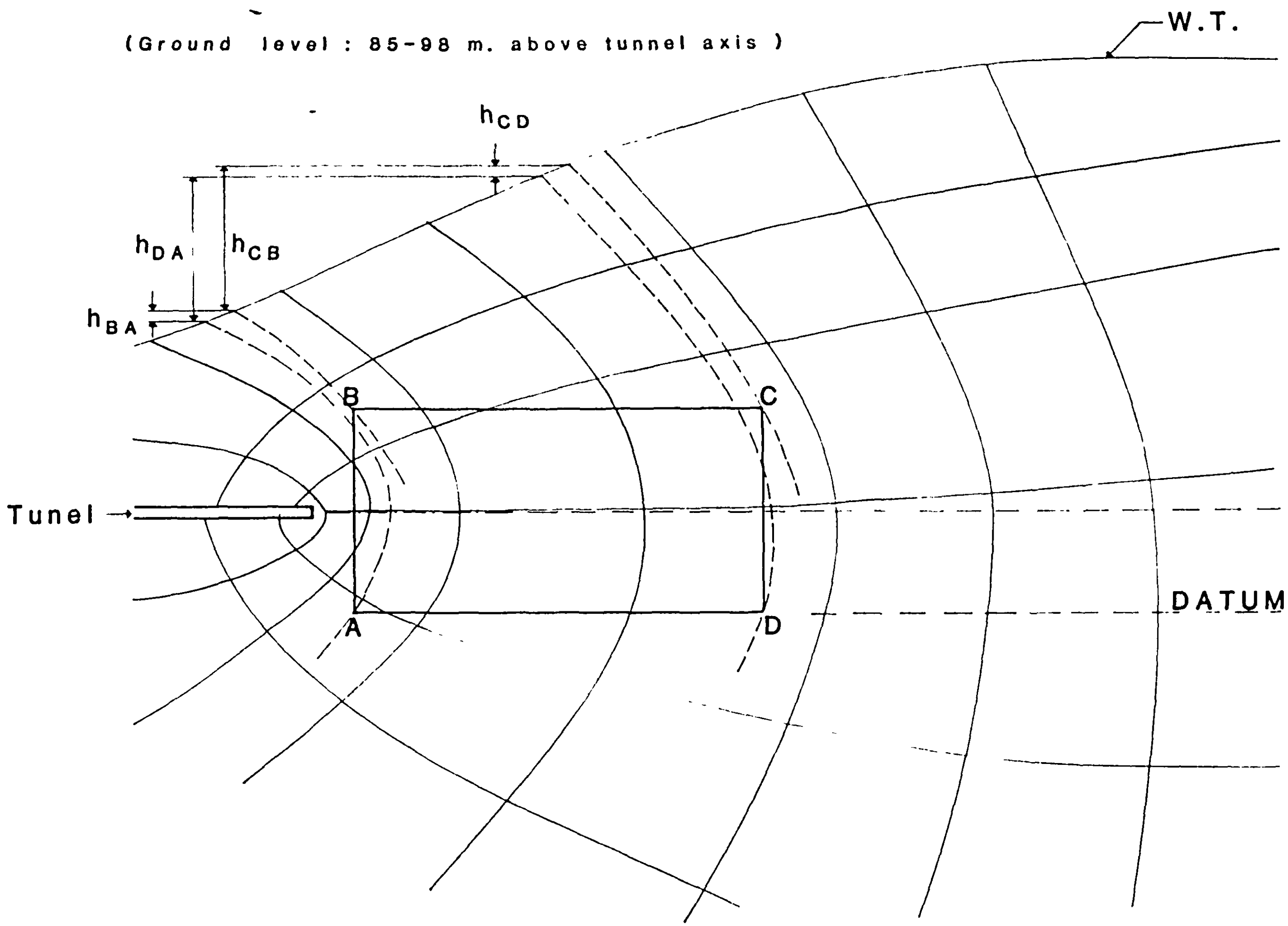

Fig. 4.53 Tentative flow net in the region of the tunnel for the case study

Realisation	Intersection frequency	Inflow litres/mins
1	28	23.85
2	26	13.99
3	32	36.37
4	38	46.94
5	22	22.91
6	33	29.12
7	32	17.27
8	28	11.84
9	32	22.88
10	34	29.72
Mean	30.50	25.50
Standard Deviation	4.55	10.60

Table 4.XVII Results of the case study

smaller in the ratio $\pi/4$ than the assumed square section. Results presented earlier in this section suggest that the discontinuity intersection frequency, and hence the inflow rates for the circular section, should approximately reflect this ratio in their perimeters. At the time of writing, inflow values for the particular length of tunnel under study are not yet available. Typical estimated inflow values for equivalent tunnel lengths nearby have ranged between 20 and 80 litres per minute.

In summary, this case study involved the collection of discontinuity data from exposed faces, the analysis of borehole measurements and the assessment of local groundwater conditions, to obtain predictions of likely water inflow quantities in the unlined section near the tunnel face. Although the predicted inflows were within the general range of the observed values, the case study underlined the difficulties of attempting to represent a three-dimensional structure by a two-dimensional model.

CHAPTER 5 DISCUSSION

The discussion presented in this Chapter is organised under the following headings: input data collection, model validity, the parametric study of discontinuity characteristics and application of the model to practical problems.

5.1 Input data collection

It was noted in Section 3.1, that the statistical model developed in the context of this work is designed to use input data derived from field measurements. The essential input data include: the means, standard deviations and the probability density functions of discontinuity trace length and orientation and also the areal density for each set. The scanline and photographic methods of sampling were found to be suitable for obtaining the necessary input data for the model. It was found that although the scanline method is a relatively inexpensive technique for obtaining discontinuity characteristics, some skill is needed in order to reduce the bias that may be introduced by the inevitably subjective nature of the process. Practical problems arise when a given discontinuity exhibits waviness or large asperities which create difficulties when measuring orientation. In some cases difficulty was encountered when classifying discontinuities that may have been induced by blasting. An additional bias, which is a function of the orientation of the scanline with respect to the normal of the discontinuity planes, can be introduced. This type of bias can, however, be corrected during the processing of the data or largely avoided during sampling by taking three mutually orthogonal scanlines.

The photograph method, which basically is an areal sampling process, was found to be a very effective, but rather laborious, way of gathering discontinuity density and trace length information. The method, explained in Chapter 3, involves examining an enlarged photographic print of the rock face and recording the coordinates of the end points of each discontinuity. A digitizer device which interfaces with the main frame computer was available for this work. Photographic distortion, caused by the camera axis not being normal to the rock face, was corrected by reference to surveying staffs that had been placed at right angles to each other on the rock face. This method could be improved further by employing photogrammetric techniques. For this purpose control points have to be established on the rock face and their orientation and location relative to the camera position accurately determined. A computer program, Stewart (1981), can be used to convert the photographic coordinates to planimetric rectangular coordinates. This process has the advantage of speeding up the calculations and also of avoiding human error that can be introduced when the coordinates are measured normally.

Areal photographic surveys in conjunction with linear scanline surveys on the actual rock face were found to be essential in collecting input data for the model. This is because three-dimensional orientation data can only be obtained easily from a scanline survey while areal density can only be estimated accurately from a two-dimensional survey. The use of these two methods together has the advantage of providing an independent check on the data. This is achieved by comparing the discontinuity frequency, λ_s, measured along a given scanline with the discontinuity frequency calculated using either equation (4.1) or measured by superimposing scanlines over the photographic print. The two independent sampling methods also provided a means of checking the estimated values of mean trace length obtained by the different analytical methods summarised in Section 3.1.3. This is crucial because, as has been shown in Chapter 4, trace length is of great importance in controlling mass permeability.

With regard to the number of discontinuities that have to be sampled in order to obtain a representative sample of the rock mass structure, it is suggested that a certain amount of pre-processing of the data be carried out by plotting the normals to the discontinuities on a hemispherical projection after the first scanline has been completed. This has the advantage of indicating which is the best orientation for the next scanline and also of keeping trace of the number of discontinuities that have been sampled from each discontinuity set present in the rock mass. In general it was found that when the minimum number of discontinuities for each set was 50, the overall sample was satisfactory. Satisfactory in this context was taken to mean that the Fisher's constant for each set exceeded 4 and that the chi-square test for the fitting of a theoretical probability density function to the experimental data indicated acceptance at the 95 percent confidence level. These criteria were also applied when sampling was done by the photographic method.

Finally it is suggested that when measuring discontinuity trace length or semi-trace length special care should be exercised, since discontinuity persistence was found to be of crucial importance in controlling the connectivity of the mesh and therefore its permeability. Special attention is needed when the trace lengths are trunicated or censored.

None of the methods mentioned above is suitable for measuring discontinuity aperture, because, with very few exceptions, the apertures on the rock exposures are bound to be disturbed, either by blasting or weathering. The apertures, as described in Section 4.4, are best estimated by using water injection tests, the theory and methodology of which have been described by Bianchi and Snow (1968), and outlined in Chapter 2.

Further measurements in scanline surveys include the roughness, waviness and hardness of the surfaces of the discontinuity planes. Only a limited number of measurements of this type have been carried out, largely because the model developed in this work makes the basic assumption that a discontinuity plane can be modelled as a smooth parallel plate.

5.2 The validity of the modelling technique

Although, in the course of this work some practical applications have been presented, it is believed that the most important features of the model are that it statistically and probabilistically represents discontinuity networks. The model permits the achievement of the following principal aims:

1. To identify and study those discontinuity characteristics that are crucial in dictating the hydraulic behaviour of discontinuity meshes, and

2. to assess when a network of discontinuities can be validly represented as a continuous, anisotropic porous medium.

A detailed discussion of these two aspects will be introduced in the next section together with comments on the practical applications of the model. In this section the discussion will be centered more on the type of model selected and on the methodology used. Bearing in mind the above aims, a numerical modelling approach was selected. This had to be of a statistical, rather than a deterministic, type in order to account for the variability of the parameters that characterise the discontinuities. Simplifying assumptions had to be made in order to rationalise the intricate and variable nature of the discontinuities. Most of the assumptions were made in order to idealise the complex geometry of the discontinuities, as had been explained in Chapter 3.

The fundamental reason for selecting a numerical model rather than a physical or an analogue model was its ability to determine analytically the flow quantities through, and also the permeability of, the discontinuity network. A numerical model also has the advantage of being amenable to extension to three-dimensional analysis. In essence the approach is based on a statistical description of a real two-dimensional discontinuity mesh, from which several random realisations of the mesh can be made. By measuring the flow quantities and permeabilities of these discontinuity mesh realisations it is possible to go some way towards achieving the above mentioned aims. There are, however, certain difficulties with this approach. Firstly, many realisations must be analysed before a mean and standard deviation of permeability and/or flow quantity, on a reliable statistical basis, can be obtained, in Section 4.2.1 it has been shown that up to 60 realisations were necessary for this purpose. Secondly, except for the special case when the discontinuities are persistent and entirely transect the test area, there is no exact method for solving analytically the permeability of a mesh whose internal potentials are unknown.

Although a more detailed way of modelling the flow across a discontinuity network could be achieved if deformability of the fractures is considered, e.g. by using Goodman's joint element method coupled to a fluid flow finite element or boundary element program, in this work an approach which assumes the rock mass to be rigid, so that each fracture could be modelled as a smooth parallel plate was adopted. This assumption is applicable to non-porous rocks that are brittle enough to develop fracture systems, and that are strong enough to sustain significant discontinuity apertures in the given stress field. A major limitation of many of the techniques that employ finite element or similar numerical methods is the size of the problems that can be efficiently and economically analysed. For example the largest mesh solved by Long (1983) using a finite element program was one containing less than five hundred discontinuities. Although no information was available concerning the number of discontinuities that can be solved with the flow/stress coupled program, it is inevitable that this would be less than that solved by Long. The model adopted in this work is one that relies on balancing energy potentials at each interval node, according to equation (3.20), and then by using the bi-factorisation technique, finding the solution of the resulting system of linear simultaneous equations. This gives the potentials at all interval nodes, from which flow and permeability can be calculated. This method can handle networks containing up to around 5000 discontinuities.

The advantage of the approach adopted in this work over the finite element method is that a larger number of discontinuities can be analysed with the same computational capacity. However, in order to account for fracture deformability, the influence of field stresses, relatively high permeability of the rock material together with complex boundary conditions it is necessary to adopt a significantly more complex approach. A major advantage of the approach presented here is that only two tests are necessary to determine the permeability tensor. Long (1983) required 24 separate tests which involved the rotation of the test area, in 15° increments, from 0° to 360°, followed by a regression analysis to determine the permeability tensor.

The current model offers two possible ways of calculating the permeability tensor. The first method, given in equation (3.26), considers total flow across the boundaries that are at right angles to the direction of the applied gradient. This gives the macroscopic flow velocity and hence, from Darcy's Law, the permeability in the direction of the gradient. The second method calculates the mean flow velocity by carrying out a summation over all of the discontinuity segments, as explained in equation (3.27). The permeability tensor is then obtained using equation (3.31). The first method, which has also been used by Long (1983) and Robinson (1982), presupposes that the discontinuity mesh behaves like an anisotropic porous medium, and, by implication, that the flow quantities across the boundaries normal to the direction of the gradient do not produce tangential components. Since this usually implies that inflow does not equal outflow on opposite sides of the sample area, some complications in defining the permeability tensor can be expected. Furthermore the value of permeability obtained in this way will depend explicity on the locations of the boundaries. For a given discontinuity mesh, the second method provides a unique permeability tensor by performing two tests, as explained in Section 3.5. The resulting permeability tensor is always independent of the location of the boundaries of the test area. There are, however, certain difficulties in defining an equivalent permeability tensor that is not only symmetric but that also predicts the correct flow quantities in all directions. It was shown in Sections 4.2.1 and 4.2.2, that there are certain errors involved in making these predictions. It is, therefore, necessary to establish an acceptable level of error for the approximation of a complex discontinuity network by a continuum model.

5.3 Parametric studies of discontinuity characteristics

As most of the parametric studies shown in Chapter 4 were carried out on the basis of a single realisation of a discontinuity mesh, it was necessary to perform a Monte Carlo analysis in order to provide substantiation for the results obtained in those studies. As expected the results of the Monte Carlo simulation have shown that permeability can vary signigicantly from one realisation to another, however, as the number of tests increases the frequency distribution of permeability tends to follow a normal distribution. This same effect was observed for the principal permeabilities, principal directions and also the flow relative errors. Confidence limits can then be established from which estimates of the precision of a random single measurement of permeability can be made. From the two sets of Monte Carlo simulation performed it can be inferred that the variability of the permeability is less when the discontinuity aperture is constant throughout the mesh. This effect was measured by comparing the coefficient of variation obtained from each set of simulations.

A series of tests in which the mean discontinuity trace length were systematically increased showed that the relative error between the expected and observed flows decreased exponentially as the node index increased. Therefore, the validity of the continuum approximation cannot be defined by a clear cut boundary but rather by a bandwith, the width of which depends upon the acceptable amount of error. P_1 and P_2 are the lower and upper bounds of the acceptable amount of error and should be established according to the required degree of precision. Fig. 5.1 illustrates this point. The wider the transition zone in Fig. 5.1 the better the continuum approximation becomes. This is because, P, the acceptable error, tends to decrease exponentially as the connectivity of the mesh increases. It was also found that both of the connectivity indices are dependant upon the geometric properties of the discontinuity mesh. The relations between the trace length to the sample size ratio, $\bar{\ell}/L$, and the connectivity indices are not linear, but are best described by a cubic polynomial function. As the density of the meshes increases the curves become steeper. As it was shown in Fig. 4.22, the same connectivity index can be obtained by three different combinations of density and $\bar{\ell}/L$ ratios. This implies that the use of discontinuity frequency solely as an index to measure permeability can sometimes be misleading and also high-lights the importance of the trace length parameter in determining permeability.

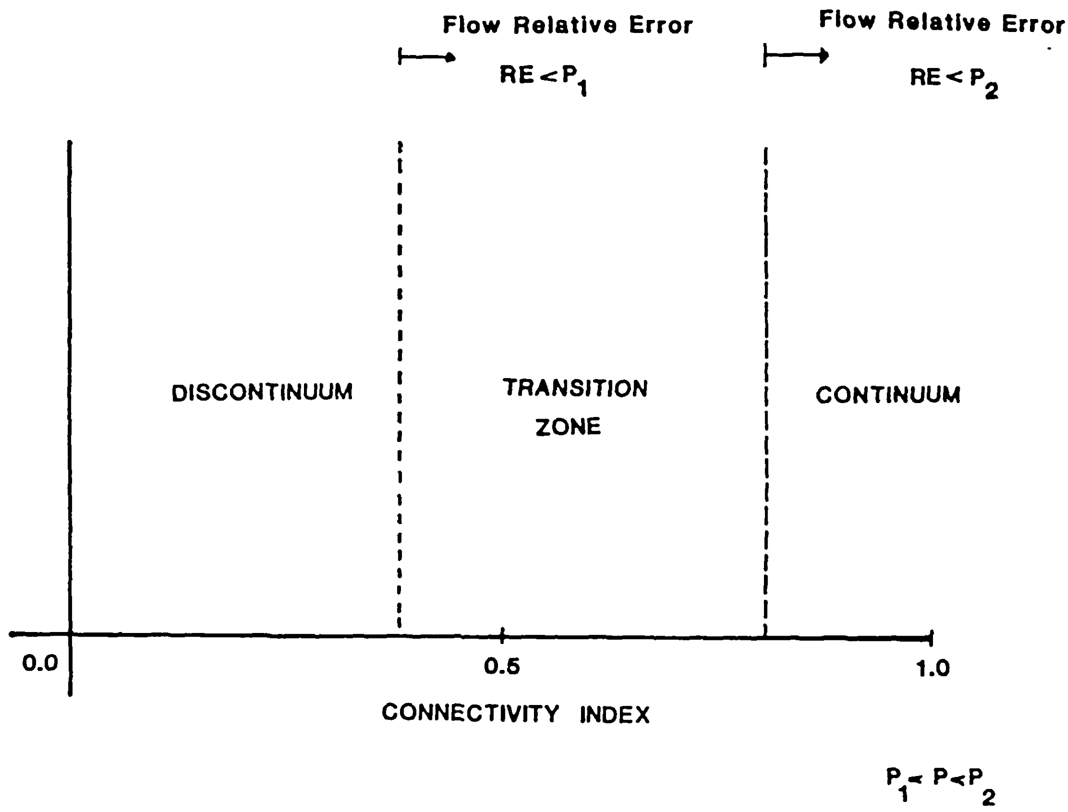

Fig. 5.1 The validity of the continuum approximation

Another series of discontinuity meshes was studied to determine the effect of discontinuity aperture on permeability. In the first set of runs, the aperture was constant within each mesh, with four different apertures being tested. As expected, it was found that the permeability tensor is proportional to the cube of the aperture. In this set of runs the change in the connectivity index was only due to the increase in mean trace length since the density and orientation parameters remained constant. However, the relationship between the connectivity index and the ratio $\overline{\ell}/L$ remained the same as in the previous set of runs, and again followed a cubic polynomial function. In the second set of runs the discontinuity aperture was allowed to vary from discontinuity to discontinuity according to a log-normal distribution. The standard deviation of this aperture distribution was varied systematically and represented by the coefficient of variation. It was found firstly, that the permeability tensor is approximately proportional to the cube of the aperture but is slightly underestimated by up to 3 percent. Secondly as the variability of the aperture was increased, up to a coefficient of variation of 20 percent, the diagonal terms of the permeability tensor increased by only 2 percent, while the off diagonal terms increased by 85 percent. For larger coefficient of variation (up to about 100 percent) the diagonal terms increased by up to 65 percent. The effect of large coefficient of variation of aperture on the off diagonal terms was also significant; e.g. for a 100 percent coefficient of variation the off diagonal terms increased by about 15 orders of magnitude. The above phenomenon was first noticed by Parsons (1966), although he varied the conductance of the discontinuity segments rather than the apertures.

The effects on permeability caused by changes in the relative orientations of the discontinuity sets was studied using a series of tests in which two orthogonal sets were analysed. The mean trace length and the standard deviation of the angle of orientation for each discontinuity set were systematically increased. It was found that an increment in the coefficient of variation of orientation of up to 30 percent had a greater effect on connectivity and permeability if the scale ratio $\bar{\ell}/L$ was less than 0.6. As this ratio increased (i.e. for larger values of mean trace length) the above effect was reduced considerably. This is because the mesh started to behave more like an isotropic continuous medium. For larger coefficients of variations the effect on connectivity and permeability becomes almost negligible. This is because the mesh behaviour was closer to the isotropic behaviour.

An attempt to define the representative elementary volume (area) was carried out. A series of tests, in which the test area was gradually reduced in size was performed. It was found that the discontinuity density, connectivity indices and the ratio $\bar{\ell}/L$ experienced some variability when the side length of the test area was less than 20 m (i.e. $\bar{\ell}/L = 5.5$). Above this value they remained approximately constant. The permeability tensor became symmetric when the side length of the test area was greater than 10 m (i.e. $\bar{\ell}/L = 3.0$). This, however, does not imply that the permeability tensor remained constant as the test area was allowed to increase in size. It was only when the side length of the test area exceeded 60 m (i.e. $\bar{\ell}/L = 16.5$) that the variability in the permeability tensor became almost negligible. The relative errors in predicting flow were calculated for all of the symmetric permeability tensors. It was found that, although the oscillation did not always decrease, the general trend was that the relative error decreased as the test area increased. It is suggested that in order to define the REV, one should first establish an acceptance level in the flow relative error which can be taken as the upper limit of REV. The lower limit can be defined as the size of test area for which the permeability ceases to change significantly. Fig. 5.2 illustrates this point. The narrower the zone between the lower and upper limits the better the continuum behaviour of the network with regard to permeability.

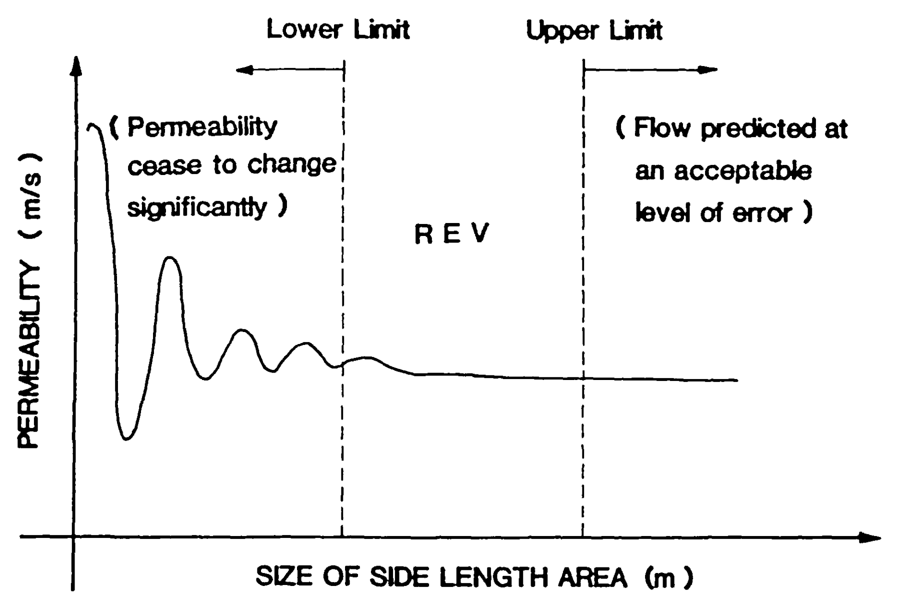

Fig. 5.2 The determination of the representative elementary volume (area)

For example, in the mesh shown in Fig. 4.34, if changes of 10 percent in measuring permeability are considered to be acceptable, and an acceptable level of error in predicting flow is 20 percent, then the lower and upper limits for the representative elementary volume are 45 m and 55 m respectively.

The anisotropy of permeability was studied by rotating the test area. The resulting polar diagrams of $1/\sqrt{K}$ were elliptical in shape. These plots were then compared with the associated discontinuity frequency rosettes. It was found that the direction of maximum discontinuity frequency approximately coincided with the direction of minor principal permeability, and that the direction of minimum discontinuity frequency approximately coincided with the direction of major principal permeability. Therefore, by observing the discontinuity frequency rosette of a given mesh it is possible to infer, approximately, the degree of anisotropy in permeability and also the orientations of the principal directions. Some caution should, however, be exercised when doing this, since discontinuity frequency, when used solely, can produce misleading results when predicting permeability; as was discussed earlier in this section.

5.4 Applications of the model to practical problems

An aim of this research was to determine an equivalent continuum permeability tensor which would represent the anisotropic flow properties of a discontinuity mesh. This approach is supported by the assumption that as the number of conducting discontinuities in a given volume of rock increases, their individual contributions to flow will tend to average out until the mass behaves like an anisotropic porous medium. The resulting equivalent permeability tensor can then be used to analyse problems with relatively complex boundary conditions, involving the iterative solution of a phreatic surface, by using more elaborate numerical techniques such as the boundary or finite element methods. There are, however, some cases when it is not possible to define an equivalent continuum, as has been shown in Chapter 4. Models such as the one proposed here provide a solution for such cases.

Two applications have been presented in this work. The first involved the analysis of water flow into circular tunnels of different diameters. The second provided a case-study which involved the collection of discontinuity data from boreholes and rock exposures, followed by the assessment of local groundwater conditions to obtain predictions of water inflow at the tunnel face.

The application of a two-dimensional model to typical three dimensional problems is, in many cases, not appropriate. This is because fractures which are not connected in the plane of a two-dimensional analysis may be connected in some other part of the rock mass. It is expected, therefore, that permeability will, in many times, be underestimated and the hydraulic behaviour appear to be less like a continuum in a two-dimensional analysis than in a three-dimensional analysis.

The basic objective of a radioactive waste repository is to achieve isolation of radionuclides from the biosphere. It is essential that the evaluation of the groundwater conditions of the area surrounding such a repository is satisfactorily carried out, so that the extent of any possible radionuclide migration can be investigated. If repository sites are to be located in hard crystalline rock masses, it is expected that the discontinuity network present in the rock mass will dictate hydrological behaviour. This is, however, only one of the mechanism influencing the groundwater flow behaviour; other mechanisms include thermal, mechanical and chemical effects. The study of these effects necessarily requires treatment of many complex coupled processes which would have to be based on the use of numerical simulation models. The application of the model, presented in this work, to radioactive waste repository assessment is indicated by the fundamental studies that were carried out and presented in Chapter 4. A site assessment of a repository by means of the statistical model presented here will consist of; first the determination of the discontinuity characteristics of the rock mass surrounding the repository area, this can be carried out by sampling rock exposures, both by linear sampling, using scanlines, and by areal sampling, using photographs, as described in Section 3.1.2. Additional geotechnical data can be obtained from boreholes drilled in the area of the repository. Mass permeability can be obtained from borehole packer tests and the mean effective discontinuity aperture also estimated for each of the discontinuity sets, as described in Appendix 8. In the case of a radioactive waste repository, however, extensive drilling may not be permissible due to problems with sealing the drill holes. The hydraulic boundary conditions can be determined from piezometric readings monitored in boreholes within the zone under study. Validation runs can be carried out and the permeability tensors obtained can be compared with those obtained from borehole packet tests. The equivalent permeability tensor of the overall area of study can then be estimated in a vertical plane. This model could be large and could certainly extend to the surface in order to see if it is possible to define the representative elementary volume. If the latter is possible then continuum models can be used in order to handle relatively complex flow systems involving the iterative solution of phreatic surface. Locally, in the near field region, the proposed model can be used in order to model the possible occurrence of individual highly conductive discontinuities so that the total fluid flow into or out the repository can be estimated. Although the fluid flow through the discontinuity network, as calculated by this model, is only due to piezometric gradients, the result of these type of studies are necessary and need to be well understood if more complex analyses of groundwater flow under the influence of a repository are to be considered.

Summarizing, the existing groundwater flow system arround a repository will inevitably be disturbed during the process of construction. The near field groundwater flow system, particularly after deposition of the radioactive waste, will be more disturbed than the far field because of the complex mechanical, thermal and chemical coupled processes that take place during the initial part of the repository life.

Models such as the equivalent continuum representation will be appropriate for regional groundwater flow in the far field. For this purpose, studies on the representative elementary volume presented in Section 4.2.5, are of great help in determining the minimum volume of rock for which the continuum approximation is valid. In the near field region, where it may not be possible to define an equivalent continuum, models such as the one proposed here can be used as a starting point in the investigation of this very complex problem. The complete model, however, should include factors such as field stresses, thermal effects and chemical effects. Although the effects of normal loads on the permeability of laboratory specimens is well understood, extrapolation of these tests to field conditions has not yet been achieved. In the case of high level radioactive waste, thermal effects, which not only create convection currents but also introduce changes in the rock mass properties, have been satisfactorily modelled for porous media; the effect of temperature on fracture permeability, however, has not been studied in sufficient detail. The high temperatures associated with high level waste can also induce vaporisation of the groundwater around the repository, leading to gas in the rock fractures. Analysis of this condition will necessitate the study of two-phase flow within the fractures. Although the study of the dispersion of contaminants in porous media has been extensively studied (Bear, 1972), the study of dispersion of contaminants in fractured rock has only recently been undertaken (Cundall, 1983 and Robinson, 1983). Further research on this and also absorbtion and adsorption is required.

CHAPTER 6 CONCLUSIONS AND RECOMMENDATIONS

6.1 Conclusions

(1) The complexity of a rock mass system is best approached from a statistical and probabilistic point of view since the exact properties of a given discontinuity geometry cannot be determined without destroying the very features that are being measured.

(2) The study of fluid flow through fractured rock masses must be based upon a representative sample of the relevant discontinuity characteristics, coupled with some form of idealised model of discontinuity geometry and fluid flow. Simplifying assumptions must be made concerning the nature of discontinuity geometry. These arise from limitations that are inherent in the numerical techniques and in the computer core available.

(3) Scanline and areal sampling techniques offer suitable methods for the determination of input parameters for the statistical model proposed.

(4) The proposed model, based upon a bi-factorisation solution routine, can be used to determine flow quantities and the equivalent permeability tensor of any random, two-dimensional network comprising up to 5000 discontinuities.

(5) A numerical validation of the model, carried out against an idealized extensive discontinuity mesh, indicated that the solutions obtained for flow quantities and permeability tensor were free of numerical error.

(6) The geometrical validation of the model was not complete; this was due to the fact that the spatial distribution of discontinuity centres on the sampled rock faces may not have resulted from a truly random process. For highly fractured rock exposures, however, a relation between discontinuity frequency, trace length and density has been proposed and validated with data from field measurements.

(7) Different random realisations based upon the same fundamental discontinuity data indicated that random effects can produce considerable variability in the equivalent permeability tensor for the network. The permeability values tended to conform with the normal distribution, which means that confidence limits can be established by applying the central limit theorem.

(8) The variability in the permeability tensor was partly caused by variability in the degree of inter-connectivity within the network and partly by the variability in discontinuity aperture. When the aperture was held constant the variability in the permeability tensor decreased substantially.

(9) The connectivity of a discontinuity network depends upon the trace length distribution, orientation distribution and areal density. Two indices of connectivity have been proposed. Firstly, the discontinuity index (I_D), defined as the ratio between the number of inter-connected discontinuities to the total number of discontinuities in the test area. Secondly, the node index (I_N), defined as the ratio between the number of inter-connected nodes to the total number of nodes in the test area. Both indices are strongly correlated by a power function and hence are both valid measures of inter-connectivity.

(10) A series of parametric studies carried out in order to determine those discontinuity characteristics that are crucial in controlling permeability gave the following results.

i. A series of tests in which discontinuity trace length and the density were increased systematically indicated that the relative error between the expected and observed flow across the boundaries decreased exponentially as the node index increased.

ii. For given values of discontinuity aperture, orientation and density, the connectivity, and hence the permeability, of the mesh increased as the trace length increased. This increase was not, however, linear but was best described by a cubic polynomial. Trace length is, therefore, a critical parameter in determining permeability.

iii. It was shown that the same connectivity index can be obtained from more than one combination of density and trace length. As discontinuity frequency is proportional to both of these parameters, it is tempting to use discontinuity frequency as an indicator of permeability. It was shown, however, that this can produce erroneous results.

iv. For a random mesh with constant aperture it was found that the permeability tensor is proportional to the cube of the aperture.

v. For a random mesh, with apertures varying according to a log-normal distribution, it was found that, although the permeability tensor remained approximately proportional to the cube of the aperture, the actual values of the permeability tensor terms changed as the variability in the aperture increased. Although these changes were more substantial in the off diagonal terms of the tensor, the overall effect ultimately depended upon the anisotropy of the discontinuity mesh.

vi. Changes in the relative orientation of the discontinuity sets in a mesh had a greater influence on permeability when the coefficient of variation was less than 30 percent and the ratio $\bar{\ell}/L$ was less than 0.6. As these two factors were increased, the effect on permeability became almost negligible because the mesh started to behave as an isotropic continuum.

vii. In all the parameter studies, as expected, the permeability tensor was symmetric. There is not, however, a single precise value of connectivity index above which it is possible to define a valid equivalent permeability tensor. It is first necessary to define an acceptable level of error in the flow quantity predictions before considering the validity of the continuum approximation.

(11) The analysis of the representative elementary volume indicated that it is possible to study how the permeability tensor, and also some characteristics of the mesh, change as the size of the test area is increased. Although the results obtained only apply for the particular meshes studied, important conclusions can be drawn from this type of study, particularly for the assessment of groundwater flow models.

(12) Studies on directional permeability showed that some indication of the anisotropy of permeability of a given discontinuity mesh can be obtained by analysing the discontinuity frequency rosette, in particular it is possible to infer the orientations of the principal directions of permeability. No quantitive estimate of the principal permeabilities themselves can be made, however, without analysing the distribution of hydraulic potentials within the discontinuity mesh.

(13) A practical application of the model, which involved the analysis of the flow into circular tunnels of different diameters indicated that although total flow quantities increased with tunnel diameter, flow variability - as measured by the coefficient of variation - decreased. In general the total flow into a given excavation increases in direct proportion to the number of inter-connected discontinuities intersecting its perimeter.

(14) A case study based upon a 2.8 m diameter tunnel excavated through a water bearing fractured rock mass illustrated the practical application of the model. This case study involved the collection of discontinuity data from rock exposures, the analysis of borehole measurements and the assessment of local groundwater conditions, to obtain predictions of likely water inflow quantities in the unlined section near the tunnel face. Although the predicted inflows were within the general range of the observed values, the case study underlined the difficulties of attempting to represent a three-dimensional structure by a two-dimensional model.

(15) The application of the model to the design of intermediate level radioactive waste repositories was discussed. This involved firstly an explanation of how the discontinuity data collection techniques and the associated data processing methods, developed specifically for the model, could be applied to rocks at the repository site. This was followed by a discussion of the applications and limitations of the flow model to the analysis of fluid migration in the near and far fields.

6.2 Recommendations

(1) Although the scanline technique together with photographic sampling methods are well suited to collecting discontinuity data for the statistically-based model proposed in this work, there is no reason why these two methods, used in conjunction, cannot provide suitable input data for other geotechnical applications, such as underground excavation design, support design and rock mass classification schemes aimed at assessing rock mass strength.

(2) There is no such thing as a truly homogenous geological medium. In order to provide a tractable analysis of flow, however, a basic assumption made in this work was that the discontinuity centres obeyed a statistically homogenous, two-dimensional Poisson process. It is suggested that the introduction of geostatistical techniques, such as those of la Pointe (1980), Miller (1979), to account for the spatial variation of discontinuity characteristics, could increase the validity of the model.

(3) The model could be improved further by introducing the effects of fracture surface roughness, and non-linear flow. In the current model, the conductivity of an individual discontinuity segment is calculated assuming that the discontinuity planes are smooth, planar and parallel. This assumption can easily be modified by adopting empirical flow laws, Louis (1969), which account for surface roughness and non-linear flow. However, depending upon the type of flow law adopted, it may be necessary to solve a system

of non-linear equations. This would involve a considerable increase in the computational complexity, and cost, of a given solution. The dispersion of contaminants and tracers in the discontinuity network could also be included. Cundall (1983), Robinson (1983), and Krizek et al (1972) have suggested ways of approaching this problem.

(4) An important upgrading in this type of modelling can be achieved by introducing the influence of the state of stress on flow and permeability. Although there is enough evidence from laboratory experiments, Iwai (1976), Sharp (1970), and Jouanna (1972) to show that fracture permeability is a function of the stress acting normal to the fracture plane, there has been little attention to the effects on fracture permeability of shear stress and shear displacement. Furthermore, problems of determining the scaling factors required to correlate laboratory tests with field conditions still remain unsolved. Bawden et al (1980), Gale (1975), and Iwai (1979) have studied the coupling of fracture flow and fracture deformation. Their approach basically consisted of coupling Goodman's Joint element (Goodman, 1976) with Wilson's linear flow element (Wilson 1970). Vargas (1982) extended Cundall's rigid block element (Cundall, 1971) to take account of the deformability of the blocks, and subsequently coupled both types of block models with finite element routines that simulated flow through the fractures. The theory and techniques used in the above studies were developed for discrete discontinuity models only. The incorporation of these coupled

methods into statistical discontinuity models should be pursued in the future, despite the fact that some limitations are envisaged concerning the sizes of problems that can be accommodated in the core memory of current computers.

(5) Finally, extension of the model to three dimensions is an important upgrading that should be pursued. This is because a two-dimensional model cannot take into account the flow through those discontinuities that are not connected in the plane of a two-dimensional analysis, but that may be connected in some other part of the rock mass. This implies that permeability will be underestimated by the two-dimensional analysis. Further assumptions are necessary in order to develop the three-dimensional model; these include assumptions about the shape and orientation of the discontinuity planes. Baecher (1978), Barton (1978) and Bridges (1975) have presented evidence to suggest that discontinuities may be equidimensional in shape, so that they can be modelled by a disc. The radii of the discs can be assumed to be distributed log-normally. As with the two-dimensional model the discontinuity centres can be assumed to be located randomly in space. Discontinuity orientations in the three-dimensional model can vary in two directions. Distributions such as Arnold's spherical normal distribution (Mahtab et al, 1972) or Bingham's distribution (Mahtab and Yegulalp, 1982) can be used to generate the orientations. The complete three-dimensional model can be constructed by generating randomly orientated discs with distributed radii, orientations and apertures within a generating

volume such as a cube. The intersection of these discs will form the connecting network. The intersection of two discontinuity planes will be a line segment. Flow will take place through a discontinuity disc if this is intersected by at least two other conducting discontinuities. Most of the connectivity analysis of the three-dimensional model can be carried out by extending the routines developed for the two dimensional model. The geometry of each discontinuity plane can be described by the equation of a disc; while its intersections with other discontinuities can be represented by the end coordinates of the line segment.

The flow solution in the three-dimensional model is the central problem of the proposed extension. Long (1983) when dealing with this problem suggested a combination of numerical and analytical solutions. She proposed to model the flow through the discontinuity planes by image theory, i.e. the total flow into or out of a discontinuity intersection is assumed to be approximately equal to the flow predicted with a source of constant strength per unit length. By assuming that hydraulic potential is the same along the discontinuity intersections, she then presented a set of equations for the average potential at each of the intersections in terms of the total flow into or out of each of the intersections. When inverted this set of equations produces an equation for the total flow into or out of each intersection in terms of the average potential at each of the intersections. Finally mass balance equations can be written by equating the flow through the associated intersections.

Solution of these equations gives the average potentials for each intersection. Knowing the potentials, the flow through each intersection can be calculated using the analytical solutions for each fracture. Flow through the boundaries can then be calculated and the permeability tensor found by rotating the test cube over a half-sphere.

The main drawback of the solution presented by Long (1983) is that there is no evidence to suggest that the hydraulic potential along the intersection segments of the discontinuity planes is constant. Indeed, this cannot be true when two or more intersection segments cross each other in a discontinuity plane. A complete numerical method of solution is necessary to account for the variable potential along the intersection segments and the complexity of the two-dimensional flow along the discontinuity planes.

It is suggested that a finite element mesh should be used to discretize each inter-connected discontinuity plane. Ideally the finite element mesh should be automatically generated, this can, however, prove to be a difficult task to accomplish. In groundwater hydrology, finite element theory has been employed by Jerandel and Witherspoon (1968), and also Zienkiewicz et al (1966) who described the use of triangular finite element theory in porous media flow. Noorishad et al (1971) and Wilson (1970) also used a triangular finite element in calculating flow through discrete fractured two-dimensional models. The techniques developed by the above researchers could serve as a basis for solving the flow through the proposed three-dimensional statistical model. It is envisaged, however, that a main frame computer, with large amount of memory and high computation speeds will be required if a statistically representative problem is to be solved.

CHAPTER 7 REFERENCES

Asfari, A. and Witherspoon, P.A. (1973) Numerical simulation of naturally fractured reservoirs. Society of Petroleum Engineers of AIME (SPE 4290), 5p.

Baca, R.G., R.C. Arnett, and I.P. King (1981) Numerical modelling of flow and transport processes in a fractured-porous rock system. Proceedings of the 22nd U.S. Symposium on Rock Mechanics, American Institute of Mining Engineers, p. 67-72.

Baecher, G.B., N.A. Lanney, and H.E. Einstein (1977) Statistical descriptions of rock properties and sampling. Proceedings of the 18th U.S. Symposium on Rock Mechanics, American Institute of Mining Engineers, p. 5C1-8.

Baecher, G.B. and N.A. Lanney (1978) Trace length biases in joint surveys. Proceedings of the 19th U.S. Symposium on Rock Mechanics, American Institute of Mining Engineers, p. 56-65.

Baecher, G.B. (1980) Progressively censored sampling of rock joint traces. Mathematical Geology 12(1), p. 33-40.

Backhouse, R.C. and B.A. Carre (1975) Regular algebra applied to path-finding problems. J. Inst. Maths. Applics. 15, p. 161-186.

Barton, C.H. (1977) A geotechnical analysis of New South Wales. CSIRO Aust., Div. of Applied Geomechanics Technical Paper No. 24, 30p.

Barton, C.M. (1978) Analysis of joint traces. Proceedings of the 19th U.S. Symposium on Rock Mechanics, American Instutite of Mining Engineers, p. 38-42.

Bawden, W.F., J.H. Curran, and J.C. Roegiers (1980) Influence of fracture deformation on secondary permeability - A numerical approach. Int. J. Rock Mech. Min. Sci. and Geomech. Abstr., 17, p. 265-279.

Bear, J. (1972) Dynamics of Fluids in Porous Media. Elsevier, New York.

Benjamin, J. and C.A. Cornell (1970) Probability Statistics and Decisions for Civil Engineers. McGraw-Hill, New York, N.Y.

Bertrand, L. et. al. (1982) Essai de determination de la distribution Regionale du tenseur de permebilité du 'Milieu Poreux Equivalent', Department Genie Geologigue, BRGM, No. 45. Orléans.

Bianchi, L. and D.T. Snow (1968) Permeability of Crystalline Rock Interpreted from Measured Orientations and Apertures of Fractures. Annals of Arid Zone, 8(2), p. 231-245

Boodt, P.I., T. Maini, and E.T. Brown (1982) Three dimensional water pressure testing of fractured rock. Proceedings of the 1st Int. Mine Water Association Congress, Budapest, p. 165-183

Brace, W.F., J.B. Walsh, and T. Frangos (1968) Permeability of Granite under high pressure, Journal of Geophysical Research, Vo. 73, No. 6, p. 2225-2236.

Bray, J.W. (1980) Unpublished Notes, Rock Mechanics Section, Imperial College.

Bray, J.W. (1983) Personal communication, Rock Mechanics Section, Imperial College.

Bridges, M.C. (1975) Presentation of Fracture Data for Rock Mechanics. 2nd Australian-New Zealand Conf. on Geomechanics, Brisbane, Publication 75(4), p. 144-148.

British Regional Geology - South Wales (1970) Natural Environment Research Council - IGS. Her Majesty's stationery office London, 152p.

Broadbent, C.D. and G.E. Rippere (1970) Fracture Studies at the Kimbley Pit. S. Afr. Inst. Min. Met., Sym. Planning Open Pit Mines, Johannesburg, p. 171-179.

Buslenko, N.P. (1967) The Monte Carlo Method, the Method of Statistical Trials, Pergamon Press, 2nd Ed.

Caldwell, J.A. (1972) The theoretical determination of the permeability tensor for jointed rock. Processings, Symposium on Percolation Through Fissured Rock, Stuttgart, International Society for Rock Mechanics and International Association of Engineering Geology, p. T1C:1-6.

Call, R.D., J.P. Savely, and P.A. Nicholas (1976) Estimation of Joint Set Characteristics from Surface Mapping. Proc. 17th U.S. Symp. on Rock Mechanics, Utah, p. 2B2-1 to 2B2-9.

Carlsson, A. and T.Olsson (1983) Rock stress influence on water flow in fracturers. 5th Congress of the ISRM, Melbourne, Vol. F, p. 31-34.

Carman, R.C. (1937) Fluid flow through a granular bed. Transactions, Institute of Chemical Engineering, London, 15, p. 150-156.

Castillo, E. (1972) Mathematical model for two-dimensional percolation through fissured rock. Proceedings, Symposium on Percolation through Fissured Rock, Stuttgart, International Society for Rock Mechanics and International Association of Engineering Geology, p. T1D:1-7.

Chatfield, C. (1978) Statistics for Technology, Chapman and Hall, London, 2 Ed.

Childs, E.C. (1957a) The anisotropic hydraulic conductivity of soil, Journal of Soil Science, 8(1), p. 42-47.

Childs, E.C. et al (1957b) Permeability measurements in the field as an assessment of anisotropy and structure development. Journal of Soil Science, Vol. 8, No. 1. (1957), p. 27-41.

Collins, R.E. (1961) Flow of Fluids Through Porous Materials, Reinhold Publishing Corporation, New York, N.Y., 275p.

Cornet, F.H. (1978) Application de la fracture hydraulique à la mesure in situ des contraintes, Colloques Scientifiques 'J. Goguel' - BRGM.Memoire No. 91, p. 173-185.

Crandall, S.H. (1956) Engineering Analysis - A survey of Numerical Procedures, McGraw-Hill, London, 417p.

Crawford, P.B. and R.E. Collins (1954) Estimating effect of vertical fractures on secondary recovery. Transactions, American Institute of Mining Engineers, 201, p. 192.

Crawford, P.B. and B.L. Landrum (1957) Effect of unsymmetrical vertical fractures on production capacity, Trans AIME, V. 204, p. 251.

Cruden, D.M. (1977) Describing the size of Discontinuities, Int. J. Rock Mechn. Min. Sci. and Geomech. Abstr., 14, p. 133-137.

Cundall, P.A. (1983) Numerical modelling of water flow in rock masses. Report DOE/RQ/83.59, England.

Cundall, P.A. (1971) The measurement and analysis of accelerations in rock slopes, PhD dissertation Imperial College.

Da Silveira, A.F. et al (1966) Quantative Characterization of the Geometric Parameters of Jointing in Rock Masses. 1st Congress ISRM, Lisbon, 1966, Vol. 1, p. 225-230.

Davis, S.N. (1969) Porosity and permeability of natural materials. In Flow Through Porous Media, ed. R.J.M. De Weist, Academic Press, New York, N.Y., p. 54-89.

De Wiest (1965) Flow through porous media, Academic Press, London.

Doe, T.R., J.C.S. Long, H.E. Endo, and C.R. Wilson (1982) Approaches to evaluating the permeability and porosity of fractured rock. Proceedings, 23rd Symposium on Rock Mechanics, University of California, Berkeley.

Einstein, H.H. and G.B. Baecher (1982) Probabilistic and Statistical methods in Engineering Geology, I. Problem statement and introduction to Solution, Rock Mechanics, Suppl. 12 (1982), p. 47-61.

Einstein, H.H. and G.B. Baecher (1983) Probabilistic and Statistical methods in Engineering Geology. Specific Methods and Examples, Part I. Exploration Rock Mechanics and Rock Engineering 16, p. 39-72.

Ewan, V.J. West, G. and Temporal, J. (1983) Variation in measuring rock joints for tunnelling. Tunnels and tunnelling, April 1983, p. 15-18.

Fatt, I (1956) The network model of porous media, I, II, and III. Transactions, American Institute of Mining Engineers, 207, p. 144-181.

Feuga, B. (1983) Characterization du Milieu Poreux Equivalent à un Milieu Rocheux fracturé par essais a l'eau in situ. Bull. of Int. Assoc. of Engineering Geology, No. 26-27, p. 403-410.

Fisher, R.A. (1953) Dispersion on a sphere. Proceedings in the Royal Society of London, Series A, 217, p. 295-306.

Freeze, R.A. (1975) A stochastic-conceptual analysis of one-dimensional groundwater flow in nonuniform homogenous media. Water Resources Research, 11(5), p. 725-741.

Friedman, M. (1976) Porosity, permeability, and rock mechanics - A Review. Proceedings of the 17th U.S. Symposium on Rock Mechanics, p. 2A1:1-17.

Gale, J.E., R.L. Taylor, P.A. Witherspoon, and M.S. Ayatollahi (1974) Flow in rocks with deformable fractures. Finite Element Methods in Flow Problems, ed. Oden J.T. et al, UAH Press, Alabama, p. 583-598.

Gale, J.E. (1975) A Numerical Field and Laboratory Study of Flow in Rocks with Deformable Fractures. Ph.D. dissertation, University of California, Berkeley, 255p.

Gale, J.E. (1982a) Assessing the permeability characteristics of Fractured Rock. Geological Society of America, Special Paper 189, p. 163-181.

Gale, J.E. et al (1982b) Hydrogeological characterization of the Stripa Site, OECD/NEA Stripa Workshop, October 1982, 20p.

Gartling, D.K. and R.K. Thomas (1982) A statistically based numerical model for heat conduction in fractured rock masses. Saudia National Laboratories Report No. SAND 82 - 0516J, 38p.

Gaziev, E.G. et al (1979) Investigations of seepage flow in block media as applied to designing structures on rock. Proc. of 4th Congress of ISRM, Montreal, (2), p. 161-166.

George, A. and J.W. Lin (1981) Computer Solution of Large Sparse Positive Definite Systems, Prentice Hall, New Jersey, 324p.

Goodman, R.E. (1976) Methods of Geological Engineering, West Publishing Company.

Gray, W.G. and K. O'Neill (1976) On the general equations for flow in porous media and their reduction to Darcy's law. Water Resources Research, 12(2), p. 148.

Greenkorn, R.A., C.R. Johnson, and L.K. Schallenbarger (1964) Directional permeability of heterogeneous anisotropic porous media. Transactions, American Institute of Mining Engineers, 231, p. 124-132.

Gringarten, A.C. and P.A. Witherspoon (1972) A method of Analysing Pump Test Data From Fractured Aquifers. Processings of the Symposium Int. Society of Rock Mechanics, Percolation Through Fissured Rock, p. T2-C, Stuttgart.

Gringarten, A.C. (1982) Flow-Test Evaluation of fractured reservoirs, Geological Society of America, Special paper 189, p. 237-263.

Grossman, N. (1978) Influéncia das descontinuidades na deformabilidade des Macicas Rochosos. Laboratorio Nacional de Engenharia Civil, Lisbon, Portugal.

Halek, V. and J. Svec (1979) Groundwater Hydraulics, Elsevier Scientific Publishing Company, Oxford 1979, 620p.

Hammersly, J.M. and D.C. Hanscomb (1964) Monte Carlo Methods. Methuen and Co., London, 178 p.

Hoek, E. and E.T. Brown (1980) Underground Excavations in Rock, IMM, London, 527p.

Hoek, E. and J.W. Bray (1977) Rock Slope Engineering, IMM, London, 2nd Ed., 402p.

Harr, M.E. (1977) Mechanics of particulate Media, A probabilistic approach, McGraw-Hill, London.

Hubbert, M.K. (1940) The theory of groundwater motion, Part I, Journal of Geology, 48(8), p. 785-944.

Hubbert, M.K. (1956) Darcy's law and the field equations of the flow of underground fluids. Petroleum Transactions, American Institute of Mining Engineers, 207, p. 222-239.

Hudson, J.A. and S.D. Priest (1979) Discontinuities and rock mass geometry. Int. J. Rock Mech. Min. Sci. and Geomech. Abstr., 16, p. 339-362.

Hudson J.A. and P.R. La Pointe (1980) Printed Circuits for Studying Rock Mass Permeability. Int. J. Rock Mech. Min. Sci. and Geomech. Abstr., 17, p. 297-301.

Hudson, J.A. and S.D. Priest (1983) Discontinuity frequency in rock masses. Int. J. Rock Mech. Min. Sci. and Geomech. Abstr., 20, p. 73-89.

Huitt, J.L. (1956) Fluid flow in simulated fractures. American Institute of Chemical Engineers Journal, 2, P. 259-264.

International Society for Rock Mechanics (1981) Rock Characterization Testing and Monitoring, ISRM Suggested Methods, Ed. E.T. Brown Pergamon Press, London, 211p.

Irmay, S. (1955) Flow of liquids through cracked media. Bulletin of the Resources Council, Israel, Jerusalem, 5A(1), p. 84.

Irmay, S. (1968) On the theoretical derivation of Darcy and Forschheimer formulas. Transactions, American Geophysical Union, 39, p. 702-707.

Iwai, K. (1976) Fundamental Studies of Fluid Flow through a Single Fracture. Ph.D. dissertation, University of California, Berkeley, 208p.

Jeffreys, H. (1931) Cartesian Tensors, Cambridge University Press, Cambridge, 92p.

Jevandel, I. and P.A. Witherspoon (1968) Application of the finite element method to transient flow in porous media, Soc. Pet. Eng. Journal (8) no. 3 p. 241.

Jouanna, P. (1972) Effet des Sollicitations Mecaniques sur les Ecoulements dans Certains Milieux Fissures, Docteur ES - Sciences Physiques These, U. de Toulouse, France.

Kennedy, J.B. and A.H. Neville (1978) Basic Statistical Methods for Engineers and Scientists, 2nd Ed., Harper International Edition.

Kiraly, L. (1969) Statistical Analysis of Fractures (orientation and density) Geologische Rundschau, 1969, V.59, No. 1, p. 125-151.

Kiraly, L. (1971) Groundwater flow in heterogeneous, anisotropic, fractured media: A simple two-dimensional electric analog, Journal of Hydrology, 12, p. 255-261.

Knoring, L.D. (1970) Correlation on joint trends with the elements of techtonic structures. Topics in Mathematical Geology, ed. M.A. Romanova, consultants Bureau, 1970, Publ. New York-London, p. 43-62.

Koch, G.S. and R.F. Link (1971) Statistical analysis of geological data Vol. 2 . John Wiley & Sons, New York, 438p.

Kovacs, G. (1981) Seepage Hydraulics, Elsevier Scientific Publishing Company, Oxford.

Kozeny, J. (1927) Uber Kajillare leitung des wassers im boden. Sitzungsber, Akad. Wiss. Wien, 136, p. 271-306.

Krapp, L. (1983) Determination of Regional Rock-Mass permeabilities. Bulletin of the international association of Engineering Geology, No. 26-27, Paris p. 443-447.

Krizek, R.J., R.M. Karadi, and E. Socias (1972) Dispersion of a contaminant in fissured rock. IRSM Sym. on percolation through Fissured Rock, Stuttgart, p. T3-C: 1-15.

Krumbein, W.C. and F.A. Graybill (1965) An introduction to statistical models in geology. McGraw-Hill, New York, 475p.

La Pointe, P.A. (1980) Analysis of the Spatial Variation in Rock Mass Properties through Geostatistics, Proceedings of the 21st U.S. Symposium on Rock Mechanics, American Institute of Rock Mechanics, p. 570-580.

Lamb, H. (1932) Hydrodynamics 6th edition, Cambridge University Press, 738p.

Lasslett, G.M. (1982) Censoring and edge effects in areal and line transect sampling of rock joint traces, J. Int. Assoc. for Math. Geology, Vol. 14, No. 2, p. 125-140.

Lomize, G. (1951) "Filtratsiia v treshchinovatykh porpdakh", (Water Flow in Jointed Rock), Gosenergoizdat, Moscow.

Long, J.C.S. (1983) Investigation of equivalent porous medium permeability in networks of discontinuous fractures. Ph.D. thesis, Univ. of California, Berkeley, 277p.

Long, J.C.S., J.S. Remer, C.R. Wilson and P.A. Witherspoon (1982) Porous media equivalents for networks of discontinuous fractures. Water Resources Research, 18(3), p. 645-658.

Louis, C. and Y.N. Maini (1970) Determination of In Situ Hydraulic Parameters in Jointed Rock. Proc. 2nd Cong. Int. Soc. Rock Mech., Belgrade, Vol. 1.

Louis, C. (1969) A study of the Groundwater Flow in Jointed Rock and Its Influence on the Stability of Rock Masses. Imperial College Rock Mechancis Research Report No. 10, 90p.

Louis, C. (1974) Rock Hydraulics, Course-Int. Centre for Mech. Sciences - Udine, Italy. (Reprinted from "Rock Mechanics", 1974, CISM 165, Edited by L. Müller.

Lyell, K.A. (1970) Interpretation of water pressure factors for the use of the slope theory. Proc. Symp. on Theoretical Background to the planning of Open Pit mines with special reference to slope stability, Johannesburg, p. 73-85.

Mahtab, M.A., D.B. Bolstad, J.R. Alldredge, and R.J. Shanley (1972) Analysis of Fractured Orientations for Input to Structural Models of Discontinuous Rock. U.S. Department of the Interior, Bureau of Mines Report, Investigation No. 7669, 76p.

Mahtab, M.A., et al (1973) Analysis of the Geometry of Fractures in San Manuel Copper Mine, Arizona. U.S. Department of the Interior, Bureau of Mines Report, Investigation No. 7715 24p.

Mahtab, M.A. and F.M. Yegulalp (1982) A rejection criterion for definition of clusters in orientation data. Proceedings, 23rd U.S. Symposium on Rock Mechanics, University of California, Berkeley.

Maini, Y.N.T. (1971) In Situ Hydraulic Parameters in Jointed Rock Fluid Measurement and Interpretation. Ph.D. dissertation, Imperial College, London.

Marcus, H. and D.E. Evanson (1961) Directional permeability in anisotropic porous media, Water Resources Center Contribution No. 31, University of California, Berkeley, 105p.

Marcus, H. (1962) The permeability of a sample of an anisotropic porous medium. Journal of Geophysical Research, 67, p. 5215-5225.

McCarter, M.K. Application of Plane Table Photogrammetry to O/P Mapping. Proceedings 17th U.S. Symposium on Rock Mechancis, p. 93-98.

McMahon, B.K. (1974) Design of Rock Slopes against Sliding on Pre-existing Fractures. Proc. 3rd Congress of the ISRM, Denver Vol. IIB p. 803-808.

Merrit, A.H. and G.B. Baecher (1981) Site Characterization in Rock Engineering. Proceedings, 22nd U.S. Symposium on Rock Mechanics, Massachusetts, p. 47-53.

Miller, S.M. (1979) Geostatistical Analysis for Evaluating Spatial Dependence in Fracture Set Characteristics. 16th Apcom Symposium, p. 537-545.

Mundry, E. On the Resolution of Mixed Frequency Distributions into Normal Components. J. Int. Assoc. for Math. Geol. (1972) Vol. 4, No. 1, p. 55.

Muskat, M. (1946) The Flow of Homogeneous Fluids through Porous Media. J.W. Edwards Inc., Ann Arbor, Michigan, 763p.

Narasimhan, T.N. (1982a) Numerical Modelling in Hydrogeology, Geological Society of America, Special Paper 189, p. 273-293.

Narasimhan, T.N. (1982b) Physics of Saturated-Unsaturated Subsurface Flow. Geological Society of America, Special Paper 189, p. 3-23.

Neretnieks, I., E.T. Eriksen, and P. Tahtinen (1982) Tracer movement in a single fissure in granitic rock: some experimental results and their interpretation, Water Resources Research 18(4), p. 849-858.

Neretnieks, I. (1983) A note on fracture flow dispersion mechanisms in the ground, Water Resources Research 19(2), p. 364-370.

Newman, S.P. et al (1979) A Statistical Approach to the inverse problem of aquifer hydrology, Part I. theory. Water Resources Research 15(4), p. 845-860.

Newman, S.P. (1982) Statistical characterization of Aquifer Heterogeneities: An Overview. Geological Society of America, Special Paper 189, p. 81-102.

Noorishad, J., P.A. Witherspoon, and T.L. Brekke (1971) A Method For Coupled Stress and Flow Analysis of Fractured Rock Masses, Geotech. Engr. Pub. No. 71-6, University of California, Berkeley.

Noyer, M.L. (1980) Calcul des directions principales et des coefficients d'anisotropie de permeabilite d'un milieu poreux equivalent a un milieu rocheux fracturé. Le programme tenseur, Note technique No. 13 BRGM, Sept. 1980, 10P.

Ollos, G. (1963) Examen hydraulique de l'ecoulement dans des roches crevassees sur des modeles reduits. Bulletin of International Association of Scientific Hydrology, 8(2) p.9.

Pahl, PJ. (1981) Estimating the Mean Length of Discontinuity Traces. Int. J. Rock. Mech. Min. Sci. and Geomech. Abstr. 18, p.221-228.

Parsons, R.W. (1966) Permeability of idealized fractured rock. Society of Petroleum Engineering Journal, 10, p. 126-136.

Parsons, M.L. (1972) Determination of Hydrogeological Properties of Fissured Rocks, Proc. 24th Geological Congress, Montreal, Canada, Section II, Hydrogeology, p. 89-99.

Piteau, D.R. (1973) Characterizing and Extrapolating Rock properties in Engineering Practice. Rock Mechanics, (Springer-Verlag), Suppl. 2, p.5-21.

Piteau, D.R. (1970) Geological Factors Significant to the Stability of Slopes Cut in Rock. Proc. Symp. on the Theoretical Background to the Planning of Open Pit Mines with Special Reference to Slope Stability, Johannesburg, p. 33-53.

Piteau, D.R. and L. Russell (1971) Cumulative Sums Technique: A New Approach to Analyzing Joints in Rock. Proceedings 13th U.S. Symposium on Rock Mechanics.

Polubarinova-Kochina, P.YA. (1962) Teoriya dvizheniya gruntovykh vod. Gosudarstr. Izdat. Tekh. Teoret. Lit. Moscow, 1952. (English translation by R. de Wiest: Theory of ground water movement. Princeton University Press, 1962).

Price, N.J. (1966) Fault and Joint Development in Brittle and Semi-Brittle Rock. Pergamon Press, London.

Priest, S.D. (1983) Hemispherical projection methods in rock mechancis. George Allen & Unwin. (in preparation).

Priest, S.D. and J. Hudson (1976) Discontinuity spacings in rock. International Journal of Rock Mechanics and Mining Science, 13, p. 135-148.

Priest, S.D. and J. Hudson (1981) Estimation of discontinuity spacing and trace length using scanline surveys. Int. J. Rock Mech. Min. Sci. and Geomech. Abstr., Vol. 18, p. 183-197.

Priest, S.D. and J.A. Samaniego (1982). Properties of discontinuous rock masses. Annual Report, Dept. of Min. Res. Eng., Imperial College.

Priest, S.D., J.A. Samaniego, J.M. Harrison, J.A. Hudson (1983) The properties of discontinuous rock masses. DOE Report No. DOE/RW/83.064, England.

Priest, S.D. and J.A. Samaniego (1983) A model for the analysis of discontinuity characteristics in two dimensions. 5th International Congress on Rock Mechanics, Melbourne, p. F199-F207.

Priest, S.D. and E.T. Brown (1983) Probabilistic Stability Analysis of variable rock slopes Trans. I.M.M.92. A:1-12.

Rats, M.V. and S.N. Chernyashov (1965) Statistical aspect of the problem on the permeability of jointed rocks. Paper No. 73, Symposium on the Hydrology of Fractured Rocks, Dubrovnik, Yugoslavia, AIHS-UNESCO, p. 227-236.

Rendu, J.M. (1981) An Introduction to Geostatistical methods of Mineral Evaluation, 2nd Edition. S. Afr. Int. of Min. and Met., Johannesburg.

Rissler, P. (1978) Determination of the Water Permeability of Jointed Rock. English Edition of Volume 5, Publication of the Institute for Foundation Engineering Mechanics, Rock Mechanics and Waterways Construction, RWTH University, Aachen, Federal Republic of Germany.

Robertson, A. (1970) The interpretation of geological factors for use in slope stability. Proceedings, Symposium on the Theoretical Background to the Planning of Open Pit Mines with Special Reference to Slope Stability, p. 55-71.

Robinson, P.C. (1981) Connectivity of fracture systems - A percolation theory approach. Report DOE/RW/81.028, London, 23p.

Robinson, P.C. (1982) NAMNET - network flow program, Report AERE - R10510, Harwell, 17p.

Robinson, P.C. (1983) DISPER - Computer program to calculate the transport of contaminants in networks. Report DOE/RW83.088. England, 12p.

Rocha, M. and F. Franciss (1977) Determination of permeability in anisotropic rock masses from integral samples. In Structural and Geotechnical Mechanics, ed. W.J. Hall, Prentice-Hall, New York, N.Y., p. 178-202.

Roegiers, J.C., J.H. Curran, and W.F. Bawden (1978) Numerical Modelling of Flow in Fractured Rock Masses. Report prepared for Energy, Mines and Resources, Canada, Earth Physics Branch, Ottawa, Ontario, 119p.

Romm, E.S. (1966) Flow Phenomena in Fissured Rocks, Moscow, 284p (In Russian).

Romm, E.S. and B.V. Pozinenko (1963) Permeability of anisotropic fractured rock (in Russian), Eng. J. 3(2), p. 381-386.

Sagar, B. and A. Runchal (1982) Permeability of fractured rock: Effect of fracture size and data uncertainties. Water Resources Research, 8 (2), p. 266-274.

Samaniego, J.A. (1981) A statistical model for simulating discontinuities in two dimensions. M.Sc. Thesis, Imperial College, London.

Samaniego, J.A. and S.D. Priest (1984) The prediction of water flows through discontinuity networks into underground excavations. ISRM Symposium, Design and Performance of Underground Excavations, Cambridge.

Scheidegger, A.E. (1954) Directional permeability of porous media to homogeneous fluids. Geofisica pura Applicata, 28, p. 75-90.

Scheidegger, A.E. (1974) The Physics of Flow Through Porous Media (Revised Edition). University of Toronto Press.

Schrauf, T.W. and D.D. Evans (1984) Relationship between the gas conductivity and geometry of a natural fracture. Report NUREG/CR-3680, US Nuclear Regulatory Commission, 131p.

Sen, Z. and A. Kazi (1984) Discontinuity spacing and RQD estimates from finite length scanlines. Int. J. Rock Mech. Min. Sci. and Geomech. Abstr. 21(4), p. 203-212.

Serafim, J.L. and A. del Campo (1965) Interstitial pressures on rock foundations of dams. Journal Soil Mechanics and Foundations Division, ASCE, 91(5), p. 65-85.

Sharp, J.C. (1970) Fluid Flow through Fissured Media. Ph.D. dissertation, Imperial College, London, 181p.

Sharp, J.C. and Y.N.T. Maini (1972) Fundamental Considerations on the Hydraulic Characteristics of Joints in Rock. Proc. Symp. on percolation through fissured rock, Int. Soc. Rock Mech., Stuttgart, p. T1F:1-15.

Smith, L. and R.A. Freeze (1979a) Stochastic analysis of steady state groundwater in a bounded domain, 1: One dimensional simulations. Water Resources Research, 15, (3), p. 521-528.

Smith, L. and R.A. Freeze (1979b) Stochastic analysis of steady groundwater flow in a bounded domain, 2: Two-dimensional simulations. Water Resources Research, 15(6), p. 1543-1559.

Snow, D.T. (1965) A Parallel Plate Model of Fractured Permeable Media. Ph.D. dissertation, University of California, Berkeley, 331p.

Snow, D.T. (1966) Three hold Pressure Test for Anisotropic Foundation Permeability, 1966. Fels. U. Ing. Geol., V.4, p. 298.

Snow, D.T. (1968) Rock Fracture Spacings, Openings and Porosities. J. Soil Mechanics and Foundations Division, American Society of Civil Engineers. (SM1) p. 73-91.

Snow, D.T. (1969) Anisotropic permeability of fractured media. Water Resources Research, 5(6), p. 1273-1289.

Snow, D.T. (1970) The Frequency and Apertures of Fractures in Rock, Int. J. Rock Mech. Min. Sci., 7, p. 23-40.

Steffen, O.K.H., and J.E. Jennings (1974) Definition of Design Joints for 2D Rock Slope Analysis. Proc. of the 3rd ISRM Congress, Vol. IIB p. 827-838.

Steffen, O.K.H., J.E. Kerrich, and J.E. Jennings (1975) Recent Developments in the Interpretation of Data from Joint Surveys in Rock Masses. Sixth Regional Conf. for Africa on Soil Mech. and Foundation Eng., Durban.

Steward, I.J. (1981) Numerical and Physical modelling on underground excavations in discontinuous rock. Ph.D. dissertation, Imperial College, London.

Terzaghi, R. (1965) Sources of error in joint surveys. Geotechnique, 15, p. 287-303.

Tewarson, R.P. (1973) Sparse Matrices Mathematics in Science and Engineering, Volume 99, Academic Press, 160p.

Thomas, A., P. Therme and P. Richard (1980) A New Method for Quick Measuring and Computing Parameters of Rock Jointing, Proceedings 22nd U.S. Rock Mechanics Symposium, p. 408-413.

Vargas, E. Jr. (1982) Development and Application of Numerical Models to simulate the Behaviour of Fractured Rock Masses, Ph.D. dissertation, Imperial College, London, 364p.

Underwood, E.E. (1967) Quantitative evaluation of sectional material. Proceedings 22nd Int. Congr. for Stereology, p. 49-60. Chicago.

Wallis, P.F. and M.S. King (1980) Discontinuity Spacing in a Crystalline Rock, Int. J. Rock Mech. Min. Sci. and Geomech. Abstr.,17, p. 63-66.

Warburton, P.M. (1980a) A Stererological Interpretation of Joint Trace Data, Int. J. Rock Mech. Min. Sci. and Geomech. Abstr., 17, p. 181-190.

Warburton, P.M. (1980b) Stereological Interpretation of Joint Trace Data: Influence of Joint Slope and Implications for Geological Survey. Int. J. Rock Mech. Min. Sci. and Geomech. Abstract., 17, p. 305-316.

Warren, J.E. and H.S. Price (1961) Flow in heterogeneous porous media. Society of Petroleum Engineering Journal, 1, p. 153-169.

Warren, J.E. and P.J. Root (1963) The behaviour of naturally fractured reservoirs. Society of Petroleum Engineering Journal, p. 245-255.

Whitten, E.H.T. (1966) Structural Geology of Folded Rocks, Rand McNally and Co. Chicago, p. 70-95.

Wilson, C.R. (1970) An Investigation of Laminar Flow in Fractured Porous Rocks. Ph.D. dissertation, University of California, Berkeley, 178p.

Wilson, C.R. and Witherspoon, P.A. (1976) Flow interference effects at fracture intersections, Water Resources Research 12(1), p. 102-104.

Wilson, C.R. et al (1983) Large-scale Hydraulic Conductivity Measurements in fractured granite. Int. J. Rock Mech. Min. Sci. and Geomech. Abstr. 20(6), p. 269-276.

Wilson, E.L. Et al (1974) Direct solution of large systems of linear equations. Computers and Structures Vol. 4, p. 363-372.

Witherspoon, P.A. and J.E. Gale (1977) "Mechancial and Hydraulic Properties of Rocks related to Induced Seismicity", Engineering Geology II, p. 23-55.

Witherspoon, P.A., C.H. Amick, J.E. Gale and K. Iwai (1979) Observations of a potential size effect in experimental determination of the hydraulic properties of fractures, Water Resources Research, 15(5), p. 1142-1146.

Witherspoon, P.A., J.S.Y. Wang, K. Iwai, and J.E. Gale (1979) Validity of cubic law for fluid flow in a deformable rock fracture. Water Resources Research, 16(6), p. 1016-1024.

Witherspoon, P.A. et al (1980) Validity of cubic law for fluid flow in a deformable rock fracture, Water Resources Research 16(6), p. 1016-1024.

Witherspoon, P.A., Y.W. Tsang, J.C.S. Long and J. Noorishad (1981) New approaches to problems of fluid flow in fractured rock masses. Proceedings 22nd US Symposium on Rock Mechanics, p. 1-20.

Witherspoon, P.A. and J.E. Gale (1983) Hydrogeological Testing to characterize a fractured granite. Bulletin of the International Association of Engineering Geology No. 26-27, p. 515-526.

Wittke, W. (1970) Three-dimensional percolation of fissured rock. Proc. of the Symposium on the theoretical background of the planning of open pit mines with special reference to slope stability. Johannesburg, p. 181-191.

Wittke, W. (1972) Zusammensfassender Bericht and Schluss folgerungen, Proc. Symps. Int. Soc. Rock Mech. Percolation through fissured rock, Stuttgart 1972, Z, p. 1-17.

Wittke, W., P. Rissler and S. Semprich, (1972), Raumliche, Laminare und turbulente stromung in Klutigem Fels nach zwei verschiedenen Modellen, Proc. Symp. Int. Soc. Rock Mech. Percolation through Fissured Rock, Stuttgart 1972, T1H, p. 1-18.

Young, R.D. (1978) Assessing rock discontinuities, tunnels and tunnelling, V.10, No. 5, p. 45-48.

Zienkiewicz, O., P. Mayer, and K.K. Cheung, (1966) solution of anisotropic seepage by finite element, J. Eng. Mech. Div. Proc. ASCE., Felo 1966, Vol. 92 (EM 1)

APPENDIX 1A

Procedure of scanline method

The scanline method is a well established technique for measuring discontinuity characteristics, on which many papers have already been published. However, for the sake of completeness and in order to describe field work carried out in Pembrokeshire a brief description of the procedure used is given here.

i) The equipment used included a 20 m steel tape, nails and string, Clar compass, a 2 m measuring tape, Schmidt hammer, profile gauge, geological hammer, feeler gauge, coding sheets and Ordnance and Geological Survey maps.

ii) The selection of the scanline site was based on the availability of a reasonable fresh rock exposure, the possibility of taking scanlines in three orthogonal directions and the availability of sufficient discontinuities to warrant a statistical analysis. After the decision on location of the scanline site was taken the next step was to record on the coded sheets - as shown in Table 1A.I - the main characteristics of the exposure. These were the dimensions, type of exposure, condition of the rock, rock type and the presence of any major geological features.

iii) Setting up the scanline involved attaching the steel tape to the rock face; this was usually done using the nails and string. When horizontal scanlines were used it was usually convenient to locate it 1 to 1.5 m from the base of the exposure. Finally the trend and plunge of the scanline as well as the face orientation were recorded.

iv) The intersection point of each discontinuity was then located and its position along the scanline recorded on the coding sheets. Care was exercised only to record discontinuities of geological origin and not fractures produced by blasting or stress relief. Each discontinuity was fully described before moving to the next one.

v) The discontinuity orientation was recorded by means of a Clar compass. When the discontinuity was reasonably planar one direct measurement was taken, however, when the surface was irregular, a flat board was placed over the discontinuity surface in order to obtain an average value for orientation.

vi) The semi-trace length above the scanline was measured for each intersected discontinuity; this was done in the plane of the rock face. For vertical scanlines it was necessary to adopt a convention concerning the side on which measurements were taken; this was kept consistent for each individual scanline.

vii) The type of termination of the discontinuity end above the scanline was recorded. The convention used was: 2 when the discontinuity ended in intact rock, 1 when it ended at another discontinuity and 0 when it was obscured or extended beyond the exposure (See Fig. 1A.1)

viii) The discontinuity type is a geological definition of the discontinuity. The convention adopted was (B) for bedding, (J) for joint, (Cl) for cleavage, (S) for shear, (Sch) for schistocity, (Fi) for fissure, (T) for tension crack and (F) for fault. The type of infilling was also recorded.

ix) A set of feeler gauges was used to measure discontinuity aperture. The procedure was to find the maximum thickness of feeler blade that could be fully and smoothly inserted into the discontinuity aperture. The results, however, were inconclusive. In nearly all of the exposures the discontinuities were tight and it was impossible to take any readings.

x) Roughness profiles were measured along strike and down dip directions. These were done by means of a 15 cm profile gauge and the profiles were then copied on to the coding sheets, as shown in Table 1A.II.

xi) Waviness was measured using offset distances measured from a base which consisted of a surveying staff placed first along the dip direction and then along the strike direction of the discontinuity being measured; the results were recovered on the coding sheets as shown in Table 1A.III.

xii) The hardness of the discontinuity surfaces was measured by means of a Schmidt hammer. The results obtained were, unfortunately, inconclusive since soft material or loose blocks led to great variability in the readings.

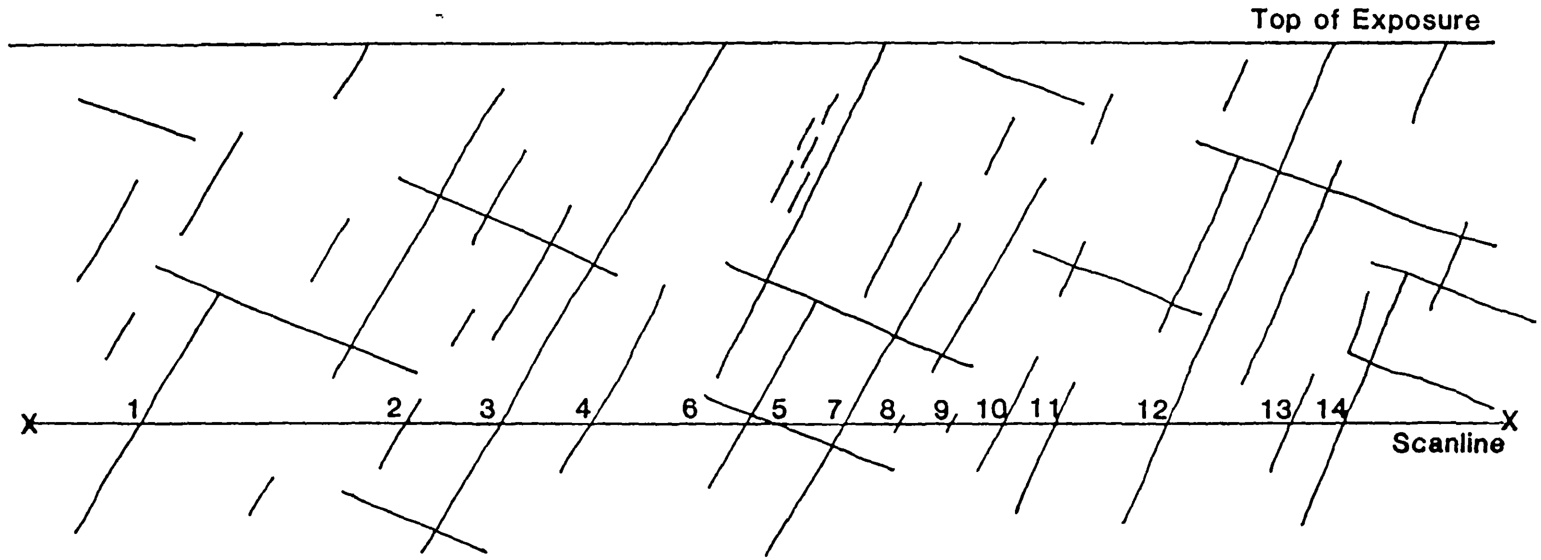

Discontinuities 2,4,6,7,8,9,10,11,13. terminate in intact rock (2)

Discontinuities 1,5,14. terminate against another discontinuity (1)

Discontinuities 3,12. are censored trace lengths (0)

Fig. 1A.1 Horizontal scanline sampling method

SCANLINE SURVEY MEASUREMENT FORM

Sheet .... of Scanline .... By.................... Date	Location Rock Type Scanline Orientation	Orientation of Rock Face Exposure Dimensions	Type of Exposure Condition of Exposure

Disc No	Position (m)	Dip Amount	Trend Value	Length (m)	Term	Disc Type	Rough- ness No	Curvat- ure No	Width (mms)	Hard- ness No	Infill Material	Comment
1												
2												
3												
4												
5												
6												
7												
8												
9												
10												
11												
12												
13												
14												
15												
16												
17												
18												
19												
20												
21												
22												
23												
24												
25												
26												
27												
28												
29												
30												
31												
32												
33												
34												
35												
36												
37												
38												
40												

Comments

Table 1A.I Scanline coding sheets

Table 1A.II Roughness coding sheets

Line Number	Disc. Reference Position	Roughness Traces Using A Profile Gaugue Down Dip* +	Hardness Values Measured				Average
1	Disc No......... Position.......m STRIKE/DIP						
2	Disc No......... Position.......m STRIKE/DIP						
3	Disc No......... Position.......m STRIKE/DIP						
4	Disc No......... Position.......m STRIKE/DIP						
5	Disc No......... Position.......m STRIKE/DIP						
6	Disc No......... Position.......m STRIKE/DIP						

Comments

*Where appropriate

Table 1A.III Waviness coding sheets

Line Number	Disc Reference Position	Waviness Readings Measured Perpendicularly from a Measuring Staff (m)	Down Dip* →
1	Disc No......	Position	
	Position ....m	Offset	
	STRIKE/DIP	Position	
		Offset	
2	Disc No..........	Position	
	Position........m	Offset	
	STRIKE/DIP	Position	
		Offset	
3	Disc No..........	Position	
	Position........m	Offset	
	STRIKE/DIP	Position	
		Offset	
4	Disc No..........	Position	
	Positon.........m	Offset	
	STRIKE/DIP	Position	
		Offset	
5	Disc No..........	Position	
	Position........m	Offset	
	STRIKE/DIP	Position	
		Offset	
6	Disc No..........	Position	
	Position........m	Offset	
	STRIKE/DIP	Position	
		Offset	

<u>Comments</u>

APPENDIX 1B

Description and locations of the field sites and data collected

The five sites visited in the Pembrokeshire area are listed in Table 1B.I. The scanline locations at each site are presented in Figs. 1B.1 to 1B.5. The raw data for the measured scanlines and the pre-processed photographic data are also presented on the enclosed micro-fiches.

Fig. 1B.1 Sketch of Tenby (Area E)

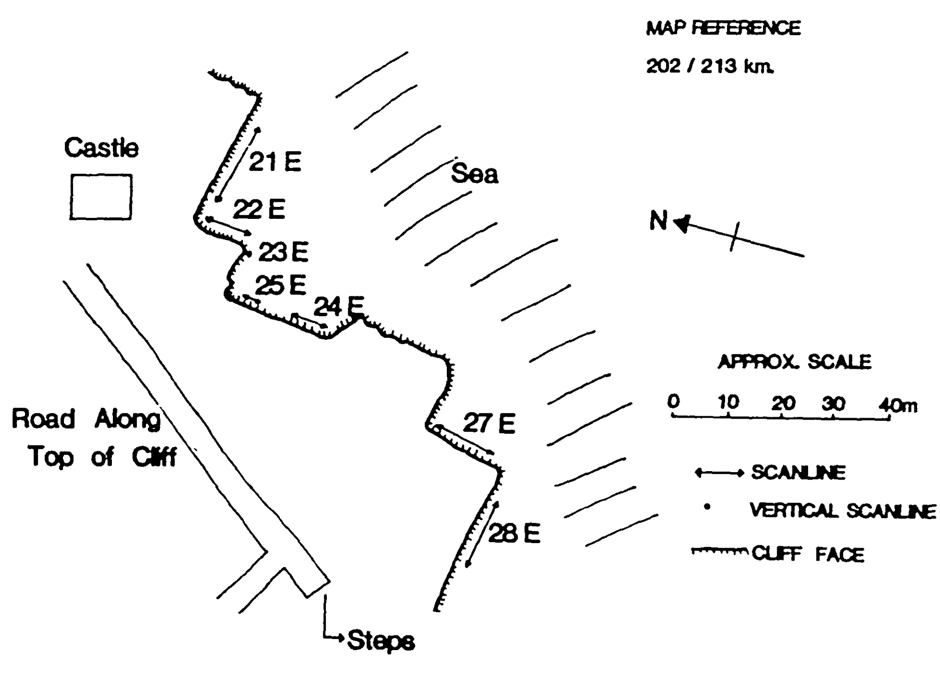

Fig 1B.2 Sketch of St. Bride's Haven (Area F)

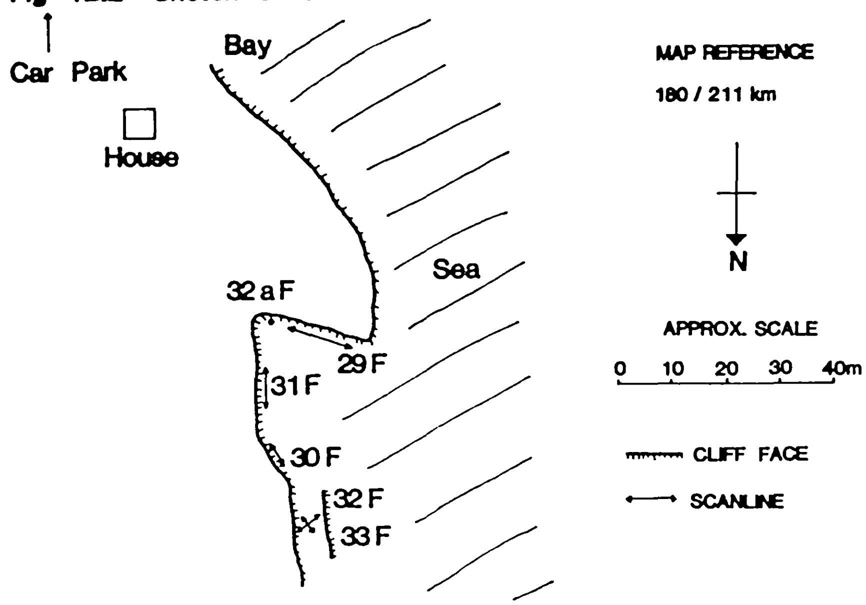

Fig. 1B.3 Sketch of N. Abereiddy Bay (Area A)

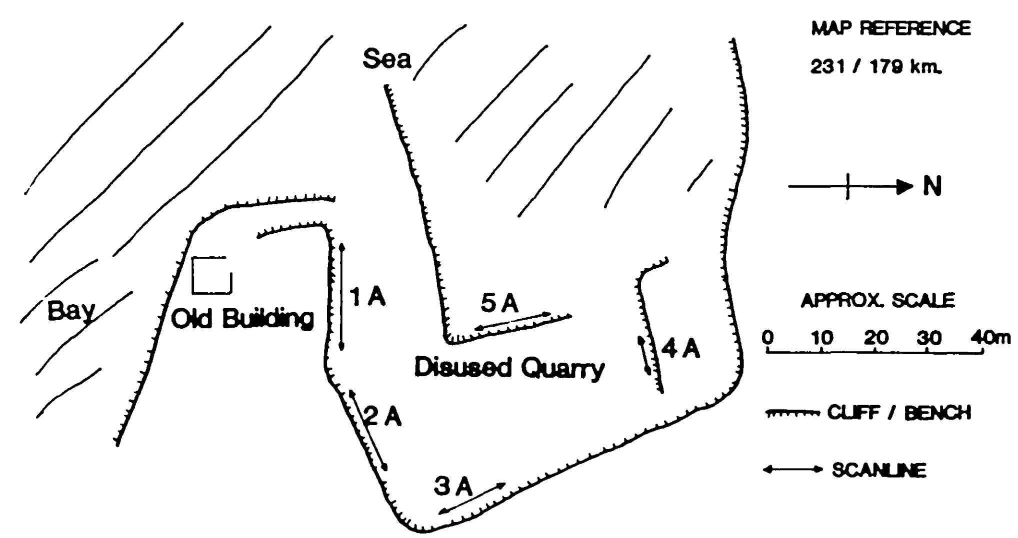

Fig. 1B.4 Sketch of Middle Mill Quarry (Area C)

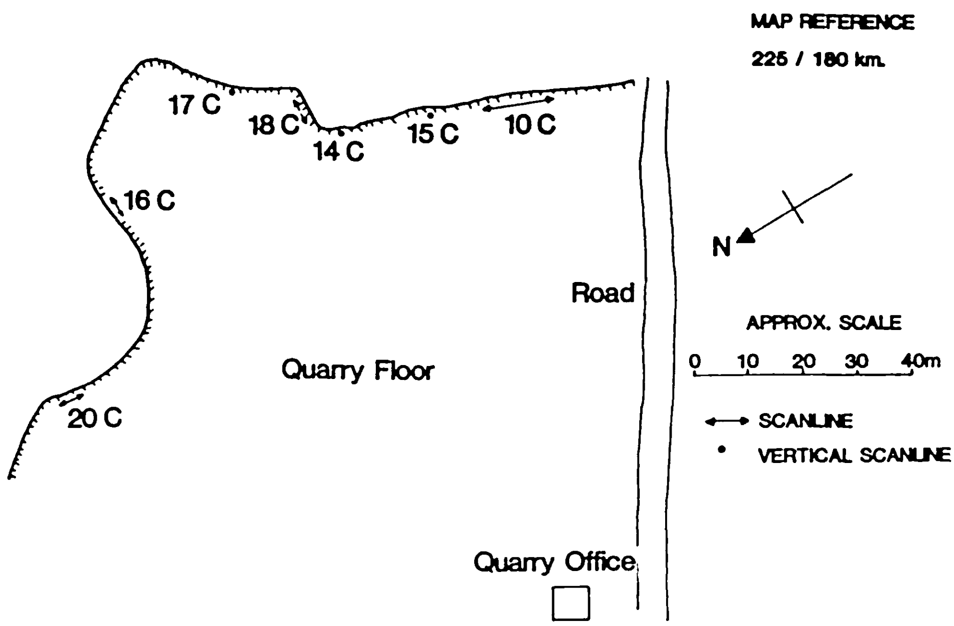

Fig. 1B.5 Sketch of Marloes Sands (Area G)

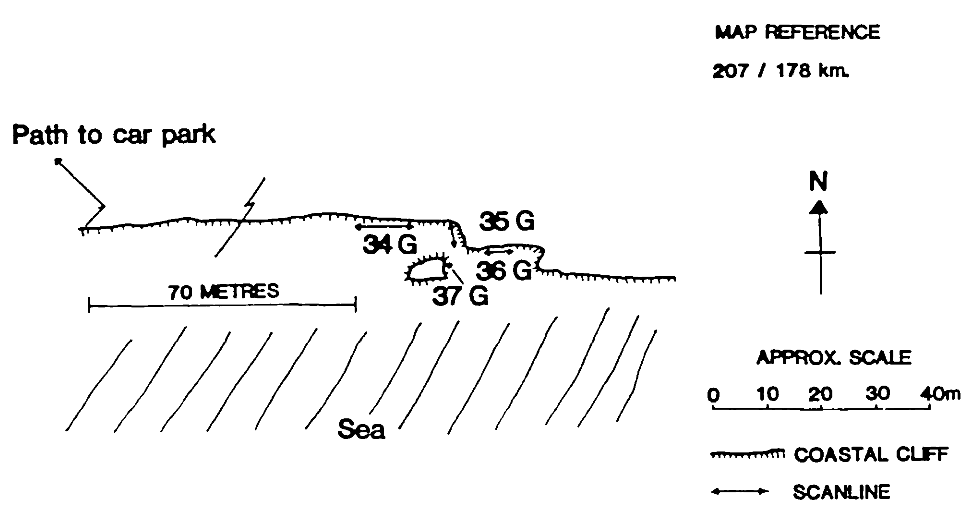

No.	Place Name	Map Co.ord.	Geological Age	Type of Rock	Dimensions of exposure	No. of Scanline	No. of Discs.	No. of Disc. sets	Condition of exposure	Sketch Fig No.	Photo Number
1	Middle Mill Quarry	N-225	Cambrian	Quartzites and Basic Intrusives	10-20m High Vertical Faces	7	150	4	Good with Blasting Breakages	7	6,7
2	North Abereiddy Bay	N-231 E-179	Ordovian (Llanvirn Series)	Slatey Volcanics	5-10m High Steeply Dipping Faces	5	248	4	Medium-Poor Some areas very weathered	6	8
3	Marloes Sands	N-207 E-178	Silurian (U.Llandovery)	Quartzitic Sandstone	3-15m High Vertical and Steeply Dipping Faces	4	328	4	Good but Surfaces Smoothed by Sea Erosion	10	9,10
4	St Brides Haven	N-180 E-211	Devonian (Lower Old Red Sandstone)	Sandy Red Marls	2-5m High Vertical Faces	6	277		Good	9	11,12
5	Tenby	N-202 E-213	Carboniferous	Limestone	5-15m High Vertical and Steeply Dipping Faces	7	322		Fair but many open discs. due to Sea Erosion	8	13,14,15

Table 1B.I Pembrokeshire field trip sites description

PEMBROKESHIRE PHOTOGRAPHIC RESULTS

APPENDIX 1C

User's instructions of SCANL and PHOCOM

The programs SCANL and PHOCOM are written in FORTRAN IV and are designed to run on a CDC computer, 850 Cyber, with line printer and microfilm plotting facilities. The compiler used was MNF5 (Minnesota Fortran Version 5).

The program SCANL can typically handle up to 15 scanlines each one containing up to 500 discontinuities and up to a maximum of 4 discontinuity sets. The data from different scanlines taken at a given site can be processed together or separately, in this work all scanline data were processed together. The input data are coded as follows:

- Card 1	format (20A4)
Cols 1-80	title
- Card 2	format (2I3)
Cols 1-3	NSL number of scanlines
Cols 4-6	NDSET number of discontinuity sets
- Card 3	format (3F5.1)
	There is one of these cards for each set
Cols 1-5	BD: Mean trend of cluster
Cols 6-10	GD: Mean pludge of cluster
Cols 11-15	ANG: Solid angle of oval

- Card 4 Format (2I4, 2F5.1)

  There is one of these cards for each scanline

Cols 1-4	IDS: Number that identifies the scanline
Cols 5-8	NTD: Number of discontinuities in each scanline
Cols 9-13	BG: Scanline trend
Cols 14-18	Scanline plunge

- Card 5 Format (4F6.2, I2)

  There is one of these cards for each discontinuity

Cols 1-6	SC(I,1): discontinuity position
Cols 7-12	SC(I,2): discontinuity dip amount
Cols 13-18	SC(I,3): discontinuity dip trend
Cols 19-24	SC(I,4): discontinuity semi-trace length
Cols 25-26	ITER(I): type of termination

The group of cards 4 and 5 is repeated for as many times as there are scanlines in the analysis.

The output of the SCANL program is organised by discontinuity sets. The basic input data are printed on the first page of the output, this is followed by data about each discontinuity set, including: number of discontinuities, mean orientation of the set, Fisher's constant, mean discontinuity spacing and standard deviation. The curve fitting for spacing is then presented using lognormal and negative exponential distributions incorporating a chi-square test. The number of discontinuities of each type of termination is then quoted. This is followed by a table which presents the two methods of analysing mean trace length as presented by Priest and Hudson (1981). Next the curve fitting plus the chisquare test for semi-trace is presented followed by a table containing the information for the estimation of mean trace length by a distribution independent method. The print out and graphical output, produced by SCANL for the data from Pembrokeshire, are included in appendix 1E and 1F respectively.

The program PHOCOM analyses data from photographs containing up to 1500 discontinuities. The program enables the user to superimpose on to the photograph up to 20 scanlines of any orientations. The input data are coded as follows:

- <u>Card 1</u> format (20A4)

  Cols 1-20 title

- <u>Card 2</u> format (I2)

  Col 1-2 NPH: number that identifies the photograph

- <u>Card 3</u> format (4I4, 5F7.3)

  Cols 1-4 NTD: total number of discontinuities

  Cols 5-8 NSLH: total number of horizontal scanlines

  Cols 9-12 NSLV: total number of vertical scanlines

  Cols 13-16 NSET: total number of discontinuity sets

  Cols 17-23 ACOR: area correction (used where the photograph area is not rectangular)

  Cols 24-30 XO1:)
) coordinates of lower left corner of photograph
  Cols 31-36 YO1:)

  Cols 37-43 YO2:)
) coordinates of upper right corner of photograph
  Cols 44-50 XO2:)

  See Fig. 1C1

- <u>Card 4</u>   format (2F7.3)

  There is one card for each discontinuity set

  Cols 1-7   THEM(I): mean angle of orientation of Set I

  Cols 8-14   5TH(I): deviation from mean

- <u>Card 5</u>   format (4F10.3)

  There is one card for each scanline

  Cols 1-10   XX1(I))
) coordinates of lower end of scanline
  Cols 11-20   YY1(I))

  Cols 21-30   XX2(I))
) coordinates of upper end of scanline (*)
  Cols 31-40   YY2(I))

  * when the scanline is horizontal XX2(I)and YY2(I) are the right end coordinate.

- <u>Card 6</u>   format (4F10.3)

  There is one card for each discontinuity

  Cols 1-10   XD1(I))
) coordinate of end 1 of a discontinuity
  Cols 11-20   YD1(I))

  Cols 21-30   XD2(I))
) coordinate of end 2 of a discontinuity
  Cols 31-40   YD2(I))

The PHOCOM ouput is organised by discontinuity sets. For each set the mean orientation, standard deviation, member of discontinuities and density are printed. A table with trace length analysis follows, in which mean values and standard deviations for non-censored, one end censored and two ends censored discontinuities are printed out. A curve fitting analysis with the chi-square test for trace length and discontinuity orientation is also printed.

The results obtained by superimposing scanlines are similar to those obtained by SCANL. The total printouts and graphical output produced by PHOCOM for the data from Pembrokeshire are presented in appendix 1G and 1H respectively. The program listings for SCANL and PHOCOM are given in Appendix 7.

APPENDIX 1D

Determination of mean trace length using a distribution independent method

The discussion presented here was originally developed by Bray (1982) following the Priest and Hudson (1981) formulation for the probability density distribution of semi-trace lengths, $h(\ell)$, sampled by a scanline. This distribution is given by

$$h_{(\ell)} = \mu\,[1-F(\ell)] \tag{1}$$

Where $1/\mu$ is the mean trace length of the population of traces intersected by a rock exposure and $F(\ell)$ its cumulative distribution. Equation (1) may be written

$$\bar{\ell} \cong \frac{1}{\mu} = [1-F(\ell)]/h_{(\ell)} \tag{2}$$

Equation (2) is a general expression for $1/\mu$ that depends on the knowledge of $F(\ell)$. As ℓ approaches zero, $F(\ell)$ also approaches zero and in the limit

$$\mu = h(o) \tag{3}$$

If a sufficiently small semi-trace length, ℓ, is selected in such a way that $F(\ell)$ approaches zero then:

$$\frac{1}{\mu} \approx \frac{n}{r} \cdot \ell \tag{4}$$

Where n is the total number of discontinuities intersecting a given scanline, and r the number of discontinuities which have a semi-trace length between zero and ℓ. As ℓ approaches zero, $\frac{n}{r}\cdot\ell$ will approach $1/\mu$. When ℓ is small, however, $\frac{n}{r}\cdot\ell$ is subject to a considerable statistical variation such that the determination of $1/\mu$ is complicated by this factor.

The following modified procedure is then preferred.

The cumulative probability for semi-trace lengths is given by

$$H(\ell) = \int_0^{\ell} h(m)dm \qquad (5)$$

from equation (1)

$$H(\ell) = \mu \int_0^{\ell}[1-F(m)]dm \qquad (6)$$

thus

$$\frac{1}{\mu} = \frac{\ell . A(\ell)}{H(\ell)} \qquad (7)$$

where
$$A(\ell) = \frac{1}{\ell}\int_0^{\ell}[1-F(m)]dm$$

but $[1-F(m)]$ has its maximum value of 1 when $m = o$. Hence $A(\ell)$ approaches 1 when ℓ approaches zero, and for all non-zero values of ℓ, $A(\ell) < 1$.

Therefore

$$\frac{1}{\mu} \leqslant \frac{\ell}{H(\ell)} \qquad (8)$$

where the equality applies in the limit when ℓ approaches zero.

Equation (8) may be written in the following form

$$\frac{1}{\mu} < \frac{n}{r}c \tag{9}$$

where n is again the sample size and r is now the number of discontinuities with a semi-trace length less than a given censoring level c.

By chosing a range of values of censoring level, c, a series of values of n.c/r can be obtained, and the results plotted graphically, with n.c/r as ordinates and c as abscissae. If more than one set of results is plotted the region which is least affected by statistical variation can be identified. Extrapolating the curves from this region to the c = 0 axis gives a reasonably accurate estimate for $1/\mu$.

Bray's approach was tested assuming that the distribution of trace lengths was known a priori. If a negative exponential distribution is first assumed the cumulative distribution can be expressed as

$$F(\ell) = 1-e^{-\mu\ell} = \frac{r}{n} \tag{10}$$

the above equation can be rearranged into

$$\frac{n.\ell}{r} = \frac{\ell}{1-e^{-\mu\ell}}$$

applying L'Hospitals rule to equation (10) in order to avoid the indetermination when $\ell \to o$ gives :

$$\frac{f(o)}{g(o)} = \frac{df(\ell)/d\ell}{dg(\ell)/d\ell}\Bigg|_{\ell = 0} \tag{11}$$

but

$$f(\ell) = \ell \text{ and } g(\ell) = 1-e^{-\mu\ell}$$

$$df(\ell)/d\ell = 1 \qquad (12)$$

$$dg(\ell)/d\ell = \mu e^{-\mu\ell}$$

replacing (12) into (11) gives

$$\frac{f(o)}{g(o)} = \frac{1}{\mu} \qquad (13)$$

Secondly, assuming that the trace lengths are uniformly distributed, the cumulative distribution can be expressed

$$H(\ell) = \mu\left[1-\frac{\mu\ell}{2}\right] \qquad (14)$$

by integration

$$H(\ell) = \int_o^c h(\ell)d\ell = \mu\ell\left[1- \quad \frac{\mu\ell}{4}\right]$$

but

$$\frac{r}{n} = H(\ell) = \mu\ell\left[1-\frac{\mu\ell}{4}\right]$$

rearranging $$\frac{n\ell}{r} = \frac{1}{\mu\left[1+\frac{\mu\ell}{4}\right]}$$

assuming $$f(\ell) = \frac{n\ell}{r} = \frac{1}{\mu\left[1+\frac{\mu\ell}{4}\right]}$$

then $$\ell\to o \quad : \quad f(o) = \frac{1}{\mu} \qquad (15)$$

Equations (13) and (15) show that the method developed by Bray (1982) gives the expected estimate of mean trace length when the type of distribution for the trace lengths was assumed to be either negative exponential or uniform.

APPENDIX 1E

Pembrokeshire Scanline Analysis

Print out of results.

01

PEMBROKESHIRE SCANLINE ANALYSIS 02

APPENDIX 1F

Pembrokeshire Scanline Analysis

Graphic output.

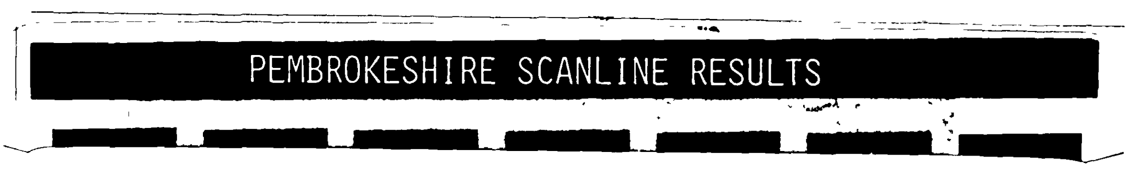

APPENDIX 1G

Pembrokeshire Photographic Analysis

Print out of results.

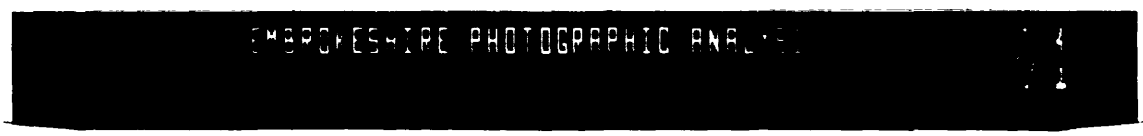

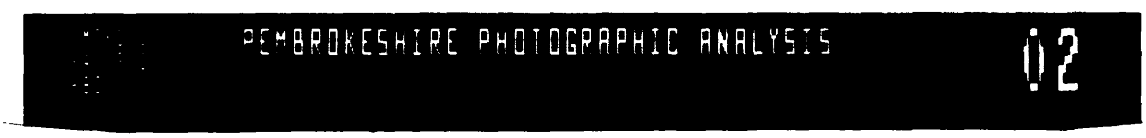

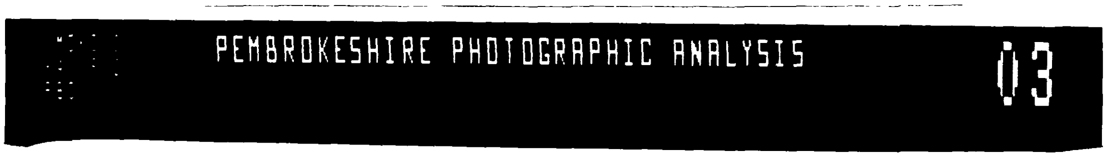

APPENDIX 1H

Pembrokeshire Photographic Analysis

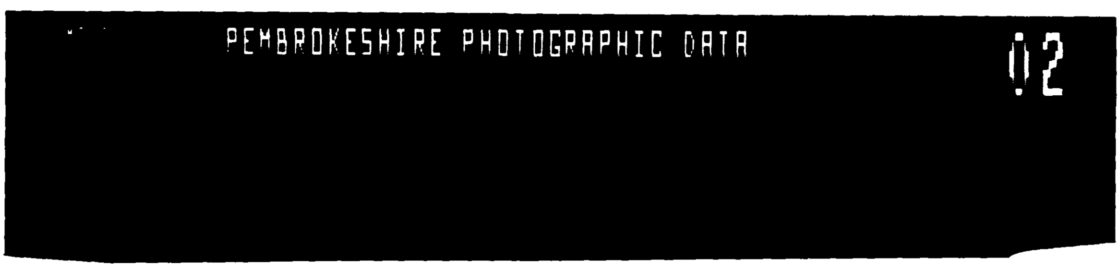

APPENDIX 2

Description of the probabililty density functions and of the random generators used in generating a discontinuity mesh

A.2.1 Poisson density function

In Section 3.2 it was assumed that the discontinuity centres were randomly distributed over the generating area such that their occurrence obeyed a two-dimensional Poisson process. This process can be represented by a discrete probability function given by:

$$f(x) = \frac{\mu^x}{x!} e^{-\mu}$$

where f(x) is the probability function, x is the number of events and μ is the population mean and variance. As μ becomes large the Poisson function tends to a normal distribution. The basic assumptions governing the Poisson process are: 1) events occur independently, that is, the occurrence of an event does not depend on previous or following events in any way. 2) Two events cannot occur simultaneously, and 3) the probability of an event occurring is proportional to the length of time since the last event - that is, the longer the time an event does not occur the more likely it is to occur. The latter has applications in describing the number of 'accidents' which could occur in a certain time interval. To obtain a Poisson distribution of discontinuities centres in a plane, two random numbers taken from a uniform distribution between zero and one are generated and taken to represent the x and y coordinates of a discontinuity centre. A description of the uniform distribution follows.

A.2.2 Uniform density function

A random variable is said to be uniformly distributed between a and b if it is equally likely to occur anywhere between a and b. Mathematically the probability density is expressed:

$$f(x) = \begin{cases} \dfrac{1}{b-a} & a < x < b \\ 0 & \text{elsewhere} \end{cases}$$

Fig 2A .1 shows the curve of the uniform probability density function. The mean, (A), and standard deviation, (B), are given by

$$\text{mean} = \quad A = \frac{b + a}{2}$$

$$\text{Standard deviation} = \quad B = \frac{b^2}{12}$$

The random number generators used in this work were taken from the NAG Libraries that are available at the Imperial College Computer Centre.

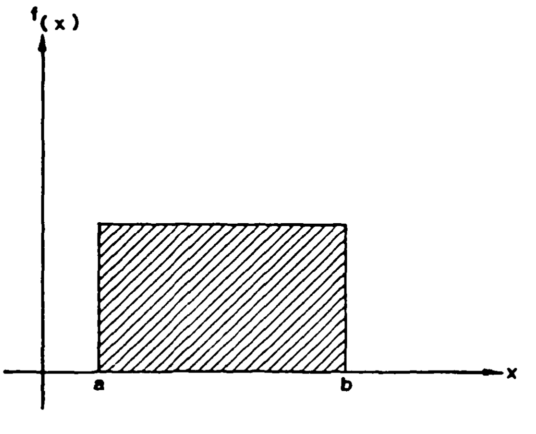

Fig. 2A.1 Uniform distribution

A.2.3 Normal density function

The discontinuity orientation of a discontinuity set was assumed to follow a normal distribution. This distribution can be expressed as:

$$f(x) = \frac{1}{B\sqrt{2\Pi}} \quad e^{-\frac{(x-A)^2}{2B^2}}$$

where A and B are the mean and standard deviation repectively. The standarised normal distribution f(z) is defined as a normal density whose mean is zero and whose standard deviation is equal to one. The density is given by

$$f(z) = \frac{1}{\sqrt{2\Pi}} \cdot e^{-\frac{z^2}{2}}$$

where z = (x - A)/B represents the variable of the standarised normal distribution. Again the random generators used are from the NAG Libraries.

A.2.4 Log-normal density function

The discontinuity aperture and sometimes the discontinuity trace length were assumed to follow a log normal distribution. This is given by:

$$f(x) = \frac{1}{xA\sqrt{2\Pi}} \cdot e^{-\frac{(\mathrm{Log}\ x - B)^2}{2A^2}}$$

where A and B are the mean and standard deviation repectively. Although it is possible to generate a random number from this distribution using the same basic generating routine as that for the normal distribution, it is necessary to carry out the following transformations:

$$B_1 = \text{Log}[(B^2/A^2) + 1]$$

$$A_1 = \text{Log } x - \frac{1}{2} B_1^2$$

The A_1 and B_1 parameters are then used in the generator routine explained in A.2.3.

A.2.5 Negative exponential density function

The distribution of discontinuity trace length and discontinuity spacing is sometimes assumed to be negative exponentially distributed. Mathematically this distribution can be expressed as:

$$f(x) = \mu e^{-\mu x}$$

where $1/\mu$ is the mean or standard deviation of the distribution. The NAG generator routine returns a random number from this distribution by simply calculating $1/\mu \log_e(Y)$, where Y is a uniformly distributed random number between 0 and 1.

APPENDIX 3

Description of the bi-factorisation method for solving sparse matrices

The bi-factorisation method, originally derived by Zollenkopf (1971), is a direct method for solving a large set of sparse linear equations.

A set of n linear equations can be expressed in matrix notation as

$$A\,x = b \qquad (1)$$

where A is a non singular n x n coefficient matrix

x is a column vector of the n unknowns, and

b is a known vector with at least one non-zero element

For applications where A remains unchanged the solution vector may be computed directly from

$$x = A^{-1}b \qquad (2)$$

The explicit computation of the inverse of A, A^{-1}, is not efficient from the point of view of storage requirements and computation time. This is particularly true for sparse matrices since it is unusual for their inverses to be other than full.

Two general approaches have been developed for obtaining repeated direct solutions without matrix inversion. In one, the coefficient matrix is factored into the products of two factor matrices by a process which is referred to as Triangular decomposition. In the other approach, the inverse is factored into the product of n factor matrices and is referred to as the product form of the inverse.

The bi-factorisation method, combines the main characteristics of the above two approaches and is based on the equation

$$L^{(n)}\, L^{(n-1)} \ldots\ldots L^{(2)}\, L^{(1)}\, A\, R^{(1)}\, R^{(2)} \ldots\ldots R^{(n-1)}\, R^{(n)} = I \qquad (3)$$

where L are the left-hand factor matrices

R are the right-hand factor matrices, and

I is the unity matrix

By matrix transformation equation (3) becomes

$$A^{-1} = R^{(1)}\, R^{(2)} \ldots\ldots R^{(n-1)}\, R^{(n)}\, L^{(n)}\, L^{(n-1)} \ldots\ldots L^{(2)}\, L^{(1)} \qquad (4)$$

Equation (4) shows that the inverse of A can be expressed by a multiple product of 2n factor matrices. This fact led Zollenkopf (1971) to name it the bi-factorisation method.

In equation (3) Zollenkopf introduces a sequence of intermediate matrices, in order to determine the factor matrices L and R.

$$\begin{aligned}
A^{(0)} &= A \\
A^{(1)} &= L^{(1)}\, A^{(0)}\, R^{(1)} \\
A^{(2)} &= L^{(2)}\, A^{(1)}\, R^{(2)} \\
A^{(j)} &= L^{(j)}\, A^{(j-1)}\, R^{(j)} \\
A^{(n)} &= L^{(n)}\, A^{(n-1)}\, R^{(n)} = I
\end{aligned} \qquad (5)$$

The aim of this representation is to transform, step by step, the initial coeffecient matrix $A = A^{(0)}$ to the unity matrix by forming successive inner triple products $L^{(j)}\ A^{(j-1)}\ R^{(j)}$ for j = 1 to n.

The following general rules are used for computing $A^{(j)}$, $L^{(j)}$ and $R^{(j)}$ from elements of $A^{(j-1)}$. The reduced matrix $A^{(j)}$:

$$a^{(j)}_{jj} = 1; \quad a^{(j)}_{ij} = 0; \quad a^{(j)}_{jk} = 0;$$

$$a^{(j)}_{ik} = a^{(j-1)}_{ik} - \frac{a^{(j-1)}_{ij} \quad a^{(j-1)}_{jk}}{a^{(j-1)}_{jj}} \qquad (6)$$

where j is the pivotal index for i, k = (j + 1) to n.

<u>Factor Matrices $L^{(j)}$</u>

The left-hand factor matrices $L^{(j)}$ are very sparse and differ form the unity matrix in only column j:

$$L^{(j)} = \begin{bmatrix} 1 & & & 0 & & & \\ & \ddots & & \vdots & & & \\ & & 1 & 0 & & & \\ & & & l^{(j)}_{j,j} & & & \\ & & & l^{(j)}_{j+1,j} & 1 & & \\ & & & l^{(j)}_{j+2,j} & & 1 & \\ & & & \vdots & & & \ddots & \\ & & & l^{(j)}_{n,j} & & & & 1 \end{bmatrix}$$

where $$l_{jj}^{(j)} = 1/a_{jj}^{(j-1)} \tag{7}$$

and $$l_{ij}^{(j)} = -a_{ij}^{(j-1)}/a_{jj}^{(j-1)} \quad \text{for } i = (j+1) \text{ to } n$$

Factor Matrices $R^{(j)}$

The right-hand factor matrices $R^{(j)}$ are also very sparse and differ from the unity matrix in only row j.

$$R^{(j)} = \begin{bmatrix} 1 & & & & & & & & \\ & \ddots & & & & & & & \\ & & 1 & & & & & & \\ 0 & \cdots & 0 & 1 & r_{j,j+1}^{(j)} & r_{j,j+2}^{(j)} & \cdots & r_{j,n}^{(j)} \\ & & & & 1 & & & & \\ & & & & & \ddots & & & \\ & & & & & & & 1 \end{bmatrix}$$

where $r_{kj}^{(j)} = -\, a_{jk}^{(j-1)}/a_{jj}^{(j-1)}$ for k = (j+1) to n

Note that the diagonal term, unlike that of $L^{(j)}$, is equal to 1 and thus $R^{(n)} = I$.

Although the method can be applied to either symmetrical or asymmetrical matrices A, only the symmetrical case will be considered here.

A symmetrical matrix A can be expressed as

$$a_{ik}^{(j-1)} = a_{ki}^{(j-1)}$$

thus $$r_{jk}^{(j)} = l_{ij}^{(j)} \quad \text{for } i = k \neq j \tag{9}$$

Equation (9) implies that the jth row of $R^{(j)}$ is identical to the jth column of $L^{(j)}$, except for the diagonal term. It is therefore unnecessary to perform any operations to the right of the diagonal, thereby obviating about half of the reduction operations.

Sparsity of the matrix is also exploited when programming the method since only non-zero terms are stored and processed. This requires, in addition to the matrix elements themselves, tables of indexing information to identify the elements and to facilitate their addressing. An optimal ordering, achieved by pivoting the reduction process, is required in order to minimise the total number of fill-in terms.

Optimal ordering can be determined during the course of the computation. Zollenkopf (1971) found that an efficient ordering can be determined by simulating the reduction process beforehand. Hence the program can be split into three parts.

(i) Simulation and ordering

(ii) Reduction

(iii) Direct solution

The simultation and ordering process is carried out at two levels. First a search for the pivoted column is performed, the column with the fewest number of non-zero elements is selected as the pivotal column. If more than one column meets this criterion, the column number in the first location on the list containing the pivotal sequence is selected. This process is carried out step by step, during which only the list containing the pivotal sequence is updated. In the second level of the simulation and ordering, fill-in terms are added and others cancelled.

The actual reduction of the coefficient matrix is guided by the pivotal sequence established by the simulation and ordering sub-routine.

The direct solution is calculated by successive factor-matrix-by vector multiplications. The simulation and ordering, reduction and direct solution steps are performed by the sub routines SIMORD, REDUCT and DIRSOL respectively. The sub-routine PREPA prepares the tables of indexing information and the tables containing the matrix elements. All of these sub-routines form part of the program DIFLOW A and DIFLOW B which are given in Appendix 7.

APPENDIX 4

Determination of the permeability tensor using the flows in the boundary nodes

The following analysis was originally developed by Cundall (1983). It was noted earlier in Chapter 3 that the mean flow velocity can be expressed

$$\overline{V}_i = \frac{1}{L^2} \sum_{m=1}^{n} q_m \, \text{Cos} \, \Theta_{im} \, \ell_m \tag{1}$$

where Θ_{im} is the angle between the mth segment and the x_i direction, ℓ_m is the length of the discontinuity segment, q_m the flow quantity in the mth segment and L is the side length of the square sample area.

Fig. 4A.1 shows the characteristics of a single discontinuity segment.

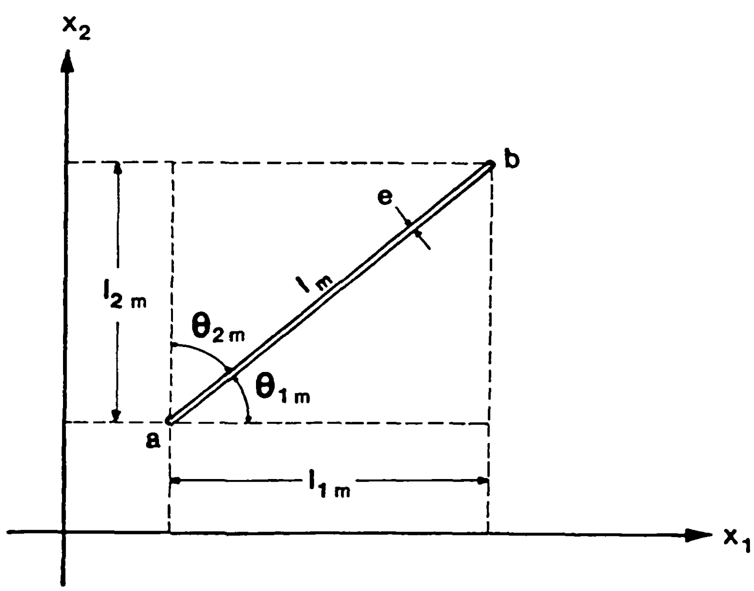

Fig. 4A.1 Characteristics of the mth segment

From Fig. 4A.1 it can be seen that $\ell_{im} = \ell_m \cos \Theta_{im}$; thus, replacing this in equation (1) gives

$$\overline{V}_i = \frac{1}{L^2} \sum_{m=1}^{n} q_m \ \ell_{im} \tag{2}$$

ℓ_{im} can also be expressed in terms of the coordinates of its end nodes, a and b.

$$\ell_{im} = x_{ia} - x_{ib} \tag{3}$$

q_m can be expressed in terms of the flow quantity going into node a and out of node b

$$q_a = q_m = - q_b \tag{4}$$

Substituting ℓ_{im} and q_m in equation (2) gives

$$\overline{V}_i = \frac{1}{L^2} \quad \sum_{m=1}^{n} q_a \ x_{ia} \ + \sum_{m=1}^{n} \ q_b \ x_{ib} \tag{5}$$

The summations in equation (5) is over the n discontinuity segments present in the network. Each node will appear in the summation as many times as there are connecting segments. Usually there is one connection for boundary segments and up to four for internal segments. The above equation can be written as a summation over the total number of nodes, N.

$$\overline{V}_i = \frac{1}{L^2} \sum_{k=1}^{N} \quad x_i \sum_{j=1}^{D} \ q_j \tag{6}$$

For i=1 to N and j=1 to D, where D can be from 1 up to 4. The term x_i is the coordinate of node i and $\sum q_j$ is the summation of all flow quantities going into or out of node i. It is clear that the above summation should be equal to zero for all internal nodes. Therefore the summation is reduced only to the boundary nodes.

$$\overline{V}_i = \frac{1}{L^2} \sum_{n=1}^{B} x_i \; q \qquad (7)$$

Where B is the total number of boundary nodes, x_i the coordinates of node i and q the quantity going into or out of the boundary node i.

APPENDIX 5

A5.1 Permeability tensor

A5.2 Principal permeability and principal direction

A5.1 Permeability tensors of the 60 realisations

K_{11}	K_{12}	K_{21}	K_{22}
.309468E-04	-.708114E-05	-.708114E-05	.333764E-04
.327430E-04	-.412461E-05	-.412461E-05	.564320E-04
.424795E-04	.267178E-05	.267178E-05	.627557E-04
.451780E-04	-.452088E-05	-.452088E-05	.619499E-04
.431867E-04	.403635E-05	.403635E-05	.859844E-04
.398505E-04	-.682925E-05	-.682925E-05	.454633E-04
.207416E-04	-.113599E-06	-.113599E-06	.384317E-04
.369162E-04	.204561E-04	.204561E-04	.876504E-04
.239022E-04	-.265339E-05	-.265339E-05	.418012E-04
.330987E-04	.155235E-04	.155235E-04	.846556E-04
.465717E-04	.866166E-05	.866166E-05	.836055E-04
.520869E-04	.121572E-04	.121572E-04	.722626E-04
.296349E-04	.523270E-05	.523270E-05	.328319E-04
.459280E-04	.842821E-05	.842821E-05	.851563E-04
.369553E-04	-.598555E-05	-.598555E-05	.556152E-04
.405123E-04	-.142813E-05	-.142813E-05	.671414E-04
.396123E-04	.766674E-05	.766674E-05	.544274E-04
.238502E-04	.934305E-05	.934305E-05	.301369E-04
.549027E-04	.137085E-05	.137085E-05	.101483E-03
.462884E-04	-.235577E-05	-.235577E-05	.112110E-03
.210096E-04	-.231882E-05	-.231882E-05	.623343E-04
.304423E-04	.381130E-05	.381130E-05	.502030E-04
.349910E-04	.425473E-06	.425473E-06	.773997E-04
.295747E-04	.170319E-05	.170319E-05	.195553E-04
.459074E-04	.377227E-05	.377227E-05	.717544E-04
.235167E-04	.712328E-05	.712328E-05	.421594E-04
.405654E-04	.467893E-05	.467893E-05	.603592E-04
.339450E-04	.444641E-05	.444641E-05	.419629E-04
.362679E-04	.383361E-05	.383361E-05	.545896E-04
.517133E-04	-.323149E-05	-.323149E-05	.562786E-04
.597637E-04	.642938E-05	.642938E-05	.132312E-03
.332882E-04	.847485E-05	.847485E-05	.748872E-04
.179923E-04	.216337E-05	.216337E-05	.235995E-04
.689762E-04	.575122E-05	.575122E-05	.844579E-04
.336159E-04	.729342E-05	.729342E-05	.603553E-04
.480578E-04	.506793E-05	.506793E-05	.140788E-03
.415022E-04	-.907273E-05	-.907273E-05	.482810E-04
.465460E-04	-.431015E-06	-.431015E-06	.628135E-04
.473332E-04	.539363E-05	.539363E-05	.108318E-03
.270600E-04	-.223793E-05	-.223793E-05	.584950E-04
.298919E-04	.123416E-04	.123416E-04	.475029E-04
.299981E-04	.467384E-05	.467384E-05	.609414E-04
.202110E-04	-.739795E-06	-.739795E-06	.474563E-04
.214549E-04	.401474E-07	.401474E-07	.529122E-04
.392849E-04	.380865E-05	.380865E-05	.677491E-04
.327430E-04	-.412461E-05	-.412461E-05	.564320E-04
.151844E-04	-.817520E-06	-.817520E-06	.172585E-04
.529105E-04	.125917E-04	.125917E-04	.787280E-04
.302579E-04	-.970092E-05	-.970092E-05	.555784E-04
.430744E-04	-.432481E-05	-.432481E-05	.516738E-04
.247827E-04	.144155E-05	.144155E-05	.536742E-04
.473564E-04	.554833E-06	.554833E-06	.504693E-04
.380632E-04	.593915E-05	.593915E-05	.419704E-04
.250003E-04	.107136E-04	.107136E-04	.614056E-04
.499378E-04	.386970E-05	.386970E-05	.894387E-04
.566636E-04	.567242E-05	.567242E-05	.119813E-03
.451780E-04	-.452088E-05	-.452088E-05	.619498E-04
.326218E-04	-.111646E-07	-.111646E-07	.584913E-04
.505071E-04	.111578E-04	.111578E-04	.684739E-04
.503692E-04	.210943E-05	.210943E-05	.126179E-03

A5.2 Principal permeabilities of the 60 realisations

	K_1	K_2	θ
1	3.934420E-05	2.497700E-05	130.133
2	5.712962E-05	3.204539E-05	99.600
3	6.310197E-05	4.213339E-05	82.616
4	6.309084E-05	4.403700E-05	104.165
5	8.636171E-05	4.280939E-05	84.659
6	5.004032E-05	3.527351E-05	123.830
7	3.843244E-05	2.074091E-05	90.368
8	9.487078E-05	2.969584E-05	70.559
9	4.218623E-05	2.351711E-05	98.257
10	8.896984E-05	2.878551E-05	74.472
11	8.553124E-05	4.464602E-05	77.466
12	7.797233E-05	4.637718E-05	64.843
13	3.670493E-05	2.576201E-05	53.494
14	8.699040E-05	4.419385E-05	78.373
15	5.737013E-05	3.520038E-05	106.341
16	6.721779E-05	4.043589E-05	93.061
17	5.768059E-05	3.635915E-05	67.008
18	3.685119E-05	1.713587E-05	54.298
19	1.015230E-04	5.486237E-05	88.316
20	1.121945E-04	4.620417E-05	92.047
21	6.246397E-05	2.087989E-05	93.202
22	5.091263E-05	2.873273E-05	79.453
23	7.740397E-05	3.498672E-05	89.425
24	2.985631E-05	1.927373E-05	9.389
25	7.229372E-05	4.536807E-05	81.864
26	4.456955E-05	2.110651E-05	71.307
27	6.140954E-05	3.951508E-05	77.348
28	4.394074E-05	3.196706E-05	66.019
29	5.535937E-05	3.549809E-05	78.646
30	5.795235E-05	5.003960E-05	117.382
31	1.328769E-04	5.919835E-05	84.974
32	7.655117E-05	3.172418E-05	78.852
33	2.433717E-05	1.725470E-05	71.172
34	8.636060E-05	6.707357E-05	71.694
35	6.221522E-05	3.175597E-05	75.693
36	1.410647E-04	4.778166E-05	86.881
37	5.457674E-05	3.520642E-05	124.758
38	6.282748E-05	4.953205E-05	91.859
39	1.387913E-04	4.685985E-05	84.985
40	5.865354E-05	2.690149E-05	94.052
41	5.385824E-05	2.353653E-05	62.754
42	6.163197E-05	2.930754E-05	81.595
43	4.747632E-05	2.019096E-05	91.554
44	5.291224E-05	2.145483E-05	89.927
45	6.824986E-05	3.878408E-05	82.509
46	5.712962E-05	3.204539E-05	99.600
47	1.754199E-05	1.490087E-05	109.124
48	8.385216E-05	4.778638E-05	67.856
49	5.886770E-05	2.696855E-05	108.731
50	5.347258E-05	4.127564E-05	112.583
51	5.374596E-05	2.471092E-05	87.151
52	5.056527E-05	4.726047E-05	80.190
53	4.626899E-05	3.376460E-05	54.104
54	6.432447E-05	2.208143E-05	74.760
55	8.981427E-05	4.956224E-05	84.457
56	1.203185E-04	5.615817E-05	84.908
57	6.309082E-05	4.403700E-05	104.165
58	5.849127E-05	3.262181E-05	90.025
59	7.391526E-05	4.516579E-05	64.419
60	1.262376E-04	5.031055E-05	88.407
MEAN VALUE =	6.682578E-05	3.597952E-05	8.469530E+01
S. DEVIATION =	2.559117E-05	1.172091E-05	1.942927E+01

APPENDIX 6

User's instructions of the DICHA, DICONN, DIFLOW A, DIFLOW B and PLOTHA programs

The programs DICHA, DICONN, DIFLOW and PLOTHA are written in FORTRAN IV aand were run in a CDC computer, 850 cyber, with line printer and microfilm facilities. The compiler used is the MNF5 (Minnesota Fortran Version 5)

6.1 The Discontinuity mesh generator program (DICHA)

The program DICHA can typically handle up to 5 discontinuity sets each containing up to 2000 discontinuities. 20 scanlines of arbitrary orientation can be superimposed onto the sample area. The input data are presented as follows:

- Card 1 format (20A4)

  cols. 1-80 title

- Card 2 format (I2, 8F6.2)

  cols. 1-2 NSL number of scanlines superimposed in the sample area

  cols. 3-24 XO2, YO2, XO1, YO1 Coordinates of the generation area

  cols. 25-50 XI2, YI2, XI1, YI1 Coordinates of the sample area

- Card 3 format (I2)

  cols. 1-2 NSED seed value to set a sequence of random numbers

- <u>Card 4</u> format (4F10.3)

  There is one of these cards for each superimposed scanline.

  cols. 1-40 XX1, YY1, XX2, YY2 Coordinates of the end points of each superimposed scanline

- <u>Card 5</u> format (2I1, I7, 4F6.2, 2F8.6)

  There is one of these cards for each discontinuity set.

  col. 1 ID an integer number that when

  ID = 0 continue to generate the next set of discontinuities

  ID = 1 last set and then stop

  col. 2 IL an integer number that indicates the trace length distribution

  IL = 0 Uniform distribution of trace lengths

  IL = 1 Log-normal distribution of trace lengths

  IL = 2 Negative exponential distribution of trace lengths

  cols. 3-9 NJC number of discontinuities per set

  cols. 10-15 AMO mean angle of orientation

  cols. 16-21 SAO standard deviation of the mean angle of orientation

  cols. 22-27 TML mean trace length

  cols. 28-33 SDL standard deviation of the mean trace length

  cols. 34-41 APM mean discontinuity aperture

  cols. 42-49 SDA standard deviation of the mean aperture

The DICHA results are of two types: the first is presented as a series of tables and is usually produced by the line printer, the second is a file containing the coordinates of the end points for each discontinuity generated within the sample area together with the aperture values generated for each discontinuity. This file is usually saved and stored in the user's file space at the computer centre.

The tables produced via the line printer are organised by discontinuity sets. For each set the following information is produced: the input parameters used in the generation process, the actual generated mean and standard deviation values and finally the discontinuity density. For each set, the following information is obtained from each superimposed scanline: scanline number, coordinates of its end points, mean and standard deviations for discontinuity spacing, semi-trace length and discontinuity frequency measured along the scanline and along the mean normal to the discontinuity set. After the information for all sets has been listed, the discontinuity frequency for all joint sets aggregated is calculated and listed. Finally the total number of discontinuities in a sample area is printed. A typical print-out produced by the program DICHA is presented later in this Appendix. A full listing of the program is given in Appendix 7.

Typical example of the print out produced by the program DICHA

```
JOINT SET NUMBER= 1

INPUT MEAN ANGLE OF ORIENTATION, (DEGREES) =        0
STANDARD DEV. OF ORIENTATION               =        0

NEGATIVE EXPONENTIAL DISTR. OF TRACE LENGTH
INPUT MEAN TRACE LENGTH        (METERS)    =     .400
STANDARD DEV. OF TRACE LENGTH   (METERS)   =     .200

INPUT MEAN APERTURE      (METERS)          =  .10000E-04
STANDARD DEV. OF APERTURE  (METERS)        =       0

NUMBER OF DISCONTINUITIES,GENERATED        =     900
--------------------------------------------------------------------------------

ACTUAL MEAN VALUES GENERATED
MEAN TRACE LENGTH=      .366    STANDARD DEV.   =       .344
MEAN ANG. ORIENT.=        0     STANDARD DEV.   =         0
MEAN DIS APERTURE= .10000E-04   STANDARD DEV.   =  .27562E-11

NUM.OF JOINTS IN SAMPLE AREA =    223

N(NUMBER OF JOINTS/UNIT AREA)=     2.230
--------------------------------------------------------------------------------

SCANLINE NUMBER= 4
START COORDS=    8.000      5.000
END COORDS  =    8.000     15.000

MEAN SPACING=   1.781     STAND. DEV.=   2.088

MEAN S-TRACE=    .390     STAND. DEV.=    .277

                         DISCONTINUITY FREQUENCY
SCANLINE NO.          LAMDA S           ANGLE I          LAMDA I
      4                .561              90.00             .561
--------------------------------------------------------------------------------

SCANLINE NUMBER= 5
START COORDS=   10.000      5.000
END COORDS  =   10.000     15.000

MEAN SPACING=    .697     STAND. DEV.=    .434

MEAN S-TRACE=    .543     STAND. DEV.=    .753

                         DISCONTINUITY FREQUENCY
SCANLINE NO.          LAMDA S           ANGLE I          LAMDA I
      5               1.434              90.00            1.434
--------------------------------------------------------------------------------

SCANLINE NUMBER= 6
START COORDS=   12.000      5.000
END COORDS  =   12.000     15.000

MEAN SPACING=   1.033     STAND. DEV.=    .772


MEAN S-TRACE=    .455     STAND. DEV.=    .295

                         DISCONTINUITY FREQUENCY
SCANLINE NO.          LAMDA S           ANGLE I          LAMDA I
      6                .968              90.00             .968
```

```
JOINT SET NUMBER= 2

INPUT MEAN ANGLE OF ORIENTATION, (DEGREES) =  45.000
STANDARD DEV. OF ORIENTATION               =       0

NEGATIVE EXPONENTIAL DISTR. OF TRACE LENGTH
INPUT MEAN TRACE LENGTH       (METERS)     =    .400
STANDARD DEV. OF TRACE LENGTH   (METERS)   =    .200

INPUT MEAN APERTURE      (METERS)          =  .10000E-04
STANDARD DEV. OF APERTURE   (METERS)       =       0

NUMBER OF DISCONTINUITIES,GENERATED        =   1550
```

```
ACTUAL MEAN VALUES GENERATED

MEAN TRACE LENGTH=       .389    STANDARD DEV.   =      .356
MEAN ANG. ORIENT.=     45.000    STANDARD DEV.   =         0
MEAN DIS APERTURE=  .10000E-04   STANDARD DEV.   =  .47184E-11

NUM.OF JOINTS IN SAMPLE AREA =    409

N(NUMBER OF JOINTS/UNIT AREA)=    4.090
```

```
SCANLINE NUMBER= 1
START COORDS=     5.000     8.000
END COORDS  =    15.000     8.000

MEAN SPACING=     .936     STAND. DEV.=     .579

MEAN S-TRACE=     .365     STAND. DEV.=     .320
```

DISCONTINUITY FREQUENCY

SCANLINE NO.	LANDA S	ANGLE I	LANDA I
1	1.068	45.00	1.510

```
SCANLINE NUMBER= 2
START COORDS=     5.000    10.000
END COORDS  =    15.000    10.000

MEAN SPACING=     .658     STAND. DEV.=     .385

MEAN S-TRACE=     .344     STAND. DEV.=     .273
```

DISCONTINUITY FREQUENCY

SCANLINE NO.	LANDA S	ANGLE I	LANDA I
2	1.520	45.00	2.150

```
SCANLINE NUMBER= 3
START COORDS=     5.000    12.000
END COORDS  =    15.000    12.000
MEAN SPACING=     .511     STAND. DEV.=     .440
MEAN S-TRACE=     .392     STAND. DEV.=     .360
```

DISCONTINUITY FREQUENCY

SCANLINE NO.	LANDA S	ANGLE I	LANDA I
3	1.955	45.00	2.765

```
SCANLINE NUMBER= 4
START COORDS=     8.000     5.000
END COORDS  =     8.000    15.000

MEAN SPACING=     .779     STAND. DEV.=     .622

MEAN S-TRACE=     .306     STAND. DEV.=     .292
```

DISCONTINUITY FREQUENCY

SCANLINE NO.	LANDA S	ANGLE I	LANDA I
4	1.284	45.00	1.816

```
SCANLINE NUMBER= 5
START COORDS=    10.000     5.000
END COORDS  =    10.000    15.000

MEAN SPACING=     .717     STAND. DEV.=     .650

MEAN S-TRACE=     .202     STAND. DEV.=     .276
```

DISCONTINUITY FREQUENCY

SCANLINE NO.	LANDA S	ANGLE I	LANDA I
5	1.394	45.00	1.971

```
SCANLINE NUMBER= 6
START COORDS=    12.000     5.000
END COORDS  =    12.000    15.000

MEAN SPACING=     .661     STAND. DEV.=     .676

MEAN S-TRACE=     .445     STAND. DEV.=     .351
```

DISCONTINUITY FREQUENCY

SCANLINE NO.	LANDA S	ANGLE I	LANDA I
6	1.513	45.00	2.140

```
JOINT SET NUMBER= 3

INPUT MEAN ANGLE OF ORIENTATION, (DEGREES) = 135.000
STANDARD DEV. OF ORIENTATION               =       0

NEGATIVE EXPONENTIAL DISTR. OF TRACE LENGTH
INPUT MEAN TRACE LENGTH        (METERS)    =    .400
STANDARD DEV. OF TRACE LENGTH  (METERS)    =    .200

INPUT MEAN APERTURE       (METERS)         = .10000E-04
STANDARD DEV. OF APERTURE (METERS)         =       0

NUMBER OF DISCONTINUITIES,GENERATED        =    1550
```

```
ACTUAL MEAN VALUES GENERATED
MEAN TRACE LENGTH=       .404   STANDARD DEV.   =      .364
MEAN ANG. ORIENT.=    135.000   STANDARD DEV.   =        0
MEAN DIS APERTURE= .10000E-04   STANDARD DEV.   = .45961E-11

NUM.OF JOINTS IN SAMPLE AREA =    411

N(NUMBER OF JOINTS/UNIT AREA)=    4.110
```

```
SCANLINE NUMBER= 1
START COORDS=     5.000      8.000
END COORDS  =    15.000      8.000

MEAN SPACING=     .811    STAND. DEV.=    .602
MEAN S-TRACE=     .288    STAND. DEV.=    .212

                      DISCONTINUITY FREQUENCY
SCANLINE NO.        LANDA S          ANGLE I         LANDA I
     1               1.233           135.00           1.743
```

```
SCANLINE NUMBER= 2
START COORDS=     5.000     10.000
END COORDS  =    15.000     10.000

MEAN SPACING=    1.401    STAND. DEV.=   1.209
MEAN S-TRACE=     .461    STAND. DEV.=    .370

                      DISCONTINUITY FREQUENCY
SCANLINE NO.        LANDA S          ANGLE I         LANDA I
     2                .714           135.00           1.009
```

```
SCANLINE NUMBER= 3
START COORDS=     5.000     12.000
END COORDS  =    15.000     12.000

MEAN SPACING=     .977    STAND. DEV.=    .745
MEAN S-TRACE=     .295    STAND. DEV.=    .273

                      DISCONTINUITY FREQUENCY
SCANLINE NO.        LANDA S          ANGLE I         LANDA I
     3               1.023           135.00           1.447
```

```
SCANLINE NUMBER= 4
START COORDS=     8.000      5.000
END COORDS  =     8.000     15.000

MEAN SPACING=    1.101    STAND. DEV.=   1.140
MEAN S-TRACE=     .428    STAND. DEV.=    .251

                      DISCONTINUITY FREQUENCY
SCANLINE NO.        LANDA S          ANGLE I         LANDA I
     4                .908            45.00           1.285
```

```
SCANLINE NUMBER= 5
START COORDS=    10.000      5.000
END COORDS  =    10.000     15.000

MEAN SPACING=     .778    STAND. DEV.=    .696
MEAN S-TRACE=     .478    STAND. DEV.=    .509

                      DISCONTINUITY FREQUENCY
SCANLINE NO.        LANDA S          ANGLE I         LANDA I
     5               1.286            45.00           1.818
```

```
SCANLINE NUMBER= 6
START COORDS=    12.000      5.000
END COORDS  =    12.000     15.000

MEAN SPACING=     .966    STAND. DEV.=    .624
MEAN S-TRACE=     .242    STAND. DEV.=    .233

                      DISCONTINUITY FREQUENCY
SCANLINE NO.        LANDA S          ANGLE I         LANDA I
     6               1.035            45.00           1.464
```

```
DISCONTINUITY FREQUENCY FOR ALL JOINT SETS
     SCANLINE          LANDA TOT.
         1               2.301
         2               2.234
         3               2.979
         4               2.754
         5               4.114
         6               3.516
TOTAL NUMBER OF DISC. IN SAMPLE AREA=   1043
```

6.2 The connectivity analysis program DICONN and the flow analysis programs DIFLOW A and DIFLOW B

It was noted earlier in Chapter 5, that when the discontinuity meshes were relatively small (containing less than 5000 discontinuities) it was more practical to merge the programs DICONN and DIFLOW in order to avoid file manipulations that are necessary when both programs are operated independently. The program which resulted from this merging was called DIFLOW A. The input data for DIFLOW A have to be stored in two different files. The first file, which contains the data for the discontinuities as generated by DICHA, is used directly without modifications. The second file is one which contains information about the size of the test area and its boundary conditions. The input data in this second file are presented as follows:

- Card 1 format (20A4)

  cols. 1-80 title

- Card 2 format (I6)

  cols. 1-6 IP number of discontinuities in the sample area

- Card 3 format (2F6.2)

  cols. 1-6 H_1 Boundary potential at the input side

  cols. 7-12 H_2 Boundary potential at the output side

- Card 4 format (4F7.3, F8.6)

  There are 4 cards all together, one for each side of the square test area.

  cols. 1-28 XX1, YY1, XX2, YY2 end coordinates of the sides of the square defining the test area.

  cols. 29-36 OPE dummy value

The output of the program DIFLOW A is summarised in a table, a typical example of the results is presented in Table 6A.I. Values under the heading "first iteration" are those obtained from the connectivity analysis of the generated mesh prior to the removal of the dead ends and the isolated closed loops of discontinuities. The values under the heading "second iteration" are the values resulting from the analysis of the inter-connected mesh. In the second part of Table 6A.I it can be seen that the measured flow rates across each side of the test area are included, together with the value of the closing error. The total aperture, defined as the sumation of aperture for all discontinuities that intersect the boundaries, is also listed for each side of the test area. As noted earlier in Figure 3.9, sides 1 and 4 are the inflow and outflow boundaries respectively with constant boundary potentials; sides 2 and 3 are permeable boundaries that can exhibit either inflow or outflow. These latter boundaries are subjected to linearly varying boundary potentials. Finally the components of the equivalent permeability tensor are presented; these are calculated in two different ways. The first pair of components are calculated using equation (3.31) which uses the flow information of all internal discontinuity segments. The second pair of components is calculated using equation (3.32), which only considers the flow through the discontinuity segments that intersect the boundaries. A second type of output is also produced; this is a file that contains the information needed to plot the interconnected mesh. This information is usually saved and stored in the user's file space. The listings of the DIFLOW A program together with the plotting program are given in Appendix 7.

```
LENGTH ORIENTATION 58

FIRST ITERATION :

NUMBER OF DISCONT.          =  1080
NUMBER OF NODES             =  1192
NUMBER OF LINKS             =  1659
NUMBER OF INTERSECTIONS     =  2434
NUMBER OF NODES ON BOUN.    =   151
NUMBER OF REJECTED NODES    =    94

SECOND ITERATION :

NUMBER OF DISCONT.          =   460
NUMBER OF NODES             =   913
NUMBER OF LINKS             =  1366
NUMBER OF INTERSECTIONS     =  1826
NUMBER OF NODES ON BOUN.    =   126
NUMBER OF EQUATIONS         =   787
NUMBER OF ADJACENT NODES    =  2732
NUMBER OF NON-ZEROS            2945


LINE NUMBER  1     FLOW RATE      1.961246E-07

LINE NUMBER  2     FLOW RATE      2.049532E-08

LINE NUMBER  3     FLOW RATE      2.002916E-07

LINE NUMBER  4     FLOW RATE     -4.169115E-07

FLOW RATE CLOSING ERROR           6.047138E-17

LINE NUMBER  1     AREA           1.650000E-03

LINE NUMBER  2     AREA           1.450000E-03

LINE NUMBER  3     AREA           1.400000E-03

LINE NUMBER  4     AREA           1.800000E-03


COMPONENTS OF EQUIVALENT PERMEABILITY TENSOR
K1=     2.164342E-08      K2=     1.451873E-09
K1=     2.164342E-08      K2=     1.451873E-09
```

Table 6A.1   Results of DIFLOW A

In order to simulate fluid flow into an underground excavation it was necessary to modify the programs DICONN and DIFLOW. Again it was found, for the same practical reasons mentioned earlier, that merging of the above two programs could be achieved if the problem being tackled contained less than 5000 discontinuities. In this case the resultant program was called DIFLOW B. The input data for this program are indentical to the data for DIFLOW A with only two differences. These differences relate to the boundary potential specifications and to the excavation size and location. The following two cards contain the additional input required by DIFLOW B.

- Card A format (9F6.2)

  cols. 1-48 H11, H12, H21, H22, H31, H32, H41, H42 The potential at each corner of the test area, see Fig. 6A.I

  cols. 49-54 HEX constant potential at the surface of the underground excavation.

- Card B format (2I2, 4F6.2)

  cols. 1-2 IEX indicates shape of the excavation

  IEX = 0 circular

  IEX = 1 elliptical

  IEX = 2 rectangular (quadrilateral in general)

  cols. 3-4 IHV used when the excavation is of elliptical shape; indicates if the major axis is horizontal or vertical.

  IHV = 0 horizontal major axis

  IHV = 1 vertical major axis

cols. 5-28 DUM 1, DUM 2, DUM 3, DUM 4 These are dummy variables that may have the following values:

(a) if the excavation is circular , i.e. IEX = 0

DUM 1 = x-coord. of the centre of the excavation

DUM 2 = y-coord. of the centre of the excavation

DUM 3 = Radius of the excavation

DUM 4 = dummy

(b) if the excavation is elliptical, i.e. IEX = 1

DUM 1 = x-coord. of the centre of the excavation

DUM 2 = y-coord. of the centre of the excavation

DUM 3 = major semi-axis length of the excavation

DUM 4 = minor semi-axis length of the excavation

(c) if the excavation is rectangular, i.e. IEX = 2

DUM 1) x and y coordinates of lower
) left corner of the excavation
DUM 2)

DUM 3) x and y coordinates of the upper
) right corner of the excavation
DUM 4)

In order to generate the complete input file for the program DIFLOW B it is only necessary to replace Card 3 from the DIFLOW A input file by Cards A and B. The rest of the input data remain the same. A typical output produced by the program DIFLOW B is presented in Table 6A.II. The listing of the program DIFLOW B is given in Appendix 7.

```
TUNNEL STUDY

FIRST ITERATION :

NUMBER OF DISCONT.            =  2142
NUMBER OF NODES               =  1913
NUMBER OF LINKS               =  2524
NUMBER OF INTERSECTIONS       =  3876
NUMBER OF NODES ON BOUN.      =   197
NUMBER OF REJECTED NODES      =   576

SECOND ITERATION :

NUMBER OF DISCONT.            =   615
NUMBER OF NODES               =  1073
NUMBER OF LINKS               =  1515
NUMBER OF INTERSECTIONS       =  2130
NUMBER OF NODES ON BOUN.      =   162
NUMBER OF EQUATIONS           =   911
NUMBER OF ADJACENT NODES      =  3030
NUMBER OF NON-ZEROS           =  3155


LINE NUMBER  1     FLOW RATE       8.819502E-08

LINE NUMBER  2     FLOW RATE       8.994389E-08

LINE NUMBER  3     FLOW RATE      -1.563065E-17

LINE NUMBER  4     FLOW RATE       4.762180E-18

FLOW RATE IN THE TUNNEL           -1.781389E-07

FLOW RATE CLOSING ERROR            1.210800E-16

LINE NUMBER  1     AREA            2.100000E-03

LINE NUMBER  2     AREA            1.750000E-03

LINE NUMBER  3     AREA            2.300000E-03

LINE NUMBER  4     AREA            1.950000E-03


COMPONENTS OF SPECIFIC DISCHARGE VECTOR
V1=    7.138175E-10     V2=    5.461668E-10
V1=    7.138175E-10     V2=    5.461668E-10
```

Table 6A.II   Results of DIFLOW B

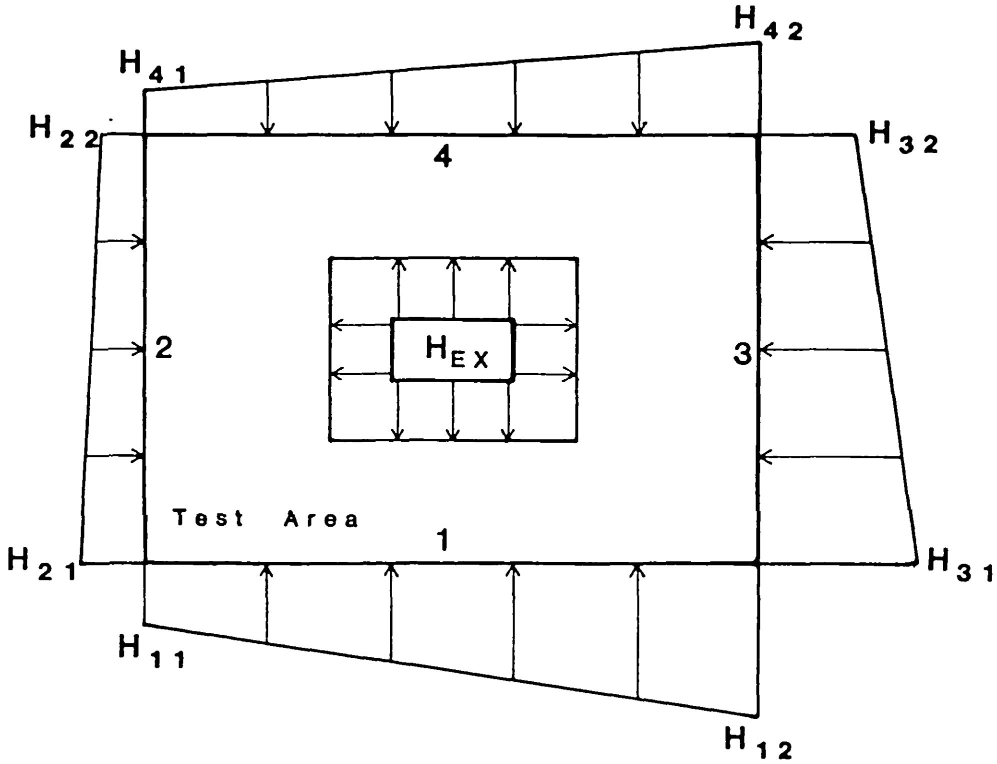

Fig. 6A.1 Boundary conditions to simulate fluid flow into underground excavations

6.3 The discontinuity mesh plotting PLOTHA

The program PLOTHA is written in Fortran IV and makes use of the Common Plotting Library available at Imperial College computer centre. The input data for this program have to be stored in two different files. The first file, which contains the data for the discontinuity network, which can be either the generated mesh or the inter-connected mesh, is used directly without modifications. The second file is one that contains information about the test area. The input data in this second file are presented as follows:

- Card 1 format (20A4)

  cols. 1-80 title

- Card 2 format (I5, 8F7.3)

  cols. 1-5 IP number of discontinuities to be plotted

  cols. 6-33 XO1, YO1, XO2, YO2 end coordinates of the sides of the square defining either the generation or the sample area

  cols. 34-61 XI1, YI1, XI2, YI2 end coordinates of the sides of the square defining the test area

The output of the program PLOTHA can be obtained either in microfilm or in flat bed plotter.

APPENDIX 7

Listing of programs:

SCANL
PHOCOM
DICHA
DICONN
DIFLOW A
DIFLOW B
PLOTHA

[redacted]

APPENDIX 8

Estimation of mean discontinuity aperture from borehole packer tests

The results of 7 packer tests, which were carried out in 3 boreholes within the area of the case-study described in Section 4.4.2, were analysed in order to estimate the mean discontinuity aperture. The information available consisted of: borehole logs, packer depths and lengths, estimated applied pressures and resulting flow rates. The water intakes in lugeons and estimated packer permeability were also available. The theory and equations used are a combination of the work presented by Snow (1969), Maini (1971) and Rissler (1978), and are applicable to constant head pressure tests. The analyses of the results obtained from this type of test are based on the following assumptions:

(i) the test section is vertical, of length L, and intersected by an arbitrary number of horizontal discontinuities

(ii) discontinuities are represented by constant apertures between smooth parallel plates that are equally spaced

(iii) the flow occurs within each discontinuity, is radial, laminar and governed by Darcy's law. No flow occurs in the rock material.

Consider a single fracture of infinite radial extent normal to the borehole axis, as shown in Fig. 8A.1. It is assumed that there is no mutual interference between the flow through this fracture and flow through other fracture planes intersecting it.

Darcy's law for the flow through the fracture plane is given by

$$\overline{V} = K_f \frac{\partial h}{\partial r} \qquad (1)$$

where K_f is the fracture permeability, $\overline{V}$ the mean velocity through a fracture of aperture e due to a pressure gradient of $\partial h/\partial r$

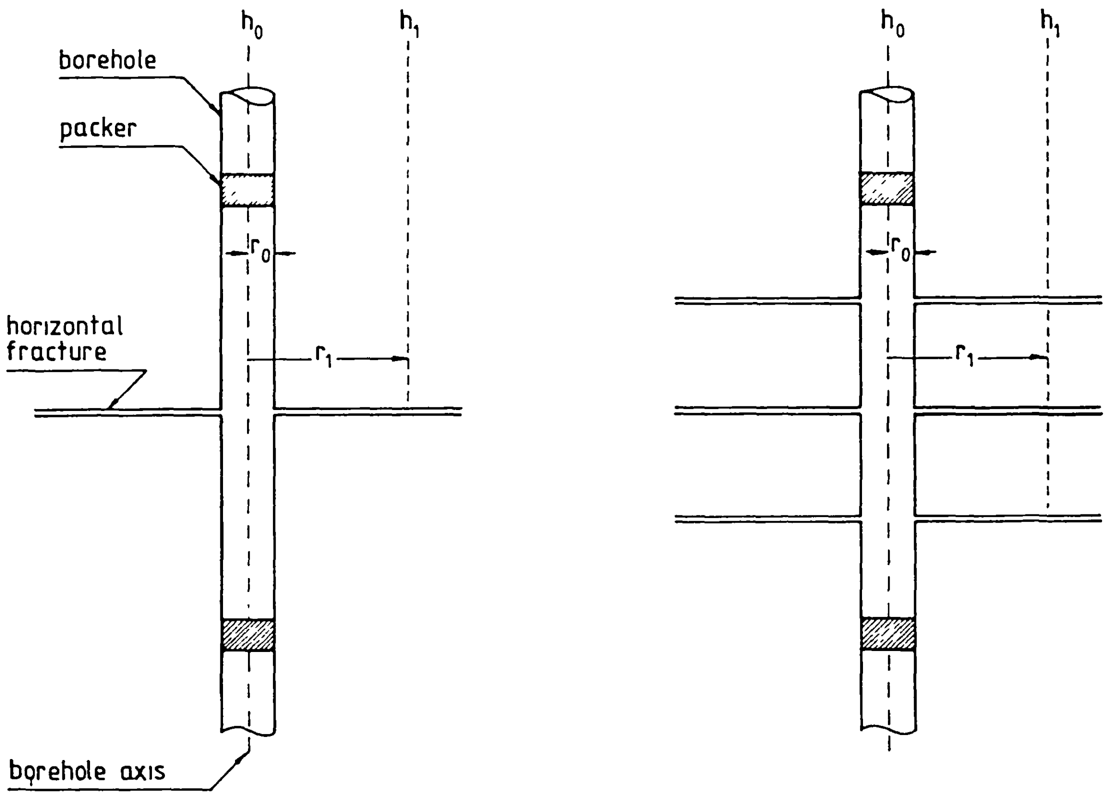

Fig. 8A.1 Single and multiple discontinuity planes normal to the borehole axis

The total flow quantity, Q, through a fracture is given by

$$Q = 2\pi r e \overline{V} \tag{2}$$

substituting equation (1) into (2) and integrating between the pressure limits of h_o to h_1 and radius limits of r_o to r_1

$$\frac{Q}{2\pi r e} = K_f \frac{\partial h}{\partial r}$$

$$\int_{r_o}^{r_1} \frac{dr}{r} = \int_{h_o}^{h_1} \frac{2\pi e}{Q} K_f \, dh$$

$$\text{Log}_e(r_1/r_o) = \frac{2\pi e}{Q} K_f \, (h_o - h_1)$$

or

$$Q = \left[\frac{2\pi e \; K_f}{\text{Log}_e \; (r_1/r_o)}\right] (h_o - h_1) \tag{3}$$

If there are n fractures within the test section, equation (3) becomes

$$Q = \left[\frac{2\pi e n \; K_f}{\text{Log}_e \; (r_1/r_o)}\right] (h_o - h_1) \tag{4}$$

or

$$K_f = \frac{Q \; \text{Log}_e \; (r_1/r_o)}{2\pi e n \; (h_o - h_1)} \tag{5}$$

According to the parallel plate model presented in Section 2.3.4 the fracture permeability is given by

$$K_f = \frac{e^2 g}{12\nu} \tag{6}$$

where ν the kinematic viscosity, g the acceleration due to gravity and e the fracture aperture. By equating equations (6) and (5) it is possible to obtain

$$e^3 = \frac{6\nu Q \operatorname{Log}_e (r_1/r_o)}{\pi g n (h_o - h_1)} \tag{7}$$

where h_o denotes the pressure at radius r_o, (i.e. the borehole radius) and h_1 the pressure at some radius r_1 from the centre of the borehole. The radius r_1 is known as the radius of influence of the test, where the fluid pressure $h_1 = 0$. Maini (1971) found that large variations in r_1 produce only small variations in the computed discontinuity apertures. For the purposes of this work a value of $r_1 = 100$m was assumed to be adequate. Therefore, equation (7) becomes

$$e^3 = \frac{6\nu Q \operatorname{Log}_e (r_1/r_o)}{\pi g n\, h_o} \tag{8}$$

The above equation was developed based upon the assumption of a vertical borehole intersected by horizontal discontinuities. In practice, however, this seldom occurs, therefore, it is necessary to consider the case where the discontinuity planes intersecting the borehole are inclined rather than horizontal. Rissler (1978) showed a relation between β, the dip angle of the discontinuity planes, and Q, the flow quantities when the borehole was vertical. He used a finite element technique to solve the flow through the intersecting discontinuities. The results obtained are shown in Fig. 8A.2.

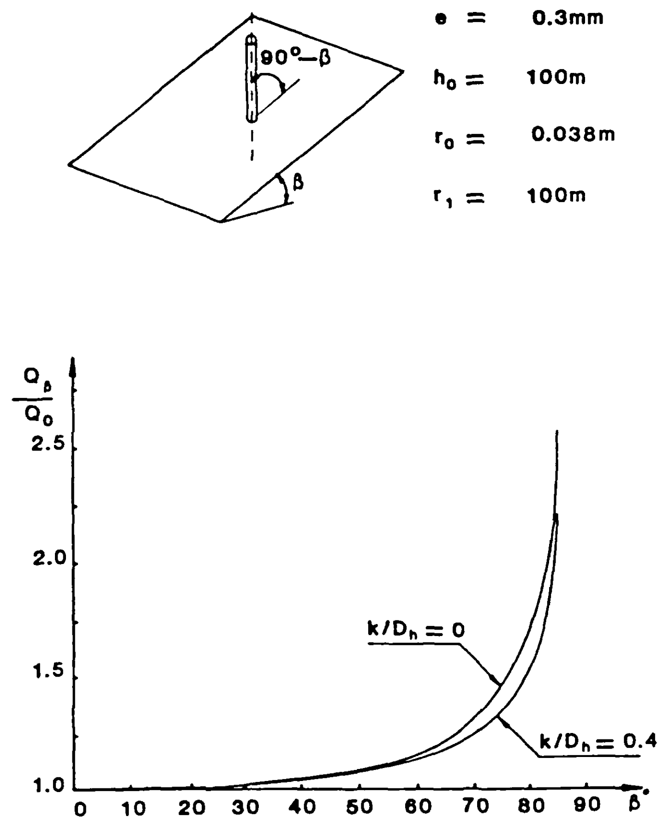

Fig. 8A.2 Influence of the dip angle of the discontinuity planes upon the flow quantities for a vertical borehole (after Rissler, 1978)

It can be seen in Fig. 8A.2 that there are two curves, each one for a different relative roughness, k/D_h. The parameter k is the absolute roughness of the discontinuity walls, i.e. the mean height of the asperities, and D_h is the hydraulic diameter which is four times the hydraulic radius R_h defined in Chapter 2. Q_β is the flow quantity through the discontinuity when its dip angle is β, and Q_o is the flow quantity when the discontinuity is horizontal, i.e. dip angle $\beta = 0$.

The sequence of calculations was as follows; from the test sections depths it was possible to identify, using the corresponding borehole loggings records, the number of discontinuities intersecting the test section, by either using the recorded values of the RQD or the measured fracture frequency. The dip angle of each of the discontinuities was found from the borehole logging records with the aid of the core photographs. If it was found that only one set of discontinuities intersected the test section, the corresponding correction factor for the flow quantity was calculated from the curves shown in Fig. 8A.2, assuming a relative roughness of zero. The corrected flow quantity, Q, was then input to equation (8) together with the corresponding pressure head, h_o, the number of intersecting discontinuities, n, and the radius of influence r_1, which was assumed to be equal to 100m in all cases. Thus the mean discontinuity aperture was estimated.

When more than one set of discontinuities was present in the test section, it was assumed that the flow quantity through each set was proportional to the number of discontinuities within each particular set. For example, assuming that there are two discontinuity sets each containing n_1 and n_2 discontinuities respectively, then,

$$Q_{\beta 1} / Q_{\beta 2} = n_1 / n_2 \quad (9)$$

but $$Q_{\beta 1} + Q_{\beta 2} = Q_t \tag{10}$$

where $Q_{\beta 1}$ and $Q_{\beta 2}$ are the flow quantities through discontinuity sets with dip angles of β_1 and β_2 respectively and Q_t is the total flow quantity across all discontinuities in the test section. When the values of $Q_{\beta 1}$ and $Q_{\beta 2}$ had been found it was possible to calculate the corresponding flow correction factors, and finally to estimate the mean apertures by using equation (8) for each set separately.

Table 8A.I shows the mean apertures calculated from three different boreholes that were located within the area of study described in Section 4.4.2. Although this method, based upon the assumptions described earlier in this Appendix, gives an estimation of the mean discontinuity aperture, it does not provide any information about their type of distribution. For the purposes of the case study described in Section 4.4.2 it was assumed that the apertures were log-normally distributed. This assumption was based on previous work presented by Snow (1969), Bianchi and Snow (1969) and Witherspoon and Gale (1983).

Borehole number	Rock type	Borehole radius (m)	Length of test section (m)	mean dip angle	number of discontinuities	mean aperture (mm)
1	grey mudstones	0.049	0.80	20°	10	0.0846
				72°	3	0.1256
			3.15	20°	38	0.0749
				75°	9	0.0943
2	strong sandstones	0.049	3.0	80°	9	0.1203
				12°	4	0.0872
			3.0	40°	93	0.0485
3	Siltstones	0.056	10.0	80°	176	0.1814
			5.0	75°	78	0.1317
			3.0	5°	34	0.0758

Table 8A.I Results of mean aperture obtained from permeability packer tests